2012-08-16

Improving the Quantitative Assessment of Intraretinal Features by Determining both Structural and Optical Properties of the Retinal Tissue with Optical Coherence Tomography

Wei Gao
University of Miami, w.gao@umiami.edu

UNIVERSITY OF MIAMI

IMPROVING THE QUANTITATIVE ASSESSMENT OF INTRARETINAL FEATURES BY DETERMINING BOTH STRUCTURAL AND OPTICAL PROPERTIES OF THE RETINAL TISSUE WITH OPTICAL COHERENCE TOMOGRAPHY

By

Wei Gao

A DISSERTATION

Submitted to the Faculty
of the University of Miami
in partial fulfillment of the requirements for
the degree of Doctor of Philosophy

Coral Gables, Florida
August 2012

UNIVERSITY OF MIAMI

A dissertation submitted in partial fulfillment of
the requirements for the degree of
Doctor of Philosophy

IMPROVING THE QUANTITATIVE ASSESSMENT OF INTRARETINAL FEATURES BY DETERMINING BOTH STRUCTURAL AND OPTICAL PROPERTIES OF THE RETINAL TISSUE WITH OPTICAL COHERENCE TOMOGRAPHY

Wei Gao

Approved:

_____ Delia Cabrera DeBuc, Ph.D. Research Associate Professor of Ophthalmology	_____ M. Brian Blake, Ph.D. Dean of the Graduate School
_____ Fabrice Manns, Ph.D. Associate Professor of Biomedical Engineering	_____ Jianhua Wang, M.D., Ph.D. Associate Professor of Ophthalmology
_____ Noël Ziebarth, Ph.D. Assistant Professor of Biomedical Engineering	_____ Weizhao Zhao, Ph.D. Associate Professor of Biomedical Engineering

GAO, WEI (Ph.D., Biomedical Engineering)

Improving the Quantitative Assessment of Intraretinal Features by Determining Both Structural and Optical Properties of the Retinal Tissue with Optical Coherence Tomography. (August 2012)

Abstract of a dissertation at the University of Miami.

Dissertation supervised by Professor Delia Cabrera DeBuc.
No. of pages in text. (310)

The goal of this project is to obtain quantitative assessments of intraretinal features by determining the structural and optical properties of retinal tissue with optical coherence tomography. To accomplish this goal, structural and optical properties, in addition to thickness measurements, were extracted from OCT-based images and were used for the discrimination of DM eyes with and without DR from healthy eyes.

First, structural parameters including the thickness, fractal dimension, energy, entropy, correlation and contrast were evaluated for each intraretinal layer using various image processing techniques such as speckle noise removal, retinal segmentation and blood vessel shadow removal. In addition, optical properties such as the mean reflectance, total reflectance, layer index and scattering coefficients were calculated. Specifically, in this dissertation, the main contribution from the biomedical engineering perspective was the development of single and multiple-scattering models using information from different cellular layers of the retina. These models were implemented to extract scattering coefficients from OCT images of healthy and diseased eyes. There is little published work addressing the optical properties of retinal tissue, and what research there

is uses a scattering model that considers the retinal tissue as a whole without taking into account its multi-layer structure. In contrast, our scattering models allow us to obtain the scattering coefficient for each intraretinal layer and better explore the optical properties of the retinal tissue.

Second, statistical analyses including ANOVA followed by Newman-Keuls post-hoc analysis and receiver operating characteristic analysis were performed on the structural and optical parameters between study groups to determine the diagnostic ability of each structural and optical characteristic to differentiate the diabetic eyes with and without MDR from healthy eyes. Based on the statistical analysis, the capacity of each structural and optical parameter to aid in diagnosis can be determined. The results indicated that the methodology shows greater capability for differentiating diabetic eyes with and without MDR from healthy eyes than the standard commercial OCT device. Moreover, the structural and optical parameters that were best able to discriminate diabetic eyes from healthy eyes were evaluated and validated by artificial neural networks with Bayesian radial basis function.

Finally, an additional evaluation in a small group of patients with multiple sclerosis, which is another type of retinal pathology manifesting as retinal neurodegeneration, was evaluated based on the developed methodology.

Our results have demonstrated that our methodology would yield better insight into the macular pathology and therefore should play an important role in the future of the diagnosis and follow-up of neurological diseases.

谨将此文献给我的父母

To my beloved parents

ACKNOWLEDGEMENTS

I extend my deepest gratitude to my advisor, Dr. Delia Cabrera DeBuc, for being an extraordinary research supervisor. Her guidance, encouragement and support were invaluable and enabled me to finish this work. It has been a great experience working under her supervision and learning from her. Dr. Cabrera DeBuc taught me how to ask questions and find solutions. Without her patience and guidance, I would not have been able to overcome many crisis situations and complete this work.

I would like to acknowledge Dr. Gábor Márk Somfai and Dr. Erika Tátrai for providing the important and necessary OCT data that helped me finish this dissertation.

I am also thankful to the committee members, Dr. Fabrice Manns, Dr. Jianhua Wang, Dr. Weizhao Zhao and Dr. Noël Ziebarth, for their time and invaluable suggestions for this work.

I am very grateful for the scholarship I received from the Department of Biomedical Engineering, Bascom Palmer Eye Institute and the College of Engineering at University of Miami.

I am also grateful for the financial support from Juvenile Diabetes Research Foundation and NIH that funded the research explored in this dissertation.

Finally, I want to express my deepest appreciation and love to my parents, my brother and his family members for all their love and support.

TABLE OF CONTENTS

LIST OF ACRONYMS

ANN:	Artificial Neural Network
ANOVA:	Analysis of Variance
AUROC:	Area Under the Receiver Operating Characteristic Curve
BCVA:	Best-Corrected Visual Acuity
CSME:	Clinically Significant Macular Edema
cpRNFL:	circumpapillary RNFL
DR:	Diabetic Retinopathy
EDSS:	Expanded Disability Status Scale
ETDRS:	Early Treatment Diabetic Retinopathy Study
FD:	Fractal Dimension
FDOCT:	Fourier Domain Optical Coherence Tomography
FN:	False Negative
FP:	False Positive
FWHM:	Full Width at Half Maximum
GCL+IPL:	Ganglion Cell Layer + Inner Plexiform Layer
INL:	Inner Nuclear Layer
IOP:	Intraocular Pressure
MDR:	Mild Diabetic Retinopathy
MS:	Multiple Sclerosis
MSFC:	Multiple Sclerosis Functional Composite
MS ON^-:	Multiple Sclerosis without Optic Neuritis
MS ON^+:	Multiple Sclerosis with Optic Neuritis
NPDR:	Nonproliferative Diabetic Retinopathy
NRIR:	Reflectivity Normalized to the Maximum Value within the Whole Retina

NRPE:	Reflectivity with Normalization to the RPE Reflectance
OCT:	Optical Coherence Tomography
ON:	Optic Neuritis
ONL+IS:	Outer Nuclear Layer + Inner Segment Photoreceptors
OPL:	Outer Plexiform Layer
OS:	Outer Segment Photoreceptors
PPV:	Positive Predicted Value
RBF:	Radial Basis Function
RNFL:	Retinal Nerve Fiber Layer
ROC:	Receiver Operating Characteristic
ROI:	Region of Interest
RPE:	Retinal Pigment Epithelium
SD:	Standard Deviation
SDOCT:	Spectral Domain Optical Coherence Tomography
SFPs:	Stereoscopic Fundus Photos
SGLDMs:	Spatial Gray Level Co-occurrence Matrices
SS:	Swept Source
TDOCT:	Time Domain Optical Coherence Tomography
TN:	True Negative
TP:	True Positive

LIST OF FIGURES

LIST OF TABLES

CHAPTER 1. SPECIFIC AIMS

Diabetic retinopathy (DR) is a severe and prevalent eye disease and is the major cause of blindness and visual disability in the United States. Therefore, an objective test for the early diagnosis and evaluation for treatment of DR is needed to identify those individuals at greater risk for this vision problem.

Most studies have focused on proliferative and severe non-proliferative stages when fundus alterations are clearly visible by ophthalmoscopy or fluorescein angiography. However, the loss of macular function may be unrelated to the stage of retinopathy. In fact, the diagnostic problem of diabetic maculopathy consists of detecting very early morphological and functional deficits related to later visual outcomes. Consequently, improved detection of early changes is needed to offer new perspectives for the follow-up and treatment of DR. Moreover, an understanding of retinal structural changes in the early stages of DR may provide information about the mechanism of its progression.

Optical coherence tomography (OCT) is a relatively new, non-invasive imaging modality that can generate high resolution and high contrast cross-sectional images of thin layers of biological tissues. OCT images can either be used to qualitatively assess retinal features and pathologies or to objectively make quantitative measurements. This is especially important in the early stages of DR when the structural changes are not yet evident with slit-lamp biomicroscopy or angiography.

The goal of this doctorate thesis is to improve the quantitative assessment of intraretinal features with OCT by determining both structural and optical properties of the

retinal tissue and to develop a methodology to better differentiate diseased eyes from healthy eyes.

The specific aims of this thesis are as following:

Specific Aim #1: To develop an objective methodology encompassing novel optical-structural measures based on image processing of two-dimensional OCT data**.**

Specific Aim #2: To test the hypothesis that novel optical-structural measures extracted from OCT images can be used to discriminate between healthy and diseased eyes.

The main goal of this thesis is to improve the detection of early retinal pathology and the measurement of its progression based on changes in imaging-derived structural and optical parameters obtained with OCT.

CHAPTER 2. BACKGROUND AND SIGNIFICANCE

2.1 OPTICAL COHERENCE TOMOGRAPHY

2.1.1 BACKGROUND

Optical coherence tomography (OCT) is a non-invasive, high-resolution imaging modality widely used in biomedical optics and medicine. The first OCT system was established at the Massachusetts Institute of Technology laboratories in 1991 by Professor Fujimoto and colleagues.[1] OCT imaging is analogous to ultrasound B-mode imaging, except that it uses light instead of sound. Cross-sectional OCT images are generated by measuring the echo time delay and intensity of backscattered light from the internal structures in biological tissues. OCT can measure and demonstrate the internal structure of biological tissues in real time with a 1-15 μm resolution without the need to process and remove the tissue as in histology. With its micrometer resolution, non-invasive and cross-sectional imaging capabilities, OCT imaging is described as "optical biopsy" for biological tissues.

OCT has a unique advantage over other medical imaging technologies (see Figure 2.1). Standard clinical ultrasound can image deep structures, but has limited resolution. The typical resolution of clinical ultrasound imaging is 0.1-1 mm when using the 2-40 MHz sound wave frequency.[2, 3] Higher resolution imaging can be achieved by high frequency ultrasound, but the ultrasonic attenuation is also increased in the biological tissue to limit the penetration depth. In contrast, confocal microscopy has an extremely high resolution (approximately1 μm) that is determined by the diffraction limit of light; however, the optical scattering limits the imaging depth to a few hundred micrometers in most biological tissues. The axial resolution of OCT images is determined by the

bandwidth and the central wavelength of the light source. An OCT image represents a cross-sectional, micron scale picture of the optical reflectance properties of the tissue.[1] This image can either be used to qualitatively assess tissue features and pathologies or to objectively make quantitative measurements.

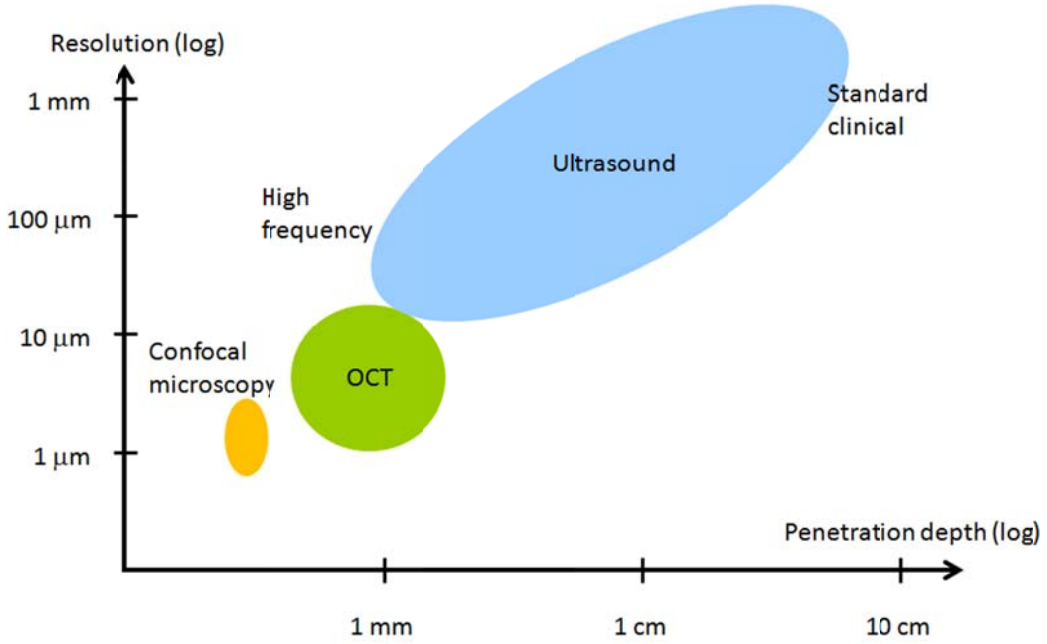

Figure 2.1 OCT vs. standard imaging (adapted from Drexler et al., 2008).

2.1.2 PRINCIPLES OF OPTICAL COHERENCE TOMOGRAPHY

OCT is an extension of optical coherence domain reflectometry to imaging in two or three dimensions (see Figure 2.2).[1,4] This imaging technique generates a cross-sectional image by recording axial reflectance profiles while the transverse position of the optical beam on the sample is scanned (see Figure 2.3). Thus, the longitudinal location of tissue structures are determined by measuring the time-of-flight delays of light backscattered from these structures (see Figure 2.2). The optical delays are measured by low coherence interferometry. Light reflected from deeper layers has a longer propagation delay than light reflected from more superficial layers.

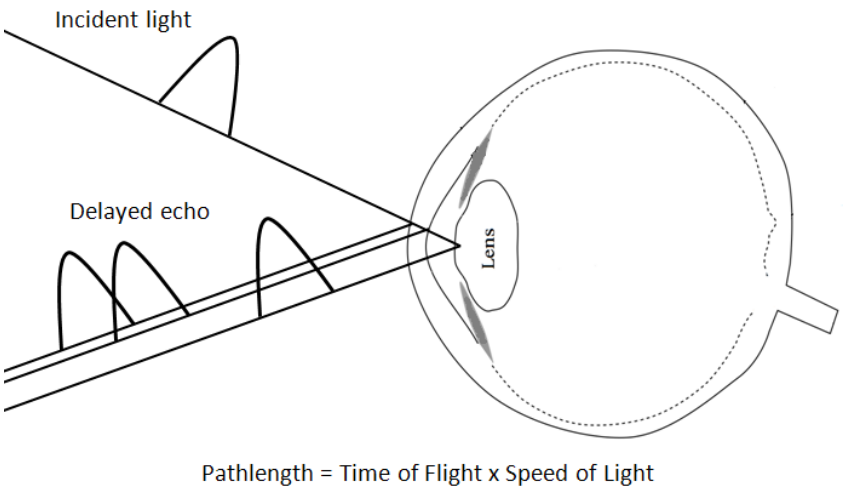

Figure 2.2 Schematic view of the principle of optical reflectometry.

The axial resolution of an OCT image depends on the coherence length, which is a fundamental property of the light source, whereas the transverse resolution for OCT imaging is determined by the focused spot size, as in microscopy. In time domain OCT (TDOCT), by rapidly varying the reference arm mirror and synchronously recording the magnitude of the resulting interference signal, a single axial profile, or A-scan, is obtained, which is a graph of the optical reflectivity versus distance in the eye (see Figure 2.3-A). A sequence of such A-scans is obtained by scanning the probe beam across the entire retina, which forms a B-scan tomogram (see Figure 2.3-B). As a result, a cross-sectional view of the structure, similar to a histologic section, is obtained. The method, and also its original display in grayscale pixels, is very similar to that of ultrasound, with the exception that light is used rather than sound, leading to the above-mentioned advantages of higher resolution resulting from a shorter wavelength.

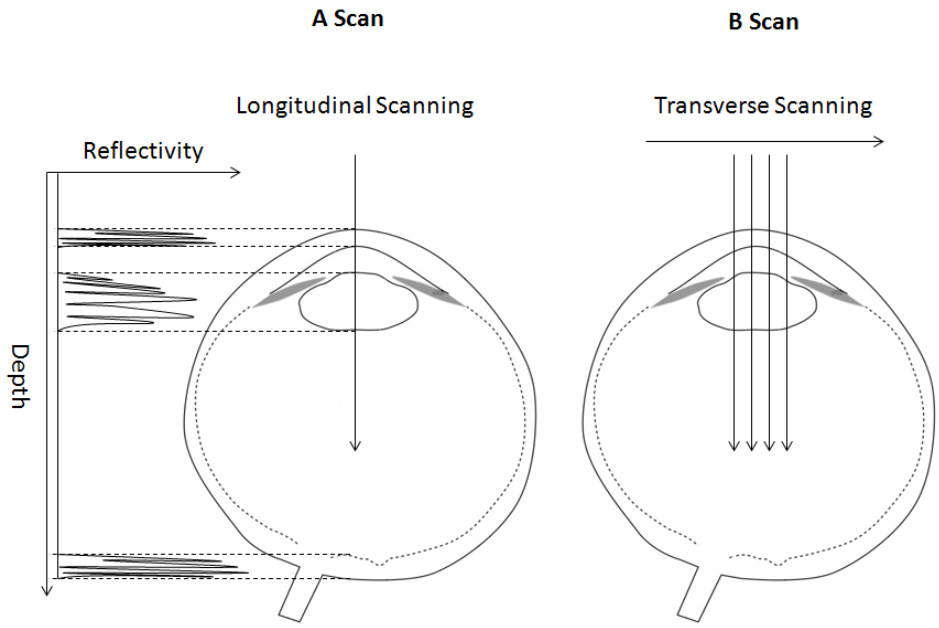

Figure 2.3 A) Longitudinal Scan. B) Scan Tomogram. Information on lateral position is provided by transverse scanning of the probe-beam.

OCT is based on the principle of low coherence interferometry, a powerful tool to "section" a transparent object. Low coherence means that the system employs a wide range of wavelengths; such as the low-coherence superluminescent diode (SLD) light sources used in the commercial stratus OCT devices (Carl Zeiss Inc.). The most straightforward and currently the most common interferometer for OCT is a simple Michelson interferometer (see Figure 2.4).[5] A low-coherence source illuminates the interferometer. The light is split by a 50/50 beam splitter into a sample and a reference path. Light retro-reflected from the reference and the sample is recombined at the beam splitter and half is collected by a photo detector in the detection arm of the interferometer. Half of the light is returned towards the source, where it is lost. In addition, the reference arm light is typically attenuated by orders of magnitude to improve the signal to noise ratio.

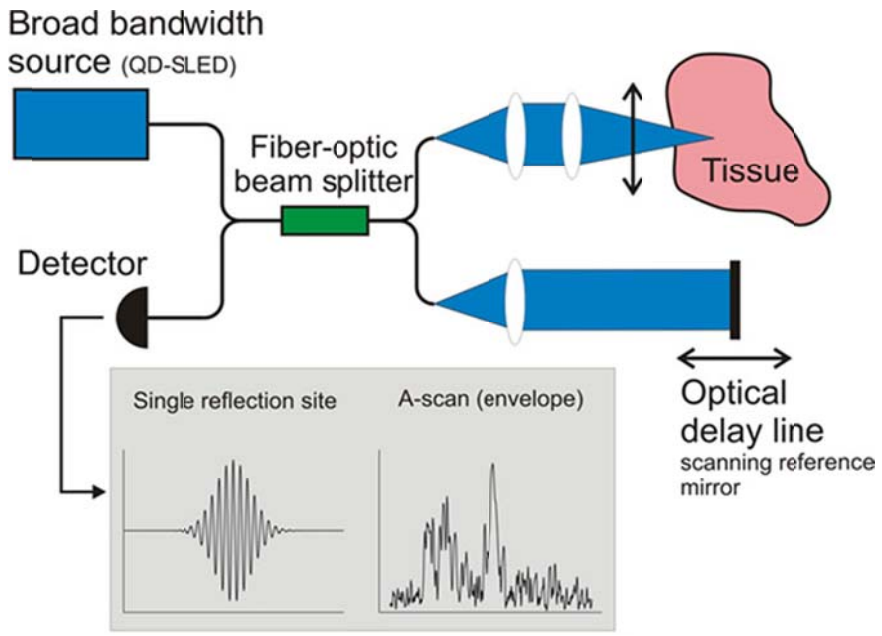

Figure 2.4 Schematic of time domain OCT system (adapted from Richard Hogg et al., 2006).

In TDOCT, the length of the reference arm in an interferometer is rapidly scanned over a distance corresponding to the imaging depth range. The mechanism of scanning largely limits the acquisition speed. In recent years, a new model of OCT based on Fourier domain interferometry has emerged, and it has been called "spectral or Fourier domain OCT" (SDOCT or FDOCT).[6-7] SDOCT can avoid scanning the reference and thus can reach a very high acquisition speed. In time domain OCT, the location of scatterers in the sample is observed by a generation of interferometric fringes at the detector as the reference reflector position is axially translated. In contrast, Fourier domain OCT calculates the entire A-scan from the spectrum of the reflected light from the given point of the sample by the use of Fourier analysis, hence the name. Two configurations have prevailed in Fourier domain systems. Spectral domain OCT uses a grating to spatially disperse the spectrum across an array-type detector. In swept source (SS) OCT, a narrow-band laser is swept across a broad spectrum, encoding the spectrum

as a function of time. SDOCT offers a significant sensitivity advantage over TDOCT.[8-11] Recently, in a direct comparison, an improvement of more than two orders of magnitude (21.7 dB) was experimentally demonstrated.[12]

OCT can be used for retinal imaging and anterior segment imaging. The instrumentation includes a video display for operator viewing of the pupil or fundus while obtaining the OCT images and a simultaneous computer display of the tomograms. Images are stored via computer for the diagnostic record.[13]

2.2 POTENTIAL CLINICAL APPLICATIONS OF OCT IN RETINAL DIAGNOSIS

2.2.1 OVERVIEW

Technological inventions and developments have created new possibilities and breakthroughs in medical diagnostics using OCT. The classic example is the major developments that have been taking place in the existing basic OCT system where components and subsystems have been changed and upgraded to give new functionalities. OCT is particularly suited for ophthalmic applications, which require micrometer resolution and millimeter penetration depth. The clinical potential of OCT technology in ophthalmology was originally recognized in the early 1990s. Particularly, OCT images of the human retina *ex vivo* were demonstrated in 1991 by Huang et al.[1] These OCT images were obtained using an OCT device with a 15 μm axial resolution at an 830 nm wavelength. The internal structure of the optic disc and vasculatures near the disc region was displayed using a log false color scale. Specifically, the retinal nerve fiber layer (RNFL) was visualized and the evident postmortem retinal detachment with subretinal fluid accumulation was observed. In 1993, the first *in vivo* human retinal images were

obtained by Fercher et al., which demonstrated the internal structures of a human retina using an OCT system with a 10 µm axial resolution at 800 nm wavelength. [14]

The development of OCT in ophthalmic applications proceeded rapidly due to its non-invasive nature, high axial resolution and cross-sectional imaging. OCT can aid in identifying, monitoring and quantitatively assessing various posterior segment conditions, including macular edema, age and non-age related macular degeneration, full and partial-thickness macular holes, epiretinal membranes, intraretinal exudates, idiopathic central serous chorioretinopathy, RPE detachment, detachment of the neurosensory retina and macular lesions associated with optic nerve head pits or glaucoma. Figure 2.5 shows exemplary images of two of the above-cited pathological cases obtained with a RTVue FD-OCT system (Optovue Inc., Freemonth, CA).

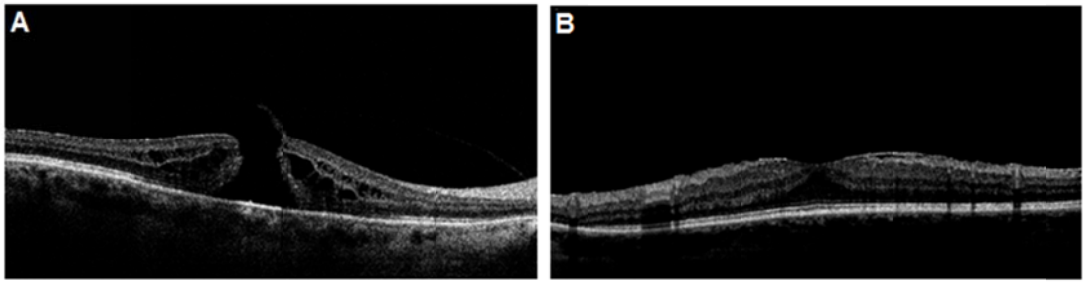

Figure 2.5 OCT images showing two OCT B-scans (6 mm length) from pathological retinas. A) Macular hole, B) Epiretinal membrane.

In fact, OCT can demonstrate the presence of edema when it is not seen through biomicroscopy or angiography. A very important feature of the OCT system is that it provides information on the retinal structures. For example, the location of a fluid accumulation in relation to the different retinal layers may be determined and the response to treatment without the need to perform invasive studies may be objectively monitored.[141] At the same time, it may be possible to explain why some patients respond to treatment while others do not. OCT has significant potential both as a diagnostic tool

and as a way to objectively monitor subtle retinal changes induced by therapeutic interventions. Thus, OCT may become a valuable tool in determining the minimum maintenance dose of a certain drug in the treatment of retinal diseases. Furthermore, it may reveal retinal changes that explain the recovery in some patients without angiographically demonstrable improvement and lack of recovery in others.

In the clinical routine, measurement of retinal thickness by the OCT software depends on the identification of the internal limiting membrane and the hyper-reflective band believed to correspond to the retinal pigment epithelium – choriocapillaris interface (or, more precisely, the photoreceptor inner-outer segment border in the case of third generation OCTs). The OCT software algorithm calculates the distance between these two boundaries across all of the sampled points and interpolates the retinal thickness in the unsampled areas between these lines. However, once the various layers can be identified and correlated with the histological structure of the retina, it may seem relevant to measure not only the entire thickness of the retina, but also the thickness of the various cellular layers. Moreover, measuring the reflectance of the various retinal layers on OCT images may also be of interest. Both *in vitro* and *in vivo* studies have shown that physiological processes of the retina lead to optical density changes that can be observed by a special M-mode OCT imaging, known as optophysiology.[15-17] Thus, it also seems rational that quantitative analysis of reflectance changes may provide clinically relevant information about retinal pathophysiology.

2.2.2 DIABETIC RETINOPATHY

OCT has also been used to investigate eye diseases related to diabetes. Diabetes remains a leading cause of blindness, increasing in incidence as the worldwide number of patients with diabetes grows. The global diabetes prevalence has been projected to

increase by 242% between 2000 and 2030.[18] Hence, it is of utmost importance to forcefully address the eye problems associated with diabetes.

There are two main types of diabetes: type 1 diabetes and type 2 diabetes. Type 1 diabetes, formerly called juvenile diabetes, is usually diagnosed in children, teenagers and young adults. In this form of diabetes, the pancreas no longer makes insulin because the body's immune system has attacked and destroyed the pancreatic cells specialized to make insulin. Type 2 diabetes, formerly called adult-onset diabetes, is the most common form of diabetes. People can develop type 2 diabetes at any age, even during childhood. This form of diabetes usually begins with insulin resistance, a condition in which muscle, liver and fat cells do not use insulin properly.[19]

Diabetes is associated with long-term complications that affect almost all of the body. The disease often leads to blindness, heart and blood vessel disease, stroke, kidney failure, amputation and nerve damage.[20] The most important retinal pathology caused by diabetes is diabetic retinopathy (DR), which is characterized by blood vessel damage. Retinopathy is common during the first five years' duration of type 1 diabetes; at least some form of retinopathy is present twenty years after the onset of type 2 diabetes.[21]

There are two stages of retinopathy: nonproliferative and proliferative.[22] Nonproliferative diabetic retinopathy develops first. Blood vessels in the eye become larger in certain spots (microaneurysms) and blood vessels may also become blocked. In addition, there may be small amounts of bleeding (retinal hemorrhages) and fluid may leak into the retina. Proliferative retinopathy is the more advanced and severe form of the disease. New blood vessels start to grow in the eye. These new vessels are fragile and can

bleed (hemorrhage). Small scars develop, both on the retina and in other parts of the eye (e.g., in the vitreous). The end result is vision loss, as well as other related problems.

Current studies of diabetic retinopathy using OCT have mainly focused on later disease stages such as proliferative and severe nonproliferative DR, when fundus alterations are clearly visible by standard imaging techniques such as ophthalmoscopy and fluorescein angiography. These standard imaging modalities do not allow cross-sectional images of the retinal tissue. However, as previously mentioned, OCT can provide high-resolution cross-sectional images of the retinal tissue structure in real time.

OCT has been recently employed to study DR at early stages.[23-27] Some of these studies have indicated either that OCT detects retinal thickening in patients with diabetes in the absence of clinically significant macular edema (CSME) or any other abnormality by slit-lamp biomicroscopy or that the morphological change in the retina may occur even in the early stages of DR. However, these studies did not evaluate whether they are discriminative enough to be useful as a clinical test and the related analysis was largely limited to retinal thickness.

Lately, it has been shown that diabetes leads to a thinning of the macula preceding the onset of severe diabetic retinopathy, which is most likely attributed to neurodegeneration of the retinal cellular structures. In this respect, early studies have shown that the thinning of the retina is due to a loss of the cellular structures in the inner retina, namely, the ganglion cells.[28] However, the loss of macular function may be unrelated to the stage of retinopathy. In fact, the diagnostic problem of diabetic maculopathy consists of detecting very early morphological and functional deficits related to later visual outcomes. Thus, improved detection of early changes is needed to

offer new perspectives for the follow-up and treatment of DR. Moreover, an understanding of retinal structural changes in early stages of DR may provide information about the mechanism of its progression.

All previous early DR studies focused on measuring retinal thickness using OCT. However, coherent light carries more information characterizing the structural and optical properties of tissue. Therefore, the changes in tissue optical properties may provide further information regarding cellular layers and early damage not only in DR but in other retinal diseases as well.

2.3 SIGNIFICANCE

Diabetic retinopathy is a sight-threatening microvascular complication leading to vision loss in millions of patients in industrialized and developing countries. The pathogenesis of DR is complex and still needs to be understood. The prevalence of DR increases with diabetes duration. Thus, an objective test for the early diagnosis and evaluation of DR treatment is needed to identify the individuals at great risk for vision-threatening problems. Our goal is to improve the early diagnosis and treatment of diabetic retinopathy with a quantitative imaging technology (i.e., OCT) that can capture detailed images of the various cellular layers of the retina affected by diabetes. OCT is a sophisticated, non-invasive technique based on optical interferometry that provides the best available spatial and temporal resolution to quantify and detect local abnormalities in the human retina. Although DR has been traditionally viewed as a disorder of retinal vasculature, retinal neurodegeneration may be the primary pathology that gives rise to microvascular changes. There is evidence of loss of function long before retinal clinical signs of DR appear.[142] However, studies describing the role of altered overall retinal

structure in the diabetic eye appear contradictory and some controversy remains. In addition, while only a few studies using OCT have demonstrated macular thinning along with selective thinning of intraretinal layers in patients with early DR, there have been no previous studies evaluating in detail the retinal optical properties in diabetic patients with and without retinopathy. In this work, we propose to measure optical parameters and thickness of the various cellular layers of the retina using OCT in diabetic patients with and without retinopathy. In addition, we plan to investigate the relationship between these quantities to develop quantitative measures to detect both early DR and DR progression. OCT data from a clinical cross-sectional study using diabetic patients with and without early retinopathy will be used. In addition, OCT data from MS patients will be used to extend and validate the analysis to a different process causing neuronal damage of the retina. The main objectives of this doctorate thesis are the following: 1) to develop an objective methodology encompassing novel optical-structural measures based on image processing of two-dimensional OCT data; and 2) to test the hypothesis that these optical-structural measures extracted from OCT images can be used to discriminate between healthy and pathological eyes. This thesis aims to improve the detection of early retinal pathology and the measurement of its progression based on changes in imaging-derived structural and optical parameters obtained with OCT. Our outcome will make it possible to provide clinicians with a powerful method for screening, follow-up and considering early prophylactic treatment of the retinal tissue.

CHAPTER 3. RESEARCH DESIGN AND METHODS

3.1 CLINICAL DATA COLLECTION FOR THE DIABETIC RETINOPATHY STUDY

The prospective data collection included participants recruited under a Juvenile Diabetes Research Foundation study. The Institutional Review Board of each institution (Bascom Palmer Eye Institute at University of Miami, FL, USA and Semmelweis University, Budapest, Hungary) involved in the study approved the study protocol. The research adhered to the tenets set forth in the Declaration of Helsinki. In this prospective study, enrollment was offered to all type 1 diabetic patients referred to a comprehensive ophthalmology clinic that has diabetic retinopathy (DR) up to ETDRS level 35 as well as to diabetic patients with no retinopathy. We note that we used OCT images from diabetic patients with no DR or with retinopathy up to ETDRS level 35, but in all cases without clinical signs of macular edema. Moreover, we did not use patients with proliferative disease, clinically significant macular edema (CSME) or with anatomic abnormalities that could distort macular architecture, such as vitreoretinal traction and epiretinal membranes. Informed consent was obtained from each subject. OCT examination was performed in healthy and diabetic eyes with and without retinopathy. The eligibility and exclusion criteria for the three groups analyzed are briefly described below.

Once the subject was enrolled in the study, one visit was required to perform a comprehensive eye examination including the following assessments: best-corrected visual acuity, intraocular pressure (using a Goldmann tonometer) and seven standard field stereoscopic fundus photos (SFPs). In addition, a hemoglobin A1c test was required at this visit for diabetic patients with no past glycemic control. No additional tests were required after this primary visit or during the time the study was completed. Inclusion

criteria for healthy controls included best-corrected visual acuity of 20/25 or better, no history of any current ocular or systematic disease and a normal-appearing macula on contact lens biomicroscopy. All eye examinations were performed by our collaborators in Hungary.

Six radial OCT scans were acquired for both eyes of each participant. While the study topic is relevant to children because children may suffer from diabetes, the development of vision-threatening retinopathy is rare in children prior to puberty.[29] Thus, the age range for the study population was 22-60 years. To independently grade and confirm patients' retinopathy levels, SFPs were obtained and classified by independent graders according to the criteria of the ETDRS protocol.[30] The graders classified SFPs without being aware of the OCT findings or clinical data. Specifically, the following parameters were used to indicate which diabetic patients without retinopathy and with retinopathy up to ETDRS level 35 in relation to the ETDRS disease severity levels:

- ETDRS level 10 indicated diabetic eyes without retinopathy (i.e., no abnormalities, DR absent).
- ETDRS level 20 indicated diabetic eyes showing only microaneurysms (very mild DR (non proliferative)).
- ETDRS level 35 indicated diabetic eyes with mild DR (more than just microaneurysms but less than severe DR (non proliferative)).

Baseline clinical and demographic information were also obtained as specified in the ETDRS design study (see Table 3.1). Specifically, eligibility was determined by the following criteria: 1) an initial history including the following elements: age at entry, gender, race, duration of diabetes, past glycemic control (hemoglobin A1c levels),

medications and medical history (e.g., onset of puberty, obesity, renal disease, systemic hypertension, serum lipid levels and pregnancy); and 2) comprehensive eye examination including best-corrected visual acuity, intraocular pressure (using Goldmann tonometer) and seven SFPs. Patients with any medical condition that might affect the visual fields other than type 1 diabetes or having undergone treatments with medications that might affect retinal thickness (e.g., chloroquine or niacin-containing anticholesterol agents) were excluded from the study. Moreover, patients who had recently undergone cataract surgery, patients with any history of vitrectomy and patients with currently unstable blood sugars or who had recently been placed on insulin pump therapy were also excluded from the study. In addition, a hemoglobin A1c level was required for diabetic patients with no past glycemic control. The hemoglobin A1c level information was used as a parameter for correlation to some findings, rather than an exclusion tool.

Table 3.1 Characteristics of the study participants.

Characteristic	Controls	DM	MDR
Number of Participants	41	29	29
Number of Eyes	74	38	43
Age (years, mean ± SD)	34 ± 12	35 ± 10	43 ± 17
Female, N (% total eyes)	52 (70%)	20 (53%)	21 (49%)
Race (% Caucasian)	100	100	91
Hemoglobin A1c level (%)	-	7.20 ± 0.90	8.51 ± 1.76
DM duration (years, mean ± SD)	-	13 ± 5	22 ± 10
IOP (mmHg, mean ± SD)	-	15.74 ± 1.77	15.09 ± 1.56
BCVA	1.00 ± 0.00	1.00 ± 0.00	0.97 ± 0.06
Total macular thickness	324.36 ± 10.27	316.72 ± 21.56	297.40 ± 21.79

Abbreviations: SD = standard deviation; NA = not applicable; DM: diabetic eyes without retinopathy; MDR: diabetic eye with mild diabetic retinopathy.

3.2 OCT SYSTEM AND MEASUREMENTS

The OCT system (Stratus OCT, Carl Zeiss Meditec, Dublin, California) used in this study employs a broadband light source, delivering an output power of 1 mW at the central wavelength of 820 nm with a bandwidth of 25 nm. It has a scanning speed of 400 A-scans per second with a resolution of 10 µm in tissue that determines the imaging axial resolution of the system. A cross-sectional image is achieved by the axial reflectance while the sample is scanned laterally. All Stratus OCT' study cases were obtained using the macular thickness map protocol. This protocol consists of six radial scan lines centered on the fovea, each having a 6 mm transverse length. To obtain the best image quality, focusing and optimization settings were controlled and scans were accepted only if the signal strength was above 6 (preferably 9-10).[31] Scans with foveal decentration (i.e., with center point thickness SD>10%) were repeated.

3.3 OCT IMAGE PROCESSING

OCT signals were collected and exported from the OCT device in the form of 16-bit grayscale images. The intensity values contained in grayscale images not only represented the amplitude of OCT signals but also contained the information about the topographic features and optical properties of the retinal tissue. The direct measurement of OCT is reflectance (intensity values), while structural parameters (i.e., thickness measurement) and some optical features (i.e., scattering coefficients) could not be obtained directly from OCT signals. Various methodologies were implemented to extract characteristics from OCT grayscale images. Moreover, to achieve more accurate structural information and optical properties, it was necessary to employ some image processing techniques to process OCT raw images initially.

All the image processing techniques that were employed in this project, such as techniques including removal of speckle noise, segmentation of intraretinal layers, partition of the macular region in sectors and detection of blood vessel shadows, played an important role in the OCT image processing and are therefore described in this section.

3.3.1 REMOVAL OF SPECKLE NOISE

Noise is a major limitation for all types of imaging modalities. Because of this, multiple imaging processing techniques have been developed to filter noise from images. Specifically, OCT images suffer from a particular type of noise called "speckle". The speckle is a common result of the limited spatial-frequency bandwidth of the interference signals in OCT.[32] Because OCT imaging systems use coherent detection to generate images, speckle noise significantly degrades the OCT image contrast by creating a grainy appearance and by obscuring small, low intensity features; therefore, this makes it more difficult for the observer to discriminate fine detail of the images in diagnostic examinations.

Various filtering approaches, such as median filtering, wavelet-based filtering, anisotropic diffusion filtering and nonlinear anisotropic filtering, were used to remove speckle noise from OCT images. Though most of these filters could effectively reduce speckle noise, some of them might blur the structural boundaries in OCT images. Therefore, a method was developed for the enhancement of OCT images as well as speckle noise removal from these OCT images. Specifically, the nonlinear complex diffusion filter was used to remove the speckle noise. This method was first introduced for speckle suppression on OCT images by Cabrera Fernandez in 2007.[32] The equation for the nonlinear complex diffusion approach used to remove noise can be described as follows:[32]

$$\frac{\partial}{\partial t} I = \nabla \cdot \left(d\left(Im(I)\right) \nabla I \right) \tag{3.1}$$

where I represents a matrix in which each element corresponds to the intensity of a pixel in an OCT image, ∇ is the gradient operator, $\nabla \cdot$ is the divergence operator and d is the diffusion conductance or the diffusivity of the equation. $Im(I)$ is the imaginary value and the diffusivity is defined as follows:

$$d\left(Im(I)\right) = \frac{\exp(i\theta)}{1 + \left(\frac{Im(I)}{k\theta}\right)^2} \tag{3.2}$$

where k is a threshold parameter and $\theta \in (-\pi/2, +\pi/2)$ is the phase angle.

Figure 3.1 demonstrates a sample OCT image before and after the speckle noise removal using the nonlinear complex diffusion filter. Obviously, the utilization of the nonlinear complex diffusion filter could not only effectively remove the speckle noise from OCT images but also enhance the sharp regions (e.g., edges).

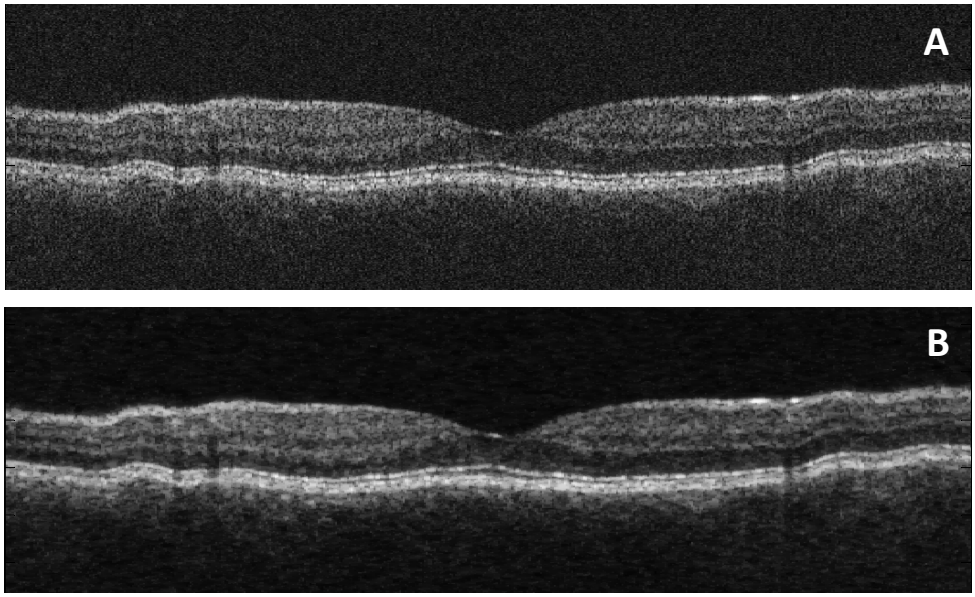

Figure 3.1 Denoising results for a sample OCT scan. (A) Original OCT image. (B) Image denoised by using the nonlinear complex diffusion filter.

3.3.2 IMAGE SEGMENTATION

To use OCT to quantitatively evaluate structural and optical property changes in the retina caused by a number of severe eye diseases, a segmentation-based calculation of the intraretinal layers' thickness is required. Segmentation is an important component of OCT image processing, in which different intraretinal layers are identified and separated from each other. There are two main drawbacks to automated segmentation approaches. The first is that diseased retinal structures can vary substantially among patients. The structural disruption observed in these patients often produces artifacts in the segmentation results. The other main drawback originates from inaccuracies in the data acquisition systems due to the noisy speckle field superimposed on imaged structures. Consequently, the intervention of a human operator is often needed to manually correct the segmentation result.

The commercial Stratus OCT (Carl Zeiss Meditec, Dublin, California) software has a measurement capability limited to thickness calculation of the macula and retinal nerve fiber layer (RNFL). Thus, quantitative information on other intraretinal layers is not provided by this instrument. This limitation in the Stratus OCT system has stimulated interest in developing segmentation algorithms to better reveal the local changes in the retinal structure.[33-48] In addition, the quantification provided by this system is often imprecise because of erroneous detection of the inner and outer borders of the retina.[49-53] As a result, potentially useful quantitative information is not extracted by the current commercial Stratus OCT. In an effort to provide additional retinal quantifications along with accurate automatic/semiautomatic detection, various computer-aided grading procedures have been introduced.[33,35-48,54] Specifically, we used a computer-aided grading methodology for OCT retinal image analysis (OCTRIMA) that is an interactive, user-

friendly stand-alone application for analyzing Stratus OCT retinal images. The OCTRIMA methodology integrates a denoising and edge enhancement technique along with a segmentation algorithm previously developed by Cabrera et al.[33] The denoising and edge enhancement techniques are part of a novel preprocessing step that facilitates better automatic segmentation results (see Figure 3.2). In addition, the semi-automatic segmentation correction tool of OCTRIMA minimizes segmentation errors generated during the OCTRIMA's automatic segmentation process, significantly reducing the need for manual error corrections. It also gives quantitative information about intraretinal structures and facilitates the analysis of other retinal features that may be of diagnostic and prognostic value, such as morphology and reflectivity.[43, 49, 51]

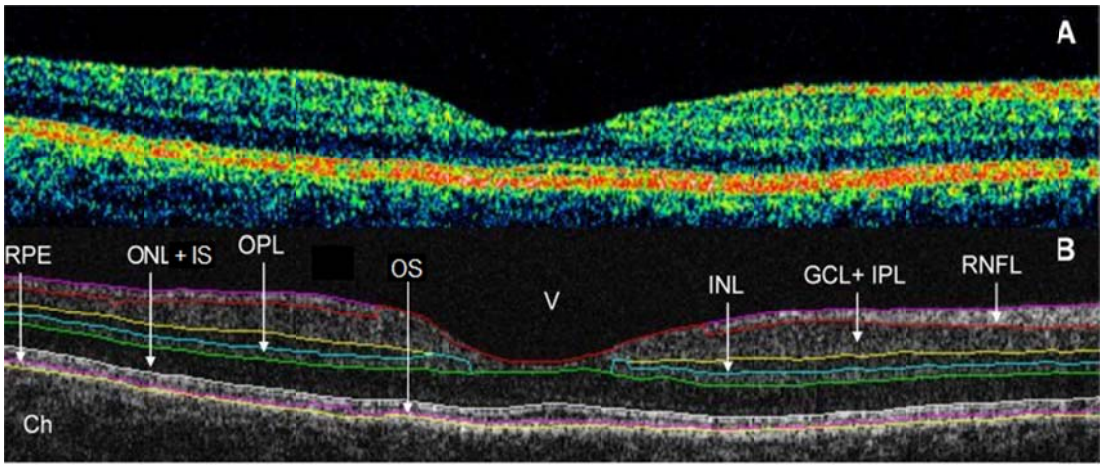

Figure 3.2 Macular image segmentation using OCTRIMA. (A) The image of a healthy macula scanned by Stratus OCT. (B) The same OCT scan processed with OCTRIMA. Abbreviations: Ch, choroid; GCL+IPL, ganglion cell layer and inner plexiform layer complex; INL, inner nuclear layer; ONL+IS, combined outer nuclear layer and inner segment of photoreceptors; OS, outer segment of photoreceptors; OPL, outer plexiform layer; RNFL, retinal nerve fiber layer; RPE, retinal pigment epithelial layer; V, vitreous. Note that OCTRIMA measures the thickness of the total retina between the inner limiting membrane and the inner boundary of the photoreceptor outer segment/RPE junction. The thickness of the combined ONL+IS structure is measured between the outer boundary of OPL and the inner boundary of the photoreceptor outer segment/RPE junction.

3.3.3 PARTITION OF THE MACULAR REGION IN SECTORS

The segmentation of intraretinal layers provides a useful way to investigate and analyze the structural information and optical properties inside the retina. For example, the mean thickness of each intraretinal layer can be obtained by averaging thickness measurements extracted from each A-scan across all B-scans. By analyzing and comparing the averaged thickness of intraretinal layers between healthy and diseased eyes with a particular condition, the difference in the thickness change can be determined and used as a diagnostic discriminator. However, the presence of local abnormalities in the retinal structure of diseased eyes may not be revealed by averaging the retinal thickness of each intraretinal layer across all B-scans. In light of this knowledge, an analysis based only on global changes seems to be insufficient to precisely describe early pathological changes in the retinal structure. Consequently, the development of classifiers to differentiate diseased eyes from healthy eyes must take into account the local changes of the retinal structure. To locally quantify these changes, the 6 mm OCT B-scans were divided in sectors.

In our method, the macular region is divided into separate regions (see Figure 3.3). The central disc is the foveola area with a diameter of 0.35 mm. The remaining rings are the fovea, parafoveal and perifoveal areas with a diameter of 1.85, 2.85 and 5.85 mm, respectively. Because an area with a diameter of 1 mm, which was defined in an early study on the treatment of diabetic retinopathy, is too large for the thickness of the foveola region, which is only approximately 0.35 mm in diameter, the custom-built map allows collection of more precise information near the foveola region compared to the ETDRS thickness map. In addition, no interpolation is used in this method.

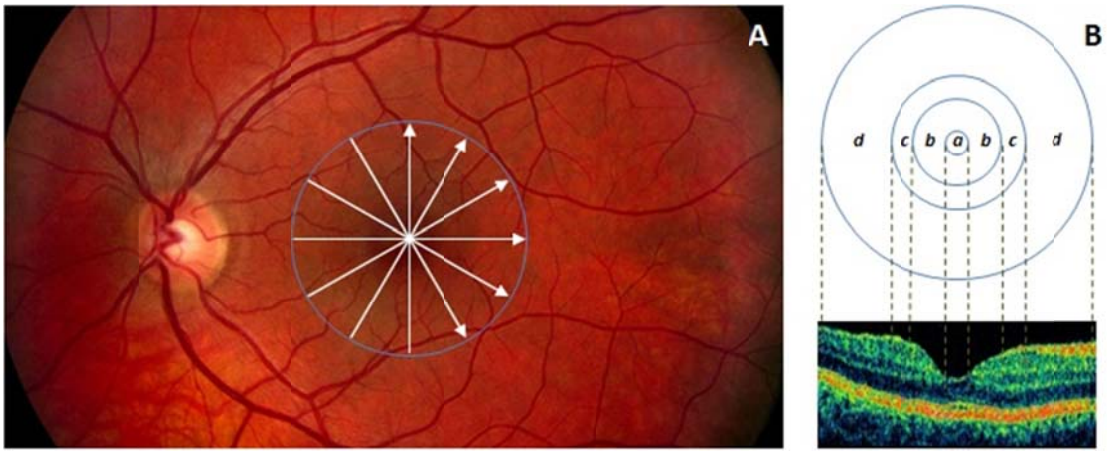

Figure 3.3 Custom-built method showing macular sectors. A) Fundus image of a healthy eye showing the Stratus OCT's radial lines protocol. B) Regions shown are: foveola (a) with a diameter of 0.35 mm, foveal region (b) with a diameter of 1.85 mm, parafoveal region (c) with a diameter of 2.85 mm and perifoveal (d) region with a diameter of 5.85 mm.

3.3.4 REMOVAL OF BLOOD VESSEL SHADOWS

Blood vessels are widely distributed in the healthy and diseased eyes and result in a rapid attenuation of incident light as it propagates through the blood vessels.[55] Blood vessels are therefore most readily identified by their shadowing effect on the reflection. In OCT images, the shadowing effect is demonstrated as the different sizes' gap where the intensity values are much lower than that of the surrounding area. Usually, blood vessels' shadows have been used to align OCT images.[56] However, the existence of blood vessel shadows in OCT images could lower the reliability of the features because the inaccurate characteristic values might be obtained from areas that contained them. To improve the precision of structural and optical features calculations, it is necessary to develop an algorithm to detect blood vessel shadows in OCT images.

Among various algorithms, the image gradient is a fundamental methodology to detect edges such as the boundaries of blood vessel shadows.[57] With a proper threshold, locations of blood vessel shadows can be found in OCT images. Although the gradient

vector field used in various algorithms could provide a good capture range, it sometimes leads to boundary delocalization.[58]

As the incident light perpendicularly penetrates into the retinal tissue, the direction of the blood vessel shadows' boundaries are vertical in OCT images. Therefore, a blood vessel shadowgram technique based on the reflectivity distribution was employed to detect the lateral coordinates of the blood vessel shadows.[53] The algorithm flowchart is shown in Figure 3.5 below.

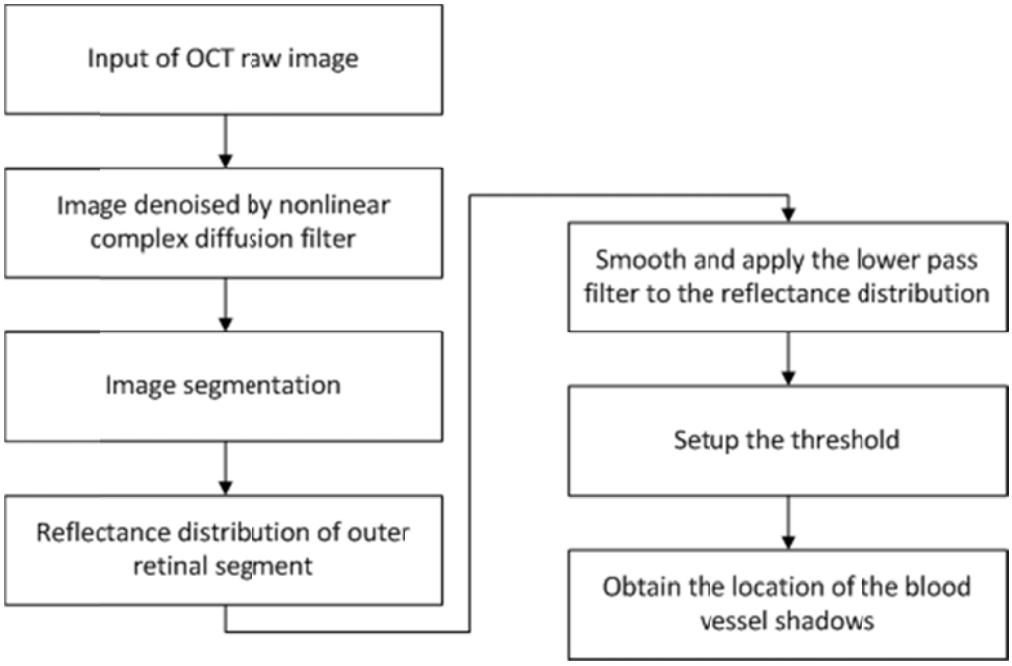

Figure 3.4 Flowchart of detection of blood vessel shadows in OCT images.

Figure 3.5 shows the results of the blood vessel shadowgram technique used to locate the blood vessel shadows in an OCT sample image. In this image, the lateral pixel intensity exhibits regions of low magnitude, which correspond to the presence of blood vessel shadows.

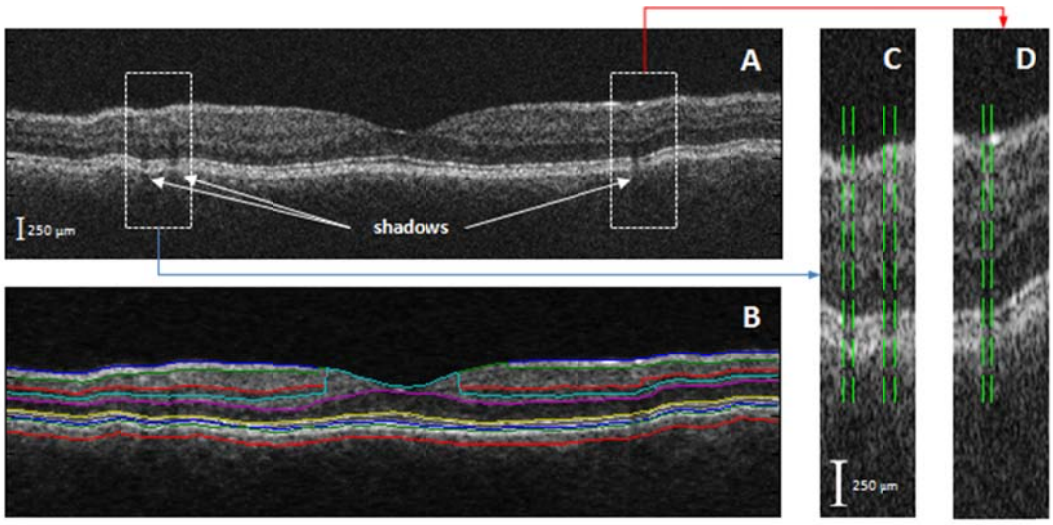

Figure 3.5 Detection of blood vessel shadows. A) OCT raw image. B) OCT image showing segmentation results after removal of speckle noise. C and D) Zoomed-in Views of the shadowed regions are showed with detected boundaries of blood vessel shadows.

3.4 CHARACTERIZING STRUCTURAL CHANGES OF THE RETINAL TISSUE

3.4.1 THICKNESS MEASUREMENTS

Measurements of the thickness of the intraretinal layers play a role in the diagnosis of retinal diseases. The thickness of intraretinal layers and their changes calculated from OCT images is a standard OCT method used to diagnose eye diseases.[143]

Traditionally, thickness measurements are calculated using the standard method provided by Stratus OCT. Specifically, this device measures mean retinal thicknesses in the nine macular ETDRS (Early Treatment Diabetic Retinopathy Study) regions.[59] Bilinear interpolation is performed to estimate the retinal thickness in the wedges between each radial OCT scan.

To more precisely describe the local changes of the retinal structure, the thickness measurements of intraretinal layers were calculated per specific macular region (see

Figure 3.3). Accordingly, the mean intraretinal layer's thickness and the macular thickness per macular region were extracted from OCT images.

3.4.2 TEXTURE ANALYSIS

Though thickness differences may characterize regions with signs of retinal disease from normal regions, differences in texture descriptors of normal and abnormal retinal tissue may also provide additional information about disease development in pathological eyes.

Texture is a property that represents the surface and structure of an image. Generally speaking, texture can be defined as a regular repetition of an element or pattern on a surface.[60] Textures are complex visual patterns composed of regions with sub-patterns with the characteristics of size, shape, shades, brightness and spatial arrangement. Moreover, a textured area in an image can be characterized by a non-uniform spatial distribution of grey levels or intensities. The variation in intensity characterizes a texture and reflects the physical variation in the underlying scene.

Texture analysis techniques can be classified into three groups: statistical technologies, spectral technologies and structural technologies.[61] Statistical texture analysis technologies derive a set of statistics from the distribution of the local features that were computed at each point in the image through the first-, second- and higher-order techniques.[61,62] Spectral texture analysis technologies detect the texture periodicities based on the autocorrelation function of a region or power spectrum, whereas structural texture analysis technologies use certain placement rules to describe the texture based on pattern primitives.[63]

The appropriateness of texture to classify tissues in OCT images has been shown in previous studies.[61] By analyzing the spatial arrangement of color or intensities in an

image or selected region of interest (ROI), the image's irregularities can be measured. Consequently, texture features, such as energy, entropy, correlation, contrast, local homogeneity and fractal dimension, could be analyzed for the macula and each intraretinal layer in specific macular sectors.

Accordingly, texture parameters such as, energy, entropy, correlation and contrast were extracted by using second-order statistical texture analysis.[64] The spatial gray level co-occurrence matrices (SGLDMs) suggested by Haralick have been widely used to estimate the texture features related to second-order statistical texture analysis.[65] SGLDMs were obtained for ROIs based on the estimation of the second-order joint conditional probability density function $s_\theta(i,j|d)$. Each $s_\theta(i,j|d)$ denotes the probability of a pixel with a grey-level value "i" being a "d" pixel away from another pixel of grey-level value "j" in the "θ" direction. Then, four texture parameters including energy, entropy, correlation and contrast were calculated from SGLDMs. Energy denotes the sum of the sum of the square of each value in a local neighborhood:

$$Energy = \sum_{i=0}^{L-1}\sum_{j=0}^{L-1}[s_\theta(i,j|d)]^2 \tag{3.3}$$

where L is the number of gray levels in the image.

Entropy denotes a measure of information content by measuring the randomness of the intensity distribution:

$$Entropy = \sum_{i=0}^{L-1}\sum_{j=0}^{L-1} s_\theta(i,j|d)log[s_\theta(i,j|d)] \tag{3.4}$$

Contrast denotes a measure of the local variations present in an image:

$$Contrast = \sum_{i=0}^{L-1}\sum_{j=0}^{L-1}(i-j)^2 s_\theta(i,j|d) \tag{3.5}$$

Correlation denotes a measure of image linearity. The value of correlation will be high if an image contains a considerable amount of linear structure:

$$Correlation = \frac{\sum_{i=0}^{L-1}\sum_{j=0}^{L-1}(i-\mu_x)(j-\mu_y)s_\theta(i,j|d)}{\sigma_x\sigma_y} \tag{3.6}$$

where μ_x, μ_y and σ_x, σ_y denote the mean and standard deviations of the row and column sums of the gray level dependence matrices $s_\theta(i,j|d)$, respectively.

$$\mu_x = \sum_{i=0}^{L-1} i \sum_{j=0}^{L-1} s_\theta(i,j|d) \tag{3.7}$$

$$\mu_y = \sum_{i=0}^{L-1} j \sum_{j=0}^{L-1} s_\theta(i,j|d) \tag{3.8}$$

$$\sigma_x = \sum_{i=0}^{L-1}(i-\mu_x)^2 \sum_{j=0}^{L-1} s_\theta(i,j|d) \tag{3.9}$$

$$\sigma_y = \sum_{i=0}^{L-1}(j-\mu_y)^2 \sum_{j=0}^{L-1} s_\theta(i,j|d) \tag{3.10}$$

3.4.3 FRACTAL ANALYSIS

The fractal dimension was first used to describe the self-similar pattern in the coastline of Britain by Mandelbrot in 1967. Mandelbrot found that the measured length of coastline changed as a different size of measuring ruler was used. The fractal dimension was introduced and interpolated as a scale that was applied to the ruler used to measure the length of coastline.

The scale can be regarded as a characterization that is used to describe the roughness of a surface such as the coastline. Due to this characterization, the fractal

dimension was commonly used for the evaluation of the complexity of an object. Higher values indicate rougher surfaces. Thus, fractal dimension as a texture parameter was mainly used in shape analysis and later for the comparison between objects. By measuring and comparing values of the fractal dimension, structural changes and shape in particular, could be differentiated.

In biology and medicine, the shapes of structures such as molecules, cells, tissues and organs play an important role in the diagnosis of diseased tissue. Because the fractal dimension can be capable of revealing differences and irregularities of these structures, quantitative measurements of the fractal dimension could be an effective approach to discriminate diseased tissue from healthy tissue. For example, fractal analysis has been successfully utilized in studies of blood cells, the human cerebellum, tumors in the brain and so on. Moreover, the utilization of various types of medical imaging techniques promotes the application of fractal analysis in biology and medicine. The abnormal tissue could be detected by performing fractal analysis for particular biological structures in medical images. Thus, fractal analysis with medical imaging techniques could provide an effective diagnostic methodology to detect diseases.

In Euclidean space, structures consist of basic Euclidean geometries including lines, planes and cubes. A straight line has exactly one dimension, a plane has exactly two dimensions and a cube has exactly three dimensions. These basic shapes in integer dimensions were called "topological dimensions". However, many complex objects are described well with the fractal dimension as a non-integer value that is between two integers. For example, a fractal curve has dimensions between a straight line and a plane (between one and two) and a fractal surface has dimensions between a plane and a cube

(between two and three). To determine the fractal dimension for complex objects, several definitions of fractal dimension have been used. One simple and understandable definition of the fractal dimension is the Hausdorff dimension, which is defined as follows:

$$FD = \lim_{r \to 0} \frac{log N_r}{\log\left(\frac{1}{r}\right)} \tag{3.11}$$

where N_r is the number of sets of cells (i.e., a ruler used to measure the coastline) and $1/r$ is the magnification factor that was used to reduce the cell in each spatial direction.

A typical example of a geometric object with a non-integer dimension is the Koch curve (see Figure 3.6). The straight line A, called the initiator, has a length of 1. The middle third of the line A was replaced with two lines that each have the same length (1/3) as the remaining lines on each side. Thus, the length of the line B has a length 4/3. This form specifies a rule that is used to generate other new forms. Thus, the curve A was used as the initiator and the curve B was used as generator for constructing the Koch Curve. Each line was replaced with four lines, each 1/3 the length of the original. Therefore, the lengths of the lines C, D and E are 16/9, 64/27 and 256/81, respectively. As indicated in Figure 3.6, the total length of the curve increases with each step, which leads to an infinite length. By applying the equation (3.11), the relationship between $logN_r$ and $\log(1/r)$ for the Koch curve, the fractal dimension *FD* could be calculated as: $\ln 4/\ln 3 = 1.26$.

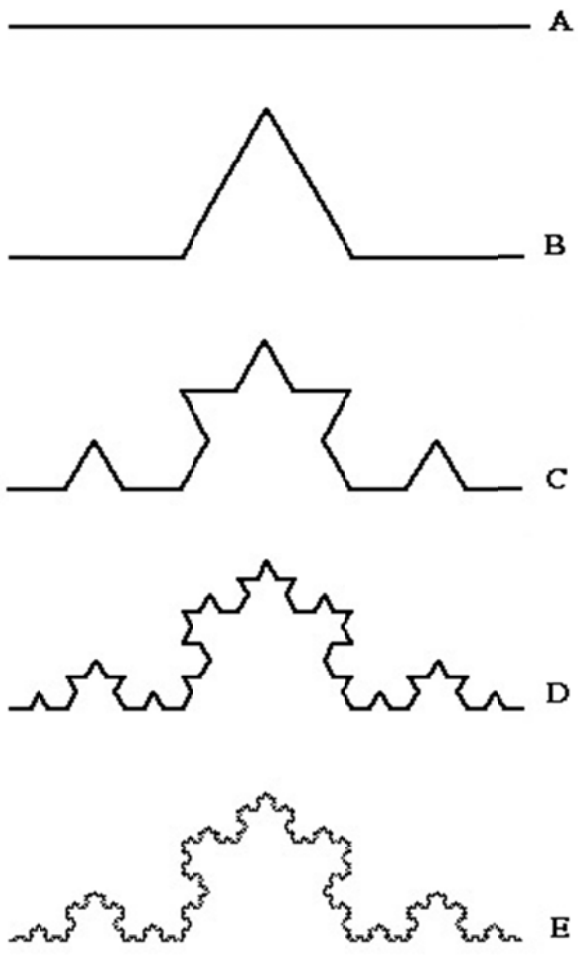

Figure 3.6 Koch curve. The initiator (A) and generator (B) is used for constructing the Koch curve, the curves C, D and E are the levels 2, 3 and 4 in the construction of the Koch curve, respectively.

Moreover, the measurement of the fractal dimension of the coastline could be treated as the Koch curve, which naturally leads to the introduction of the box-counting method. In the measurement of the coastline, the number of scaled rulers is also counted as and is the size of the cell (i.e., ruler). The same equation (3.11) is used in the calculation of the fractal dimension. Note that the typical cell is a box-shaped cell (a square) for two-dimensional objects and that the typical cell is a cube for three-dimensional objects.

The box-counting method is considered the most popular methodology to measure the fractal dimension in various applications due to its simplicity and automatic computability. However, the box-counting method was pointed to overcount or undercount the number of boxes (cells), which then led to an inaccurate calculation of the fractal dimension. Therefore, a more accurate and robust methodology, the power spectrum method, is used for the calculation of the fractal dimension.

Based on the mathematical theory, the average power spectrum of an image obeys power law scaling. The fractal dimension is calculated from the power law detected in the graph of the power spectrum as a function of the frequency in the Fourier transform of the image. When the graph is plotted in a log-log scale, the curve is approximately similar to a straight line and the dimension is provided by the slope of the line.

The fast Fourier transform (FFT) was applied to the profiles to obtain the power spectrum.

$$P(\omega) \sim \omega^{-\beta} \tag{3.12}$$

where $P(\omega)$ is the power spectrum with the frequency ω. β is the spectral exponent of the reflectivity profile.

The equation (3.12) can be converted into

$$ln\big(P(\omega)\big) \sim -\beta\, ln(\omega) \tag{3.13}$$

By investigating the relationship between the power spectrum and the frequency, fractal dimension is linked to the power-law exponent β by the following relationship: [67]

$$FD = \frac{5-\beta}{2} \tag{3.14}$$

Specifically, the fractal dimension is evaluated from the slope β of a least-square regression line fit to the data points in log-log plot of power spectrum.

In this study, the fractal dimension was used as an indicator of retinal structure disorder. As mentioned, the power spectrum method is more robust than the box counting method; we used the power spectrum method to calculate the fractal dimension in this project.[67] The power spectrum method has the unique ability to characterize scale-invariant and space-invariant physical phenomena, which are relevant to the concepts of self-similarity and self-affinity and form the essence of fractal geometry.

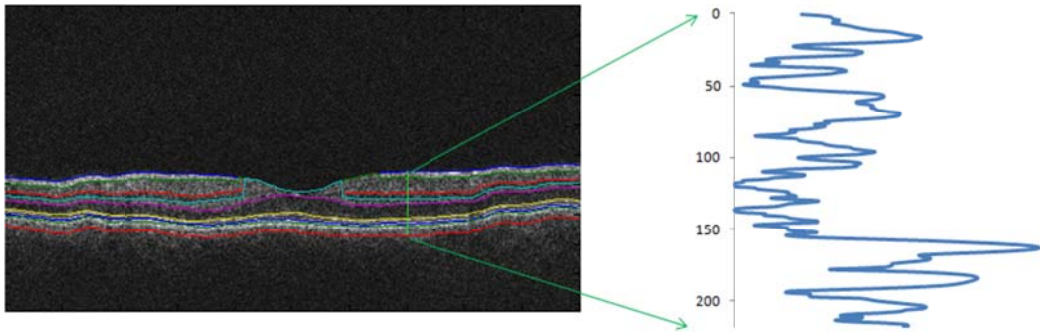

Figure 3.7 Reflectivity profile used to calculate the fractal dimension.

As indicated in Figure 3.7, the fractal dimension was calculated for the reflectivity profile within each intraretinal layer for each A-scan. The mean value of the fractal dimension was calculated by averaging the fractal dimension measurements across all A-scans in each macular region of each intraretinal layer.

3.5 CHARACTERIZING OPTICAL PROPERTY CHANGES OF THE RETINAL TISSUE

The most common parameter investigated during the OCT examination is the retinal thickness. However, the direct measurement of OCT is reflectance, while standard measurements such as thickness and volume are obtained later from reflectance information. The human retina is an optically transparent tissue that only reflects approximately 1% of the incident light.[68] Retinal tissue is characterized by many small random fluctuations in refractive index caused by the tissue ultrastructure. As a

consequence, light incident on tissue is deflected or scattered off this structure. Therefore, differences in optical properties of normal and abnormal retinal tissue may also provide additional information about disease development in diseased eyes. For example, it has been shown that DR not only causes thinning of the inner retinal layers but also reduces the amplitude of the back-reflected signal from these layers.[69] Consequently, diagnostic predictors based on reflectance changes are also of interest. Therefore, OCT could also be used for quantitative analysis of tissue optical properties, as the OCT signal depends on the total attenuation and backscattering coefficients.[70-72] This particular analysis may improve the diagnostic potential of OCT. In this section, optical features of the retinal tissue such as mean reflectance, total reflectance and layer index are introduced.

Region of Interest (ROI)

Because the selection of areas could affect the final results, specific regions of interest (ROIs) were defined within each intraretinal layer or macular sector. As was mentioned before, the blood vessel shadows have to be carefully removed from the ROIs to improve the precision of the optical properties' calculations. Each selected ROI was discretized before the extraction of structural and optical features. In addition, the size of the ROI was defined by the particular dimension (e.g., thickness range, area) of each intraretinal layer and macular sector.

In the Figure 3.8, each grid represents a pixel and the $I(j,k)$ is the intensity value in the column k of the row j. Additionally, Δx and Δy are the lateral and axial resolutions determined by the OCT system. The former is a function of the optical properties and the latter is related to the coherence length of the light source. The coherence length of a source and hence the axial resolution of OCT, is defined as follows:

(3.15)

where is the central wavelength of source and is the wavelength bandwidth, defined as the full width at half maximum (FWHM) of its wavelength spectrum..

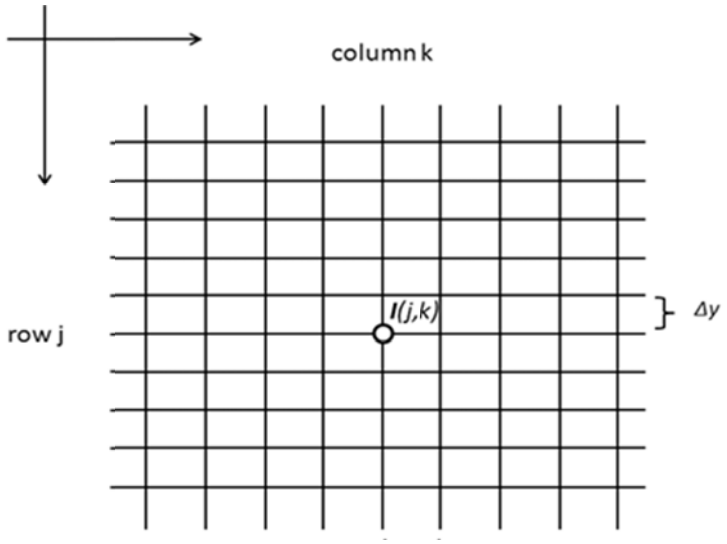

Figure 3.8 Discretization of region of interest.

The apparent reflectivity measured by OCT is a combination of the actual reflectivity and the scattering and absorption characteristics of the overlying media. Accordingly, the apparent reflectivity measured by OCT may be affected by abnormalities in the retinal tissue.

Mean reflectance was calculated by averaging the reflectivity profile, called A-scan, in the region of interest (ROI):

(3.16)

where denotes the reflectivity values of the element in the row of column of the selected ROI. is the total number of elements in the longitudinal direction of column within the selected ROI.

Since intensities recorded in OCT image could be thought as the amplitude of the signal.[68] Mean reflectance is converted into decibel (dB) units:

$$MR_{k,dB} = 20\,log_{10}(MR_k) = 20\,log_{10}\left(\frac{1}{N_k}\sum_{j=1}^{N_k} I_{j,k}\right) \quad (3.17)$$

Total reflectance TR_k was calculated by summing reflectivity values of the elements in the column k of the selected ROI:

$$TR_k = MR_k \times \frac{H_k}{\Delta y} \quad (3.18)$$

where $I_{j,k}$ denotes the reflectivity values of the element in the row j of column k of the selected ROI and N_k is the total number of elements in the longitudinal direction of column k within the selected ROI.

Because intensities recorded in an OCT image could be thought as the amplitude of the signal[68], mean reflectance is converted into decibel (dB) units:

$$TR_{k,dB} = 20\,log_{10}(TR_k) = 20\,log_{10}\left(\frac{1}{N_k}\sum_{j=1}^{N_k} I_{j,k} \times \frac{H_k}{\Delta y}\right) \quad (3.19)$$

Layer index LI_k was defined as follows:[71]

$$LI_k = MR_k \times \frac{H_k}{I_{sa}} = \frac{1}{N_k}\sum_{j=1}^{N_k} I_{j,k} \times \frac{H_k}{I_{sa}} \quad (3.20)$$

where MR_k is the mean reflectance in the column k of the selected ROI, H_k is the local thickness of the ROI in the column of k, I_{sa} is a reflectivity value and *99%* of all recorded reflectivity values in a given retinal OCT image are less than this specific value.[71]

3.6 LIGHT SCATTERING MODELS FOR THE OCT SIGNAL

3.6.1 OVERVIEW

The human retina, like other biological tissues, is a turbid medium composed of different types of cells and organelles. Each type of cell or organelle has a unique light absorption and scattering properties due to their particular shape and composition. Therefore, the optical features of the retinal tissue are more difficult to obtain because of the high non-homogeneity within the retinal structure.

In this section, typical scattering models, including Mie scattering theory and radiative transport theory with related solutions, are introduced. The single- and multiple-scattering regimes used to extract the scattering coefficients from the OCT signal are also introduced.

3.6.1.1 MIE SCATTERING THEORY

Mie scattering theory is a theoretical solution for the scattering of a plane electromagnetic (EM) wave by a single, homogenous, isotropic sphere.[74, 75] As the EM wave interacts with the discrete particle, the electron orbits within the particle's constituent molecules are perturbed periodically with the same frequency as the electric field of the incident wave. The majority of light scattered by the particle is emitted at an identical frequency as the incident light, a process referred to as elastic scattering. Mie scattering theory, therefore, may be used to describe most spherical particle scattering systems, including Rayleigh scattering.[76] Rayleigh scattering theory can be recognized as an approximation of Mie scattering theory in the small size parameter regime $a \ll 1$ with a a dimensionless size parameter defined as follows:

$$a = \frac{2\pi r}{\lambda} \tag{3.21}$$

where r is the spherical particle radius and λ is the relative wavelength determined by the incident wavelength and the refractive index of the surrounding medium.

A Mie theory calculation for a spherical particle will yield the efficiency of scattering, which relates to the cross-sectional area of scattering as follows:

$$\sigma_s = Q_s A \tag{3.22}$$

where Q_s is the scattering efficiency. A is the true geometrical cross-sectional area of the particle defined as follows:

$$A = \pi a^2 \tag{3.23}$$

The scattering coefficient is related to the product of scatter (spherical particles) number density ρ_s and the cross-sectional area of scattering:

$$\mu_s = \rho_s \sigma_s \tag{3.24}$$

3.6.1.2 RADIATIVE TRANSPORT THEORY

In addition to Mie scattering theory, radiative transport theory has been widely used to describe light energy transfer in biological tissues.[77] In radiative transport theory, light propagation in the tissue is affected by the absorption, scattering and emission, though the effects of interference, diffraction and polarization can be ignored with the assumption that the distances between particles are sufficiently far away. Radiative transport theory can be formulated as follows:

$$\begin{aligned} \boldsymbol{s} \cdot \nabla I(\boldsymbol{r}, \boldsymbol{s}) &= -(\mu_a + \mu_s) I(\boldsymbol{r}, \boldsymbol{s})_s \\ &\quad + \mu_s \int_{4\pi} \rho(\boldsymbol{s}, \boldsymbol{s}') I(\boldsymbol{r}, \boldsymbol{s}') d\,\Omega \end{aligned} \tag{3.25}$$

where $\boldsymbol{s}$ is the unit vector defining the direction of light propagation, $I(\boldsymbol{r}, \boldsymbol{s})$ is the intensity of the light wave at position $\boldsymbol{r}$ and propagating in the direction of unit vector $\boldsymbol{s}$, μ_a is the absorption coefficient, μ_s is the scattering coefficient, $d\Omega$ is the differential solid

angle in the direction of $\boldsymbol{s}'$ and $\rho(\boldsymbol{s}, \boldsymbol{s}')$ is the scattering phase function, representing the probability of light with propagation direction $\boldsymbol{s}'$ being scattered into solid angle $d\Omega$ around direction $\boldsymbol{s}$.

The absorption and scattering coefficients have units of inverse length and describe the probability that a photon is absorbed or scattered. The first term on the right side of the equation (3.25) indicates that the light intensity $I(\boldsymbol{r}, \boldsymbol{s})$ is decreased due to the absorption and scattering in the direction $\boldsymbol{s}$. The second term on the right side of the equation (3.25) represents that the light intensity $I(\boldsymbol{r}, \boldsymbol{s})$ is increased due to scattering from the direction $\boldsymbol{s}'$ back to the direction $\boldsymbol{s}$.

To solve the radiative transfer equation (3.25), two common methodologies with the proper assumptions have been developed. One methodology is the diffusion approximation and the other one is the Monte Carlo simulation.[78, 79]

In diffusion approximation, two assumptions, called directional broadening and temporal broadening, are made. Directional broadening assumes that few absorption events occur and radiance becomes isotropic after abundant scattering events. Temporal broadening assumes that the time for substantial energy flux (the integral term in the equation 3.25) is much longer than the time to traverse one mean free path. Thus, the scattered component of the irradiance can be approximated by the first two terms of its Legendre polynomials. Based on the diffusion approximation, the analytical solution for radiative transfer equation could be obtained by solving a steady diffusion equation. One limitation of the diffusion approximation is that the absorption and scattering coefficients are inaccurate near the light source and boundaries because the assumption that light is nearly isotropic is too restrictive to take into account source and boundary conditions.[144]

The diffusion coefficient composed of absorption and scattering coefficients could be solved as follows:

$$D = \frac{1}{3[\mu_a + \mu_s(1-g)]} \tag{3.26}$$

where g is the anisotropy factor, which represents the effects of the phase function in the radiative transfer equation.

In the Monte Carlo simulation, each photon is considered independently and its trajectory is computed based on the probability predicted by the radiative transfer equation during each time interval. Each photon has a probability of absorption or scattering and the direction of each scattering event is determined by a random number weighted by an assumed phase function. The Monte Carlo method propagates each photon with small, fixed incremental stepsizes. The fixed stepsize Δs must be small relative to the average mean free path of a photon in the tissue. Each stepsize of each photon is defined with the total attenuation coefficient and a function of a random variable ξ that is uniformly distributed in the range [0 1].

$$\Delta s = \frac{-ln\xi}{(\mu_a + \mu_s)} \tag{3.27}$$

Unlike diffusion theory, the Monte Carlo method is applicable near tissue boundaries and sources, even for few scattering events. However, the Monte Carlo method requires a longer computational time to achieve better precision due to its statistical characteristics.

3.6.1.3 SCATTERING REGIMES

OCT signals are predominantly made up of light from single- and multiple-scattering regimes and each regime is characterized differently in OCT modeling. Though multiple scattering events are more frequent than single scattering events as the light

propagates in the biological tissue, the single scattering theory is still valuable to describe the interaction of photons and particles in the shallow regime of the biological tissue. [68] Therefore, it is necessary to implement a criterion to determine the primary scattering events that happens in the biological tissue.

Among various optical parameters, optical depth was often used to differentiate the single- and multiple-scattering regimes in the tissue.[80] The optical depth, or optical thickness, represents the quantity of light removed from a beam by absorption and scattering as a result of the light propagation in the tissue. The optical depth can be defined as follows:

$$l_{op} = \mu_t z \tag{3.28}$$

where μ_t is the total attenuation coefficient in the tissue, which can be expressed as:

$$\mu_t = \mu_a + \mu_s \tag{3.29}$$

where μ_a is the absorption attenuation coefficient in the tissue and μ_s is the scattering coefficient in the tissue.

When $l_{op} < 1$ in the medium, the light is said to be in the single scattering regime, meaning that the light averagely has only undergone a single scattering event or less. When $1 < l_{op} < 10$, the light is said to be in the multiple-scattering regime, meaning that light has undergone an average of several scattering events before being detected. When $l_{op} > 10$, the light is said to be in the diffusion regime, meaning that the light travels through the medium by means of the diffusion approximation.

3.6.2 SCATTERING MODELS FOR THE OCT SIGNAL

Until now, few attempts have been made to measure the scattering properties of retinal tissue using OCT imaging. Hammer et al. investigated the optical scattering of four posterior eye segments from bovine/porcine samples.[70] Faber et al. demonstrated the

optical scattering of oxygenated and deoxygenated hemoglobin by using spectral domain OCT.[81] In addition, a characterization of atherosclerotic plaques using a single, multiple-scattering layer model has been reported.[82]

Modeling light propagation and scattering in biological tissue is a complex problem. As mentioned above, several methodologies based on different approximations have been widely utilized, which include Mie theory, radiative transport theory and diffusion theory. However, to investigate optical properties of the retinal tissue from OCT images, easily operational models need to be implemented.

In this study, the scattering properties of the human retina were first extracted from OCT images using a single-scattering OCT model. However, because of the fact that multiple scattered photons contribute to the OCT signal, the single-scattering model may be insufficient for this purpose. Therefore, a multiple-scattering model was also used to extract the scattering coefficients from OCT images.[83]

3.6.2.1 SINGLE SCATTERING MODEL

In the single-scattering model, a single-scattering event was assumed for each ballistic photon. In general, the single-scattering model is capable of describing the light propagation in the superficial tissue layer where the optical depth $l_{op} < 1$ for most of biological tissue. While retinal tissue is very transparent to infrared light, the OCT signal backscattered from the retinal tissue is mainly composed of by single-scattering events. Therefore, the OCT signals contributed from multiple scattering events can be ignored.[68] The single-scattering model has been widely used to explain the OCT signal backscattered from retinal tissue.[73] Under the single-scattering assumption, the interaction between light and tissue can be simplified as illustrated in Figure 3.9.

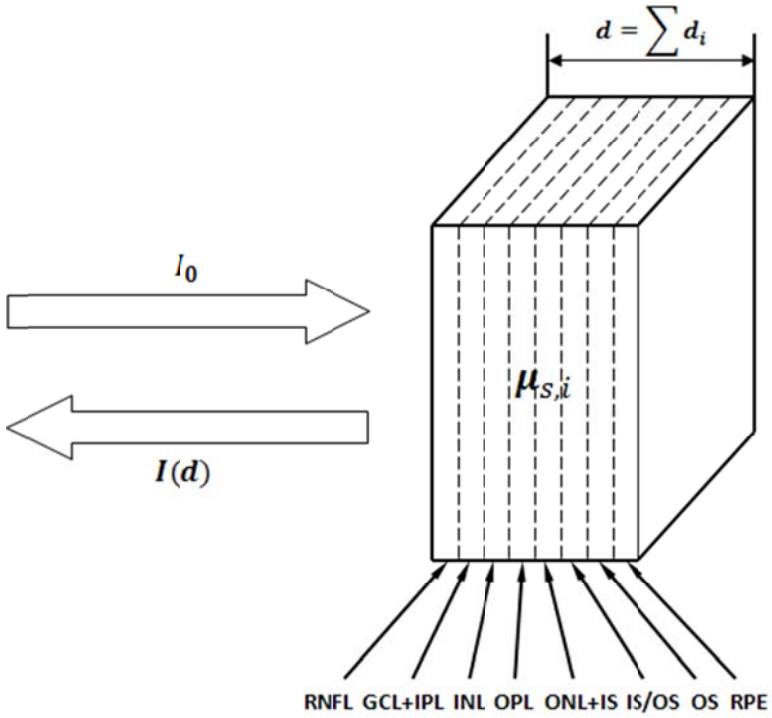

Figure 3. 9 The diagram of light attenuation in multiple layers.

OCT detects the reflected light that is a portion of the incident light. The ratio of the backscattered light intensity to the incident light is related to the path-length-resolved reflectance *R(d)* of the retinal tissue at depth *d*. *R(d)* is the proportional to the attenuation coefficient and decays exponentially at a rate equal to twice the integration of the local attenuation coefficient from the surface to depth d in the retinal tissue.

(3.30)

where is the dimensionless light intensity in the depth detected by OCT, which is equal to the intensity of light, is the normalization to and is the local total attenuation coefficient at the depth .

The total attenuation coefficient is the sum of the absorption and scattering coefficients. Due to transparence in the retinal tissue, the absorption of photons can be

ignored.[68] Therefore, the total attenuation coefficient can be approximated by the scattering coefficient. Then, the equation (3.30) can be rewritten as follows:

$$\bar{I}(d) \propto \exp\left[-2\int_0^d \mu_s(z)dz\right] \tag{3.31}$$

By applying the logarithm operation to both of two sides in the equation (3.31), it could be converted into the following:

$$logI(d) - logI_0 = -2\int_0^d \mu_s(z)dz + C \tag{3.32}$$

where C is a constant parameter. Because the value of the term $logI_0$ is fixed, the equation (3.32) could be rewritten as follows:

$$logI(d) = -2\int_0^d \mu_s(z)dz + C' \tag{3.33}$$

Obviously, if the scattering coefficient in the retina was assumed to be a constant, the scattering coefficient in the equation (3.33) could be obtained by using the curve fitting method (see Figure 3.10A).

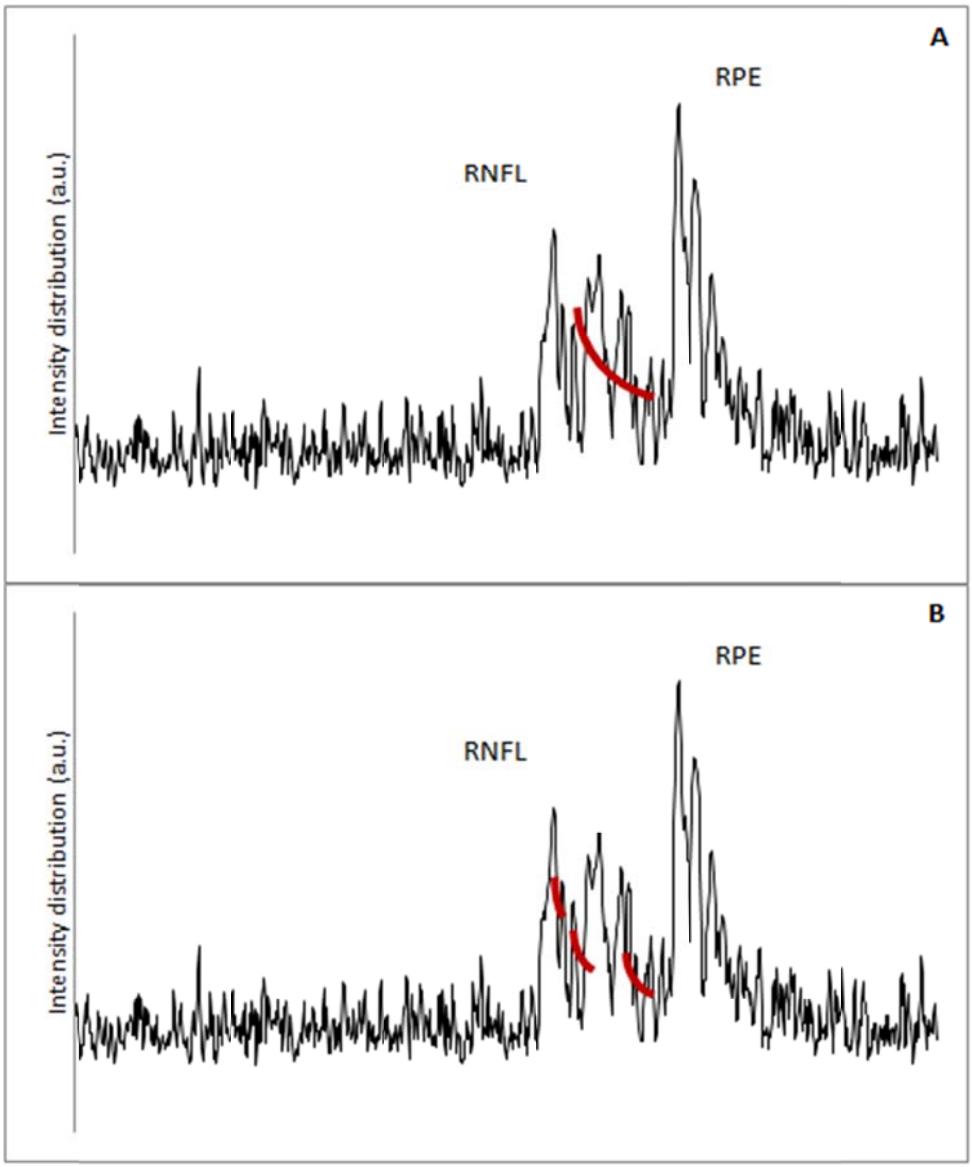

Figure 3.10 Measured OCT A-scan through the retina as well as calculations of single scattering coefficients using the curve fitting method. A) The curve fitting method for the scattering coefficient in the retina; B) the curve fitting method for scattering coefficients of intraretinal layers.

However, different intraretinal layers have different types of cellular organelles and therefore their optical properties are different. Thus, different scattering coefficients are assumed in intraretinal layers (see Figure 3.10B). The equation (3.31) can be written in a discrete form:

$$\bar{I}(d) \propto \exp\left[-2\sum_{i=1}^{n}\mu_{s,i}d_i\right] \tag{3.34}$$

where $\mu_{s,i}$ is the scattering coefficient of the ith intraretinal layer and d_i is the thickness of the ith intraretinal layer.

The equation (3.34) could be converted to the following:

$$log\bar{I}(d) = logI(d) - logI_0 = -2\sum_{i=1}^{n}\mu_{s,i}d_i + D \tag{3.35}$$

$$logI(d) = -2\sum_{i=1}^{n}\mu_{s,i}d_i + D' \tag{3.36}$$

where D and D' are the constants in the equation (3.35) and (3.36), respectively.

The scattering coefficient in each intraretinal layer was considered uniform. Therefore, the scattering coefficient of each intraretinal layer could also be calculated with the curve fitting method (see Figure 3.10B) from each A-scan. Mean values of the scattering confidents of all intraretinal layers could be obtained by averages across all A-scans.

3.6.2.2 MULTIPLE SCATTERING MODEL

Though the single-scattering model could describe the interaction between photons and particles in the retinal tissue as well as in the superficial layer of other turbid tissue, the multiple scattering events during light propagation the biological tissue cannot be ignored. Therefore, multiple scattering events may affect the precision of optical properties that are extracted from OCT signals.

In this study, the extended Huygens-Fresnel (EHF) principle was used to extract the scattering coefficients considering multiple scattering events in the retinal tissue.[84] The Huygens-Fresnel principle was first used to describe beam propagation in a turbulent

atmosphere.[85] By including the shower curtain effect, the extended Huygens-Fresnel principle was implemented and was used to describe the multiple scattering events in OCT.

The extended Huygens-Fresnel principle can be used to describe light propagation in tissue, retaining both amplitude and phase information but neglecting absorption in retinal tissue. Thus, the retinal tissue is characterized by a scattering coefficient. Furthermore, the retinal tissue is modeled as a material with scatterers randomly distributed over the volume of interest. Note that in the present analysis, the polarization effect is ignored.

By mixing the sample filed U_S reflected at the discontinuity in the tissue at depth z, with the reference field U_R on the photon detector of the OCT system, we obtain the heterodyne signal current $I(z)$ as follows:

$$I(z) \propto Re\left[\int U_R(p,t)U_S^*(p,t+\tau)dp\right] \tag{3.37}$$

where the integration is taken over the area of the photon detector, *Re* denotes the real part of a complex number and τ is the difference of the propagation times between the reference and sample beams. In addition, Gaussian shapes are assumed for the reference field U_R and input sample filed U_S:

$$U_R(p,t) = \sqrt{\frac{P_R}{\pi\omega_0^2}}exp\left[-\frac{p^2}{2}\left(\frac{1}{\omega_0^2}+\frac{ik}{f}\right)\right]exp[i\omega_R t+\varphi_R(t)] \tag{3.38}$$

$$U_S(p,t) = \sqrt{\frac{P_S}{\pi\omega_0^2}}exp\left[-\frac{p^2}{2}\left(\frac{1}{\omega_0^2}+\frac{ik}{f}\right)\right]exp[i\omega_S t] \tag{3.39}$$

where P_R and P_S are the powers of the reference and the input sample beams, respectively, ω_0 is the *1/e* intensity radius of these beams in the lens plan, k is the wavenumber, f is the focal length of the lens, ω_R and ω_S are the angular frequencies of the reference and the input sample beams, respectively and φ_R is the phase of the reference field relative to the input sample field.

By applying the average operation for the equation (3.37), the mean square heterodyne signal current could be obtained:

$$\langle I^2(z)\rangle \propto |g(\tau)|^2 Re\left[\iint \Gamma_S(p_1,p_2)\Gamma_R(p_1,p_2)dp_1dp_2\right] \tag{3.40}$$

where $g(\tau)$ is the modulus of the normalized temporal coherence function of the source, $p_1$and p_2 are two-dimensional vectors in the plane transverse to the optical axis and Γ_R and Γ_S are the mutual coherence functions of the reference and the reflected sample optical fields in the mixing plane, respectively. From this, we derive the following:

$$\Gamma_R(p_1,p_2) = U_R(p_1,t)U_S^*(p_2,t) \tag{3.41}$$

$$\Gamma_S(p_1,p_2) = U_S(p_1,t)U_R^*(p_2,t) \tag{3.42}$$

The final equation for the OCT signal current at probing depth z can be expressed as follows:

$$\langle I^2(z)\rangle \propto \left[e^{-2\mu_s z} + \frac{2\exp(-2e^{-2\mu_s z}(1-e^{-2\mu_s z}))}{1+\frac{\omega_s^2}{\omega_H^2}} + (1-e^{-2\mu_s z})^2\frac{\omega_s^2}{\omega_H^2}\right] \tag{3.43}$$

The parameters ω_H and ω_S are the *1/e* irradiance radius at the probing depth in the absence and presence of scattering, respectively.

$$\omega_H^2 = \omega_0^2\left(A - \frac{B}{f}\right)^2 + \left(\frac{B}{k\omega_0}\right)^2 \quad (3.44)$$

$$\omega_s^2 = \omega_0^2\left(A - \frac{B}{f}\right)^2 + \left(\frac{B}{k\omega_0}\right)^2 + \left(\frac{2B}{k\rho_0}\right)^2 \quad (3.45)$$

where A and B are elements from the $ABCD$ ray matrix for light propagation from the lens plane to the probing depth in the sample.[86] ρ_0 is the lateral coherence length that can be expressed as follows:

$$\rho_0(z) = \sqrt{\frac{3}{\mu_s z}}\frac{\lambda_0}{\pi\theta_{rms}}\left(\frac{nB}{z}\right)^2 \quad (3.46)$$

where θ_{rms} is the root-mean-square scattering angle; it can be approximated as $\theta_{rms} \simeq \sqrt{2(1-g)}$ of which g is the anisotropy factor.

The first term on the right side of the equation (3.43) represents the contribution from the single scattering evens, which has been introduced in the previous subsection. The third term represents the contribution from the multiple scattering events and the second is the cross term.

3.6.3 VALIDATION OF SCATTERING MODELS USING A PHANTOM MODEL

To use the single- and multiple-scattering models to extract the scattering coefficients from OCT signals, a validity study needs to be performed. Specifically, the accuracy of the scattering coefficient calculations was obtained from OCT signals using a well-characterized phantom.

The scattering coefficient estimation was investigated by scanning a custom-built test object containing a specific enclosed specimen of known size. The specimen was enclosed in a chamber that consisted of a 400 μm thick washer delimited by two external 150 micron thick glass plates and it was held in the space between these two glass plates.

To ensure that the strong reflections from the glass-air interfaces did not interfere with the measurement, glass plates with a thickness at least ten times the temporal coherence length of the source were used. Because the Stratus OCT system is designed specifically for visualization of the human retina, its image acquisition setup was modified to visualize the specimens. Thus, the chamber was introduced in an apparatus that included a flat mirror tilted 45^{o} to an objective lens (see Figure 3.11) to acquire images of horizontally oriented specimens.[87]

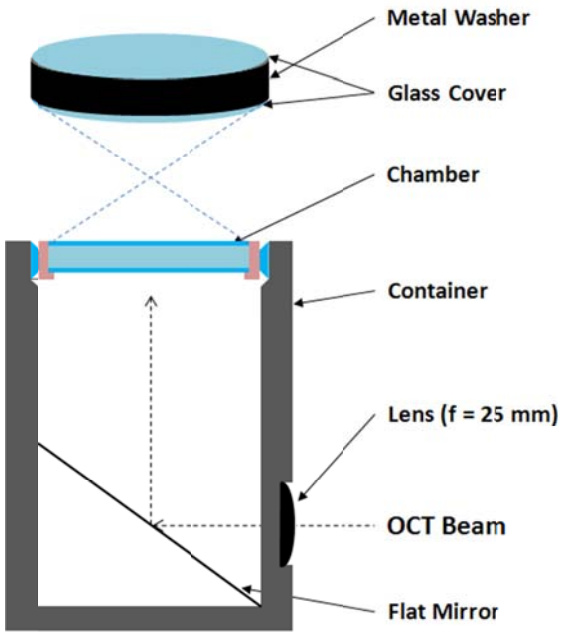

Figure 3.11 Cross-sectional view of the apparatus. The travel distance of the beam from the lens until the chamber is 25 mm.

The specimens used in this test were polystyrene microspheres, which are widely used for lateral flow tests, latex agglutination tests, flow cytometry, fluorescence microscopy and other applications. Because the 10 μm polystyrene microsphere is similar to the size of the organelles in retinal tissue, 10 μm polystyrene microspheres was chosen for the calculation. Scattering coefficients were calculated using the Mie scattering theory

and compared to experimental results. Table 3.2 lists the microspheres' physical properties.

Table 3.2 Physical properties of polystyrene microspheres.

Parameters	Physical Properties
Diameter	10 µm
Density	1.05 g/ml
Mass of Particles	0.025 g/ml
Refractive Index	1.60

OCT raw data (see Figure 3.12) was exported and used to extract the optical properties of the specimen using the scattering models. Single- and multiple-scattering coefficients were calculated using the scattering models introduced in this section and were compared to results calculated using Mie scattering theory. Ten regions of interest (ROIs) were selected in the areas near the upper and lower glass covers to account for the single- and multiple-scattering regimes, respectively.

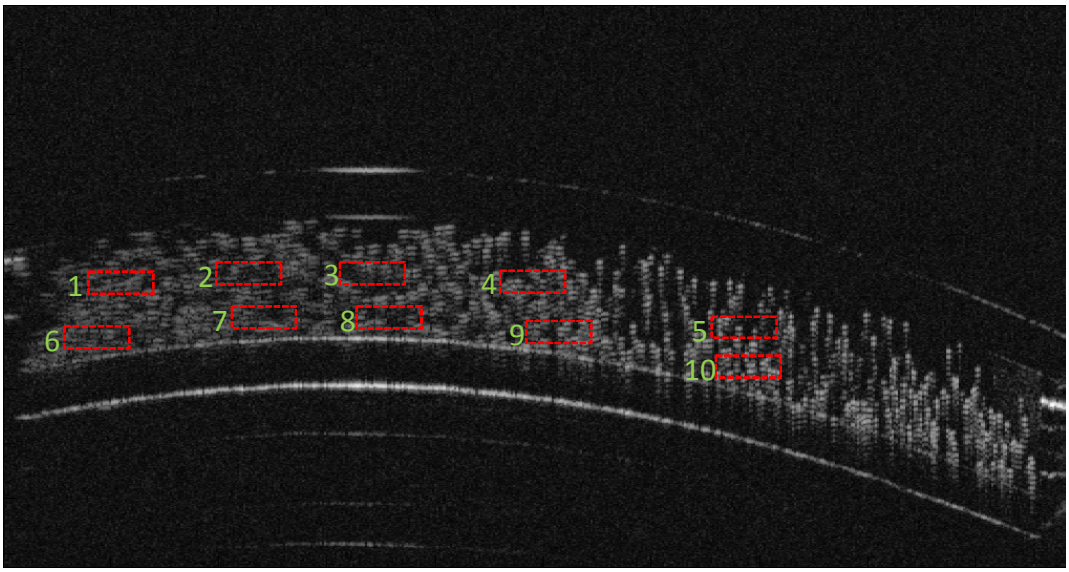

Figure 3.12 ROIs in the OCT phantom image

Compared to the results calculated by the Mie scattering theory (0.70 mm^{-1}), the scattering coefficients were calculated by using the scattering models introduced in section 3.6.2. Table 3.3 shows the results obtained after calculating the scattering coefficients using an experimental OCT phantom image (see Figure 3.12). Scattering coefficients in ROIs 1 to 5 were calculated using the single-scattering model and scattering coefficients in ROIs 6 to 7 were calculated using the multiple-scattering model. The results indicated that the single-scattering model slightly underestimated the theoretical value calculated by Mie scattering theory in region 1 (0.67 mm^{-1} vs. 0.70 mm^{-1}) and 2 (0.71 mm^{-1} vs. 0.70 mm^{-1}), which are near the upper glass cover. The multiple-scattering model slightly overestimated the scattering coefficient calculated by the Mie scattering theory in region 6 (0.75 mm^{-1} vs. 0.70 mm^{-1}), which is near the lower glass cover. Moreover, relatively larger deviations from the theoretical values were observed for the scattering coefficients in the other ROIs, which could be caused by the non-uniform distribution of polystyrene microspheres inside the air-filled chamber (e.g., compared to the uniform distribution in ROIs 1 and 6), as indicated in the OCT image. Scattering coefficients extracted from ROIs 1, 2 and 6 showed that the single- and multiple-scattering models could be used to calculate the optical properties in shallow and deeper regions of the test object when the polystyrene microspheres were relatively uniformly distributed in the region of analysis.

Table 3.3 Scattering coefficient results obtained with the single- and multiple-scattering models.

Single-Scattering		Multiple-Scattering	
ROI	Scattering Coefficient (mm^{-1})	ROI	Scattering Coefficient (mm^{-1})
1	0.67 (-4%)	6	0.75 (7%)
2	0.71 (1%)	7	1.64 (134%)
3	1.59 (127%)	8	1.41 (101%)
4	1.73 (147%)	9	1.22 (74%)
5	1.49 (128%)	10	1.87 (167%)

3.7 EVALUATION ON FACTORS THAT MAY AFFECT THE ESTIMATION OF STRUCTURAL AND OPTICAL PARAMETERS

As previously mentioned, OCT is typically employed for the measurement of retinal thickness. However, coherent reflected light carries more information characterizing the optical properties of tissue. Before the question can be answered affirmatively regarding whether or not OCT can quantitatively measure the optical properties of retinal tissue, a better understanding and modeling of the OCT signal backscattered from the retinal structure is needed. As indicated, the desired characteristics are related to the intensity information in OCT images, while multiple factors could cause varying intensities and therefore affect the structural and optical features extracted from OCT images. For example, speckle noise distorts the distribution of intensities in OCT images and blood vessel shadows lower the intensities locally. OCT scanning pitfalls could also change the values of characteristics.[88]

The purpose of this study was to evaluate the effects of several key factors on the estimation of structural and optical features that were related to intensity values in OCT images. Typical features, such as fractal dimension and scattering coefficients, were used in the evaluations.

3.7.1 EVALUATION OF THE EFFECT OF REMOVING BLOOD VESSEL SHADOWS

As mentioned in subsection 3.3.4, blood vessel shadows result in areas with lower intensities in OCT images. The information carried in the shadowed area might be distorted, and therefore, inaccurate characteristics might be obtained from the shadowed areas. Hence, it is important to evaluate the effect of blood vessel shadows on the estimation of structural and optical properties from OCT images. A total of ten healthy eyes (60 B-scans), ten diabetic eyes with mild retinopathy (60 B-scans) and ten diabetic eyes without mild retinopathy (60 B-scans) were selected from the database. The nonlinear complex diffusion filter was applied to remove the speckle noise. The blood vessel shadows were detected on each OCT image. Fractal dimension and scattering coefficients using the single-scattering model were calculated for each intraretinal layer before and after removing the blood vessel shadows present in OCT images. Because the absolute reflectivity can vary according to a wide variety of factors, such as media opacity, astigmatism and scan technique, relative numbers should be used to facilitate the comparison of different scans in the same subject as well as among different subjects or groups. Consequently, when an estimate of the mean reflectivity is being calculated, the intensity at each point of a specific A-scan should be computed relative to the value of the highest intensity value along the length of the entire A-scan from the vitreous to the choroids. Therefore, any studies considering quantifiable differentiation of intraretinal spaces on the basis of their optical reflectivity need to consider each value as a percentage of the local maximum. Moreover, taking into account that the RPE layer apparently has constant backscatter properties and therefore behaves like a diffuse reflector, an assumption that could be valid when the RPE is more or less flat, this layer

could be fairly insensitive to the direction of incidence of the light beam.[89] Accordingly, reflectivity with normalization to the RPE reflectance (NRPE) was used in our analysis. In addition, reflectivity normalized to the maximum value within the whole retina (NRIR) was also included in the analysis. Accordingly, scattering coefficients were calculated by using the single-scattering model with two normalization methods, NRIR and NRPE (NRIR: reflectivity normalized to the maximum value within the whole retina and NRPE: reflectivity with normalization to the RPE reflectance).

The differences in the fractal dimension and scattering coefficients of healthy and diabetic eyes with and without mild retinopathy before and after removing blood vessel shadows are shown in Figures 3.11-3.13. The figures clearly indicated that the fractal dimension and scattering coefficients only changed slightly after removing blood vessel shadows. Overall, the numerical results showed that the fractal dimension increased by 0.1-0.2% and that the scattering coefficients decreased by 1-3% after removing blood vessel shadows.

In this evaluation, we found that blood vessel shadows affected the scattering coefficients more than the fractal dimension because scattering coefficients are more directly related to the intensity distributions than the fractal dimension. Therefore, the scattering coefficients demonstrated a larger change than the fractal dimensions. Moreover, the fractal dimension is a characteristic that is used to describe the disorder of the internal structure of the retinal tissue. When blood vessel shadows that contained blurred information were removed from OCT images, the values of the fractal dimension increased slightly. Moreover, when using the single-scattering model and assuming that the absorption attenuation could be neglected due to the transparency in the retinal tissue,

the scattering coefficients decreased slightly after removing blood vessel shadows because lower intensities in the blood vessel shadows represent a stronger attenuation in the shadowing regions.

According to our results, it appears that the effect of blood vessel shadows on the estimation of structural and optical features could be ignored. Although blood vessel shadows would not change the trends in characteristics of the intraretinal layers, the removal of blood vessel shadows could improve the performance of methods used in OCT image analysis (e.g., reduce segmentation errors).

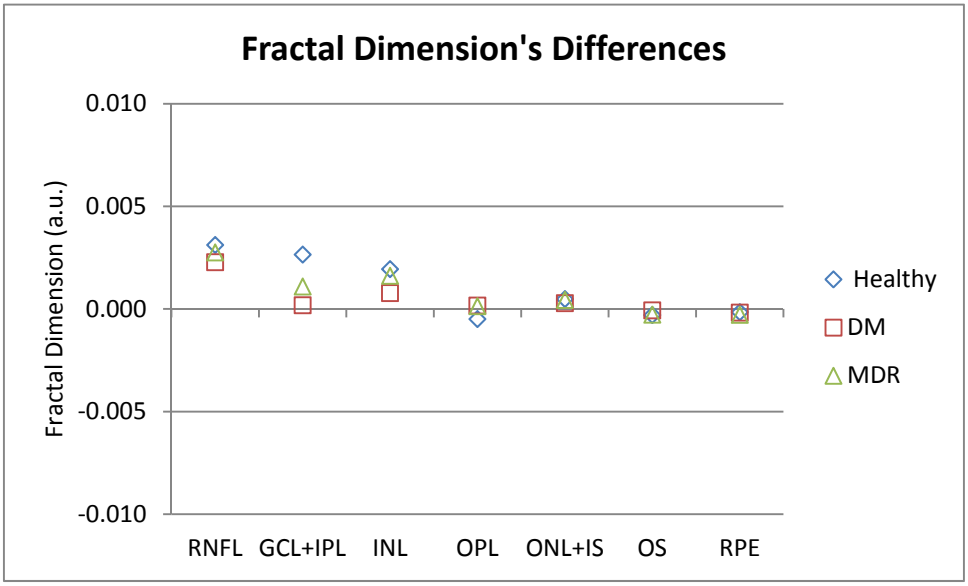

Figure 3.13 Differences of the fractal dimension calculated before and after removing the blood vessel shadows.

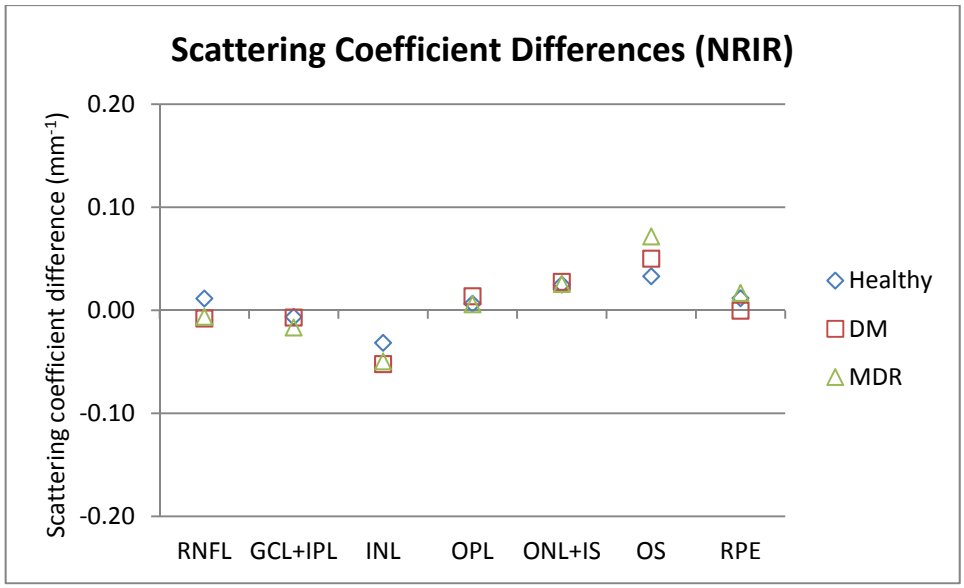

Figure 3.14 Differences of the scattering coefficient (NRIR) calculated before and after removing the blood vessel shadows.

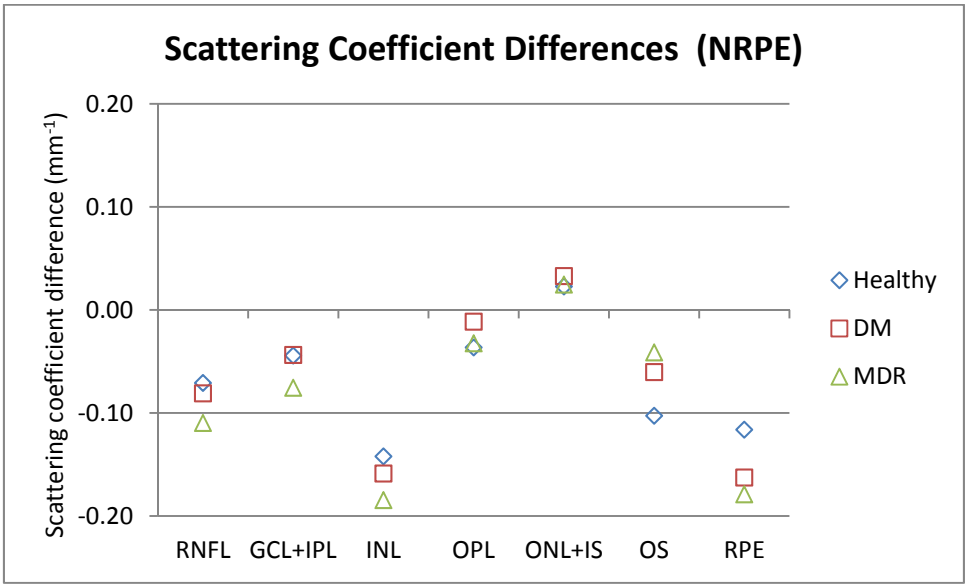

Figure 3.15 Differences of the scattering coefficient (NRPE) calculated before and after removing the blood vessel shadows.

3.7.2 EVALUATION OF THE EFFECT OF SPECKLE NOISE REMOVAL

Speckle-free Stratus OCT test images from ten healthy eyes (60 B-scans), ten diabetic eyes with mild retinopathy (60 B-scans) and ten diabetic eyes without mild

retinopathy (60 B-scans) were obtained after applying median filtering. Because the speckle pattern becomes additive white noise after the log-transformation, a Gaussian distribution approach to speckles was considered. Therefore, the experiments were conducted on the OCT test images at different levels of Gaussian additive noise (5%, 10% and 15%). Relative light-backscattering of two particular segments characterized by low (ONL+IS) and high light-backscatter (OS) were chosen for the analysis. The fractal dimension and scattering coefficients were calculated for each intraretinal segment before and after removing the blood vessel shadows from OCT images. The scattering coefficients were calculated by using the single-scattering model with two normalization methods (NRIR and NRPE). Although blood vessel shadows would not change the parameter's properties in intraretinal layers according to the previous evaluation, the blood vessel shadows were removed to improve the segmentation performance as well as the numerical accuracy of the fractal dimension and scattering coefficient calculations.

The fractal dimension increased in both the ONL+IS and OS when the noise level was augmented from 5 to 15% in OCT data from diseased subjects (DM and MDR). A similar trend was observed in healthy eyes (see Table 3.4). Once the Gaussian additive noise was removed, the accuracy of the fractal dimension in the ONL+IS and OS improved in both healthy and pathological OCT data (see Table 3.4). The fractal dimensions for healthy and pathological eyes were less varied in the OS compared to the fractal dimension in the ONL+IS.

The scattering coefficients decreased in the ONL+IS and increased in the OS when the noise level was augmented from 5 to 15% in OCT data from MDR subjects, but the scattering coefficients increased in both the ONL+IS and OS from healthy and DM

patients. Once the Gaussian additive noise was removed, the accuracy of the scattering coefficients in the OS improved in both healthy and pathological OCT data, but no improvement was observed in the ONL, except in one case in the DM group (see Table 3.5 and 3.6). The scattering coefficients for healthy and diseased eyes decreased when the noise level was increased from 5 to 15% for the low scattering structure (ONL+IS). However, the scattering coefficients in the high scattering structure (OS) increased when a 15% noise level was added.

In this evaluation, we found that the scattering coefficients extracted from OCT images were more affected as the noise level increased. In addition, higher scattering coefficients were obtained for the diseased eyes independently of the noise level added to the OCT test images. As expected, the scattering coefficients obtained for the OS were higher than the scattering coefficients obtained for the low contrast segments (ONL+IS). In addition, scattering coefficient extraction was more affected by the speckle noise in the OS where multiple-scattered light could be more predominant.

Table 3.4 Fractal dimension results for each intraretinal layer (mean±SD).

Intraretinal layers	5P	5PF	10P	10PF	15P	15PF
Healthy						
ONL+IS	1.96 ± 0.05	1.79 ± 0.03	2.14 ± 0.05	1.82 ± 0.03	2.24 ± 0.05	1.87 ± 0.04
OS	1.73 ± 0.02	1.70 ± 0.02	1.78 ± 0.02	1.71 ± 0.02	1.84 ± 0.02	1.72 ± 0.02
DM						
ONL+IS	2.00 ± 0.04	1.80 ± 0.03	2.18 ± 0.03	1.83 ± 0.03	2.28 ± 0.03	1.88 ± 0.03
OS	1.74 ± 0.01	1.70 ± 0.01	1.80 ± 0.02	1.71 ± 0.01	1.87 ± 0.03	1.72 ± 0.01
MDR						
ONL+IS	2.04 ± 0.05	1.82 ± 0.03	2.22 ± 0.04	1.86 ± 0.03	2.31 ± 0.03	1.91 ± 0.03
OS	1.76 ± 0.02	1.72 ± 0.02	1.82 ± 0.03	1.73 ± 0.02	1.89 ± 0.04	1.74 ± 0.01

5P, 10P and 15P means the OCT raw image was added with Gaussian additive noise 5%, 10% and 15%, respectively. 5PF, 10PF and 15PF means the OCT raw image was added with Gaussian additive noise 5%, 10% and 15% and then were filtered with nonlinear complex diffusion filter.

Table 3.5 Scattering coefficients (mm^{-1}) of intraretinal layers by using the single-scattering model results with normalization NRIR (mean±SD).

Intraretinal layers	5P	5PF	10P	10PF	15P	15PF
Healthy						
ONL+IS	2.40 ± 0.21	2.55 ± 0.23	2.41 ± 0.16	2.48 ± 0.20	2.47 ± 0.16	2.41 ± 0.24
OS	10.72 ± 2.62	8.18 ± 2.11	12.13 ± 2.50	9.06 ± 2.27	13.45 ± 2.74	9.87 ± 2.56
DM						
ONL+IS	2.35 ± 0.42	2.52 ± 0.54	2.43 ± 0.42	2.43 ± 0.53	2.57 ± 0.48	2.42 ± 0.46
OS	10.28 ± 1.79	8.22 ± 1.65	11.27 ± 2.17	9.05 ± 1.95	12.46 ± 2.88	9.47 ± 1.97
MDR						
ONL+IS	2.51 ± 0.51	2.63 ± 0.62	2.49 ± 0.35	2.59 ± 0.56	2.48 ± 0.25	2.50 ± 0.50
OS	13.22 ± 2.24	10.38 ± 2.74	14.64 ± 2.57	11.54 ± 2.42	16.23 ± 3.42	12.15 ± 2.1

5P, 10P and 15P denote the OCT raw image was added with Gaussian additive noise 5%, 10% and 15%, respectively. 5PF, 10PF and 15PF means the OCT raw image was added with Gaussian additive noise 5%, 10% and 15% and then were filtered with nonlinear complex diffusion filter.

Table 3.6 Scattering coefficients (mm^{-1}) of intraretinal layers by using the single-scattering model results with normalization NRPE (mean±SD).

Intraretinal layers	5P	5PF	10P	10PF	15P	15PF
Healthy						
ONL+IS	3.80 ± 0.45	3.85 ± 0.52	3.96 ± 0.36	3.84 ± 0.49	4.31 ± 0.44	3.86 ± 0.50
OS	16.76 ± 5.11	12.3 ± 3.96	19.72 ± 5.32	13.99 ± 4.37	23.06 ± 5.85	15.66 ± 5.01
DM						
ONL+IS	3.96 ± 0.99	4.06 ± 1.13	4.23 ± 0.98	4.02 ± 1.08	4.72 ± 1.17	4.12 ± 1.04
OS	17.07 ± 4.20	13.1 ± 3.47	19.27 ± 4.97	14.75 ± 4.15	22.61 ± 6.88	15.91 ± 4.56
MDR						
ONL+IS	4.05 ± 0.92	4.05 ± 1.06	4.20 ± 0.68	4.08 ± 0.99	4.37 ± 0.57	4.05 ± 0.90
OS	21.3 ± 3.52	15.91 ± 3.2	24.55 ± 4.42	18.12 ± 2.88	28.57 ± 6.31	19.63 ± 2.73

5P, 10P and 15P means the OCT raw image was added with Gaussian additive noise 5%, 10% and 15%, respectively. 5PF, 10PF and 15PF means the OCT raw image was added with Gaussian additive noise 5%, 10% and 15% and then were filtered with nonlinear complex diffusion filter.

3.7.3 EVALUATION OF THE EFFECT OF CHANGES IN ANGLES OF INCIDENCE OF THE OCT LIGHT ON THE RETINA

OCT images may differ because of the different angle of incidence of the OCT light on the retina. Therefore, multiple subject re-positioning and image quality controls are normally used to avoid scanning pitfalls and improve the stability and repeatability of

OCT measurements during clinical data collection. Therefore, it is necessary to investigate their effects on the estimation of structural and optical properties.

In this experiment, three sets of OCT images were collected repeatedly for the same eye with different angles of incidence of the OCT light on the retina (see Figures 3.16-3.17). In one set, the OCT beam was constrained to lie perpendicular to the center of the pupil. The OCT beam was constrained to lie symmetrically near the perpendicular to the pupil center for the remaining two sets. The OCT images from the three sets were denoised by the nonlinear complex diffusion filter and segmentation of intraretinal layers was performed. To improve the segmentation performance, the blood vessel shadows were removed using the methodology introduced in subsection 3.3.4 before calculating the structural and optical properties.

Because the calculations of the fractal dimension and scattering coefficients strongly depend on the intensity distribution in OCT images, these two parameters were extracted and used in this evaluation for the three sets of OCT images. The fractal dimension was calculated using the power spectrum method. The scattering coefficients were calculated using the single-scattering model with two normalization methods (NRIR and NRPE).

The fractal dimension and scattering coefficients for all sets of OCT images are shown in Figures 3.18-3.20. Our results indicate that the largest fractal dimension difference was obtained for the RNFL when comparing three sets of measurements, with a relative difference of less than 4%. The relative difference obtained for the other intraretinal layers was in the 0.2-2% range. Figure 3.18 indicates that the fractal dimension's accuracy in each intraretinal layer was high except for the RNFL. Compared

to the fractal dimension results, the scattering coefficient differences between the three sets of OCT images were relatively higher. Additionally, the largest and smallest scattering coefficient differences were obtained in the OS and GCL+IPL, respectively (both with NRIR and NRPE).

In this evaluation, we found that the scattering coefficients extracted from OCT images were more affected than the fractal dimension as the OCT light beam changes its incidence angle. Of note, the fractal dimension is a structural parameter and it is determined by the roughness of structure inside the retinal tissue. Therefore, similar structures could be recorded by OCT imaging despite different angles of incidence of the OCT light on the retina, which could explain why the fractal dimension values are close. However, the scattering coefficient is an optical parameter that it is mainly determined by the photon's interaction with cellular organelles; therefore, a minor change in position of the incident light beam could cause a different light path inside the retinal tissue even for neighboring scanned locations containing similar structures. Accordingly, larger relative differences were obtained for the scattering coefficients compared to the fractal dimensions. However, in the superficial layers, relatively few interactions happened between the photon and cellular organelles compared to the deeper layers (see section 3.6.1.3). Therefore, smaller scattering coefficient differences were found in the superficial layers, such as the RNFL and GCL+IPL.

In general, the minor incident angle changes of the OCT light beam could slightly affect the structural and optical characteristics extracted from OCT images. The effect on the estimation of structural features could be ignored, while the effect on the estimation of optical properties should be carefully treated, though the variation of results was in the

acceptable range.[90] However, results may be significantly affected for higher values of the resultant angle of incidence on the retina.

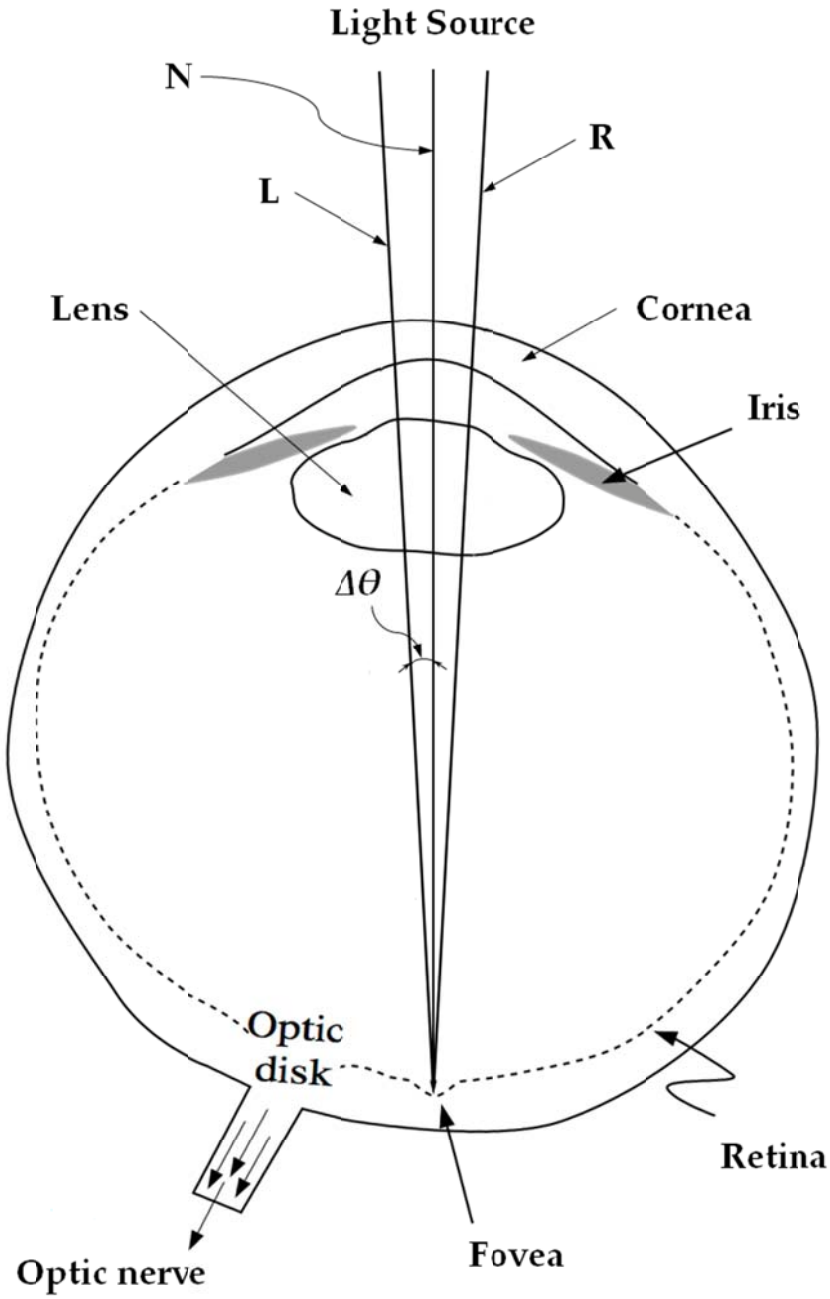

Figure 3.16 Diagram showing the angles of incidence of the OCT light on the retina for the scan lines left (L), normal (N) and right (R). The L and R scan lines were slightly tilted from the normal scan line by displacing the fixation target to an equal distance/angle ($\Delta\theta \approx 5^{\circ}$) from the normal position on both sides.

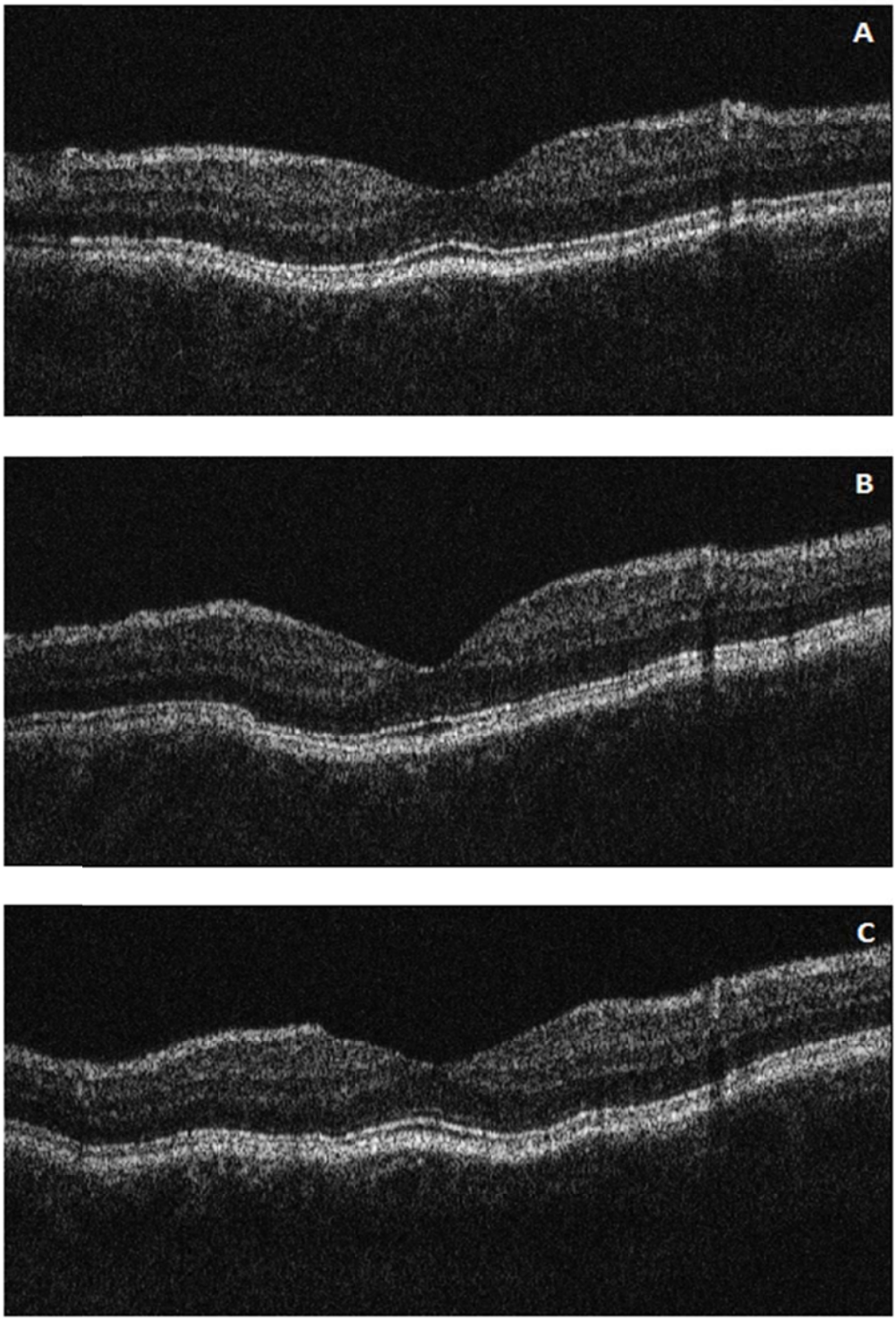

Figure 3.17 OCT radial scans (A, B and C) in the position of the initial radial scan lines , and respectively.

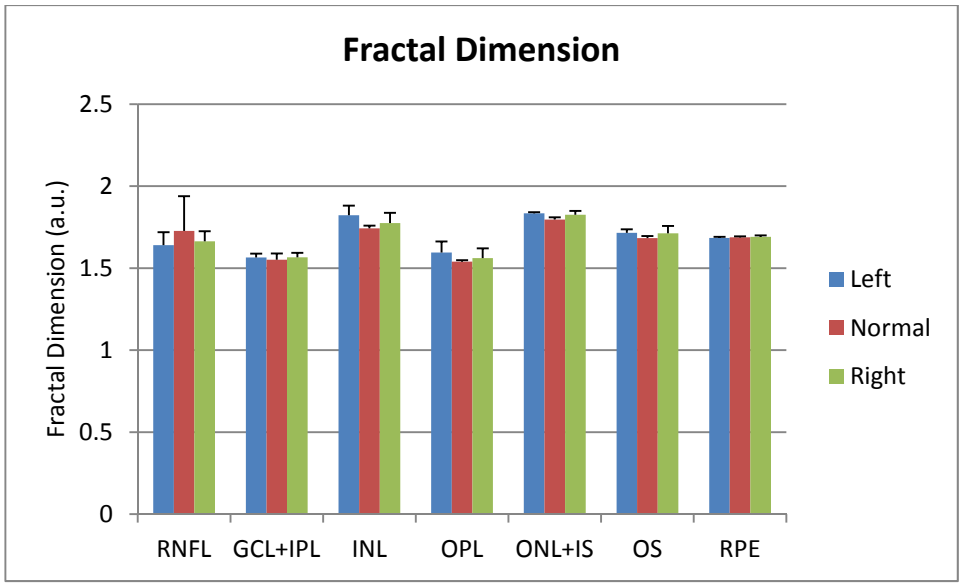

Figure 3.18 Comparison of fractal dimension of intraretinal layers for three sets of OCT images.

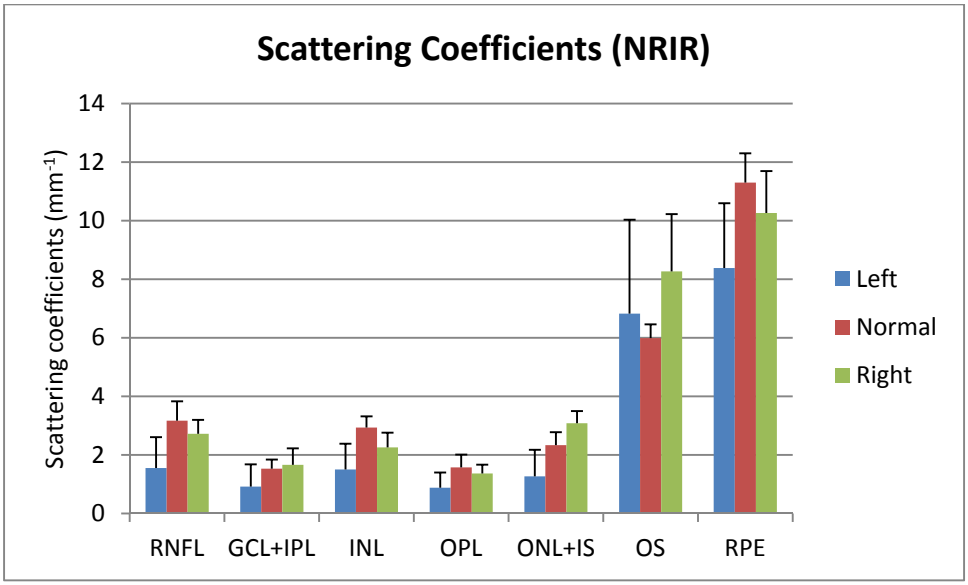

Figure 3.19 Comparison of scattering coefficients (NRIR) of intraretinal layers for three sets of OCT images by using the single-scattering model.

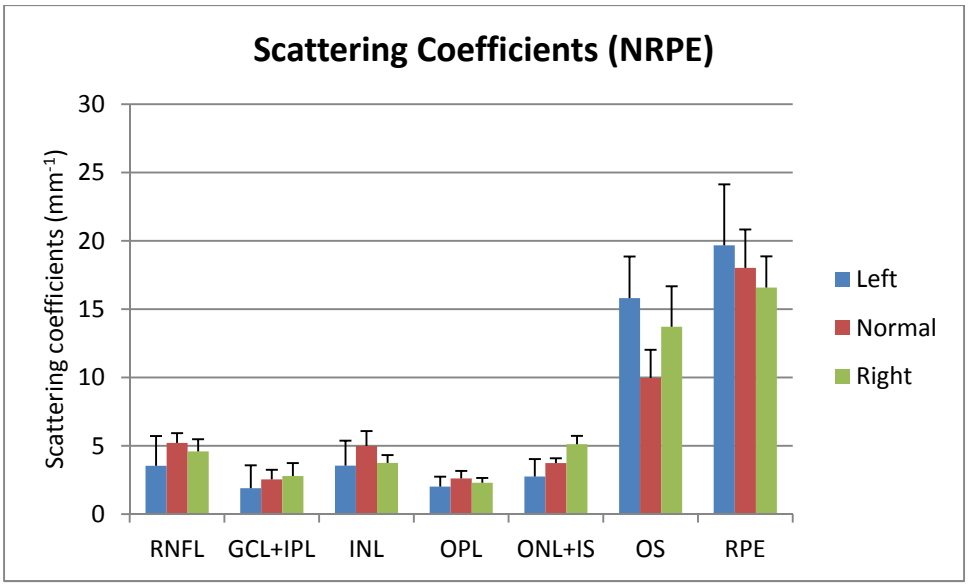

Figure 3.20 Comparison of scattering coefficients (NRPE) of intraretinal layers for two sets of OCT images by using the single scattering model.

CHAPTER 4. QUANTITATIVE ANALYSIS OF THE STRUCTURAL MORPHOLOGY

4.1 OVERVIEW

The importance of OCT imaging arises from the need to diagnose and treat diseased eyes where the internal structure can be visualized and imaged at a micro scale resolution. Specifically, OCT is capable of measuring the thickness of intraretinal layers by using segmented OCT images. By comparing the thickness of intraretinal layers of diseased eyes to healthy eyes, the thickness changes in intraretinal layers can be determined and then used to diagnose disease. In addition, structural information measured from commercial OCT devices could be used to detect diseased eyes.

In this chapter, structural characteristics, including the thickness measurements and texture parameters, are reported after calculating them from the OCT images of healthy and diabetic eyes with and without mild diabetic retinopathy (MDR). The differences in structural parameters between study groups were tested using an ANOVA followed by Newman-Keuls post-hoc analysis.[91] Because of the number of comparisons, $p \leq 0.001$ was considered statistically significant ($0.001 < p \leq 0.05$ missed significant). Receiver operating characteristic (ROC) analysis was also performed on the structural parameters between study groups to determine the ability of each structural characteristic to differentiate diabetic eyes with and without MDR from healthy eyes.[92] Area under the receiver operating characteristic curve (AUROC) was used to compare diagnostic power. This area summarizes the sensitivity and specificity of diagnosis over the total range of valid diagnostic thresholds. An AUROC of 1.0 indicated perfect discrimination. An AUROC of 0.5 indicated no discrimination. The AUROC calculations and statistical

analyses were performed using the software package SPSS version 16 (SPSS Inc., Chicago, Illinois).

4.2 QUANTITATIVE MEASUREMENTS

Healthy eyes (74 eyes) and diabetic eyes with and without mild diabetic retinopathy (43 MDR and 38 DM eyes, respectively) were used in this study. A total of six radial scans per study eye were collected with the Stratus OCT system. Thickness measurements and texture parameters were extracted from the OCT images for each intraretinal layer and macular region in all study groups. The foveola region was not included in the analysis because segmentation was less reliable due to the low OCT signal in this region.

4.2.1 THICKNESS MEASUREMENTS

The mean thickness in each intraretinal layer was calculated by averaging the local thickness across all macular regions for the healthy and diabetic eyes with and without MDR. The thickness in each macular region and intraretinal layer was also measured, except in the foveola. The thickness measurements are given in Table 4.1 and the values are expressed in the form of the mean ± SD (SD: standard deviation).

The thickness changes were analyzed using ANOVA followed by Newman-Keuls post-hoc analysis between DM, MDR and healthy eyes. Significant differences between study groups are also reported in Table 4.1.

4.2.1.1 INTRARETINAL LAYER THICKNESS CHANGES PER EYE

The mean thicknesses in each intraretinal layer for all study groups are plotted in Figure 4.1. In the DM, MDR and healthy eyes, the highest and lowest intraretinal layer thicknesses were found in the ONL+IS and RPE, respectively. The mean thickness of the GCL+IPL, OPL and OS showed a significant decrease (8%, 13% and 12%, respectively)

in the MDR eyes compared to healthy eyes (see Figure 4.1 and Table 4.1). The mean thickness in the other intraretinal layers (except in the RNFL) showed a non-significant tendency towards thickening compared to healthy eyes.

Moreover, the mean thickness in the OPL, OS and RPE showed a significant decrease (10%, 20% and 7%, respectively) in the MDR eyes compared to the DM eyes. The mean thickness of the remaining intraretinal layers (except in the RNFL) showed a non-significant tendency towards thinning compared to DM eyes.

4.2.1.2 INTRARETINAL LAYER THICKNESS CHANGES IN THE FOVEAL REGION

The OPL and OS foveal thicknesses showed a significant decrease (13% and 12%, respectively) in the MDR eyes compared to healthy eyes (see Figure 4.2 and Table 4.1). The GCL+IPL and INL foveal thickness showed a significant increase (26% and 19%, respectively), while the thickness in the other intraretinal layers (except in the RNFL) showed a non-significant tendency towards thickening compared to healthy eyes.

When comparing MDR with DM eyes, the RNFL, OPL and OS foveal thickness showed a significant decrease (30%, 27% and 17%, respectively). The foveal thickness in the other intraretinal layers (except in the GCL+IPL and ONL+IS) showed a non-significant tendency towards thinning compared to DM eyes (see Table 4.1 and Figure. 4.2).

4.2.1.3 INTRARETINAL LAYER THICKNESS CHANGES IN THE PARAFOVEAL REGION

The RNFL, GCL+IPL and OS parafoveal thickness showed a significant decrease (7%, 8% and 13%, respectively) in MDR eyes compared to healthy eyes (see Figure 4.3 and Table 4.1). However, the parafoveal thickness in the other intraretinal layers (except

in the ONL+IS and RPE) showed a non-significant tendency towards thinning compared to healthy eyes.

When comparing MDR with DM eyes, the RNFL, GCL+IPL and OS parafoveal thickness showed a significant decrease (8%, 7% and 24%, respectively). The parafoveal thickness in the other intraretinal layers (except in the ONL+IS) showed a non-significant tendency towards thinning compared to DM eyes (see Table 4.1 and Figure. 4.3).

4.2.1.4 INTRARETINAL LAYER THICKNESS CHANGES IN THE PERIFOVEAL REGION

The RNFL and OS parafoveal thickness showed a significant decrease (8% and 13%, respectively) in the MDR eyes compared to healthy eyes (see Figure 4.4 and Table 4.1). The perifoveal thickness in the other intraretinal layers (except in the ONL+IS) showed a non-significant tendency towards thinning compared to healthy eyes.

When comparing MDR with DM eyes, the perifoveal thickness in the RNFL and OS showed a significant decrease (6% and 23%, respectively). The perifoveal thickness in the other intraretinal layers (except in the INL and ONL+IS) showed a non-significant tendency towards thinning compared to DM eyes (see Table 4.1 and Figure. 4.4).

4.2.1.5 THICKNESS CHANGES ACROSS ALL MACULAR REGIONS

A summary of the statistical analyses for thickness changes in each macular region and intraretinal layer is shown in Figure 4.5. It is worth noting that results across all macular regions were averaged in each eye. The thickness in each intraretinal layer was significantly thinner in the GCL+IPL, OPL and OS in the MDR eyes compared to healthy eyes. Moreover, Figure 4.5 clearly indicates that the statistically significant thickness changes observed in the GCL+IPL and OS were distributed across all macular

regions, while in the OPL, the thickness changes were only observed in the foveal region. Therefore, the GCL+IPL and OS showed diffuse thinning in MDR eyes.

When comparing MDR with DM eyes, a significant thickness change in the OS was also observed across all macular regions, while in the OPL, the significant thickness change was only observed in the foveal region. Therefore, the OS showed diffuse thinning in MDR eyes.

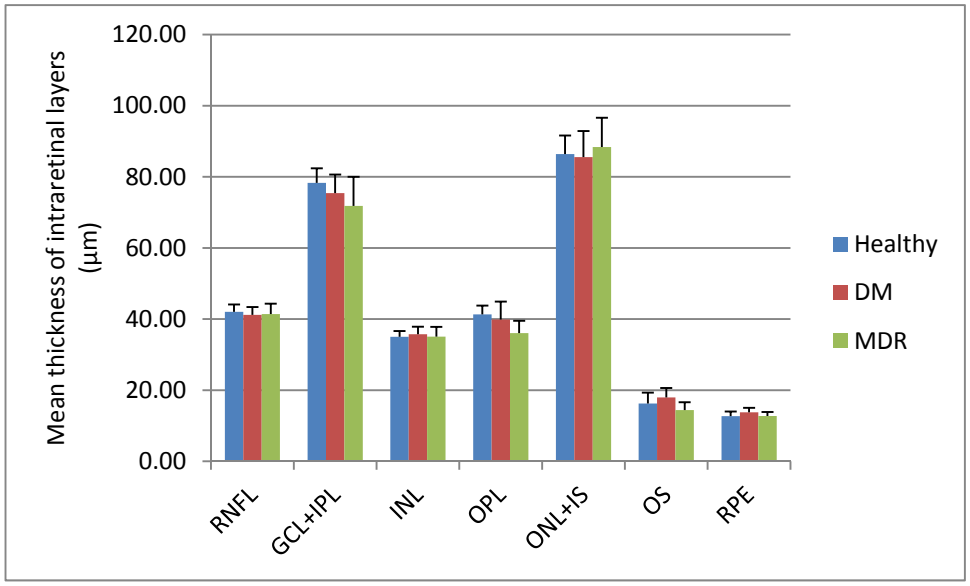

Figure 4.1 Thickness across all macular regions by study groups.

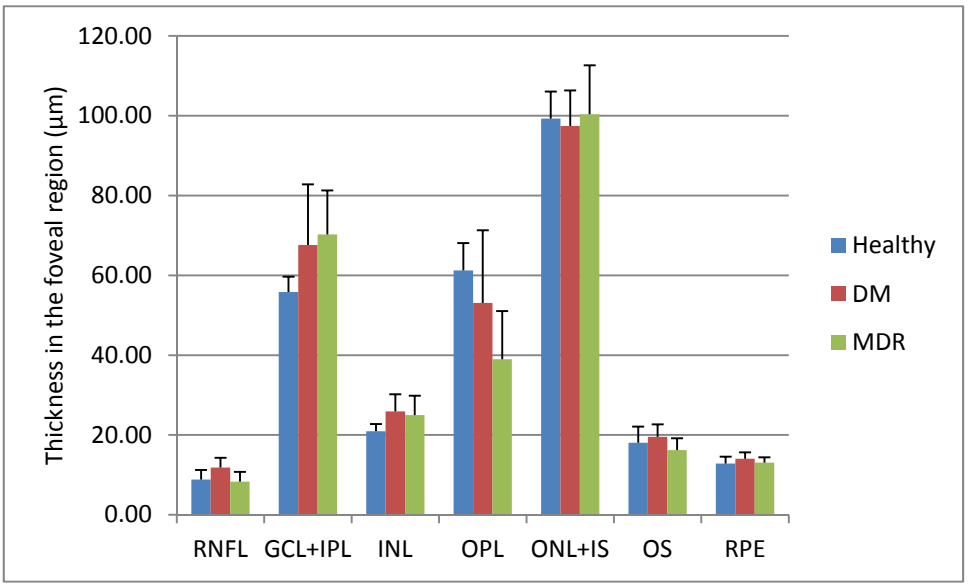

Figure 4.2 Thickness in the foveal region by study groups.

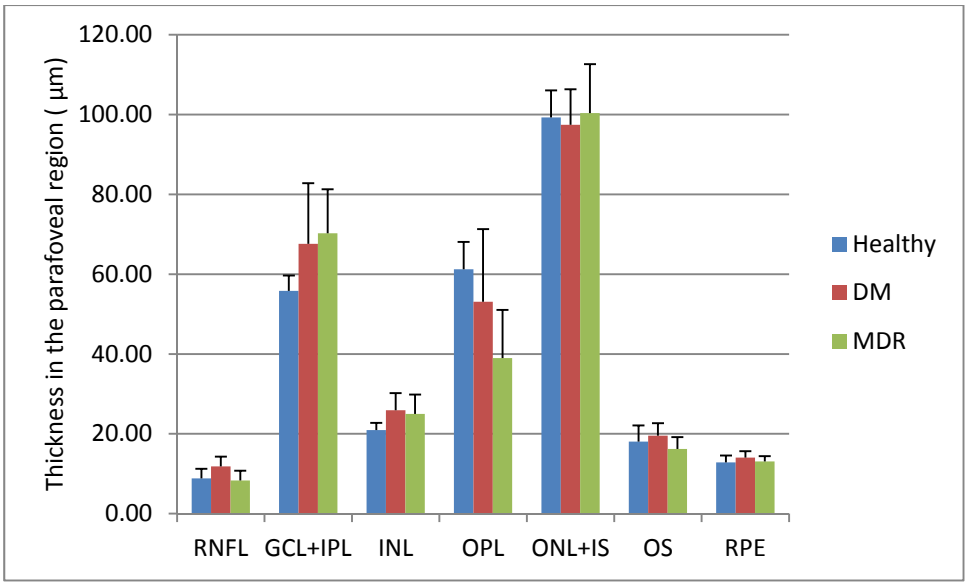

Figure 4.3 Thickness in the parafoveal region by study groups.

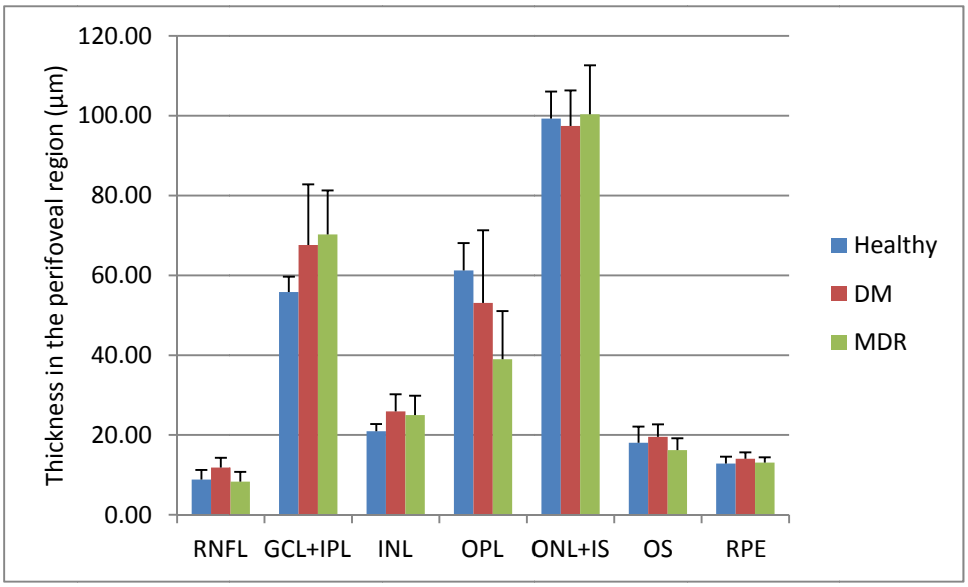

Figure 4.4 Thickness in the perifoveal region by study groups.

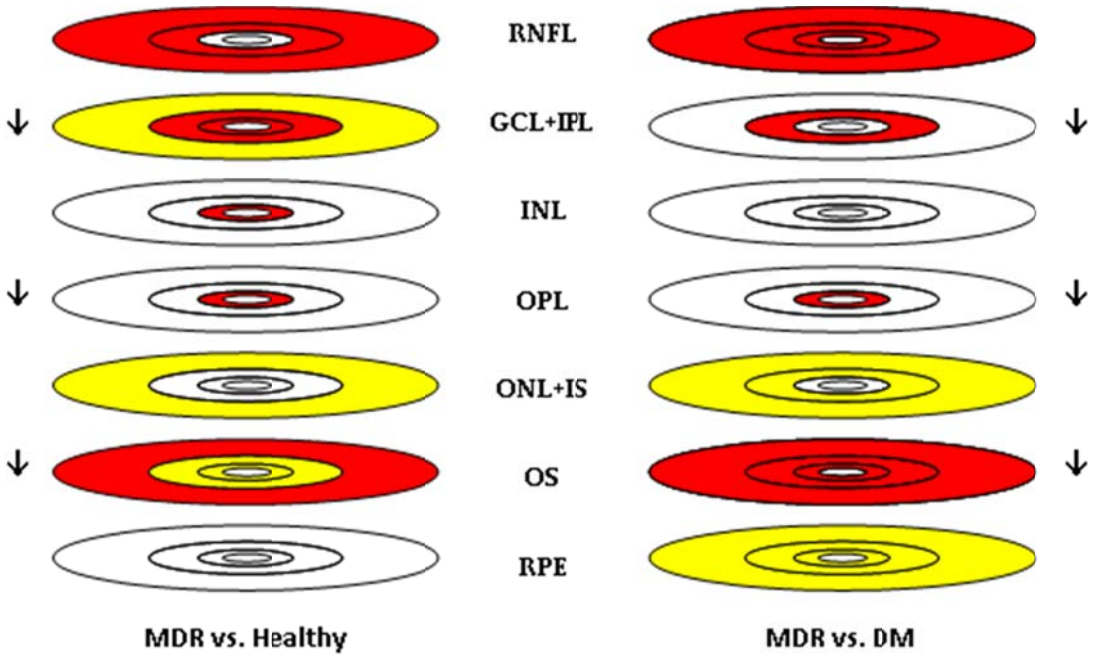

Figure 4.5 Thickness changes in each macular region and intraretinal layer for MDR vs. healthy and MDR vs. DM eyes. Comparisons were performed by using an ANOVA followed by Newman-Keuls post hoc analysis. The red and yellow color denotes $p<0.001$ and $0.001<p<0.05$, respectively. Arrows denote an increasing (decreasing) trend when pointing up (down).

4.2.2 TEXTURE PARAMETERS

Energy, entropy, correlation and contrast parameters were chosen to evaluate the OCT images by study group. The texture parameters extracted for each intraretinal layer and macular region in each eye are shown in Tables 4.2-4.6. The changes in texture parameters were investigated for the MDR group and compared to healthy and DM eyes.

4.2.2.1 TEXTURE PARAMETERS CHANGES OF INTRARETINAL LAYERS IN EACH EYE

When comparing MDR eyes with healthy eyes, the energy measurements showed a significant decrease in the INL and OPL (17% and 16%, respectively). The energy measurements appeared to have no significant changes in all other intraretinal layers except in the OS (see Table 4.2). The entropy measurement showed a statistically significant increase in the INL and OPL (22% and 13%, respectively). The entropy measurement showed a non-significant decrease in the RNFL and a non-significant increase in the OS when compared to healthy eyes (see Table 4.3). The correlation measurements showed a significant decrease in the OPL and a non-significant decrease in the RFL and INL; the correlation measurements in all other intraretinal layers were not significantly different from to healthy eyes (see Table 4.4). The contrast measurement showed a significant increase (5%, 59% and 55%, respectively) in the GCL+IPL, INL and OPL. Additionally, the contrast measurement showed a non-significant increase in all other intraretinal layers (see Table 4.5).

Moreover, when comparing MDR eyes with DM eyes, the energy measurement showed a significant increase (4%) in the RNFL and a significant decrease (6%) in the OS. Additionally, the energy measurement showed a non-significant decrease in the INL, OPL and OS (except in the ONL+IS; see Table 4.2). The entropy measurement showed a

significant decrease (5%) in the RNFL and showed a significant increase (4%) in the OS. The entropy measurement also showed a non-significant decrease in the ONL+IS and RPE and a non-significant increase in the INL and OPL (see Table 4.3). The correlation measurement showed a significant decrease (2%) in the OPL and a non-significant decrease in the INL and OPL (see Table 4.4). The contrast measurement showed a significant increase (18% and 17%, respectively) in the INL and OPL. However, a non-significant increase was observed in the GCL+IPL, ONL+IS and OS (see Table 4.5).

Overall, the comparisons indicated that the significant differences in intraretinal layers in terms of texture parameters were mainly found in the INL and OPL in the MDR eyes compared to healthy eyes. Additionally, when comparing MDR with DM eyes, the significant differences in texture parameters were mainly found in the RNFL, OPL and OS.

4.2.2.2 TEXTURE PARAMETERS CHANGES IN THE FOVEAL REGION

When comparing MDR with healthy eyes, the foveal energy measurements showed a significant decrease in the INL, OPL and OS (20%, 2% and 8%, respectively). The foveal energy showed a non-significant increase in all other intraretinal layers (except in the ONL+IS). The foveal entropy measurements showed a significant increase in the INL and a significant decrease in the OPL. Moreover, foveal entropy showed a non-significant increase in the ONL+IS and OS. The foveal correlation measurement in the RNFL, INL and OPL showed a significant decrease (13%, 4% and 5%, respectively). The foveal correlation measurements also showed a non-significant increase in the GCL+IPL, ONL+IS and OS. The foveal contrast measurements in the INL and OPL showed a significant increase (75% and 58%, respectively). In addition, the foveal

contrast showed a non-significant increase in the RNFL, ONL+IS and OS and a non-significant decrease in the GCL+IPL and RPE.

When comparing MDR with DM eyes, the foveal energy measurements showed a significant increase (9%) in the RNFL. Additionally, a significant decrease (8% and 10%, respectively) was observed in the INL and OS. There were no statistically significant changes in all other intraretinal layers (except in the ONL+IS). The foveal entropy measurement showed a significant decrease in the RNFL and OPL (23% and 2%, respectively) and a significant increase in the OS (11%). No statistically significant foveal entropy changes were found in the GCL+IPL and RPE. The foveal correlation measurement showed a significant decrease in the RNFL, INL and OPL (19%, 2% and 2%, respectively). No statistically significant foveal correlation changes were found in all other intraretinal layers except in the OS, where the foveal correlation measurement increased. The foveal contrast measurement showed a significant increase in the INL and OPL (21% and 20%, respectively). The contrast measurements in all other intraretinal layers showed no significant differences.

Overall, the comparisons indicated that significant differences in texture parameters in the foveal region were mainly found in the INL and OPL in the MDR eyes compared to healthy eyes. When comparing MDR with DM eyes, significant differences in texture parameters in the foveal region were mainly found in the RNFL, INL, OPL and OS.

4.2.2.3 TEXTURE PARAMETERS CHANGES IN THE PARAFOVEAL REGION

When comparing MDR with healthy eyes, the parafoveal energy measurement showed a significant increase (5%) in the RNFL and a significant decrease in the

GCL+IPL, INL, OPL and ONL+IS (5%, 5%, 5% and 3%, respectively). The parafoveal entropy measurement also showed a significant increase (11%, 6%, 6%and 15%, respectively) in the GCL+IPL, INL, OPL and ONL+IS. The parafoveal correlation measurements showed a significant decrease (8%) in the RNFL and a significant increase (2%, 3% and 3%) in the INL, OPL and ONL+IS. In addition, the parafoveal contrast measurement showed a significant increase (10%) in the GCL+IPL and a significant decrease (5%) in the OPL.

When comparing MDR with DM eyes, the parafoveal energy measurement showed a significant increase (6%) in the RNFL; a non-significant decrease was observed in all other intraretinal layers. The parafoveal entropy measurement parameters showed a significant increase (6%, 5% and 12%, respectively) in the INL, OPL and ONL+IS and a non-significant increase in the GCL+IPL, OS and RPE. The parafoveal correlation measurement showed a significant decrease (10%) in the RNFL and a non-significant increase in the INL, OPL, ONL+IS, OS and RPE. The parafoveal contrast measurement only showed a significant increase (8%) in the GCL+IPL.

Overall, the comparisons indicated that significant differences in texture parameters in the parafoveal region were mainly found in the GCL+IPL, INL, OPL and ONL+IS in the MDR compared to healthy eyes. Moreover, when comparing MDR with DM eyes, significant differences in the parafoveal region were found in the INL, OPL and ONL+IS for the entropy measurements only.

4.2.2.4 TEXTURE PARAMETERS CHANGES IN THE PERIFOVEAL REGION

When comparing MDR with healthy eyes, the perifoveal energy measurement showed a non-significant increase in the RNFL and GCL+IPL and a non-significant decrease in the OPL, ONL+IS, OS and RPE. The perifoveal entropy measurements

showed a significant decrease (4%) in the RNFL and a significant increase (10%) in the ONL+IS and a non-significant increase in the OPL and OS. The perifoveal correlation measurement showed a significant decrease in the RNFL and GCL+IPL. The perifoveal contrast measurement showed a significant increase in the RNFL and GCL+IPL (12% and 7%, respectively) and a non-significant decrease in the INL and ONL as well as a non-significant increase in the ONL+IS, OS and RPE.

When comparing MDR with DM eyes, the perifoveal energy measurement showed a non-significant increase in the RNFL and GCL+IPL as well as a non-significant decrease in the OPL, ONL+IS, OS and RPE without reaching statistical significance. The perifoveal entropy measurements showed a significant increase (2% and 8%, respectively) in the OPL and ONL+IS as well as a non-significant decrease in the RNFL and a non-significant increase in the. The perifoveal correlation measurement showed a significant decrease (8%) in the RNFL and a non-significant decrease in the OS. Moreover, the perifoveal contrast measurement showed a significant increase (8%) in the RNFL and a non-significant increase in the GCL+IPL, ONL+IS, OS and RPE as compared to DM eyes.

Overall, the comparisons indicated that significant differences in texture parameters in the perifoveal region were mainly found in the RNFL and GCL+IPL in MDR eyes compared to healthy eyes. Compared to DM eyes, significant differences in texture parameters in the perifoveal region were mainly found in the RNFL for the MDR group.

4.2.2.5 TEXTURE PARAMETERS CHANGES ACROSS ALL MACULAR REGIONS

Our previous results in each macular region demonstrated that more significant differences between groups were observed for the contrast parameters among the selected texture parameters; a summary of the statistical trends in each macular region and for each intraretinal layer is shown in Figure 4.6. In general, the contrast measurements (in each intraretinal layer) showed a significant increase in the GCL+IPL, INL and OPL when comparing MDR with healthy eyes. Additionally, the contrast measurements in the MDR group showed a significant increase in the INL and OPL as compared to DM eyes.

As seen in Figure 4.6, when comparing MDR with healthy eyes, a diffuse contrast change in the GCL+IPL and OPL is observed across the foveal, parafoveal and perifoveal regions. However, in the INL, the contrast difference was only observed in the foveal region. When comparing MDR with DM eyes, a similar trend was observed for the INL and OPL, where statistically significant changes were only observed in the foveal region.

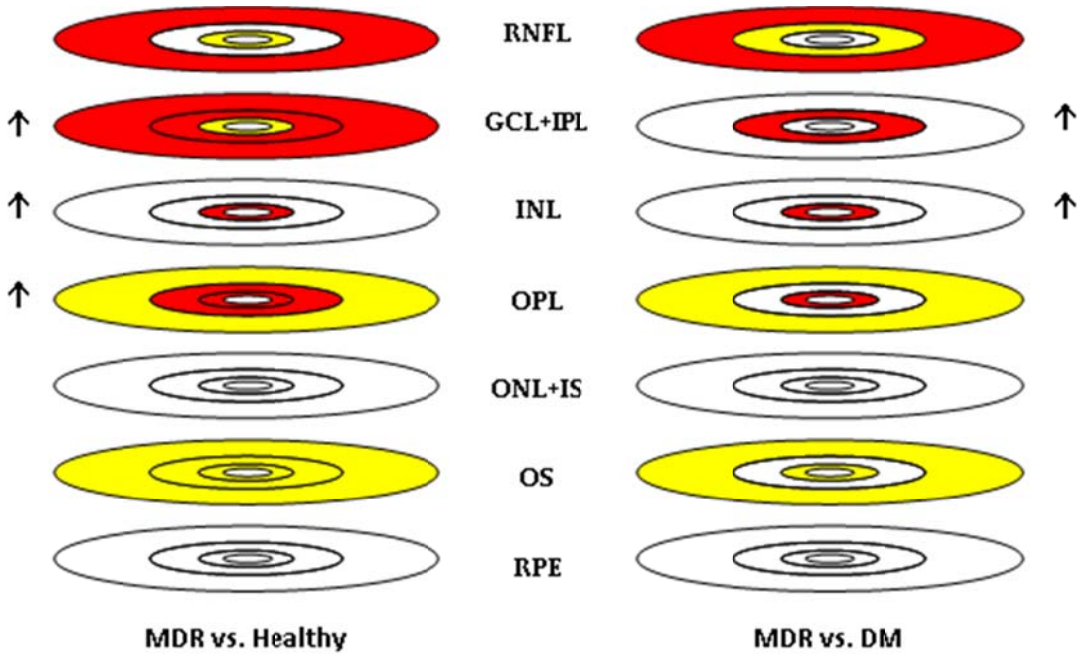

Figure 4.6 Contrast changes in each macular sector in each intraretinal layer for MDR vs. healthy and MDR vs. DM. Comparisons were performed using ANOVA followed by Newman-Keuls post hoc analysis. The red and yellow color denotes $p<0.001$ and $0.001<p<0.05$, respectively. Arrows denote an increasing (decreasing) trend when pointing up (down).

4.2.3 FRACTAL DIMENSION MEASUREMENTS

Conventionally, the fractal dimension is used to describe the roughness of an object's surface. For various texture parameters, the fractal dimension can be more capable of evaluating the internal structural change. Therefore, structure disorder in the retinal tissue can be assessed when the fractal dimension is calculated using the intensity profile along the direction of depth in OCT images.

The fractal dimension in each macular region was calculated for each intraretinal layer and all study groups. The fractal dimension changes were compared using ANOVA followed by Newman-Keuls post-hoc analysis between the MDR eyes, healthy eyes and DM eyes. Statistically significant fractal dimension changes are shown in Table 4.6.

4.2.3.1 FRACTAL DIMENSION CHANGES ACROSS ALL MACULAR REGIONS

The fractal dimension results in each intraretinal layer by study group are shown in Figure 4.7 and Table 4.6. The results indicated that compared to healthy eyes, MDR eyes had significant differences in the fractal dimension in the RNFL, GCL+IPL, INL, OPL and OS. Specifically, the fractal dimension decreased 6% in the GCL+IPL and increased 3% in the OPL as compared to healthy eyes. The fractal dimension in the ONL+IS showed a non-significant increase.

When comparing MDR with DM eyes, the fractal dimension had a significant increase (4%, 2%, 2% and 1%) in the RNFL, OPL, OS and RPE and a significant decrease (3%) in the GCL+IPL in MDR eyes; a non-significant increase was observed in the INL and ONL+IS.

4.2.3.2 FRACTAL DIMENSION CHANGES IN THE FOVEAL REGION

The foveal fractal dimension results are shown in Figure 4.8 and Table 4.6. When comparing MDR and healthy eyes, the foveal fractal dimension measurement showed a statistically significant decrease (18% and 4%, respectively) in the GCL+IPL and INL; and a statistically significant increase in the OPL and OS in the MDR group. Particularly, the foveal fractal dimension measurement increased 11% in the OPL. In addition, the foveal fractal dimension measurement in all other intraretinal layers showed an increasing trend without reaching statistical significance.

When comparing MDR and DM eyes, the foveal fractal dimension measurement showed a statistically significant increase (6%, 6% and 1%) in the RNFL, OPL and OS while a statistically significant decrease (9%) was observed in the GCL+IPL of MDR eyes.

4.2.3.3 FRACTAL DIMENSION CHANGES IN THE PARAFOVEAL REGION

The foveal fractal dimension results are shown in Figure 4.8 and Table 4.6. When comparing MDR with healthy eyes, the foveal fractal dimension was significantly lower in the GCL+IPL and INL (18% and 4%, respectively) and significantly higher in the OPL and OS in the MDR group. Specifically, the foveal fractal dimension increased 11% in the OPL. In addition, the foveal fractal dimension in all other intraretinal layers showed a non-significant increase.

When comparing MDR with DM eyes, the foveal fractal dimension showed a significant increase (6%, 6% and 1%) in the RNFL, OPL and OS, while a significant decrease (9%) was observed in the GCL+IPL of MDR eyes.

4.2.3.4 FRACTAL DIMENSION CHANGES IN THE PERIFOVEAL REGION

The perifoveal fractal dimension measurements by study groups are shown in Figure 4.10 and Table 4.6. When comparing MDR eyes with healthy eyes, the perifoveal fractal dimension was significantly increased in the OS (2%). Moreover, a non-significant increase was observed in the RNFL and ONL+IS.

When comparing MDR eyes with DM eyes, the perifoveal fractal dimension was significantly increased in the OS and RPE. Additionally, the perifoveal fractal dimension in all other intraretinal layers except in the RNFL showed no statistically significant changes.

4.2.3.5 FRACTAL DIMENSION CHANGES ACROSS ALL MACULAR REGIONS

Distribution statistics of the fractal dimension results across all macular regions for each intraretinal layer are shown in Figure 4.11. The results across all macular regions were averaged per eye. The results indicated that fractal dimension measurements of

intraretinal layers are statistically significant and different in the RNFL, GCL+IPL, INL, OPL and OS of MDR eyes compared to healthy eyes. The fractal dimension across all macular regions was significantly different in the RNFL, GCL+IPL, OPL, OS and RPE of MDR eyes compared to DM eyes.

As seen in the scan results (Figure 4.11 and Table 4.6), the fractal dimension in the foveal region was significantly different for the same intraretinal layer where the fractal dimension measurement across all regions was significantly different, except for one case (in the RNFL between the MDR eyes and healthy eyes). The statistically significant trend in the RNFL across all regions is mainly due to changes in the fractal dimension in the parafoveal and perifoveal region when comparing MDR eyes to healthy eyes.

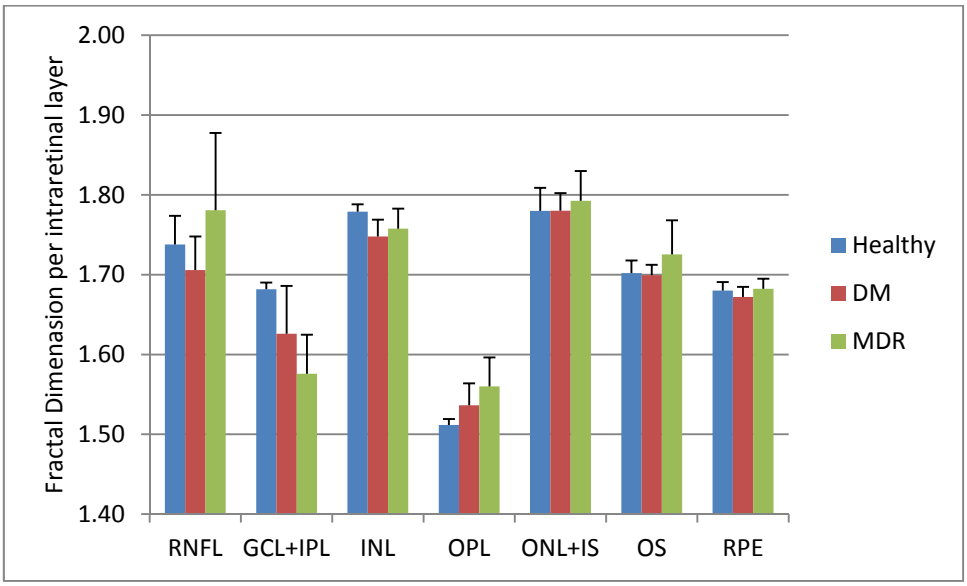

Figure 4.7 Fractal dimension per intraretinal layer by study groups.

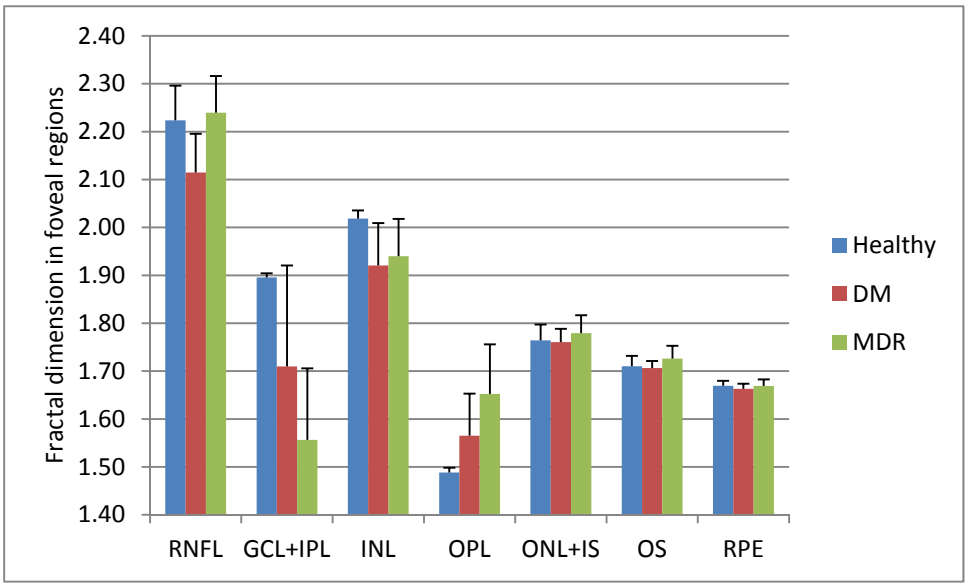

Figure 4.8 Fractal dimension in the fovea region by study groups.

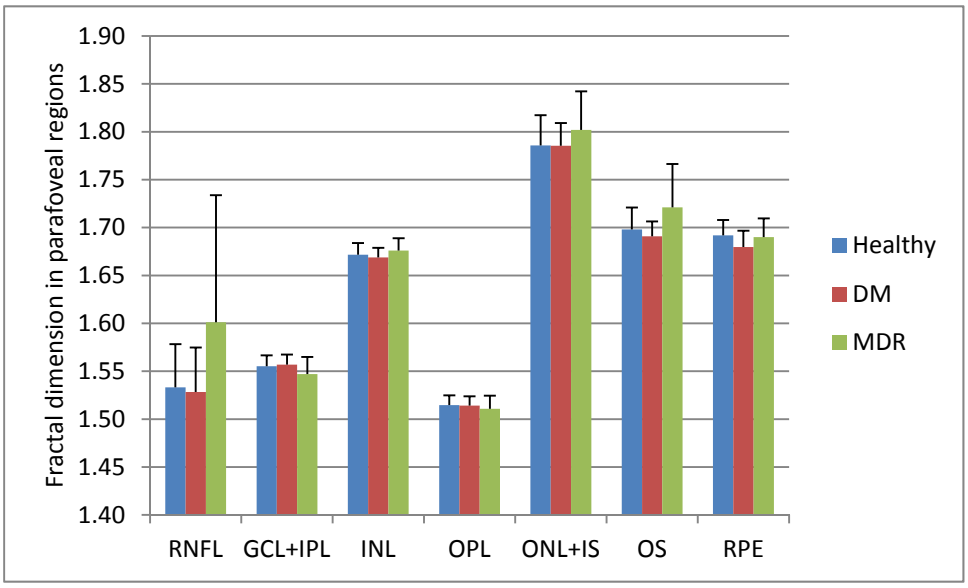

Figure 4.9 Fractal dimension in the parafoveal region by study groups.

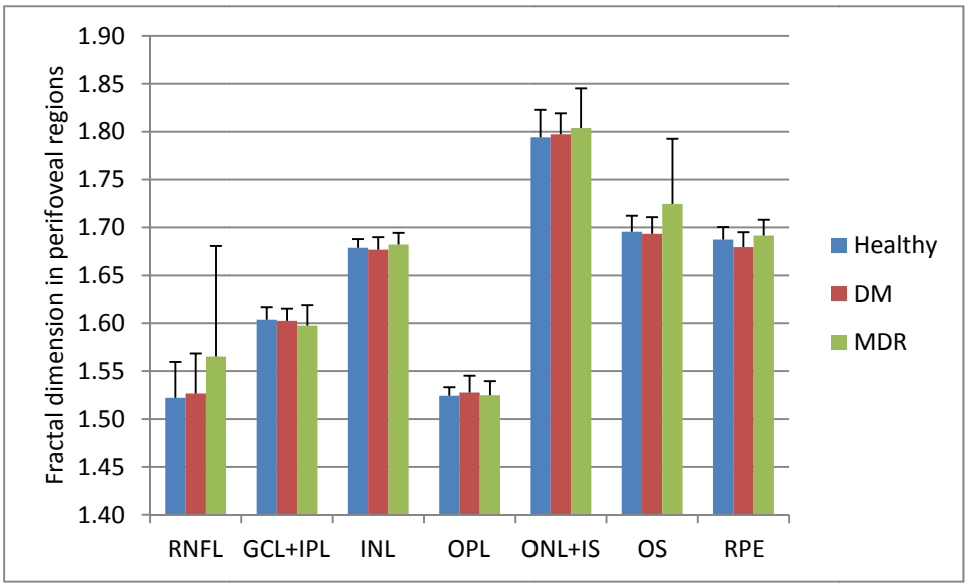

Figure 4.10 Fractal dimension in the perifoveal region by study groups.

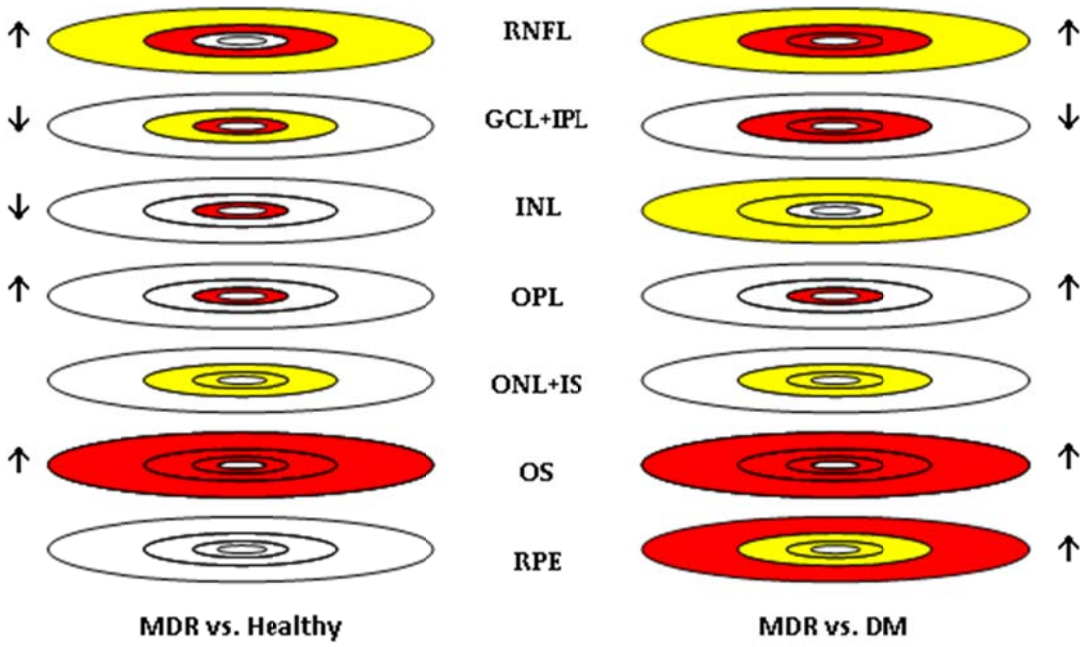

Figure 4.11 Fractal dimension changes in each macular region and intraretinal layer for MDR vs. Healthy and MDR vs. DM eyes. Comparisons were performed using ANOVA followed by Newman-Keuls post hoc analysis. The red and yellow color denotes $p<0.001$ and $0.001<p<0.05$, respectively. Arrows denote an increasing (decreasing) trend when pointing up (down).

4.3 RECEIVER OPERATING CHARACTERISTIC (ROC) ANALYSIS

In the previous section, structural characteristics were extracted from OCT images and their changes were investigated for each intraretinal layer in predefined macular regions and across all macular regions. Statistically significant changes in these parameters in each macular region were found in several particular intraretinal layers and therefore were used to discriminate the MDR eyes from healthy and DM eyes. As demonstrated by our results, thickness and fractal dimension parameters appear to more powerfully discriminate the MDR eyes from healthy eyes or DM eyes. However, the discriminating power of these two structural parameters in each macular region needs to be determined. Accordingly, a receiver operating characteristic (ROC) analysis was utilized to determine the discriminating power of the fractal dimension and thickness parameters in each macular region. An area under the ROC (AUROC) curve was calculated. An area under the curve of 1.0 indicates perfect discrimination, while an AUROC of 0.50 indicates no discrimination.

4.3.1 ROC ANALYSIS FOR THICKNESS MEASUREMENTS

The ROC analyses with corresponding sensitivity and specificity tests were only performed for intraretinal layers that showed significant thickness differences in each macular region when comparing MDR eyes to healthy and DM eyes. These layers were the RNFL, GCL+IPL, OPL and OS. The ROC curves are shown in figures 4.12 and 4.13. AUROC values are shown in Table 4.9 for each discrimination test. Cutoff values of thickness measurements derived from the ROC analyses are shown in Table 4.10 and Table 4.11.

When comparing MDR with healthy eyes, the highest AUROC values were observed in the GCL+IPL, OPL and OS (0.76, 0.88 and 0.67, respectively). The cutoff point for the GCL+IPL was suggested to be 75.86 µm with a sensitivity and specificity of 0.74 and 0.64, respectively. The cutoff point for the OPL was suggested to be 38.12 µm with a sensitivity and specificity of 0.91 and 0.81, respectively. Moreover, the cutoff point for the OS was suggested to be 14.59 µm with a sensitivity and specificity of 0.68 and 0.58, respectively. Additionally, by observing and comparing ROC curves (see Figure 4.12), we found that the most significant thickness changes were obtained for the GCL+IPL, OPL and OS in the parafoveal, foveal and perifoveal macular region, respectively. In the parafoveal region, the AUROC for the GCL+IPL was 0.72 with a cutoff point of 92.00 µm. Similarly, the AUROC for the OPL (OS) in the foveal (perifoveal) region was 0.91 (0.87) with a cutoff point of 49.66 (13.84) µm.

The highest AUROC values obtained when comparing MDR with DM eyes were observed in the OPL and OS (0.73 and 0.86, respectively). The cutoff point for the OPL was suggested to be 35.94 µm with a sensitivity and specificity of 0.71 and 0.61, respectively. The cutoff point for the OS was suggested to be 15.41 µm with a sensitivity and specificity of 0.82 and 0.72, respectively. By observing and comparing the ROC curves (see Figure 4.13), we found that the most significant thickness changes were observed in the OPL in all macular regions (i.e., foveal, parafoveal and perifoveal regions). The AUROC for the OPL in the foveal region was estimated to be 0.74 with a cutoff point of 36.33 µm. The AUROC for the OPL in the perifoveal (parafoveal) region was estimated to be 0.87 (0.86) with a cutoff point of 13.84 (14.23) µm.

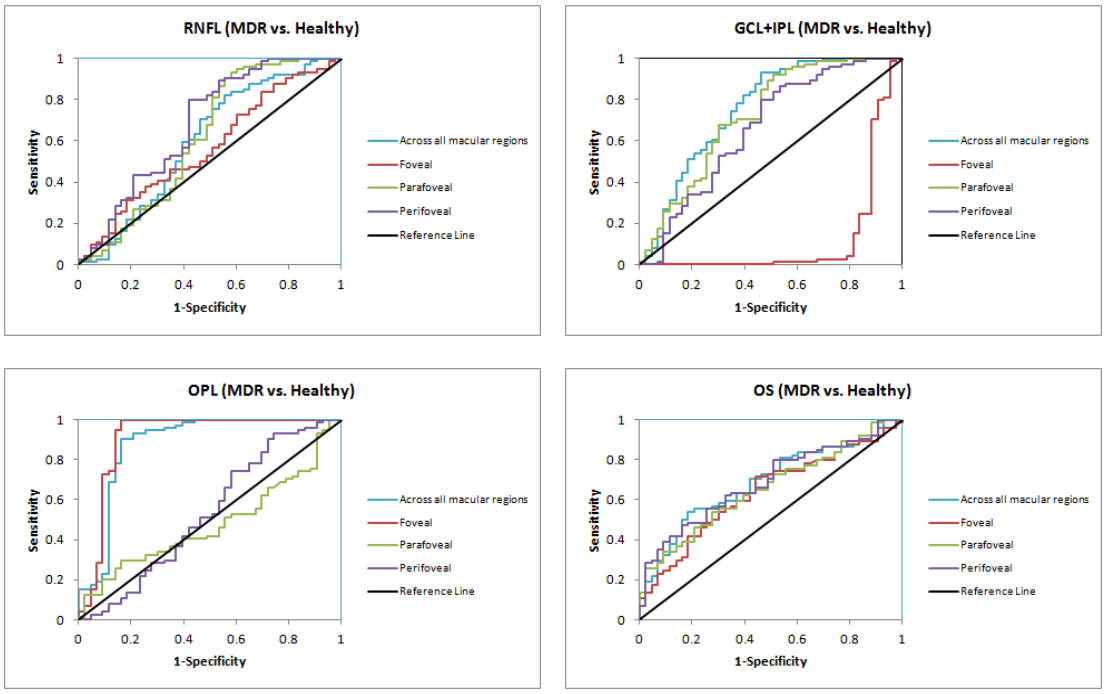

Figure 4.12 Receiver operating characteristic (ROC) curves for the detection of early diabetic retinopathy using thickness measurements of the RNFL, GCL+IPL, OPL and OS as predictor variables when comparing MDR with healthy eyes.

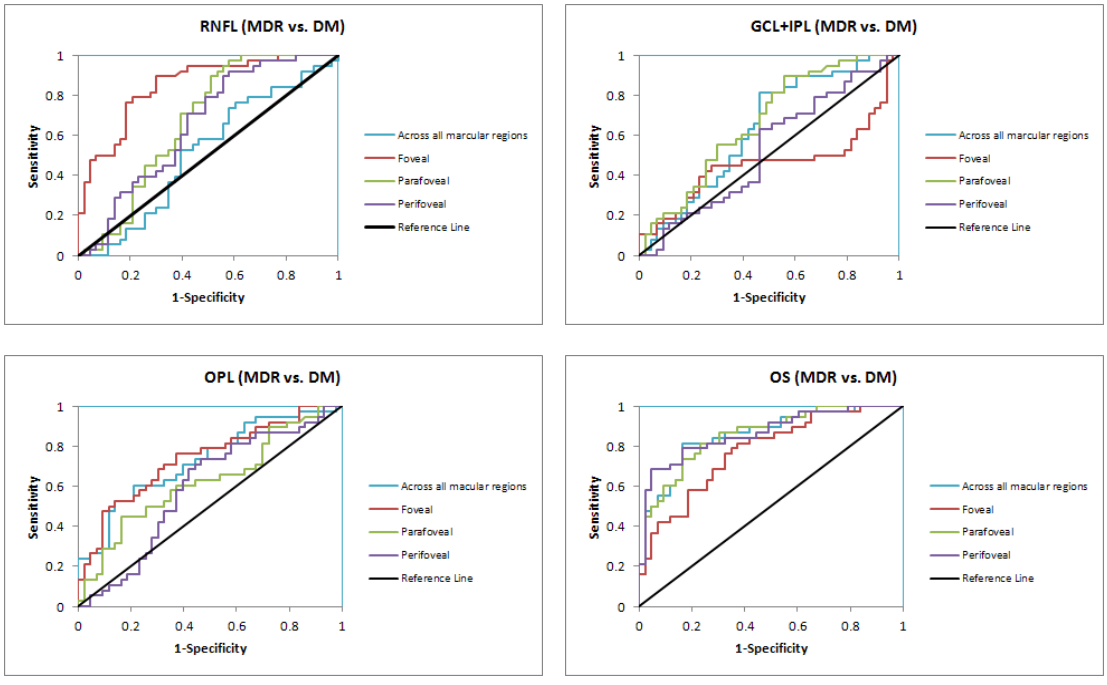

Figure 4.13 Receiver operating characteristic (ROC) curves for the detection of early diabetic retinopathy using thickness measurements of the RNFL, GCL+IPL, OPL and OS as predictor variables when comparing MDR with DM eyes.

4.3.2 ROC ANALYSIS FOR FRACTAL DIMENSION MEASUREMENTS

The ROC analyses with corresponding sensitivity and specificity values were only performed for intraretinal layers that showed significant differences in the fractal dimension both across all macular regions and in each macular region. AUROC and cutoff values are shown in Table 4.12 and Tables 4.13-4.15, respectively.

The highest AUROC values estimated for the fractal dimension measurements were observed in the GCL+IPL and INL (0.95 and 0.79, respectively) when comparing MDR with healthy eyes. The cutoff point for the GCL+IPL was suggested to be 1.66 with a sensitivity and specificity of 0.98 and 0.88, respectively. The cutoff point for the INL was suggested to be 1.77 with a sensitivity and specificity of 0.80 and 0.70, respectively. Moreover, ROC curves indicated that the most significant thickness changes were observed in the GCL+IPL and INL in the foveal region (see Figure 4.14). In this region, the AUROC for the GCL+IPL (INL) was estimated to be 0.96 (0.83) with a cutoff point of 1.85 (2.00) (sensitivity: 1.00 (0.84) and specificity: 0.90 (0.74).

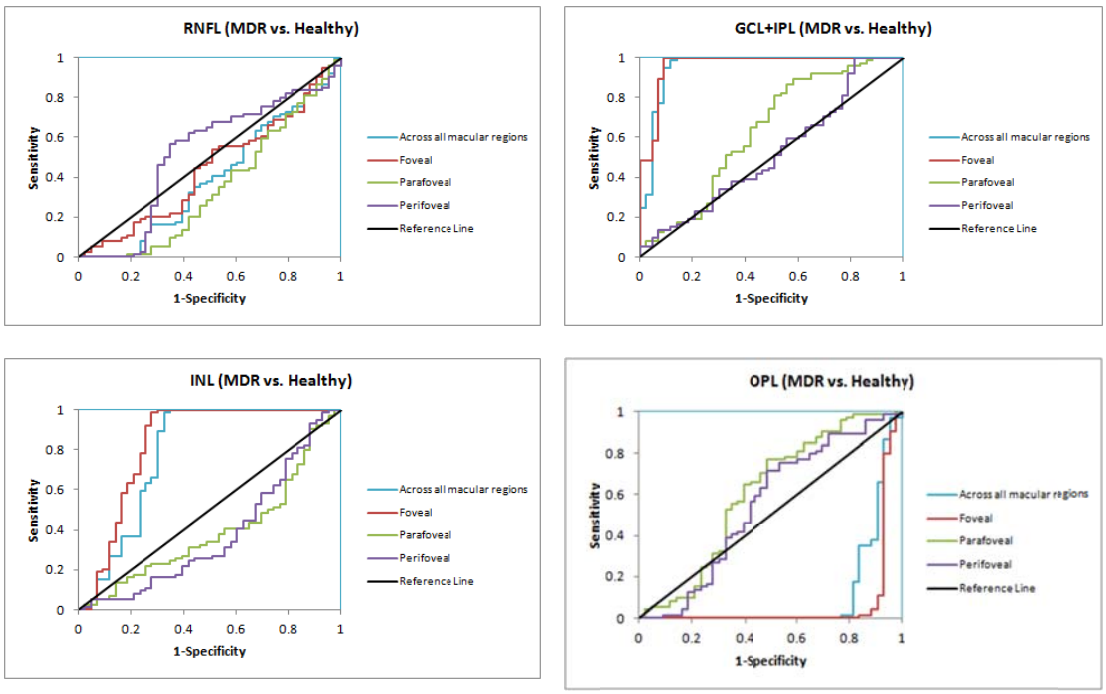

Figure 4.14 Receiver operating characteristic (ROC) curves for the detection of early diabetic retinopathy using fractal dimension measurements of the RNFL, GCL+IPL INL and OPL as predictor variables when comparing MDR with healthy eyes.

The highest AUROC value was observed in the GCL+IPL (0.77) when comparing MDR with DM eyes. The cutoff point for the GCL+IPL was suggested to be 1.75 with a sensitivity and specificity of 0.55 and 0.45, respectively. Moreover, ROC curves indicated that the most significant fractal dimension changes were observed for the GCL+IPL in the foveal region (see Figure 4.15). The AUROC was estimated to be 0.77 with a suggested cutoff point of 1.49 (sensitivity: 0.74 and specificity: 0.64).

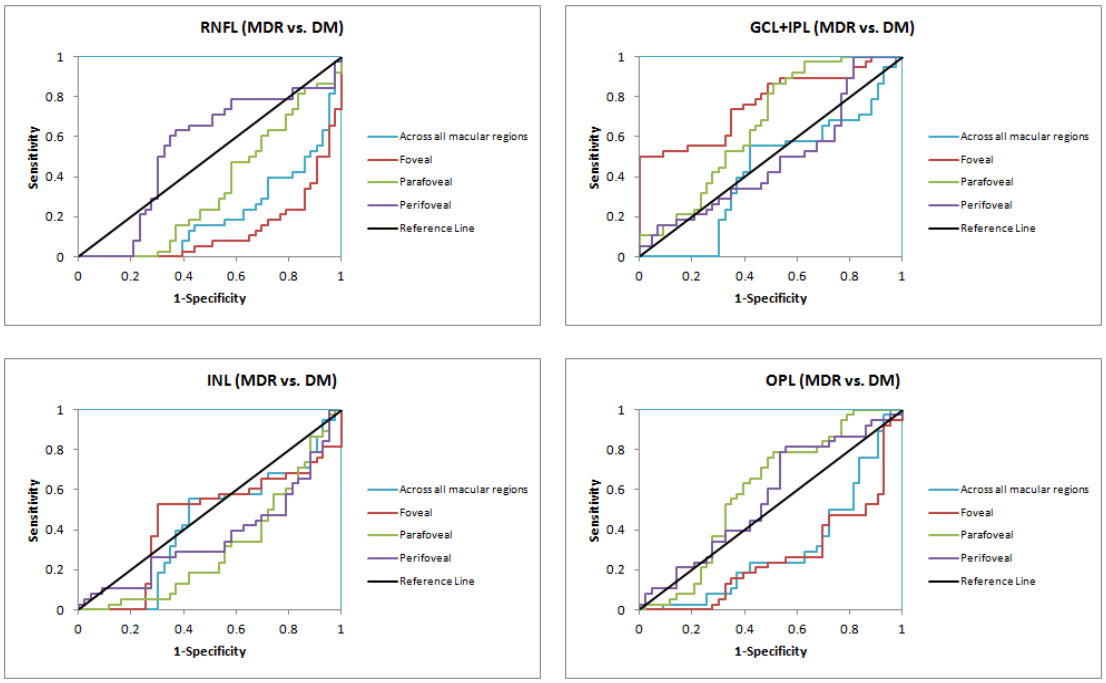

Figure 4.15 Receiver operating characteristic (ROC) curves for the detection of early diabetic retinopathy using fractal dimension measurements of the RNFL, GCL+IPL INL and OPL as predictor variables when comparing MDR with DM eyes.

4.4 SUMMARY

In this chapter, we used structural parameters such as thickness and fractal dimension to look for indicators of early retinopathy in the diabetic macula. OCT is typically employed for the measurement of retinal thickness. However, texture measurements may provide additional information to characterize abnormalities in the early stages of retinopathy. Therefore, changes in texture descriptors may provide further information regarding cellular layers and early damage in diabetic ocular disease.

Our findings indicate that the thickness of the GCL+IPL complex, OPL and OS showed a significant decrease (8%, 13% and 10%, respectively) in MDR eyes compared to controls. The thickness in the other layers (except in the ONL+IS and RPE) showed a non-significant tendency towards thinning as compared to DM and healthy eyes. The thickness of the OPL and OS showed a significant decrease (10% and 19%, respectively)

in the MDR eyes compared to eyes in the DM group. Moreover, the fractal dimension increased for all layers (except the GCL+IPL and INL) in MDR eyes compared to controls. When comparing MDR with DM eyes, the fractal dimension increased for all layers (except the GCL+IPL).

Our results indicated that significant thickness differences (mean values) between study groups, particularly for the GCL+IPL, OP and OS, were in the range of 1 to 8 microns. These differences were obtained after extracting the mean thickness of each intraretinal layer, which was calculated by averaging the local thickness measurement across all A-scans in each B-scan. It is worth noting that the axial resolution of the Stratus OCT is less than 10 microns, according to the manufacturer's data, but the B-scan's pixel resolution is 2 μm (across the retinal tissue depth). Therefore, thickness differences (i.e., mean values) between study groups were around or less than the stated Stratus OCT resolution data. For example, the absolute value of the mean thickness difference (across all macular regions) for the GCL+IPL was 6.50 μm when comparing MDR and healthy groups, which is less than the axial resolution (10 μm) but greater than the pixel resolution (across the retinal tissue depth).

Moreover, our results are consistent with results from a similar study using the Stratus OCT. Specifically, a mean thickness difference of 5.42 μm was observed in the pericentral ETDRS region between MDR and healthy eyes for the GCL+IPL complex. The thickness variation of the GCL+IPL was in the range of 2.26 μm to 8.56 μm.[145] Similarly, our results showed that a mean thickness difference of 7.98 μm was observed in the perifoveal (i.e., pericentral as in ETDRS regions) macular region between MDR and healthy eyes for the GCL+IPL complex. The thickness variation of the GCL+IPL

was in the range of 5.73 μm to 11.2 μm. We also note that our smaller thickness measurement variability could be related to the reduced interpolation error and improved accuracy near the foveal region as a result of our custom-built macular region analysis.

Furthermore, the ROC analysis shows that some structural and texture-derived parameters are superior to the standard thickness measurements. Specifically, when comparing MDR eyes with DM and control eyes, we found that the thickness of the inner retinal layers (RNFL and the GCL+IPL complex) was significantly better at diagnosing early DR compared to the total retinal thickness measured by OCTRIMA.[33, 52] This result indicates that isolating the inner layers from the outer retinal layers improved diagnostic power. This could be justified by the fact the outer retinal layers, which are not as affected by DR, take up 60% to 70% of the total retinal thickness. Therefore, these outer layers could add variation in thickness that decreases the diagnostic discriminating power. The highest AUROC values estimated for thickness were observed for the GCL+IPL complex and OPL when comparing MDR with healthy eyes and for the OS when comparing MDR with DM eyes. In addition, the highest estimated values for the fractal dimension were observed for the GCL+IPL when comparing MDR with healthy and DM eyes. Interestingly, the highest AUROC values estimated for the fractal dimension were observed in the INL when comparing DM with healthy eyes.

The maximum discrimination value for intraretinal thickness, as assessed by the c-statistic, was 0.87 for the OPL and 0.76 for the GCL+IPL complex and was obtained at a thickness of ≤ 38.12 μm and 75.86 μm, respectively. In a comparison of randomly selected diabetic subjects and control subjects, this result implies there is an 88% (76%) probability that the diabetic subject will have an abnormal OPL (GCL+IPL) thickness

value. The ≤ 38.12 (75.86) µm threshold for the OPL (GCL+IPL) coincides with the mean ± SD for the OCT measurements. At this value, the sensitivity for the OPL (GCL+IPL) is 91% (74%) with a specificity of 81% (64%). Similarly, the maximum discrimination value for a fractal dimension of 0.95 for the GCL+IPL complex was obtained at a FD ≤ 1.66 (see Tables 7 and 9). Therefore, there is a 95% probability that the diabetic subject will have an abnormal GCL+IPL structure (i.e., disordered structure compared to controls). The ≤ 1.66 threshold for the GCL+IPL complex coincides with the mean ± SD for the OCT measurements. At this value, the sensitivity for the GCL+IPL complex is 98% with a specificity of 88%.

Compared to the standard thickness measurements provided by OCT devices, the combination of thickness and the fractal dimension was significantly better at discriminating MDR eyes from healthy and DM eyes. Thus, the diagnostic power was improved by adding diagnostic parameters measured locally and based on texture descriptors in diabetic eyes. Our results showed that when looking for abnormalities in the GCL+IPL complex, OPL and OS could detect DR earlier.

In general, thickness and fractal dimension showed better discriminating power for retinal abnormalities localized in the inner retina (mainly in the GCL+IPL complex) between MDR eyes and healthy eyes. When comparing MDR with healthy eyes, thickness showed better discriminating power for outer retinal abnormalities localized in the OPL. When comparing MDR with DM eyes, thickness showed better discriminating power for outer retinal abnormalities localized in the OPL and OS. In addition, when comparing MDR with DM eyes, the fractal dimension showed better discriminating power for inner retinal abnormalities localized in the GCL+IPL complex. Moreover, for

the diagnosis of MDR versus control and DM eyes, we found no advantage in using texture measures such as energy, contrast, homogeneity, entropy and correlation.

Our results suggest that the RNFL, GCL+IPL complex, OPL and OS are more susceptible to initial damage when comparing MDR with control and DM eyes. Specifically, the trend observed for the thickness (thinning) of the RNFL and GCL+IPL complex in MDR eyes might be associated with pathological metabolic changes in the retina and may reflect neurodegenerative changes in the diabetic retina. These findings also have possible implications for the early detection of macular damage associated with diabetes. Because the macular region is rich in retinal ganglion cells, diabetic damage to this central region might occur early in the disease process. In fact, animal models of DR show significant loss of macular ganglion cells.[93-97] Interestingly, our results showed for the first time that the thickness of the OPL in MDR eyes was significantly reduced compared with similar measures in healthy eyes. This result is supported by previous results from in vitro and in vivo experiments inducing apoptosis in animal models of diabetic eyes.[94] Previous studies have shown that not only are retinal pericytes and endothelial cells susceptible to hyperglycemia, but neuroglial elements of the retina are also involved in the retinal damage caused by diabetes.[93, 95] According to Barber and colleagues, apoptotic cells are likely to include ganglion cells and other neurons in the retina (such as cells of the plexiform and nuclear layers).[98, 99] Thus, the possibility that damage to the neuroglial retina causes or contributes to the capillary degeneration may be consistent with evidence that neuroglial degeneration precedes the degeneration of retinal capillaries in diabetic retinopathy.[88]

Interestingly, a significant decrease in the fractal dimension was only observed for the GCL+IPL complex of MDR eyes compared to controls. This result is in agreement with previous reports showing a significant reduction of the fractal dimension during induced apoptosis throughout early apoptotic phases in breast cancer cells.

In summary, we have introduced a novel approach using thickness- and texture-based diagnostic parameters to predict early DR. The structural parameters analyzed for the particular intraretinal layers (GCL+IPL, OPL and OS) were able to discriminate diabetic eyes with early retinopathy from healthy and diabetic eyes with a higher sensitivity and specificity than standard thickness parameters. These results validate the observations and provide some potential for therapeutic interventions to prevent early DR in diabetic subjects. Given the results from our study, we conclude that obtaining the fractal dimension as well as thickness measurements for the RNFL, GCL+IPL complex, OPL and OS may be a beneficial tool for diagnosing early diabetic retinopathy in DM patients. In our population (or a similar population), a GCL+IPL (OPL) thickness of $\leq$ 75.85 (38.12) µm and a GCL+IPL fractal dimension of $\leq$ 1.66 can be used to select diabetic patients who may benefit from trials of interventions to prevent the onset of diabetic retinopathy. We conclude that our novel approach using structural and texture-based parameters extracted from OCT images could have the potential to differentiate diabetic eyes with early retinopathy from healthy and diabetic eyes without retinopathy.

Table 4.1 Distribution statistics of thickness (µm) measurements by study groups

Thickness (µm)	Healthy	DM	MDR
Across All Macular Regions			
RNFL	42.02 ± 2.11	41.19 ± 2.19	41.38 ± 2.93
GCL+IPL	78.30 ± 4.09	75.41 ± 5.23 †	71.80 ± 8.22 ‡
INL	35.02 ± 1.60	35.74 ± 2.13	35.05 ± 2.76
OPL	41.30 ± 2.49	39.88 ± 5.04 ‡	36.07 ± 3.45 ‡
ONL+IS	86.41 ± 5.21	85.55 ± 7.32	88.39 ± 8.21
OS	16.27 ± 3.06	17.97 ± 2.64 ‡	14.40 ± 2.20 ‡
RPE	12.71 ± 1.32	13.78 ± 1.28 ‡	12.76 ± 1.09
Foveal Region			
RNFL	8.85 ± 2.37	11.83 ± 2.45 ‡	8.30 ± 2.44
GCL+IPL	55.80 ± 3.87	67.58 ± 15.20	70.26 ± 11.02 ‡
INL	20.93 ± 1.82	25.89 ± 4.30	25.00 ± 4.85 ‡
OPL	61.24 ± 6.83	53.08 ± 18.22 ‡	38.97 ± 12.09 ‡
ONL+IS	99.26 ± 6.79	97.42 ± 8.92	100.35 ± 12.27
OS	18.05 ± 4.03	19.53 ± 3.14 ‡	16.22 ± 2.96 †
RPE	12.84 ± 1.72	14.06 ± 1.59 †	13.10 ± 1.32
Parafoveal Region			
RNFL	33.72 ± 1.85	34.16 ± 1.48 ‡	31.33 ± 5.23 ‡
GCL+IPL	94.71 ± 5.73	92.93 ± 6.75 ‡	86.73 ± 11.2 ‡
INL	39.60 ± 2.17	40.49 ± 2.68	39.24 ± 3.32
OPL	37.17 ± 2.68	38.15 ± 2.54	37.07 ± 2.21
ONL+IS	84.89 ± 6.11	83.24 ± 8.16 †	86.85 ± 8.35
OS	14.80 ± 3.58	16.97 ± 2.99 ‡	12.84 ± 2.50 †
RPE	11.57 ± 1.59	13.08 ± 1.74 †	12.02 ± 1.64
Perifoveal Region			
RNFL	41.87 ± 2.94	41.39 ± 2.68 ‡	38.7 ± 5.47 ‡
GCL+IPL	67.36 ± 4.52	64.39 ± 6.07	63.89 ± 8.40 †
INL	33.00 ± 1.67	33.38 ± 1.91	32.77 ± 3.12
OPL	31.54 ± 1.38	31.86 ± 1.49	31.49 ± 2.17
ONL+IS	75.27 ± 4.84	74.67 ± 7.01 †	78.01 ± 6.50 †
OS	14.59 ± 2.81	16.45 ± 2.64 ‡	12.72 ± 2.31 ‡
RPE	12.54 ± 1.39	13.33 ± 1.51 †	12.44 ± 1.34

† $0.001<p<0.05$ and ‡ $p<0.001$ (ANOVA followed by Newman-Keuls post hoc analysis) between MDR and healthy eyes (see MDR column) and between MDR and DM eyes (see DM column).

Table 4.2 Distribution statistics of energy (a.u.) by study groups

Energy	Healthy	DM	MDR
Across All Macular Regions			
RNFL	0.64 ± 0.03	0.63 ± 0.02 ‡	0.65 ± 0.04
GCL+IPL	0.50 ± 0.01	0.50 ± 0.01	0.50 ± 0.01
INL	0.66 ± 0.02	0.58 ± 0.09 †	0.55 ± 0.05 ‡
OPL	0.63 ± 0.01	0.57 ± 0.06 †	0.56 ± 0.04 ‡
ONL+IS	0.54 ± 0.03	0.53 ± 0.03	0.54 ± 0.03
OS	0.48 ± 0.02	0.49 ± 0.03 ‡	0.47 ± 0.02 †
RPE	0.48 ± 0.03	0.47 ± 0.02 †	0.48 ± 0.03
Foveal Region			
RNFL	0.79 ± 0.06	0.74 ± 0.06 ‡	0.81 ± 0.05
GCL+IPL	0.49 ± 0.01	0.50 ± 0.02	0.49 ± 0.02 †
INL	0.66 ± 0.04	0.57 ± 0.09 ‡	0.52 ± 0.06 ‡
OPL	0.49 ± 0.01	0.48 ± 0.01	0.48 ± 0.02 ‡
ONL+IS	0.72 ± 0.05	0.70 ± 0.05	0.70 ± 0.06
OS	0.61 ± 0.07	0.62 ± 0.06 ‡	0.56 ± 0.06 ‡
RPE	0.42 ± 0.02	0.43 ± 0.02	0.43 ± 0.02
Parafoveal Region			
RNFL	0.53 ± 0.03	0.53 ± 0.03 ‡	0.56 ± 0.06 ‡
GCL+IPL	0.72 ± 0.04	0.70 ± 0.05	0.69 ± 0.06 ‡
INL	0.59 ± 0.03	0.58 ± 0.03 †	0.56 ± 0.04 ‡
OPL	0.59 ± 0.03	0.59 ± 0.03 †	0.57 ± 0.04 ‡
ONL+IS	0.88 ± 0.02	0.87 ± 0.03 †	0.85 ± 0.04 ‡
OS	0.76 ± 0.11	0.73 ± 0.09	0.70 ± 0.13 †
RPE	0.48 ± 0.05	0.49 ± 0.09	0.48 ± 0.07
Perifoveal Region			
RNFL	0.56 ± 0.03	0.55 ± 0.03 †	0.59 ± 0.08 †
GCL+IPL	0.49 ± 0.01	0.49 ± 0.01	0.49 ± 0.01
INL	0.46 ± 0.01	0.46 ± 0.01	0.46 ± 0.01
OPL	0.48 ± 0.02	0.48 ± 0.02 †	0.47 ± 0.01 †
ONL+IS	0.78 ± 0.03	0.78 ± 0.04 †	0.76 ± 0.04 †
OS	0.63 ± 0.10	0.62 ± 0.07	0.59 ± 0.09
RPE	0.43 ± 0.02	0.43 ± 0.03	0.43 ± 0.02

† $0.001<p<0.05$ and ‡ $p<0.001$ (ANOVA followed by Newman-Keuls post hoc analysis) between MDR and healthy eyes (see MDR column) and between MDR and DM eyes (see DM column).

Table 4.3 Distribution statistics of entropy (a.u.) by study groups

Entropy	Healthy	DM	MDR
Across All Macular Regions			
RNFL	0.74 ± 0.04	0.77 ± 0.03 ‡	0.73 ± 0.06
GCL+IPL	0.97 ± 0.01	0.97 ± 0.02	0.97 ± 0.02
INL	0.71 ± 0.03	0.82 ± 0.13 †	0.87 ± 0.07 ‡
OPL	0.76 ± 0.02	0.84 ± 0.08	0.86 ± 0.05 ‡
ONL+IS	0.92 ± 0.05	0.94 ± 0.04	0.92 ± 0.05
OS	0.96 ± 0.03	0.94 ± 0.04 ‡	0.97 ± 0.03 †
RPE	0.91 ± 0.03	0.93 ± 0.02 †	0.91 ± 0.04
Foveal Region			
RNFL	0.40 ± 0.08	0.51 ± 0.10 ‡	0.40 ± 0.07
GCL+IPL	0.97 ± 0.01	0.96 ± 0.02	0.97 ± 0.02
INL	0.71 ± 0.03	0.82 ± 0.13 †	0.87 ± 0.08 ‡
OPL	0.97 ± 0.01	0.97 ± 0.01 ‡	0.95 ± 0.03 ‡
ONL+IS	0.66 ± 0.08	0.69 ± 0.08	0.67 ± 0.09
OS	0.78 ± 0.08	0.74 ± 0.08 ‡	0.83 ± 0.07 †
RPE	0.97 ± 0.02	0.97 ± 0.01	0.97 ± 0.03
Parafoveal Region			
RNFL	0.87 ± 0.04	0.88 ± 0.05 †	0.85 ± 0.06 †
GCL+IPL	0.61 ± 0.05	0.65 ± 0.07 †	0.68 ± 0.08 ‡
INL	0.80 ± 0.03	0.80 ± 0.03 ‡	0.85 ± 0.05 ‡
OPL	0.79 ± 0.03	0.80 ± 0.03 ‡	0.84 ± 0.05 ‡
ONL+IS	0.34 ± 0.04	0.35 ± 0.05 ‡	0.39 ± 0.07 ‡
OS	0.47 ± 0.19	0.51 ± 0.15	0.55 ± 0.18
RPE	0.90 ± 0.07	0.87 ± 0.11	0.90 ± 0.07
Perifoveal Region			
RNFL	0.91 ± 0.03	0.92 ± 0.03 †	0.88 ± 0.09 ‡
GCL+IPL	0.98 ± 0.02	0.98 ± 0.01	0.98 ± 0.02
INL	0.99 ± 0.01	0.98 ± 0.01	0.99 ± 0.01
OPL	0.96 ± 0.02	0.95 ± 0.02 ‡	0.97 ± 0.02 †
ONL+IS	0.51 ± 0.04	0.52 ± 0.06 ‡	0.56 ± 0.06 ‡
OS	0.70 ± 0.13	0.71 ± 0.11 †	0.76 ± 0.12 †
RPE	0.97 ± 0.02	0.97 ± 0.02	0.97 ± 0.02

† $0.001<p<0.05$ and ‡ $p<0.001$ (ANOVA followed by Newman-Keuls post hoc analysis) between MDR and healthy eyes (see MDR column) and between MDR and DM eyes (see DM column).

Table 4.4 Distribution statistics of correlation (a.u.) by study groups

Correlation	Healthy	DM	MDR
Across All Macular Regions			
RNFL	0.93 ± 0.00	0.93 ± 0.00	0.92 ± 0.02
GCL+IPL	0.95 ± 0.00	0.95 ± 0.00	0.95 ± 0.00
INL	0.93 ± 0.00	0.93 ± 0.01 †	0.92 ± 0.01 †
OPL	0.94 ± 0.00	0.93 ± 0.01 ‡	0.92 ± 0.01 ‡
ONL+IS	0.97 ± 0.00	0.97 ± 0.00 †	0.97 ± 0.01
OS	0.89 ± 0.01	0.89 ± 0.01	0.88 ± 0.02
RPE	0.83 ± 0.01	0.83 ± 0.01	0.82 ± 0.01
Foveal Region			
RNFL	0.67 ± 0.08	0.72 ± 0.07 ‡	0.58 ± 0.13 ‡
GCL+IPL	0.92 ± 0.00	0.93 ± 0.01	0.93 ± 0.01
INL	0.89 ± 0.01	0.88 ± 0.02 ‡	0.86 ± 0.03 ‡
OPL	0.93 ± 0.01	0.91 ± 0.03 ‡	0.89 ± 0.02 ‡
ONL+IS	0.93 ± 0.02	0.94 ± 0.02	0.94 ± 0.02
OS	0.81 ± 0.04	0.81 ± 0.04	0.82 ± 0.03
RPE	0.76 ± 0.03	0.77 ± 0.03	0.76 ± 0.03
Parafoveal Region			
RNFL	0.76 ± 0.06	0.77 ± 0.06 ‡	0.69 ± 0.14 ‡
GCL+IPL	0.87 ± 0.03	0.88 ± 0.03	0.87 ± 0.03
INL	0.81 ± 0.03	0.82 ± 0.02 †	0.83 ± 0.03 ‡
OPL	0.79 ± 0.03	0.81 ± 0.03 †	0.82 ± 0.03 ‡
ONL+IS	0.81 ± 0.04	0.82 ± 0.04 †	0.84 ± 0.03 ‡
OS	0.76 ± 0.06	0.74 ± 0.07	0.74 ± 0.06
RPE	0.72 ± 0.04	0.69 ± 0.05 †	0.72 ± 0.04
Perifoveal Region			
RNFL	0.83 ± 0.04	0.83 ± 0.04 ‡	0.77 ± 0.15 ‡
GCL+IPL	0.94 ± 0.00	0.94 ± 0.01	0.93 ± 0.01 ‡
INL	0.89 ± 0.01	0.89 ± 0.01	0.89 ± 0.01
OPL	0.86 ± 0.01	0.86 ± 0.01 †	0.87 ± 0.01 †
ONL+IS	0.89 ± 0.02	0.89 ± 0.02	0.90 ± 0.02 †
OS	0.81 ± 0.03	0.81 ± 0.03 †	0.79 ± 0.05 †
RPE	0.76 ± 0.03	0.76 ± 0.03	0.76 ± 0.03

† $0.001<p<0.05$ and ‡ $p<0.001$ (ANOVA followed by Newman-Keuls post hoc analysis) between MDR and healthy eyes (see MDR column) and between MDR and DM eyes (see DM column).

Table 4.5 Distribution statistics of contrast (a.u.) by study groups

Contrast	Healthy	DM	MDR
Across All Macular Regions			
RNFL	1516.30 ± 117.28	1580.95 ± 116.02	1609.70 ± 160.84 †
GCL+IPL	1457.80 ± 83.51	1455.97 ± 115.11 †	1531.74 ± 134.40 ‡
INL	1404.58 ± 129.70	1900.10 ± 583.39 ‡	2237.81 ± 429.88 ‡
OPL	1333.37 ± 88.44	1763.18 ± 516.55 ‡	2069.46 ± 414.56 ‡
ONL+IS	874.95 ± 105.71	831.74 ± 55.18 †	921.70 ± 217.11
OS	3613.71 ± 405.61	3501.71 ± 349.19 †	3790.32 ± 529.86 †
RPE	5014.53 ± 420.37	5057.19 ± 418.54	5095.36 ± 528.15
Foveal Region			
RNFL	2088.32 ± 333.82	2331.96 ± 529.5	2325.43 ± 480.43 †
GCL+IPL	2362.71 ± 134.64	2194.92 ± 289.29	2224.63 ± 245.03 †
INL	2077.17 ± 337.04	3002.71 ± 1070.36 ‡	3628.65 ± 701.00 ‡
OPL	2099.11 ± 221.11	2768.28 ± 879.00 ‡	3314.65 ± 566.41 ‡
ONL+IS	995.01 ± 168.37	961.32 ± 82.15	1057.67 ± 300.89
OS	4116.37 ± 556.12	4027.69 ± 513.64 †	4404.23 ± 617.70 †
RPE	7308.22 ± 655.20	7081.34 ± 823.06	7112.06 ± 831.75
Parafoveal Region			
RNFL	5128.67 ± 1305.11	4610.53 ± 1541.17 †	5426.65 ± 1314.43
GCL+IPL	1863.24 ± 116.70	1905.07 ± 124.10 ‡	2058.11 ± 271.50 ‡
INL	3983.85 ± 240.79	3950.13 ± 258.88	3912.58 ± 314.57
OPL	4272.54 ± 241.98	4120.25 ± 241.74	4079.55 ± 274.40 ‡
ONL+IS	1122.66 ± 120.42	1139.84 ± 141.99	1179.05 ± 239.18
OS	3214.98 ± 1485.33	3653.88 ± 926.63	3974.89 ± 1559.35 †
RPE	7803.44 ± 1093.91	7844.12 ± 1252.47	7722.92 ± 1305.43
Perifoveal Region			
RNFL	2260.49 ± 176.31	2334.06 ± 227.01 ‡	2521.83 ± 350.87 ‡
GCL+IPL	1879.89 ± 120.80	1981.19 ± 166.02	2010.94 ± 242.32 ‡
INL	3546.13 ± 210.98	3540.40 ± 276.15	3460.76 ± 282.84
OPL	4036.11 ± 233.66	3998.26 ± 247.95 †	3872.81 ± 271.47 †
ONL+IS	1291.61 ± 117.39	1287.32 ± 116.23	1314.39 ± 251.53
OS	3986.67 ± 1088.46	4057.73 ± 679.88 †	4692.39 ± 1021.98 †
RPE	7292.01 ± 789.99	7254.33 ± 683.27	7362.44 ± 744.05

† $0.001<p<0.05$ and ‡ $p<0.001$ (ANOVA followed by Newman-Keuls post hoc analysis) between MDR and healthy eyes (see MDR column) and between MDR and DM eyes (see DM column).

Table 4.6 Distribution statistics of fractal dimension (a.u.) by study groups

Fractal Dimension	Healthy	DM	MDR
Across All Macular Regions			
RNFL	1.74 ± 0.04	1.71 ± 0.04 ‡	1.78 ± 0.10 ‡
GCL+IPL	1.68 ± 0.01	1.63 ± 0.06 ‡	1.58 ± 0.05 ‡
INL	1.78 ± 0.01	1.75 ± 0.02 †	1.76 ± 0.03 ‡
OPL	1.51 ± 0.01	1.54 ± 0.03 ‡	1.56 ± 0.04 ‡
ONL+IS	1.78 ± 0.03	1.78 ± 0.02 †	1.79 ± 0.04
OS	1.70 ± 0.02	1.70 ± 0.01 ‡	1.73 ± 0.04 ‡
RPE	1.68 ± 0.01	1.67 ± 0.01 ‡	1.68 ± 0.01
Foveal Region			
RNFL	2.22 ± 0.07	2.11 ± 0.08 ‡	2.24 ± 0.08
GCL+IPL	1.90 ± 0.01	1.71 ± 0.21 ‡	1.56 ± 0.15 ‡
INL	2.02 ± 0.02	1.92 ± 0.09	1.94 ± 0.08 ‡
OPL	1.49 ± 0.01	1.57 ± 0.09 ‡	1.65 ± 0.10 ‡
ONL+IS	1.76 ± 0.03	1.76 ± 0.03 †	1.78 ± 0.04 †
OS	1.71 ± 0.02	1.71 ± 0.01 ‡	1.73 ± 0.03 ‡
RPE	1.67 ± 0.01	1.66 ± 0.01 †	1.67 ± 0.01
Parafoveal Region			
RNFL	1.53 ± 0.05	1.53 ± 0.05 ‡	1.6 ± 0.13 ‡
GCL+IPL	1.56 ± 0.01	1.56 ± 0.01 ‡	1.55 ± 0.02 †
INL	1.67 ± 0.01	1.67 ± 0.01 †	1.68 ± 0.01
OPL	1.51 ± 0.01	1.51 ± 0.01	1.51 ± 0.01
ONL+IS	1.79 ± 0.03	1.79 ± 0.02 †	1.80 ± 0.04 †
OS	1.70 ± 0.02	1.69 ± 0.02 ‡	1.72 ± 0.05 ‡
RPE	1.69 ± 0.02	1.68 ± 0.02 †	1.69 ± 0.02
Perifoveal Region			
RNFL	1.52 ± 0.04	1.53 ± 0.04 †	1.57 ± 0.12 †
GCL+IPL	1.60 ± 0.01	1.60 ± 0.01	1.60 ± 0.02
INL	1.68 ± 0.01	1.68 ± 0.01 †	1.68 ± 0.01
OPL	1.52 ± 0.01	1.53 ± 0.02	1.52 ± 0.01
ONL+IS	1.79 ± 0.03	1.80 ± 0.02	1.80 ± 0.04
OS	1.70 ± 0.02	1.69 ± 0.02 ‡	1.72 ± 0.07 ‡
RPE	1.69 ± 0.01	1.68 ± 0.02 ‡	1.69 ± 0.02

† $0.001<p<0.05$ and ‡ $p<0.001$ (ANOVA followed by Newman-Keuls post hoc analysis) between MDR and healthy eyes (see MDR column) and between MDR and DM eyes (see DM column).

Table 4.7 Statistically significant differences of structural features between MDR and healthy eyes

MDR vs. Healthy	Thickness	Energy	Entropy	Correlation	Contrast	Fractal Dimension
Across All Macular Regions						
RNFL						**X**
GCL+IPL	**X**				**X**	**X**
INL		**X**	**X**		**X**	**X**
OPL	**X**	**X**	**X**	**X**	**X**	**X**
ONL+IS						
OS	**X**					**X**
RPE						
Foveal Region						
RNFL				**X**		
GCL+IPL	**X**					**X**
INL	**X**	**X**	**X**	**X**	**X**	**X**
OPL	**X**	**X**	**X**	**X**	**X**	**X**
ONL+IS						
OS		**X**				**X**
RPE						
Parafoveal Region						
RNFL	**X**	**X**		**X**		**X**
GCL+IPL	**X**	**X**	**X**		**X**	
INL		**X**	**X**	**X**		
OPL		**X**	**X**	**X**	**X**	
ONL+IS		**X**	**X**	**X**		
OS						**X**
RPE						
Perifoveal Region						
RNFL	**X**		**X**	**X**	**X**	
GCL+IPL				**X**	**X**	
INL						
OPL						
ONL+IS			**X**			
OS	**X**					**X**
RPE						

Symbol "X" denotes the intraretinal layer and regional sector in which the structural feature change showed a statistically significant difference ($p<0.001$) by using ANOVA followed by Newman-Keuls post hoc analysis.

Table 4.8 Statistically significant differences of structural features between MDR and DM eyes

MDR vs. DM	Thickness	Energy	Entropy	Correlation	Contrast	Fractal Dimension
Across All Macular Regions						
RNFL		X	X			X
GCL+IPL						X
INL					X	
OPL	X			X	X	X
ONL+IS						
OS	X	X	X			X
RPE	X					X
Foveal Region						
RNFL	X	X	X	X		X
GCL+IPL						□
INL		X		X	X	
OPL	X		X	X	X	X
ONL+IS						
OS	X	X	X			X
RPE						
Parafoveal Region						
RNFL	X	X		X		X
GCL+IPL	X				X	
INL	X		X			
OPL			X			
ONL+IS			X			
OS	X					X
RPE						
Perifoveal Region						
RNFL	X			X	X	
GCL+IPL						
INL						
OPL			X			
ONL+IS			X			
OS	X					X
RPE						

Symbol "x" denotes the intraretinal layer and macular region in which the structural feature change showed a statistically significant difference ($p<0.001$) by using ANOVA followed by Newman-Keuls post hoc analysis.

Table 4.9 AUROC values of thickness measurements by study groups

AUROC	MDR vs. Healthy	MDR vs. DM	DM vs. Healthy
Across All Macular Regions			
RNFL	0.60	0.51	0.60
GCL+IPL	0.76 *	0.63	0.67
INL	0.51	0.59	0.40
OPL	0.88 **	0.73 *	0.60
ONL+IS	0.39	0.42	0.50
OS	0.69	0.86 **	0.32
RPE	0.48	0.77 *	0.28
Foveal Region			
RNFL	0.57	0.85 **	0.20
GCL+IPL	0.12	0.46	0.32
INL	0.21	0.56	0.16
OPL	0.91 **	0.74 *	0.61
ONL+IS	0.49	0.43	0.55
OS	0.64	0.78 *	0.37
RPE	0.44	0.69	0.30
Parafoveal region			
RNFL	0.62	0.67	0.41
GCL+IPL	0.72 *	0.67	0.57
INL	0.53	0.62	0.39
OPL	0.48	0.63	0.38
ONL+IS	0.40	0.40	0.53
OS	0.66	0.86 **	0.30
RPE	0.42	0.68	0.24
Perifoveal Region			
RNFL	0.68	0.65	0.53
GCL+IPL	0.66	0.53	0.66
INL	0.55	0.58	0.44
OPL	0.53	0.59	0.41
ONL+IS	0.35	0.38	0.49
OS	0.69	0.87 **	0.30
RPE	0.52	0.66	0.36

*0.70≤AUROC<0.80, **0.80≤AUROC

Table 4.10 Cutoff values of thickness measurements (μm) derived from ROC analyses between MDR and healthy eyes

Intraretinal Layer	AUROC	95% CI		Cutoff Point (μm)	Sensitivity	Specificity
		Lower Bound	Upper Bound			
Across All Macular Regions						
RNFL	0.60 ± 0.06	0.48	0.71	41.03	0.64	0.54
GCL+IPL	0.76 ± 0.05	0.66	0.86	75.85	0.74	0.64
INL	0.51 ± 0.06	0.39	0.63	34.85	0.55	0.45
OPL	0.88 ± 0.04	0.80	0.96	38.12	0.91	0.81
ONL+IS	0.39 ± 0.06	0.29	0.50	86.87	0.47	0.37
OS	0.69 ± 0.05	0.59	0.78	14.59	0.68	0.58
RPE	0.48 ± 0.05	0.38	0.59	12.41	0.57	0.47
Foveal Region						
RNFL	0.57 ± 0.06	0.46	0.68	8.22	0.57	0.47
GCL+IPL	0.12 ± 0.04	0.04	0.21	58.11	0.24	0.14
INL	0.21 ± 0.05	0.12	0.31	21.69	0.36	0.26
OPL	0.91 ± 0.04	0.83	0.98	49.66	0.95	0.85
ONL+IS	0.49 ± 0.06	0.37	0.60	99.40	0.57	0.47
OS	0.64 ± 0.05	0.53	0.74	16.43	0.66	0.56
RPE	0.44 ± 0.05	0.34	0.54	12.57	0.47	0.37
Parafoveal Region						
RNFL	0.62 ± 0.06	0.50	0.74	33.06	0.61	0.51
GCL+IPL	0.72 ± 0.05	0.62	0.83	92.00	0.70	0.60
INL	0.53 ± 0.06	0.42	0.65	39.03	0.59	0.49
OPL	0.48 ± 0.05	0.37	0.59	36.69	0.52	0.42
ONL+IS	0.40 ± 0.06	0.30	0.51	84.95	0.50	0.40
OS	0.66 ± 0.05	0.56	0.76	13.02	0.65	0.55
RPE	0.42 ± 0.06	0.31	0.53	11.66	0.52	0.42
Perifoveal Region						
RNFL	0.68 ± 0.06	0.57	0.79	40.29	0.68	0.58
GCL+IPL	0.66 ± 0.06	0.55	0.77	65.53	0.68	0.58
INL	0.55± 0.06	0.43	0.67	32.37	0.61	0.51
OPL	0.53 ± 0.06	0.42	0.65	31.17	0.57	0.47
ONL+IS	0.35 ± 0.05	0.24	0.45	75.74	0.45	0.35
OS	0.69 ± 0.05	0.59	0.78	13.17	0.66	0.56
RPE	0.52 ± 0.06	0.41	0.63	12.27	0.54	0.44

Table 4.11 Cutoff values of thickness measurements (μm) derived from ROC analyses between MDR and DM eyes

Intraretinal Layer	AUROC	95% CI		Cutoff Point (μm)	Sensitivity	Specificity
		Lower Bound	Upper Bound			
Across All Macular Regions						
RNFL	0.51 ± 0.07	0.39	0.64	40.59	0.58	0.48
GCL+IPL	0.63 ± 0.06	0.51	0.75	73.83	0.66	0.56
INL	0.59 ± 0.06	0.46	0.71	35.31	0.63	0.53
OPL	0.73 ± 0.06	0.62	0.84	35.94	0.71	0.61
ONL+IS	0.42 ± 0.07	0.29	0.55	86.65	0.47	0.37
OS	0.86 ± 0.04	0.77	0.94	15.41	0.82	0.72
RPE	0.74 ± 0.06	0.63	0.85	13.22	0.71	0.61
Foveal Region						
RNFL	0.85 ± 0.04	0.77	0.93	9.59	0.82	0.72
GCL+IPL	0.46 ± 0.07	0.32	0.59	68.09	0.47	0.37
INL	0.56 ± 0.06	0.44	0.69	24.42	0.59	0.49
OPL	0.74 ± 0.06	0.63	0.85	36.33	0.73	0.63
ONL+IS	0.43 ± 0.06	0.31	0.56	98.19	0.50	0.40
OS	0.78 ± 0.05	0.68	0.88	17.34	0.76	0.66
RPE	0.69 ± 0.06	0.57	0.80	13.30	0.68	0.58
Parafoveal Region						
RNFL	0.67 ± 0.06	0.55	0.79	33.28	0.71	0.61
GCL+IPL	0.67 ± 0.06	0.55	0.78	91.14	0.64	0.54
INL	0.62 ± 0.06	0.50	0.74	39.78	0.61	0.51
OPL	0.63 ± 0.06	0.50	0.75	37.14	0.63	0.53
ONL+IS	0.40 ± 0.06	0.28	0.53	85.17	0.50	0.40
OS	0.86 ± 0.04	0.78	0.94	14.23	0.82	0.72
RPE	0.68 ± 0.06	0.57	0.80	12.62	0.71	0.61
Perifoveal Region						
RNFL	0.65 ± 0.06	0.53	0.77	40.15	0.68	0.58
GCL+IPL	0.53 ± 0.07	0.40	0.65	63.03	0.63	0.53
INL	0.58 ± 0.06	0.46	0.71	32.51	0.66	0.56
OPL	0.59 ± 0.06	0.47	0.72	31.48	0.68	0.58
ONL+IS	0.38 ± 0.06	0.26	0.50	76.29	0.50	0.40
OS	0.87 ± 0.04	0.79	0.95	13.84	0.82	0.72
RPE	0.66 ± 0.06	0.54	0.78	12.55	0.64	0.54

Table 4.12 AUROC values of fractal dimension (a.u.) by study groups

AUROC	MDR vs. Healthy	MDR vs. DM	DM vs. Healthy
Across All Macular Regions			
RNFL	0.39	0.21	0.72 *
GCL+IPL	0.95 **	0.77 *	0.73 *
INL	0.79 *	0.43	0.97 **
OPL	0.11	0.31	0.19
ONL+IS	0.34	0.33	0.45
OS	0.27	0.22	0.54
RPE	0.43	0.27	0.69
Foveal Region			
RNFL	0.44	0.13	0.84 **
GCL+IPL	0.96 **	0.77 *	0.55
INL	0.83 **	0.45	0.97 **
OPL	0.07	0.26	0.25
ONL+IS	0.35	0.30	0.50
OS	0.32	0.26	0.54
RPE	0.51	0.36	0.66
Parafoveal region			
RNFL	0.35	0.34	0.51
GCL+IPL	0.63	0.66	0.46
INL	0.39	0.31	0.56
OPL	0.61	0.60	0.52
ONL+IS	0.34	0.33	0.46
OS	0.33	0.23	0.58
RPE	0.52	0.33	0.72 *
Perifoveal Region			
RNFL	0.51	0.54	0.45
GCL+IPL	0.52	0.48	0.54
INL	0.38	0.37	0.56
OPL	0.55	0.56	0.50
ONL+IS	0.36	0.38	0.43
OS	0.31	0.29	0.54
RPE	0.42	0.29	0.66

*0.70≤AUROC<0.80, **0.80≤AUROC

Table 4.13 Cutoff values of fractal dimension (a.u.) derived from ROC analyses between MDR and healthy eyes

Intraretinal Layer	AUROC	95% CI		Cutoff Point (μm)	Sensitivity	Specificity
		Lower Bound	Upper Bound			
Across All Macular Regions						
RNFL	0.39 ± 0.06	0.28	0.50	1.74	0.47	0.37
GCL+IPL	0.95 ± 0.03	0.91	1.00	1.66	0.98	0.88
INL	0.79 ± 0.05	0.68	0.89	1.77	0.80	0.70
OPL	0.11 ± 0.04	0.03	0.19	1.52	0.26	0.16
ONL+IS	0.34 ± 0.06	0.23	0.44	1.78	0.40	0.30
OS	0.27 ± 0.05	0.18	0.36	1.71	0.43	0.33
RPE	0.43 ± 0.06	0.32	0.54	1.68	0.50	0.40
Foveal Region						
RNFL	0.44 ± 0.06	0.33	0.55	2.22	0.55	0.45
GCL+IPL	0.96 ± 0.02	0.93	1.00	1.85	1.00	0.90
INL	0.83 ± 0.05	0.74	0.93	2.00	0.84	0.74
OPL	0.07 ± 0.04	0.00	0.14	1.50	0.17	0.07
ONL+IS	0.35 ± 0.06	0.24	0.46	1.77	0.38	0.28
OS	0.32 ± 0.05	0.22	0.42	1.71	0.43	0.33
RPE	0.51 ± 0.06	0.40	0.62	1.67	0.54	0.44
Parafoveal Region						
RNFL	0.35 ± 0.06	0.24	0.45	1.54	0.45	0.35
GCL+IPL	0.63 ± 0.06	0.52	0.74	1.55	0.66	0.56
INL	0.39 ± 0.05	0.28	0.50	1.67	0.43	0.33
OPL	0.61 ± 0.06	0.49	0.72	1.51	0.66	0.56
ONL+IS	0.34 ± 0.06	0.24	0.45	1.79	0.38	0.28
OS	0.33 ± 0.05	0.22	0.43	1.70	0.40	0.30
RPE	0.52 ± 0.06	0.41	0.63	1.69	0.57	0.47
Perifoveal Region						
RNFL	0.51 ± 0.06	0.40	0.63	1.53	0.64	0.54
GCL+IPL	0.52 ± 0.06	0.41	0.63	1.60	0.55	0.45
INL	0.38 ± 0.06	0.27	0.49	1.68	0.45	0.35
OPL	0.55 ± 0.06	0.43	0.67	1.52	0.64	0.54
ONL+IS	0.36 ± 0.06	0.24	0.47	1.80	0.36	0.26
OS	0.31 ± 0.05	0.20	0.41	1.70	0.45	0.35
RPE	0.42 ± 0.06	0.31	0.53	1.69	0.47	0.37

Table 4.14 Cutoff values of fractal dimension (a.u.) derived from ROC analyses between MDR and DM eyes

Intraretinal Layer	AUROC	95% CI		Cutoff Point (μm)	Sensitivity	Specificity
		Lower Bound	Upper Bound			
Across All Macular Regions						
RNFL	0.21 ± 0.05	0.11	0.31	1.73	0.38	0.28
GCL+IPL	0.77 ± 0.05	0.67	0.87	1.75	0.55	0.45
INL	0.43 ± 0.07	0.30	0.56	1.75	0.55	0.45
OPL	0.31 ± 0.06	0.19	0.42	1.54	0.38	0.28
ONL+IS	0.33 ± 0.06	0.21	0.44	1.79	0.45	0.35
OS	0.22 ± 0.05	0.12	0.32	1.70	0.40	0.30
RPE	0.27 ± 0.06	0.16	0.38	1.68	0.38	0.28
Foveal Region						
RNFL	0.13 ± 0.04	0.05	0.20	2.17	0.24	0.14
GCL+IPL	0.77 ± 0.05	0.66	0.87	1.49	0.74	0.64
INL	0.45 ± 0.07	0.32	0.58	1.94	0.57	0.47
OPL	0.26 ± 0.06	0.15	0.37	1.59	0.40	0.30
ONL+IS	0.30 ± 0.06	0.19	0.42	1.77	0.38	0.28
OS	0.26 ± 0.05	0.15	0.36	1.71	0.43	0.33
RPE	0.36 ± 0.06	0.24	0.48	1.67	0.45	0.35
Parafoveal Region						
RNFL	0.34 ± 0.06	0.22	0.46	1.54	0.47	0.37
GCL+IPL	0.66 ± 0.06	0.54	0.78	1.55	0.66	0.56
INL	0.31 ± 0.06	0.20	0.43	1.67	0.40	0.30
OPL	0.60 ± 0.06	0.47	0.72	1.51	0.66	0.56
ONL+IS	0.33 ± 0.06	0.21	0.45	1.79	0.42	0.32
OS	0.23 ± 0.05	0.13	0.33	1.70	0.36	0.26
RPE	0.33 ± 0.06	0.21	0.44	1.68	0.43	0.33
Perifoveal Region						
RNFL	0.54 ± 0.07	0.41	0.67	1.53	0.66	0.56
GCL+IPL	0.48 ± 0.07	0.36	0.61	1.60	0.50	0.40
INL	0.37 ± 0.06	0.24	0.49	1.68	0.43	0.33
OPL	0.56 ± 0.06	0.44	0.69	1.52	0.61	0.51
ONL+IS	0.38 ± 0.06	0.26	0.50	1.80	0.45	0.35
OS	0.29 ± 0.06	0.17	0.40	1.70	0.38	0.28
RPE	0.29 ± 0.06	0.17	0.40	1.68	0.40	0.30

Table 4.15 Cutoff values of fractal dimension (a.u.) derived from ROC analyses between DM and healthy eyes

Intraretinal Layer	AUROC	95% CI		Cutoff Point (μm)	Sensitivity	Specificity
		Lower Bound	Upper Bound			
Across All Macular Regions						
RNFL	0.72 ± 0.05	0.62	0.82	1.72	0.71	0.61
GCL+IPL	0.73 ± 0.06	0.61	0.84	1.68	0.73	0.63
INL	0.97 ± 0.01	0.94	0.99	1.77	0.89	0.79
OPL	0.19 ± 0.05	0.10	0.29	1.52	0.34	0.24
ONL+IS	0.45 ± 0.06	0.34	0.56	1.78	0.50	0.40
OS	0.54 ± 0.06	0.43	0.65	1.70	0.57	0.47
RPE	0.69 ± 0.05	0.58	0.80	1.67	0.68	0.58
Foveal Region						
RNFL	0.84 ± 0.04	0.77	0.92	2.16	0.78	0.68
GCL+IPL	0.55 ± 0.08	0.40	0.70	1.89	0.60	0.50
INL	0.97 ± 0.01	0.94	0.99	2.00	0.92	0.82
OPL	0.25 ± 0.06	0.14	0.36	1.49	0.39	0.29
ONL+IS	0.50 ± 0.06	0.39	0.61	1.76	0.53	0.43
OS	0.54 ± 0.06	0.43	0.64	1.71	0.54	0.44
RPE	0.66 ± 0.06	0.56	0.77	1.66	0.64	0.54
Parafoveal Region						
RNFL	0.51 ± 0.06	0.40	0.62	1.53	0.55	0.45
GCL+IPL	0.46 ± 0.06	0.35	0.57	1.55	0.55	0.45
INL	0.56 ± 0.06	0.45	0.67	1.67	0.52	0.42
OPL	0.52 ± 0.06	0.40	0.63	1.51	0.55	0.45
ONL+IS	0.46 ± 0.06	0.35	0.58	1.78	0.44	0.34
OS	0.58 ± 0.05	0.48	0.69	1.69	0.58	0.48
RPE	0.72 ± 0.05	0.61	0.82	1.68	0.71	0.61
Perifoveal Region						
RNFL	0.45 ± 0.06	0.33	0.57	1.54	0.53	0.43
GCL+IPL	0.54 ± 0.06	0.43	0.66	1.60	0.60	0.50
INL	0.56 ± 0.06	0.44	0.69	1.68	0.63	0.53
OPL	0.50 ± 0.06	0.38	0.62	1.52	0.62	0.52
ONL+IS	0.43 ± 0.06	0.32	0.54	1.79	0.44	0.34
OS	0.54 ± 0.06	0.42	0.65	1.69	0.60	0.50
RPE	0.66 ± 0.06	0.55	0.77	1.68	0.68	0.58

CHAPTER 5. QUANTITATIVE ANALYSIS OF OPTICAL PROPERTIES

5.1 OVERVIEW

OCT is typically employed for the measurement of retinal thickness. However, the reflected light carries more information characterizing the optical properties of tissue. Therefore, changes in the tissue's optical properties may provide further information about cellular layers and early damage in diabetic ocular disease. Consequently, the diagnostic power may be improved by adding diagnostic parameters based on the measurement of optical properties, including the backscattered signal from layered retinal structures in diabetic eyes.

In this chapter, optical parameters are reported after calculating them from OCT images of healthy and diabetic eyes with and without mild diabetic retinopathy. The differences in optical parameters between study groups were investigated using ANOVA followed by Newman-Keuls post-hoc analysis. Because of the number of comparisons, a $p \leq 0.001$ was considered statistically significant ($0.001 < p \leq 0.05$ missed significant). Receiver operating characteristic (ROC) analysis was also performed on the optical parameters between study groups to determine the diagnostic ability of each optical characteristic to differentiate diabetic eyes with and without MDR from healthy eyes. An area under the receiver operating characteristic curve (AUROC) was used to compare diagnostic power. The AUROC calculations and statistical analyses were performed using the software package SPSS version 16 (SPSS Inc., Chicago, Illinois).

5.2 QUANTITATIVE MEASUREMENTS

Healthy eyes (74 eyes) and diabetic eyes with and without diabetic retinopathy (43 MDR and 38 DM eyes, respectively) were used in this study. A total of six radial

scans per study eye were collected by the Stratus OCT system. Optical parameters such as mean reflectance, total reflectance, layer index and scattering coefficients were extracted from the OCT images for each intraretinal layer and in each macular region in all study groups. The foveola region was not included in the analysis because segmentation was less reliable due to the low OCT signal in this region.

5.2.1 MEAN REFLECTANCE MEASUREMENTS

Mean reflectance in each intraretinal layer was calculated by averaging the local reflectivity (see equation 3.16) across all macular regions for healthy and DM eyes with and without MDR. The mean reflectance in each macular region and intraretinal layer was also measured, except in the foveola. The mean reflectance measurements are shown in Table 5.1. The values are expressed in the form of the mean ± SD (SD: standard deviation).

The mean reflectance changes between DM, MDR and healthy eyes were analyzed using ANOVA followed by Newman-Keuls post-hoc analysis. Significant differences between study groups are also reported in Table 5.1.

5.2.1.1 MEAN REFLECTANCE CHANGES IN THE INTRARETINAL LAYERS OF EACH EYE

The mean reflectance of each intraretinal layer for all study groups is plotted in Figure 5.1. The data clearly demonstrate that in the DM, MDR and healthy eyes, the highest and lowest mean reflectance was achieved by the RPE and ONL+IS, respectively. Specifically, the mean reflectance showed a statistically significant decrease in all intraretinal layers (i.e., 4%, 5%, 5%, 5% and 6% for the RNFL, GCL+IPL, INL, OPL and ONL+IS, respectively) when comparing MDR with healthy eyes (see Figure 5.1 and Table 5.1).

Moreover, when comparing MDR with DM eyes, the mean reflectance of the GCL+IPL, INL, OPL and ONL+IS showed a significant decrease (3%, 4%, 4% and 4%, respectively) and a non-significant decrease for the OS and RPE.

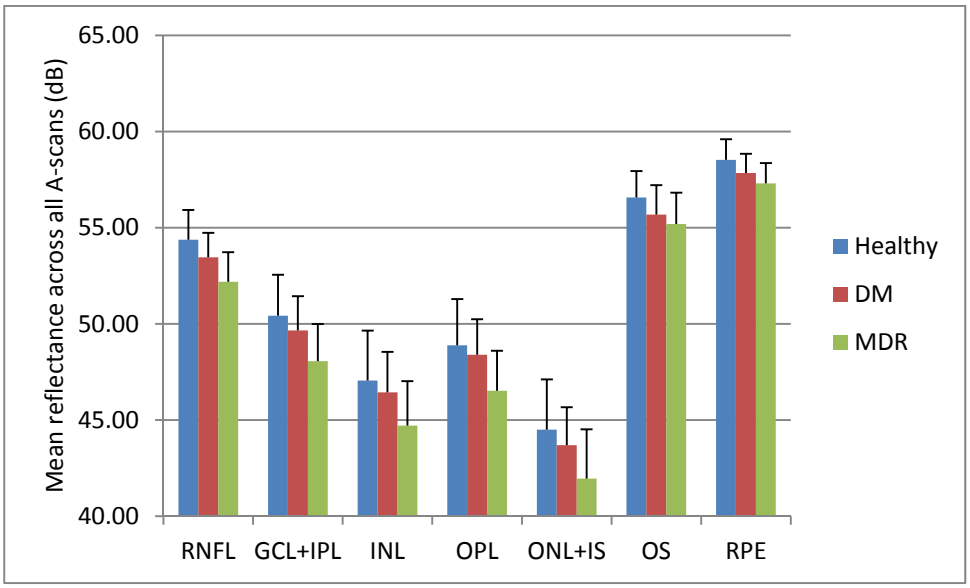

Figure 5.1 Mean reflectance across all macular regions by study groups

5.2.1.2 MEAN REFLECTANCE CHANGES IN THE INTRARETINAL LAYERS OF THE FOVEAL REGION

The foveal mean reflectance in MDR compared to healthy eyes showed a significant decrease for all intraretinal layers (i.e., 5%, 5% and 6% for the GCL+IPL, INL and ONL+IS, respectively).

When comparing MDR with DM eyes, the foveal mean reflectance showed a significant decrease (4%) in the GCL+IPL, INL, OPL and ONL+IS. Moreover, the foveal mean reflectance showed a non-significant decrease for the OS and RPE.

5.2.1.3 MEAN REFLECTANCE CHANGES IN THE INTRARETINAL LAYERS OF THE PARAFOVEAL REGION

The parafoveal mean reflectance in MDR compared to healthy eyes was significantly decreased in all intraretinal layers (i.e., 5%, 5% and 6% for the INL, OPL and ONL+IS, respectively).

When comparing MDR with DM eyes, the parafoveal mean reflectance was significantly decreased (4%) in the GCL+IPL, INL, OPL and ONL+IS. In addition, the parafoveal mean reflectance showed a non-significant decrease for the OS and RPE.

5.2.1.4 MEAN REFLECTANCE CHANGES IN THE INTRARETINAL LAYERS OF THE PERIFOVEAL REGION

The perifoveal mean reflectance in MDR compared to healthy eyes was significantly decreased in all intraretinal layers (i.e., 5%, 5%, 5% and 6% for the GCL+IPL, INL, OPL and ONL+IS, respectively).

When comparing MDR with DM eyes, the perifoveal mean reflectance was significantly decreased in the RNFL, GCL+IPL, INL, OPL and ONL+IS (2%, 3%, 4%, 4% and 4%, respectively). In addition, the perifoveal mean reflectance measurement showed a non-significant decrease for the OS and RPE.

5.2.1.5 MEAN REFLECTANCE CHANGES IN THE INTRARETINAL LAYERS ACROSS ALL MACULAR REGIONS

A summary of the statistical analysis obtained for mean reflectance changes in each macular region for each intraretinal layer is shown in Figure 5.2. The results across all macular regions were averaged in each eye. The mean reflectance in each intraretinal layer showed a significant decrease for all intraretinal layers in MDR compared to healthy eyes. Moreover, Figure 5.2 clearly indicates that the statistically significant mean reflectance changes observed in all intraretinal layers were distributed across all macular

regions. When comparing MDR with DM eyes, statistically significant thickness changes were distributed across all macular regions, except the OS.

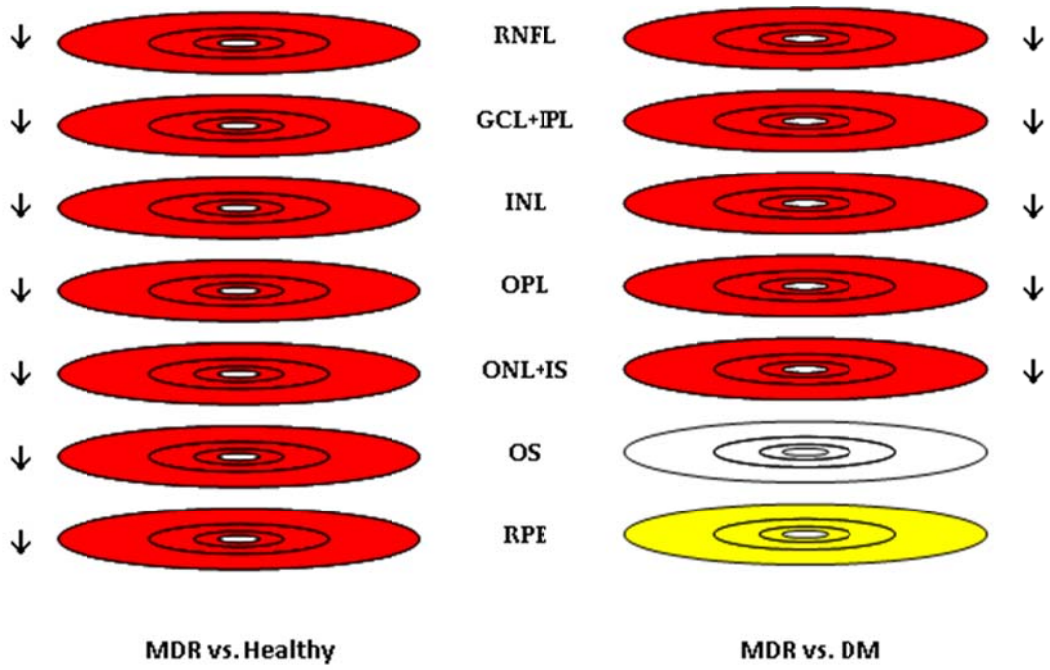

Figure 5.2 Mean reflectance changes in each macular region and intraretinal layer for MDR vs. Healthy and MDR vs. DM eyes. Comparisons were performed using an ANOVA followed by Newman-Keuls post hoc analysis. The red and yellow color denotes $p<0.001$ and $0.001<p<0.05$, respectively. Arrows denote an increasing (decreasing) trend when pointing up (down).

5.2.2 TOTAL REFLECTANCE MEASUREMENTS

Total reflectance per intraretinal layer was calculated by summarizing the local reflectivity (see equation 3.18) across all macular regions for healthy and DM eyes with and without MDR. The total reflectance in each macular region and intraretinal layer was also measured, except in the foveola. Total reflectance measurements are given in Table 5.2. The values are expressed in the form of the mean ± SD (SD: standard deviation). Total reflectance changes were analyzed using ANOVA followed by Newman-Keuls post-hoc analysis between DM, MDR and healthy eyes. Significant differences between study groups are also reported in Table 5.2.

5.2.2.1 CHANGES IN THE TOTAL REFLECTANCE OF THE INTRARETINAL LAYERS

The total reflectance measurements in each intraretinal layer for all study groups are plotted in Figure 5.3. The data clearly demonstrate that in the DM, MDR and healthy eyes, the highest and lowest mean reflectance of the intraretinal layers were found in the INL and GCL+IPL, respectively. The total reflectance showed statistically significant differences in all intraretinal layers when comparing MDR with healthy eyes (see Figure 5.3 and Table 5.2). Specifically, the total reflectance showed a significant decrease in the GCL+IPL and OPL (4% and 5%, respectively). Moreover, when comparing MDR with DM eyes, the total reflectance showed a significant decrease for all intraretinal layers (except in the ONL+IS). Specifically, the total reflectance showed a significant decrease (4%) for the OPL.

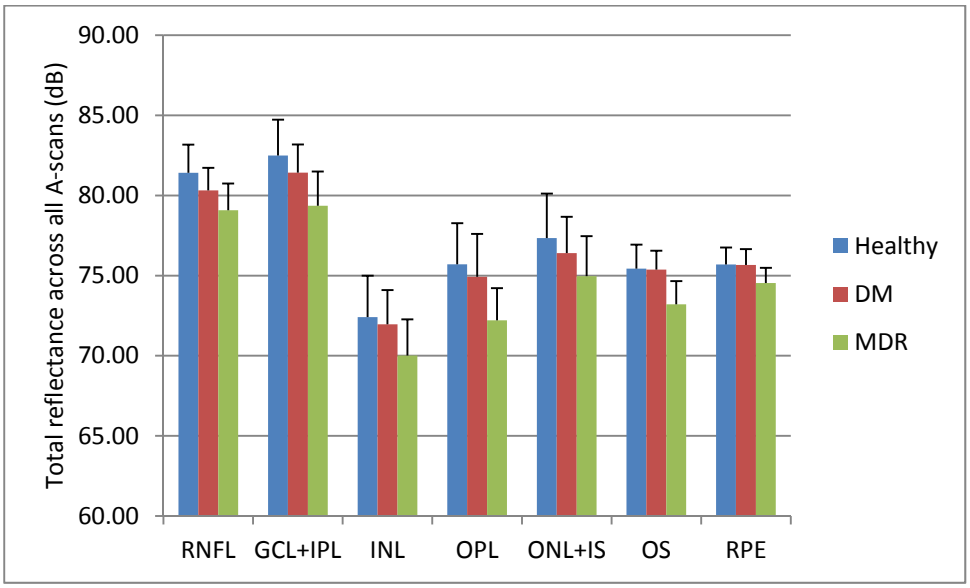

Figure 5.3 Total reflectance across all macular regions by study groups

5.2.2.2 TOTAL REFLECTANCE CHANGES IN THE INTRARETINAL LAYERS OF THE FOVEAL REGION

The foveal total reflectance in the MDR compared to healthy eyes showed a significant decrease in all intraretinal layers (i.e., 5% and 6% for the GCL+IPL and OPL, respectively).

When comparing MDR with DM eyes, the foveal total reflectance showed a significant decrease for all intraretinal layer (except in the ONL+IS). Specifically, the foveal total reflectance showed a significant decrease (5%) for the OPL. In addition, the foveal total reflectance showed a non-significant decrease in the ONL+IS.

5.2.2.3 TOTAL REFLECTANCE CHANGES IN THE INTRARETINAL LAYERS OF THE PARAFOVEAL REGION

The parafoveal total reflectance in the MDR compared to healthy eyes showed a significant decrease in all intraretinal layers. Specifically, the parafoveal total reflectance showed a significant decrease for the RNFL, INL, OPL, ONL+IS and OS (3%, 4%, 3%, 3% and 3%, respectively).

When comparing MDR with DM eyes, the parafoveal total reflectance showed a significant decrease in all intraretinal layers (except in the ONL+IS). The foveal mean reflectance showed a significant decrease (3%) in the GCL+IPL, INL and OPL. In addition, the parafoveal total reflectance showed a non-significant decrease in the ONL+IS.

5.2.2.4 TOTAL REFLECTANCE CHANGES IN THE INTRARETINAL LAYERS OF THE PERIFOVEAL REGION

The perifoveal total reflectance in the MDR compared to healthy eyes showed a significant decrease in all intraretinal layers. Specifically, the perifoveal total reflectance

showed a significant decrease in the RNFL, GCL+IPL, INL, OPL, ONL+IS and OS (3%, 4%, 4%, 4%, 3% and 3%, respectively).

When comparing MDR with DM eyes, the perifoveal total reflectance showed a significant decrease in all intraretinal layers (except in the ONL+IS). Specifically, the perifoveal total reflectance showed a significant decrease (3%) in the INL, OPL and OS.

5.2.2.5 TOTAL REFLECTANCE CHANGES IN THE INTRARETINAL LAYERS ACROSS ALL REGIONS

A summary of the statistical analysis for the total reflectance changes in each macular region and intraretinal layer is shown in Figure 5.4. The results across all macular regions were averaged in each eye. The total reflectance in each intraretinal layer showed a significant decrease in all intraretinal layers in MDR compared to healthy eyes. Moreover, Figure 5.4 clearly indicates that the statistically significant total reflectance changes observed for all intraretinal layers were distributed across all macular regions.

When comparing MDR with DM eyes, the total reflectance in each intraretinal layer showed a significant decrease for all intraretinal layers (except in the ONL+IS). In addition, Figure 5.4 clearly indicates that the statistically significant total reflectance changes observed in all intraretinal layers (except in the ONL+IS) were distributed across all macular regions.

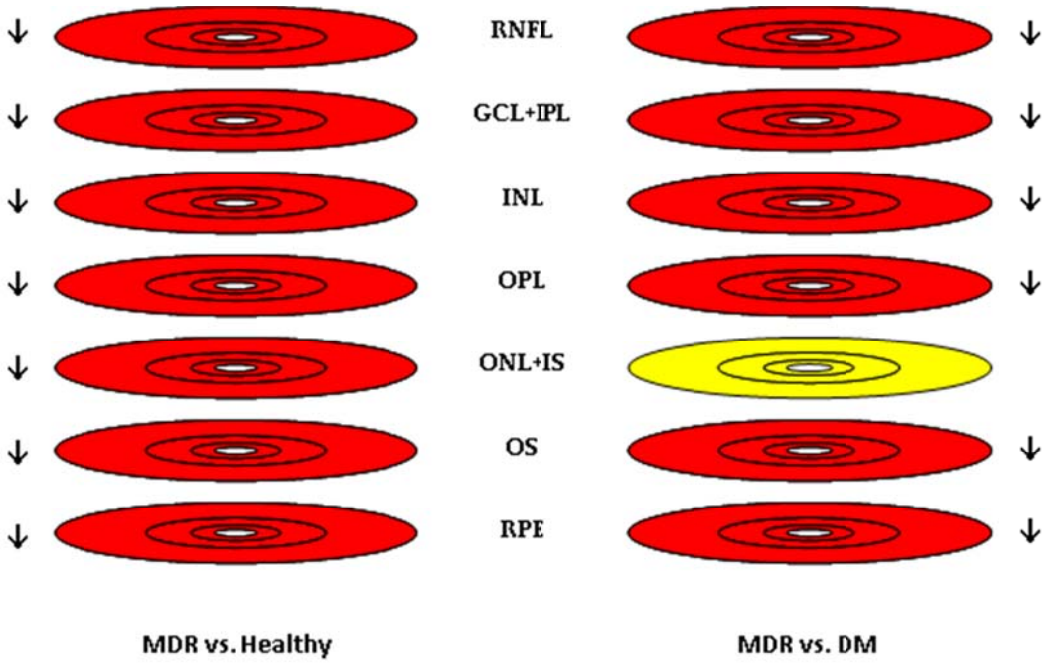

Figure 5.4 Total reflectance changes in each macular region in each intraretinal layer for MDR vs. Healthy and MDR vs. DM. Comparisons were performed by using ANOVA followed by Newman-Keuls post hoc analysis. The red and yellow color denotes $p<0.001$ and $0.001<p<0.05$, respectively. Arrows denote an increasing (decreasing) trend when pointing up (down).

5.2.3 LAYER INDEX MEASUREMENTS

The layer index in each intraretinal layer was calculated by using the equation 3.20 across all macular regions for the healthy and DM eyes with and without MDR. The layer index in each macular region and intraretinal layer was also measured, except in the foveola. The layer index measurements are given in Table 5.3. The values are expressed in the form of mean ± SD (SD: standard deviation).

The layer index changes were analyzed using an ANOVA followed by Newman-Keuls post-hoc analysis between DM, MDR and healthy eyes. Significant differences between study groups are also reported in Table 5.3.

5.2.3.1 LAYER INDEX CHANGES IN THE INTRARETINAL LAYERS OF EACH EYE

The layer index in each intraretinal layer for all study groups are plotted in Figure 5.5. The figure clearly demonstrates that in the DM, MDR and healthy eyes, the highest and lowest mean reflectance of the intraretinal layers were found in the INL and GCL+IPL, respectively. The layer index in each intraretinal layer in the MDR compared to healthy eyes showed a significant decrease for the RNFL, GCL+IPL, INL, OPL and OS (13%, 21%, 14%, 24% and 23%, respectively). However, the layer index in each intraretinal layer showed a non-significant decrease in the ONL+IS.

When comparing MDR with DM eyes, the layer index showed significant differences for all intraretinal layers (except in the ONL+IS). Specifically, the layer index showed a significant decrease in the GCL+IPL, INL and OPL (16%, 15% and 15%, respectively).

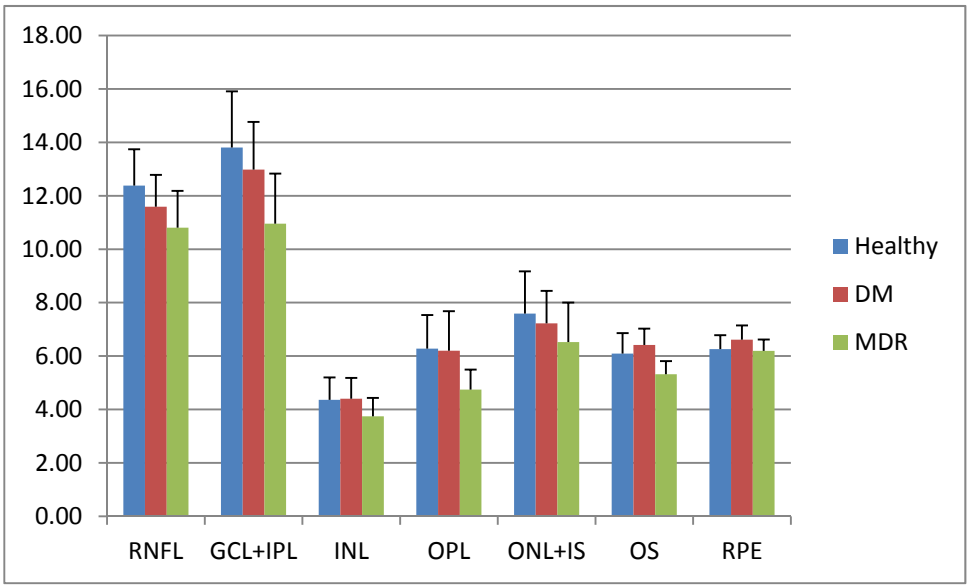

Figure 5.5 Layer index per intraretinal layer by study groups

5.2.3.2 CHANGES IN THE LAYER INDEX OF THE INTRARETINAL LAYERS IN THE FOVEAL REGION

The foveal layer index in MDR compared to healthy eyes showed a significant decrease in the RNFL, GCL+IPL, OPL and OS (29% and 36% for the GCL+IPL and OPL).

When comparing MDR with DM eyes, the foveal layer index showed a significant decrease in the GCL+IPL, INL, OPL and OS (i.e., 24% and 35% in the GCL+IPL and OPL, respectively). In addition, the foveal layer index showed a non-significant decrease in the RNFL and ONL+IS.

5.2.3.3 CHANGES IN THE LAYER INDEX OF THE INTRARETINAL LAYERS IN THE PARAFOVEAL REGION

The parafoveal layer index in MDR compared to healthy eyes showed a significant decrease in all intraretinal layers (except in the RPE). Specifically, the parafoveal layer index showed a significant decrease in the GCL+IPL, INL, OPL, ONL+IS and OS (20%, 15%, 14% 14% and 14%, respectively).

When comparing MDR with DM eyes, the parafoveal layer index showed a significant decrease in the RNFL, GCL+IPL, INL,OPL and OS (11%, 17%, 16%, 17% and 21%, respectively). In addition, the parafoveal layer index showed a non-significant decrease in the ONL+IS.

5.2.3.4 CHANGES IN THE LAYER INDEX OF THE INTRARETINAL LAYERS IN THE PERIFOVEAL REGION

The perifoveal layer index in MDR compared to healthy eyes showed a significant decrease in the RNFL, GCL+IPL, INL, OPL and OS (i.e., 17% and 16% in the

GCL+IPL and OPL, respectively). However, the perifoveal layer index showed a non-significant decrease in the ONL+IS and RPE.

When comparing MDR with DM eyes, the parafoveal layer index showed a significant decrease in the RNFL, INL, OPL and OS (8%, 13%, 14% and 18%, respectively). In addition, the parafoveal layer index showed a non-significant decrease in all the other intraretinal layers.

5.2.3.5 CHANGES IN THE LAYER INDEX OF THE INTRARETINAL LAYERS ACROSS ALL REGIONS

A summary of the statistical analyses for layer index changes in each macular region for each intraretinal layer is shown in Figure 5.6. We note that the results across all macular regions were averaged in each eye. The layer index in each intraretinal layer showed significant differences in the RNFL, GCL+IPL, INL, OPL and OS in MDR compared to healthy eyes. Moreover, Figure 5.6 clearly indicates that the statistically significant layer index changes observed in the RNFL, GCL+IPL, OPL and OS were distributed across all macular regions (except for the INL in the foveal region).

When comparing MDR with DM eyes, the layer index in each intraretinal layer showed significant differences in the GCL+IPL, INL, OPL, OS and RPE. Moreover, Figure 5.6 clearly indicates that the statistically significant layer index changes in the INL, OPL and OS were also observed across all macular regions.

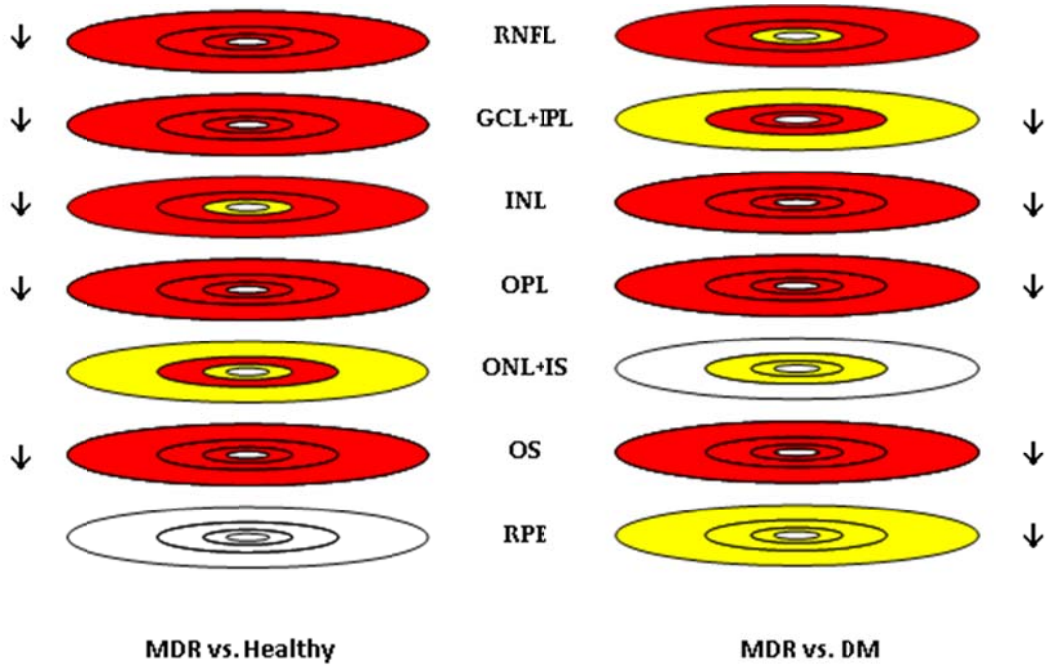

Figure 5.6 Layer index changes in each macular region and intraretinal layer for MDR vs. Healthy and MDR vs. DM. Comparisons were performed using ANOVA followed by Newman-Keuls post hoc analysis. The red and yellow color denotes $p<0.001$ and $0.001<p<0.05$, respectively. Arrows denote an increasing (decreasing) trend when pointing up (down).

5.2.4 SCATTERING COEFFICIENTS

The scattering coefficient in each intraretinal layer was calculated across all macular regions for the healthy and DM eyes with and without MDR. The scattering coefficient in each macular region in each intraretinal layer was also measured, except in the foveola. Two normalization methods were used in the calculations performed with both the single and multiple scattering models: 1. Reflectivity normalized to the maximum value within the whole retina (NRIR); and 2. Reflectivity normalized with respect to the RPE reflectance (NRPE). The scattering coefficients are given in Tables 5.4-5.7. The values are expressed in the form of the mean ± SD (SD: standard deviation).

The scattering coefficient changes were analyzed using ANOVA followed by Newman-Keuls post-hoc analysis between DM, MDR and healthy eyes. Significant differences between study groups are also reported in Tables 5.4-5.7.

5.2.4.1 SCATTERING COEFFICIENT CHANGES CALCULATED USING THE SINGLE-SCATTERING MODEL AND THE NRIR METHOD

The scattering coefficient measurements are given in Table 5.4.

5.2.4.1.1 CHANGES IN THE SCATTERING COEFFICIENT OF THE INTRARETINAL LAYERS

When comparing MDR with healthy eyes, the scattering coefficient in each intraretinal layer showed a statistically significant increase in the OS and RPE (24% and 13%, respectively). However, the scattering coefficient showed a non-significant decrease in all other intraretinal layers.

When comparing MDR with DM eyes, the scattering coefficient in each intraretinal layer showed a significant decrease (14%) in the OPL as well as a significant increase in the OS and RPE (28% and 13%, respectively). In addition, the scattering coefficient showed a non-significant decrease in the RNFL, GCL+IPL and INL.

5.2.4.1.2 SCATTERING COEFFICIENT CHANGES IN THE INTRARETINAL LAYERS OF THE FOVEAL REGION

In MDR, compared to healthy eyes, the foveal scattering coefficient showed a significant increase for in GCL+IPL and RPE (9% and 13%, respectively). However, the foveal scattering coefficient showed a non-significant decrease in the RNFL, OPL, ONL+IS and OS.

When comparing MDR with DM eyes, the foveal scattering coefficient showed a significant increase in the OS and RPE (38% and 12%, respectively). In addition, the

foveal scattering coefficient showed a non-significant decrease in the RNFL and INL and a non-significant increasing in the GCL+IPL, OPL and ONL+IS.

5.2.4.1.3 SCATTERING COEFFICIENT CHANGES IN THE INTRARETINAL LAYERS OF THE PARAFOVEAL REGION

The parafoveal scattering coefficient in MDR compared to healthy eyes showed a significant increase in the OS and RPE (20% and 14%, respectively). However, the parafoveal scattering coefficient showed a non-significant decrease in the RNFL, INL and OPL and a non-significant increase in the GCL+IPL and ONL+IS.

When comparing MDR with DM eyes, the parafoveal scattering coefficient showed a significant increase in the OS and RPE (44% and 13%, respectively). In addition, the parafoveal scattering coefficient also showed a non-significant decrease for the RNFL, INL and OPL and a non-significant increase in the GCL+IPL and ONL+IS.

5.2.4.1.4 SCATTERING COEFFICIENT CHANGES IN THE INTRARETINAL LAYERS OF THE PERIFOVEAL REGION

The perifoveal scattering coefficient in MDR compared to healthy eyes showed a significant increase in the OS and RPE (21% and 12%, respectively). However, the perifoveal scattering coefficient showed a non-significant decrease in all other intraretinal layers (except in the ONL+IS).

When comparing MDR with DM eyes, the perifoveal scattering coefficient showed a significant increase in the OS and RPE (29% and 12%, respectively). In addition, the perifoveal scattering coefficient showed a non-significant decrease in all other intraretinal layers (except in the ONL+IS).

5.2.4.1.5 SCATTERING COEFFICIENT CHANGES IN THE INTRARETINAL LAYERS ACROSS ALL MACULAR REGIONS

A summary of the statistical analyses for the scattering coefficient changes in each macular region for each intraretinal layer is shown in Figure 5.7. We note that results across all macular regions were averaged per eye. The scattering coefficient in each intraretinal layer showed a significant increase in the OS and RPE in MDR compared to healthy and DM eyes. Moreover, Figure 5.9 clearly indicates that the significant layer index changes observed in the OS and RPE were distributed across all macular regions (except for the foveal region in the OS when compared MDR to healthy eyes).

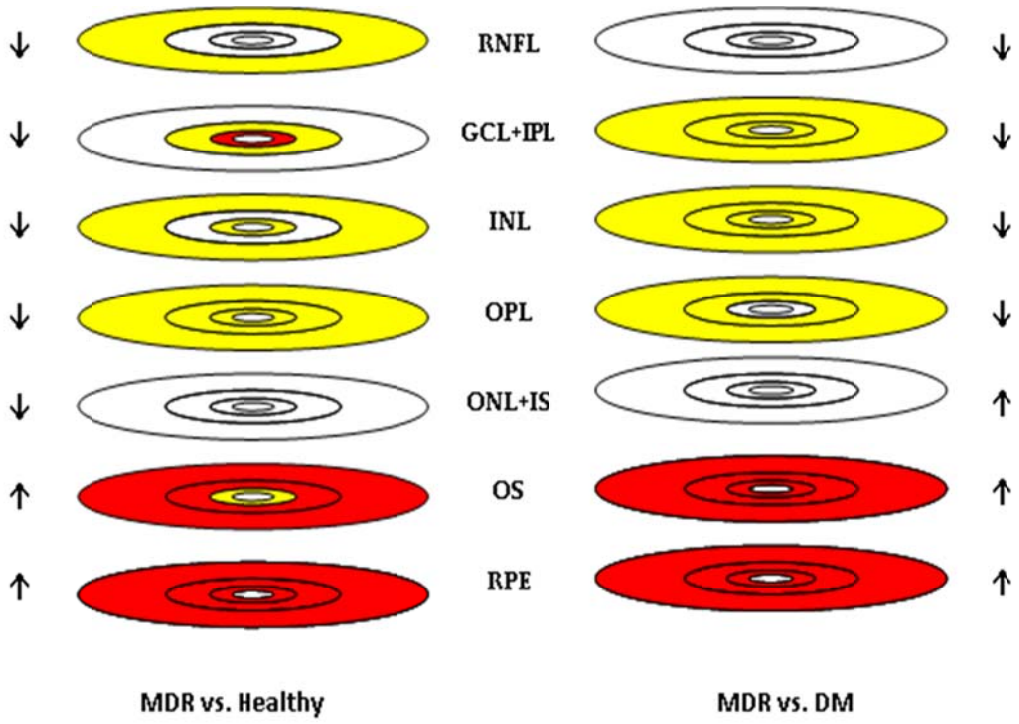

Figure 5.7 Scattering coefficient changes in each macular region and intraretinal layer. Comparisons were performed using ANOVA followed by Newman-Keuls post hoc analysis. The red and yellow color denotes $p<0.001$ and $0.001<p<0.05$, respectively. Arrows denote an increasing (decreasing) trend when pointing up (down).

5.2.4.2 SCATTERING COEFFICIENT CHANGES CALCULATED USING THE SINGLE-SCATTERING MODEL AND THE NRPE METHOD

The scattering coefficient measurements are given in Table 5.5.

5.2.4.2.1 INTRARETINAL LAYER SCATTERING COEFFICIENT CHANGES PER EYE

The scattering coefficient per intraretinal layer in MDR compared with that for healthy eyes showed a statistically significant increase for the OS and RPE (29% and 18%, respectively). However, the scattering coefficient showed a decreasing trend without reaching statistical significances for the RNFL, INL and OPL.

When comparing MDR and DM eyes, the scattering coefficient per intraretinal layer showed a statistically significant decrease (10%) for OPL as well as a statistically significant increase for the OS and RPE (33% and 18%, respectively). In addition, the scattering coefficient showed a decreasing trend without reaching statistical significances for the GCL+IPL, INL and ONL+IS.

5.2.4.2.2 INTRARETINAL LAYER SCATTERING COEFFICIENT CHANGES IN THE FOVEAL REGION

The foveal scattering coefficient in MDR compared with that for healthy eyes showed a statistically significant increase for the GCL+IPL, OPL, OS and RPE (12%, 13%, 23% and 16%, respectively). Moreover, the foveal scattering coefficient showed a decreasing trend for the INL as well as an increasing trend for the RNFL and ONL+IS without reaching statistical significances.

When comparing MDR and DM eyes, the foveal scattering coefficient showed a statistically increase for the OS and RPE (40% and 13%, respectively). In addition, the foveal scattering coefficient showed a decreasing trend for the RNFL and INL and an

increasing trend for the GCL+IPL, OPL and ONL+IS without reaching statistical significances.

5.2.4.2.3 INTRARETINAL LAYER SCATTERING COEFFICIENT CHANGES IN THE PARAFOVEAL REGION

The parafoveal scattering coefficient in MDR compared with that for healthy eyes showed a statistically significant increase for the GCL+IPL, OS and RPE (11%, 23% and 17%, respectively). However, the parafoveal scattering coefficient showed a decreasing trend for the INL and OPL and an increasing trend for the RNFL and ONL+IS without reaching statistical significances.

When comparing MDR and DM eyes, the parafoveal scattering coefficient showed a statistically significant increase for the OS and RPE (46% and 15%, respectively). In addition, the parafoveal scattering coefficient also showed a decreasing trend for the INL and OPL and an increasing trend for the GCL+IPL and ONL+IS without reaching statistical significances.

5.2.4.2.4 INTRARETINAL LAYER SCATTERING COEFFICIENT CHANGES IN THE PERIFOVEAL REGION

The perifoveal scattering coefficient in MDR compared with that for healthy eyes showed a statistically significant increase for the OS and RPE (26% and 18%, respectively). Moreover, the perifoveal scattering coefficient showed a decreasing trend for the RNFL and INL and an increasing trend for the GCL+IPL, OPL and ONL+IS without reaching statistical significances.

When comparing MDR with healthy eyes, the perifoveal scattering coefficient showed a statistically significant increase for the OS and RPE (33% and 10%, respectively). In addition, the perifoveal scattering coefficient showed a decreasing trend

for the GCL+IPL, INL and OPL and an increasing trend for the ONL+IS without reaching statistical significances.

5.2.4.2.5 INTRARETINAL LAYER SCATTERING COEFFICIENT CHANGES ACROSS ALL MACULAR REGIONS

A summary of the statistical analyses for the scattering coefficients' changes per macular region for each intraretinal layer is shown in Figure 5.8. We note that results across all macular regions were averaged per eye. The scattering coefficient per intraretinal layer showed a statistically significant increase for the OS and RPE in the MDR compared to healthy and DM eyes. Moreover, Figure 5.10 clearly indicates that the statistically significant layer index changes observed for the OS and RPE were distributed across all macular regions.

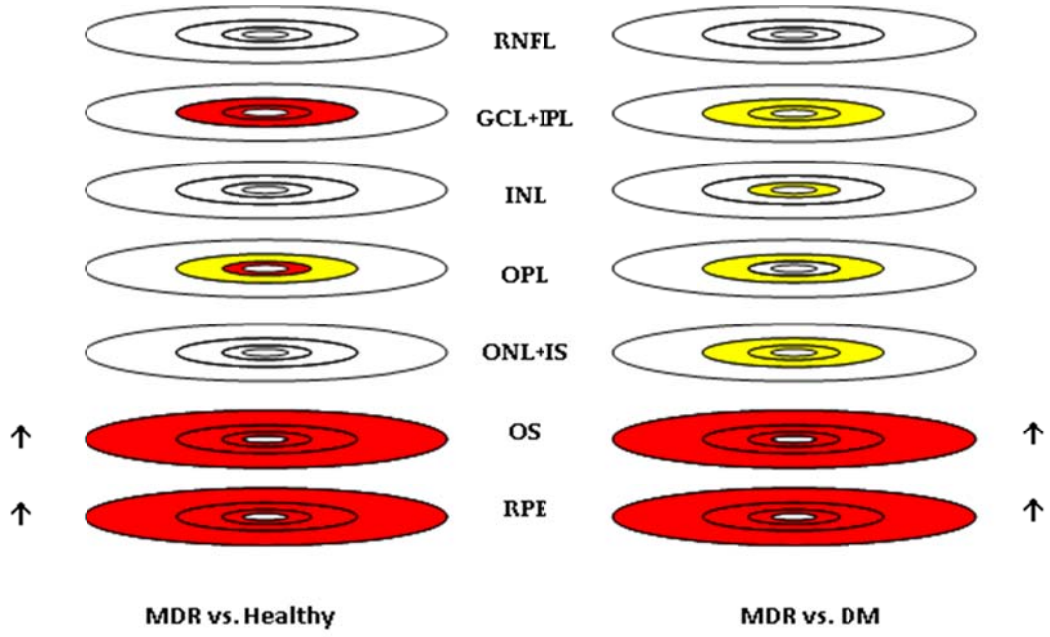

Figure 5.8 Scattering coefficient changes per macular region per intraretinal layer. Comparisons were performed with ANOVA followed by Newman-Keuls post hoc analysis. The red and yellow colors denote $p<0.001$ and $0.001<p<0.05$, respectively. Arrows denote an increasing (decreasing) trend when pointing up (down).

5.2.4.3 SCATTERING COEFFICIENT CHANGES CALCULATED USING THE MULTIPLE-SCATTERING MODEL AND THE NRIR METHOD

The scattering coefficient per intraretinal layer was calculated across all macular regions for healthy and DM eyes with and without MDR. The scattering coefficient per macular region per intraretinal layer was also measured, except in the foveola. The multiple-scattering model with the NRIR normalization method was used for the calculation. The scattering coefficient measurements are given in Table 5.6. Values are expressed in the form of mean ± SD (SD: standard deviation).

The scattering coefficient changes were analyzed using ANOVA followed by Newman-Keuls post-hoc analysis between DM, MDR and healthy eyes. Significant differences between the study groups are also reported in Table 5.6.

5.2.4.3.1 INTRARETINAL LAYER SCATTERING COEFFICIENT CHANGES PER EYE

The scattering coefficient per intraretinal layer in MDR compared with that for healthy eyes showed a statistically significant increase for the OS and RPE (18% and 11%, respectively). However, the scattering coefficient showed a decreasing trend for all other intraretinal layers without reaching statistical significance.

When comparing MDR with DM eyes, the scattering coefficient per intraretinal layer showed a statistically significant decrease for the OPL (11%), as well as a statistically significant increase for the OS and RPE (20% and 11%, respectively). In addition, the scattering coefficient showed a decreasing trend for the RNFL, GCL+IPL and INL and an increasing trend for the ONL+IS without reaching statistical significance.

5.2.4.3.2 INTRARETINAL LAYER SCATTERING COEFFICIENT CHANGES IN THE FOVEAL REGION

The foveal scattering coefficient in MDR compared with that for healthy eyes showed a statistically significant increase for the GCL+IPL, OPL and RPE (16%, 11%

and 10%, respectively). Additionally, the foveal scattering coefficient showed a decreasing trend for the INL and an increasing trend in the RNFL and OS without reaching statistical significance.

When comparing MDR and DM eyes, the foveal scattering coefficient showed a statistically significant increase for the OS and RPE (24% and 9%, respectively). In addition, the foveal scattering coefficient showed a decreasing trend for the RNFL and INL and an increasing trend in the GCL+IPL, OPL and ONL+IS without reaching statistical significance.

5.2.4.3.3 INTRARETINAL LAYER SCATTERING COEFFICIENT CHANGES IN THE PARAFOVEAL REGION

The parafoveal scattering coefficient in MDR compared with that for healthy eyes showed a statistically significant increase for the OS and RPE (13% and 12%, respectively). In addition, the parafoveal scattering coefficient showed a decreasing trend for the INL and OPL and an increasing trend in the RNFL and GCL+IPL without reaching statistical significance.

When comparing MDR and DM eyes, the parafoveal scattering coefficient showed a statistically significant increase for the OS and RPE (31% and 10%, respectively). In addition, the parafoveal scattering coefficient showed a decreasing trend for the RNFL, INL and OPL and an increasing trend in the GCL+IPL and ONL+IS without reaching statistical significance.

5.2.4.3.4 INTRARETINAL LAYER SCATTERING COEFFICIENT CHANGES IN THE PERIFOVEAL REGION

The perifoveal scattering coefficient in MDR compared with that for healthy eyes showed a statistically significant increase for the OS and RPE (15% and 10%, respectively). Additionally, the perifoveal scattering coefficient showed a decreasing

trend for the RNFL, INL, OPL and ONL+IS and an increasing trend for the GCL+IPL without reaching statistical significance.

When comparing MDR and DM eyes, the perifoveal scattering coefficient showed a statistically significant increase for the OS and RPE (20% and 10%, respectively). In addition, the perifoveal scattering coefficient showed a decreasing trend for the RNFL, GCL+IPL, INL and OPL and an increasing trend for the ONL+IS without reaching statistical significance.

5.2.4.3.5 INTRARETINAL LAYER SCATTERING COEFFICIENT CHANGES ACROSS ALL MACULAR REGIONS

A summary of the statistical analyses for the scattering coefficient changes per macular region for each intraretinal layer is shown in Figure 5.9. We note that the results across all macular regions were averaged per eye. The scattering coefficient per intraretinal layer showed a statistically significant increase for the OS and RPE in the MDR compared with that for healthy and DM eyes. Moreover, Figure 5.10 clearly indicates that the statistically significant layer index changes observed for the OS and RPE were distributed across all macular regions.

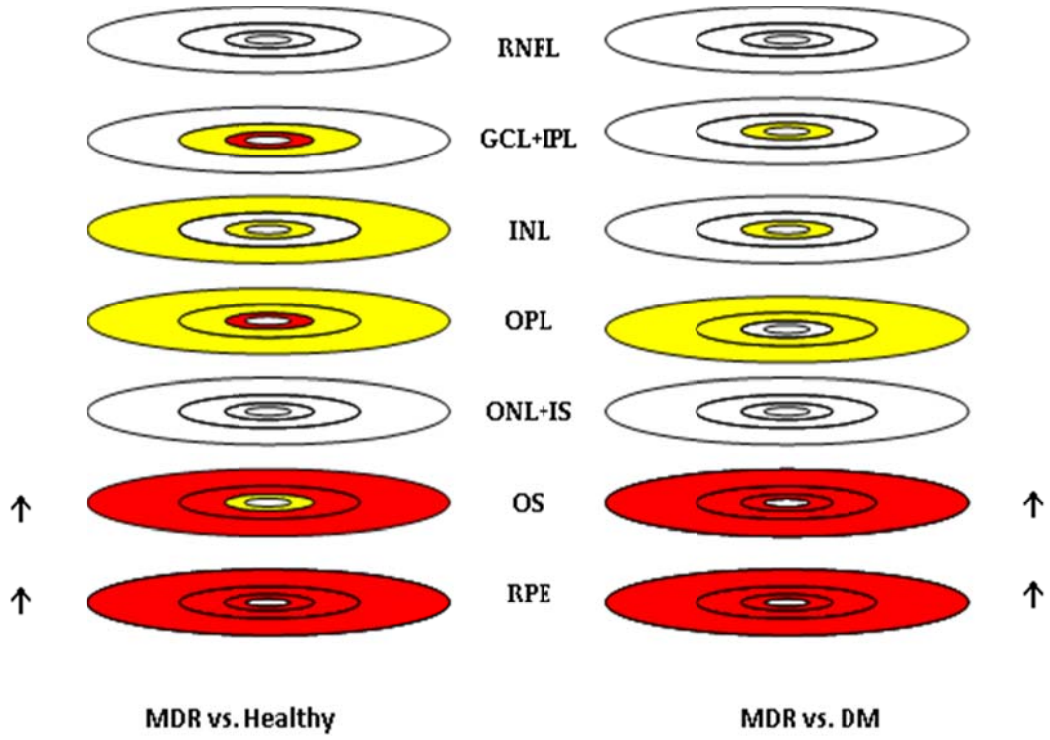

Figure 5.9 Scattering coefficient (multiple, NRIR) changes per macular region per intraretinal layer. Comparisons were performed using ANOVA followed by Newman-Keuls post hoc analysis. The red and yellow colors denote $p<0.001$ and $0.001<p<0.05$, respectively. Arrows denote an increasing (decreasing) trend when pointing up (down).

5.2.4.4 SCATTERING COEFFICIENTS CALCULATED USING THE MULTIPLE-SCATTERING MODEL WITH THE NRPE METHOD

The scattering coefficient per intraretinal layer was calculated across all macular regions for the healthy and DM eyes with and without MDR. The scattering coefficient per macular region per intraretinal layer was also measured, except in the foveola. The multiple-scattering model with the NRPE normalization method was used for the calculation. The scattering coefficient measurements are given in Table 5.7. Values are expressed as the mean ± SD (SD: standard deviation).

The scattering coefficient changes were analyzed using ANOVA followed by Newman-Keuls post hoc analysis between DM, MDR and healthy eyes. Significant differences between the study groups are also reported in Table 5.7.

5.2.4.4.1 INTRARETINAL LAYER SCATTERING COEFFICIENT CHANGES PER EYE

The scattering coefficient showed a statistically significant increase for the OS and RPE (23% and 16%, respectively) in MDR compared with that for healthy eyes. Additionally, the scattering coefficient per intraretinal layer showed a decreasing trend for the INL and OPL and showed an increasing trend for the RNFL, GCL+IPL and ONL+IS without reaching statistical significance.

When comparing MDR and DM eyes, the scattering coefficient showed a statistically significant increase for the OS and RPE (25% and 15%, respectively) and a statistically significant decrease for the OPL (9%). Moreover, the scattering coefficient per intraretinal layer showed a decreasing trend for the GCL+IPL and INL and an increasing tread for the RNFL and ONL+IS without reaching statistical significance.

5.2.4.4.2 INTRARETINAL LAYER SCATTERING COEFFICIENT CHANGES IN THE FOVEAL REGION

The foveal scattering coefficient in MDR compared with that for healthy eyes showed a statistically significant increase for the GCL+IPL, OPL, OS and RPE (19%, 14%, 11% and 11%, respectively). Moreover, the foveal scattering coefficient showed a decreasing trend for the INL and an increasing trend for the RNFL and ONL+IS without reaching statistical significance.

When comparing MDR and DM eyes, the foveal scattering coefficient showed a statistically significant increase in the GCL+IPL, OS and RPE (10%, 27% and 11%,

respectively). Moreover, the foveal scattering coefficient showed a decreasing trend for the RNFL and INL and an increasing trend for the OPL and ONL+IS without reaching statistical significance.

5.2.4.4.3 INTRARETINAL LAYER SCATTERING COEFFICIENT CHANGES IN THE PARAFOVEAL REGION

The parafoveal scattering coefficient showed a statistically significant increase for the GCL+IPL, OS and RPE (10%, 17% and 15%, respectively) in MDR compared with that for healthy eyes. Additionally, the parafoveal scattering coefficient per intraretinal layer showed a decreasing trend for the INL and OPL and an increasing trend for the RNFL and ONL+IS without reaching statistical significance.

When comparing MDR and DM eyes, the parafoveal scattering coefficient showed a statistically significant increase for the OS and RPE (35% and 12%, respectively). Moreover, the parafoveal scattering coefficient per intraretinal layer showed a decreasing trend for the INL and OPL and showed an increasing trend for the RNFL, GCL+IPL and ONL+IS without reaching statistical significance.

5.2.4.4.4 INTRARETINAL LAYER SCATTERING COEFFICIENT CHANGES IN THE PERIFOVEAL REGION

The perifoveal scattering coefficient in MDR compared with that for healthy eyes showed a statistically significant increase for the OS and RPE (21% and 15%, respectively). Moreover, the perifoveal scattering coefficient showed a decreasing trend for the INL and OPL and an increasing trend for the RNFL, GCL+IPL and ONL+IS without reaching statistical significance.

When comparing MDR and DM eyes, the perifoveal scattering coefficient showed a statistically significant increase for the OS and RPE (26% and 14%, respectively). Moreover, the perifoveal scattering coefficient showed a decreasing trend

for the GCL+IPL, INL and OPL and an increasing trend for the RNFL and ONL+IS without reaching statistical significance.

5.2.4.4.5 INTRARETINAL LAYER SCATTERING COEFFICIENT CHANGES ACROSS ALL MACULAR REGIONS

Figure 5.10 provides a summary of the statistical analyses for the scattering coefficient changes per macular region for each intraretinal layer. We note that the results across all macular regions were averaged per eye. The scattering coefficient per intraretinal layer showed a statistically significant increase for the OS and RPE in the MDR compared with those for healthy and DM eyes. Moreover, Figure 5.10 clearly indicates that the statistically significant layer index changes observed for the OS and RPE were distributed across all macular regions.

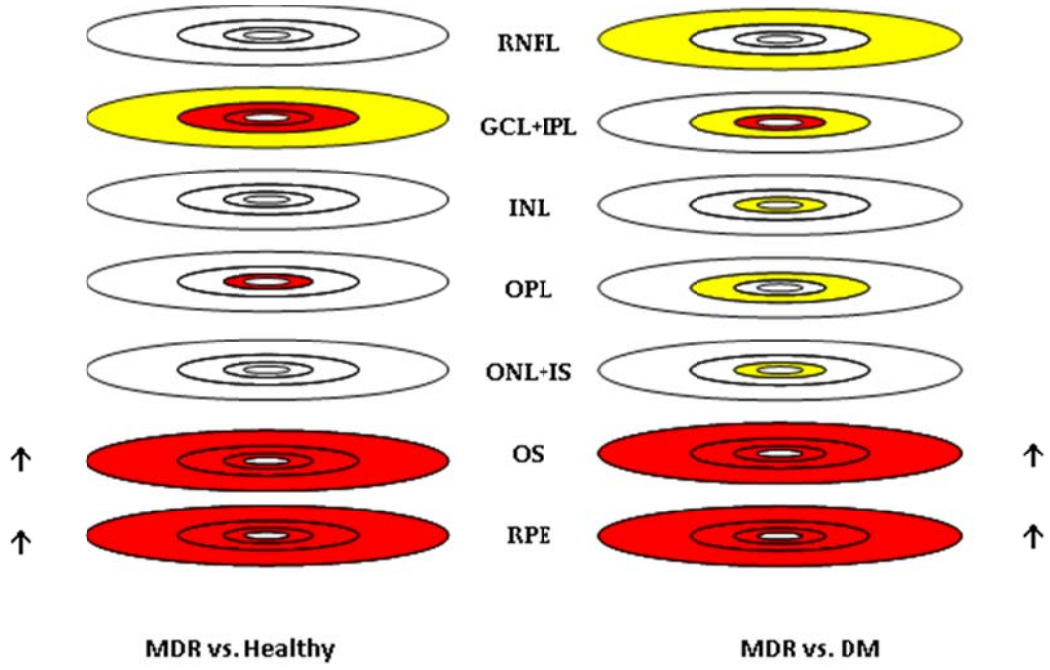

Figure 5.10 Scattering coefficient changes per macular region per intraretinal layer. Comparisons were performed with ANOVA followed by Newman-Keuls post hoc analysis. The red and yellow colors denote $p<0.001$ and $0.001<p<0.05$, respectively. Arrows denote an increasing (decreasing) trend when pointing up (down).

5.3 RECEIVER OPERATING CHARACTERISTIC (ROC) ANALYSIS

In the previous section, optical characteristics were extracted from the OCT images and their changes were investigated in each intraretinal layer using different normalization methods and scattering models. Statistically significant changes in these parameters per macular region were found in several particular intraretinal layers and therefore could be used as indicators to discriminate MDR eyes from healthy eyes and DM eyes. As our results demonstrate, mean reflectance, total reflectance and layer index parameters appear to more powerfully differentiate MDR eyes from healthy eyes than from DM eyes. However, the discriminating power of these optical parameters per macular region needs to be determined. Accordingly, a receiver operating characteristic (ROC) analysis was used to determine the discriminating power of the optical parameters per macular region. The area under the ROC (AUROC) curve was calculated as described in the previous chapter.

5.3.1 ROC ANALYSIS FOR MEAN REFLECTANCE MEASUREMENTS

ROC analyses with corresponding sensitivity and specificity tests were only performed for the intraretinal layers that showed statistically significant mean reflectance differences per macular region when comparing MDR eyes with healthy and DM eyes. These layers were the RNFL, GCL+IPL, INL, OPL and ONL+IS. The ROC curves are shown in Figures 5.11 and 5.12. Table 5.10 displays the AUROC values for each discrimination test. Cutoff values for the mean reflectance derived from ROC analyses are shown in Table 5.11 and Table 5.12, respectively.

When comparing MDR and healthy eyes, the highest AUROC values were observed in the RNFL, GCL+IPL, INL, OPL and ONL+IS (0.81, 0.79, 0.75, 0.77 and

0.75, respectively). The cutoff point for the RNFL was suggested as 52.91 dB with the sensitivity and specificity at 0.80 and 0.70, respectively. The cutoff point for the GCL+IPL was suggested as 48.55 dB with the sensitivity and specificity at 0.78 and 0.68, respectively. The cutoff point for the INL was suggested as 45.36 dB with the sensitivity and specificity at 0.73 and 0.63, respectively. The cutoff point for the OPL was suggested as 47.03 dB with the sensitivity and specificity at 0.74 and 0.64, respectively. Furthermore, the cutoff point for the ONL+IS was suggested as 42.37 dB with the sensitivity and specificity at 0.77 and 0.67, respectively. Additionally, by comparing ROC curves (see Figure 5.12), we found that the most significant mean reflectance changes were obtained for the RNFL in the foveal, parafoveal and perifoveal macular region. In the foveal region, the AUROC for the RNFL was 0.79 with a cutoff point at 50.86 dB. Likewise, the AUROC for the RNFL in the parafoveal (perifoveal) region was 0.83 (0.84) with a cutoff point at 52.29 (53.44) dB.

The highest AUROC values obtained while comparing MDR and DM eyes were observed in the RNFL, GCL+IPL, INL, OPL and ONL+IS (0.75, 0.72, 0.70, 0.74 and 0.72, respectively). The cutoff point for the RNFL was suggested as 52.46 dB with the sensitivity and specificity at 0.75 and 0.65, respectively. The cutoff point for the GCL+IPL was suggested as 48.22 dB with the sensitivity and specificity at 0.71 and 0.61, respectively. The cutoff point for the INL was suggested as 44.93 dB with the sensitivity and specificity at 0.66 and 0.56, respectively. The cutoff point for the OPL was suggested as 46.98 dB with the sensitivity and specificity at 0.71 and 0.61, respectively. Moreover, the cutoff point for the ONL+IS was suggested as 42.25 dB with the sensitivity and specificity at 0.71 and 0.61, respectively. Additionally, by comparing ROC curves (see

Figure 5.12), we found that the most significant mean reflectance changes were obtained for the OPL, RNFL and RNFL in the foveal, parafoveal and perifoveal macular region. In the foveal region, the AUROC for the OPL was 0.75 with a cutoff point at 47.32 dB. Likewise, the AUROC for the RNFL in the parafoveal (perifoveal) region was 0.76 (0.75) with a cutoff point at 52.08 (53.05) dB.

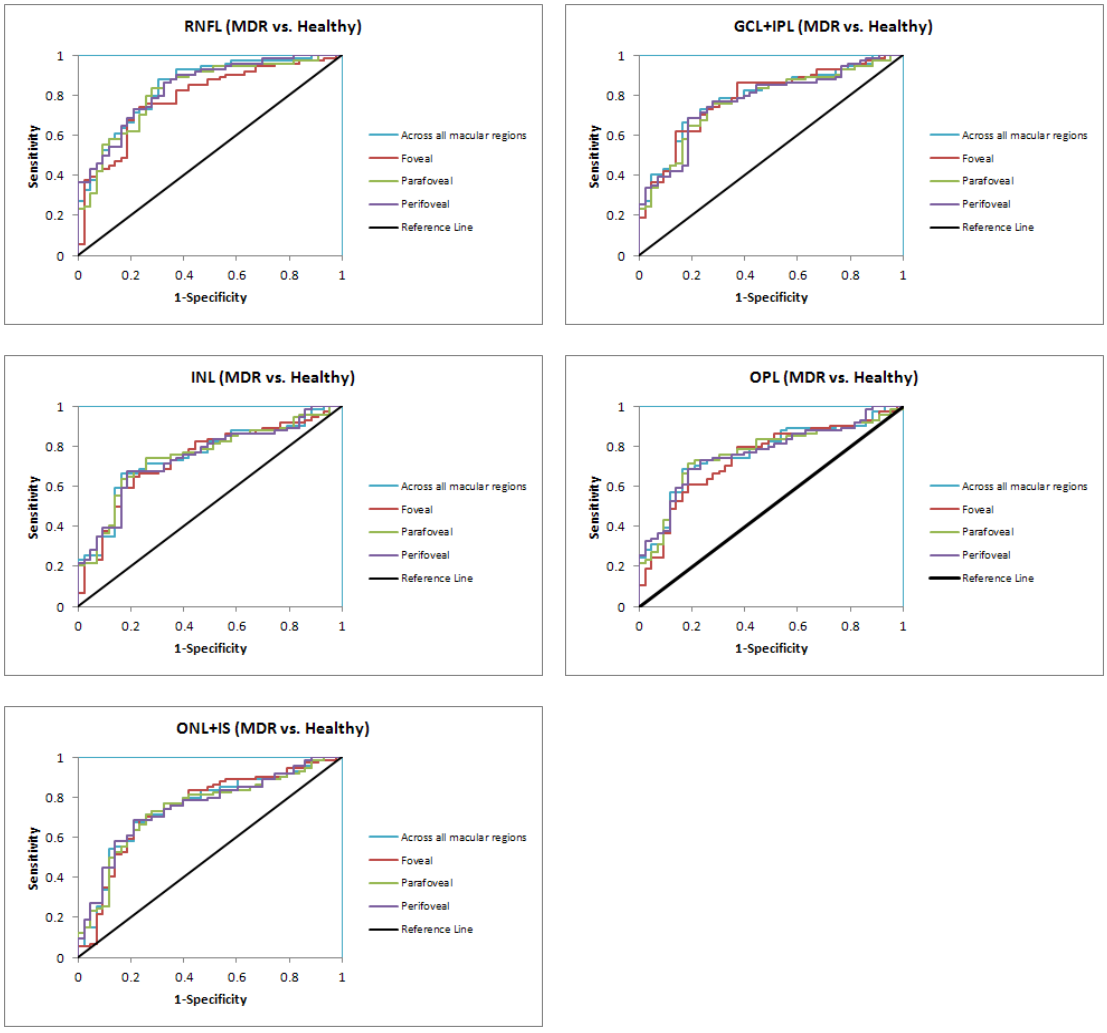

Figure 5.11 Receiver operating characteristic (ROC) curves for the detection of early DR using mean reflectance measurements of the RNFL, GCL+IPL, INL, OPL and ONL+IS as predictor variables when comparing MDR with healthy eyes.

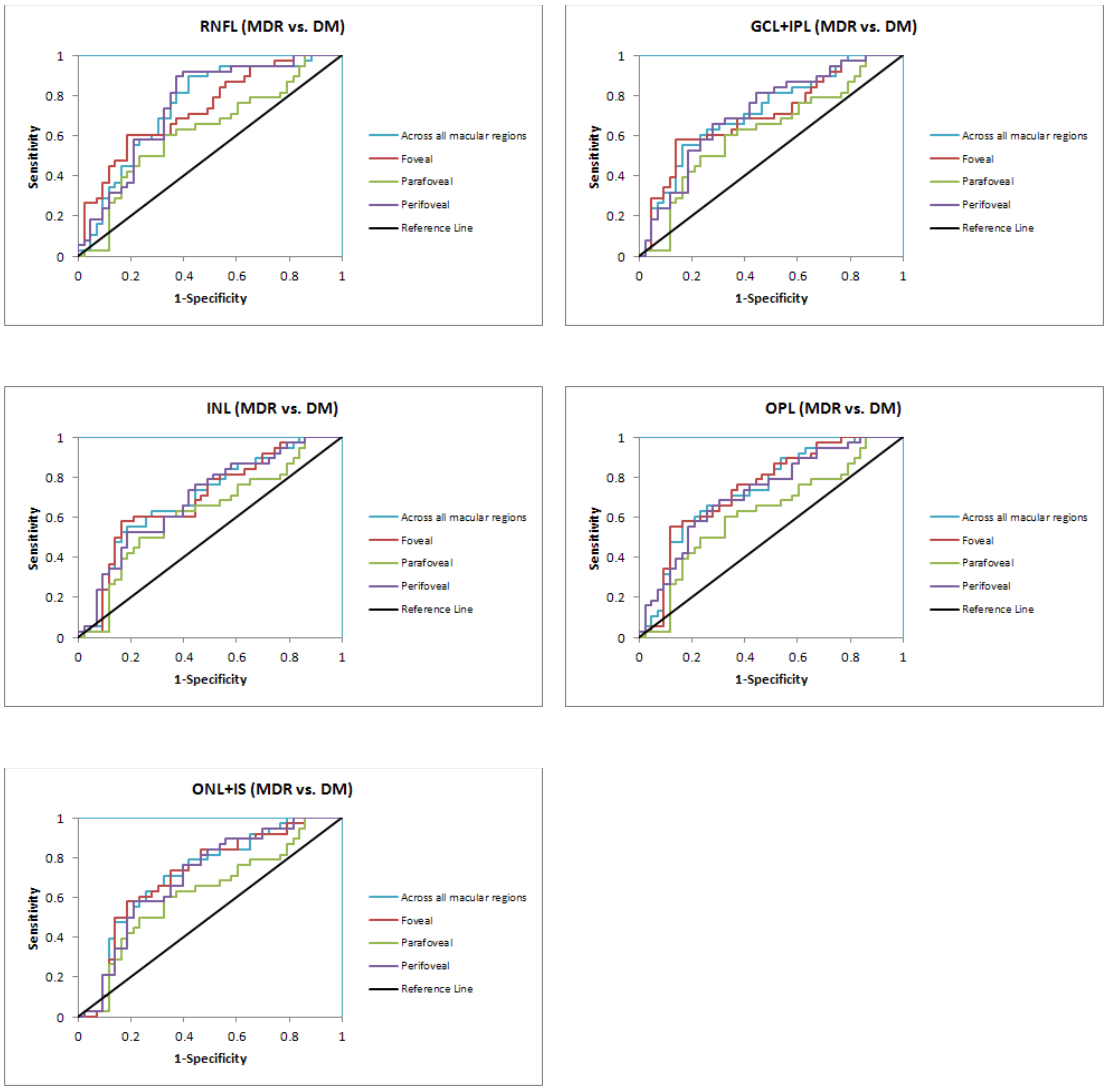

Figure 5.12 Receiver operating characteristic (ROC) curves for the detection of early DR using mean reflectance measurements of the RNFL, GCL+IPL, INL, OPL and ONL+IS as predictor variables when comparing MDR with DM eyes

5.3.2 ROC ANALYSIS FOR TOTAL REFLECTANCE MEASUREMENTS

ROC analyses with corresponding sensitivity and specificity tests were only performed for the intraretinal layers that showed statistically significant total reflectance differences per macular region when comparing MDR eyes with healthy and DM eyes. These layers were the RNFL, GCL+IPL, INL, OPL, ONL+IS and OS. The ROC curves are shown in Figures 5.15 and 5.16. Table 5.13 presents the AUROC values for each

discrimination test. Cutoff values of total reflectance derived from the ROC analyses are shown in Table 5.14 and Table 5.15, respectively.

When comparing MDR eyes and healthy eyes, the highest AUROC values were observed in the RNFL, GCL+IPL, INL, OPL, ONL+IS and OS (0.83, 0.84, 0.76, 0.84, 0.74 and 0.85, respectively). The cutoff point for the RNFL was suggested as 79.89 dB with the sensitivity and specificity at 0.80 and 0.70, respectively. The cutoff point for the GCL+IPL was suggested as 80.57 dB with the sensitivity and specificity at 0.82 and 0.72, respectively. The cutoff point for the INL was suggested as 70.47 dB with the sensitivity and specificity at 0.74 and 0.64, respectively. The cutoff point for the OPL was suggested as 72.97 dB with the sensitivity and specificity at 0.81 and 0.71, respectively. The cutoff point for the ONL+IS was suggested as 75.33 dB with the sensitivity and specificity at 0.73 and 0.63, respectively. Moreover, the cutoff point for the OS was suggested as 74.22 dB with the sensitivity and specificity at 0.80 and 0.70, respectively. Additionally, by comparing ROC curves (see Figure 5.15), we found that the most significant total reflectance changes were obtained for the OPL, OS and OS in the foveal, parafoveal and perifoveal macular region. In the foveal region, the AUROC for the OPL was 0.90 with a cutoff point at 75.56 dB. Likewise, the AUROC for the OS in the parafoveal (perifoveal) region was 0.83 (0.84) with a cutoff point at 74.31 (73.56) dB.

The highest AUROC values obtained when comparing MDR and DM eyes were observed in the RNFL, GCL+IPL, INL, OPL and OS (0.73, 0.78, 0.74, 0.76 and 0.86, respectively). The cutoff point for the RNFL was suggested as 79.41 dB with the sensitivity and specificity at 0.71 and 0.61, respectively. The cutoff point for the GCL+IPL was suggested as 79.91 dB with the sensitivity and specificity at 0.75 and 0.65,

respectively. The cutoff point for the INL was suggested as 70.38 dB with the sensitivity and specificity at 0.68 and 0.58, respectively. The cutoff point for the OPL was suggested as 72.73 dB with the sensitivity and specificity at 0.68 and 0.58, respectively. Moreover, the cutoff point for the OS was suggested as 74.29 dB with the sensitivity and specificity at 0.82 and 0.72, respectively. Additionally, by comparing ROC curves (see Figure 5.16), we found that the most significant total reflectance changes were obtained for the OS in the foveal, parafoveal and perifoveal macular region. In the foveal region, the AUROC for the OS was 0.86 with a cutoff point at 74.83 dB. Likewise, the AUROC for the RNFL in the parafoveal (perifoveal) region was 0.87 (0.84) with a cutoff point at 74.40 (73.83) dB.

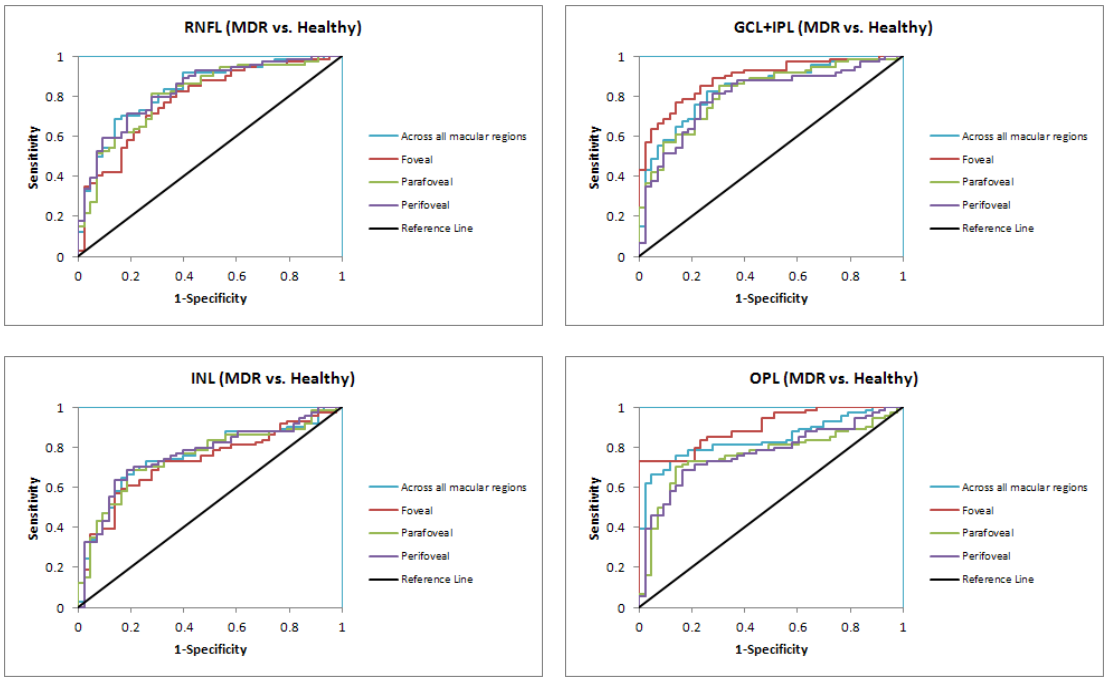

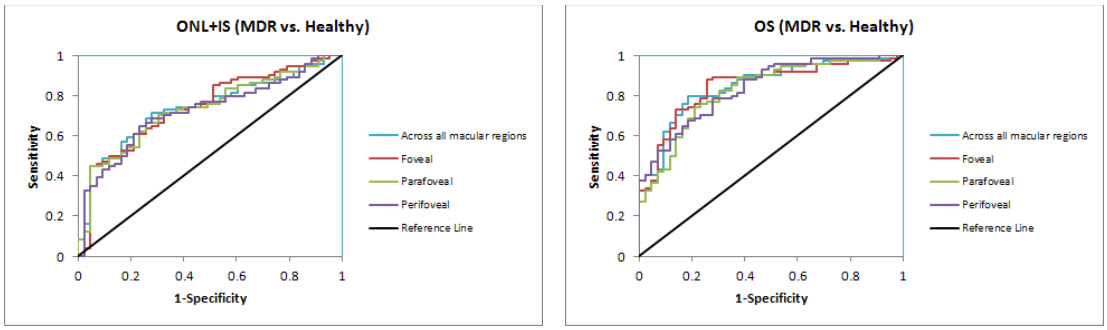

Figure 5.13 Receiver operating characteristic (ROC) curves for the detection of early DR using total reflectance measurements of the RNFL, GCL+IPL, INL, OPL, ONL+IS and OS as predictor variables when comparing MDR with healthy eyes.

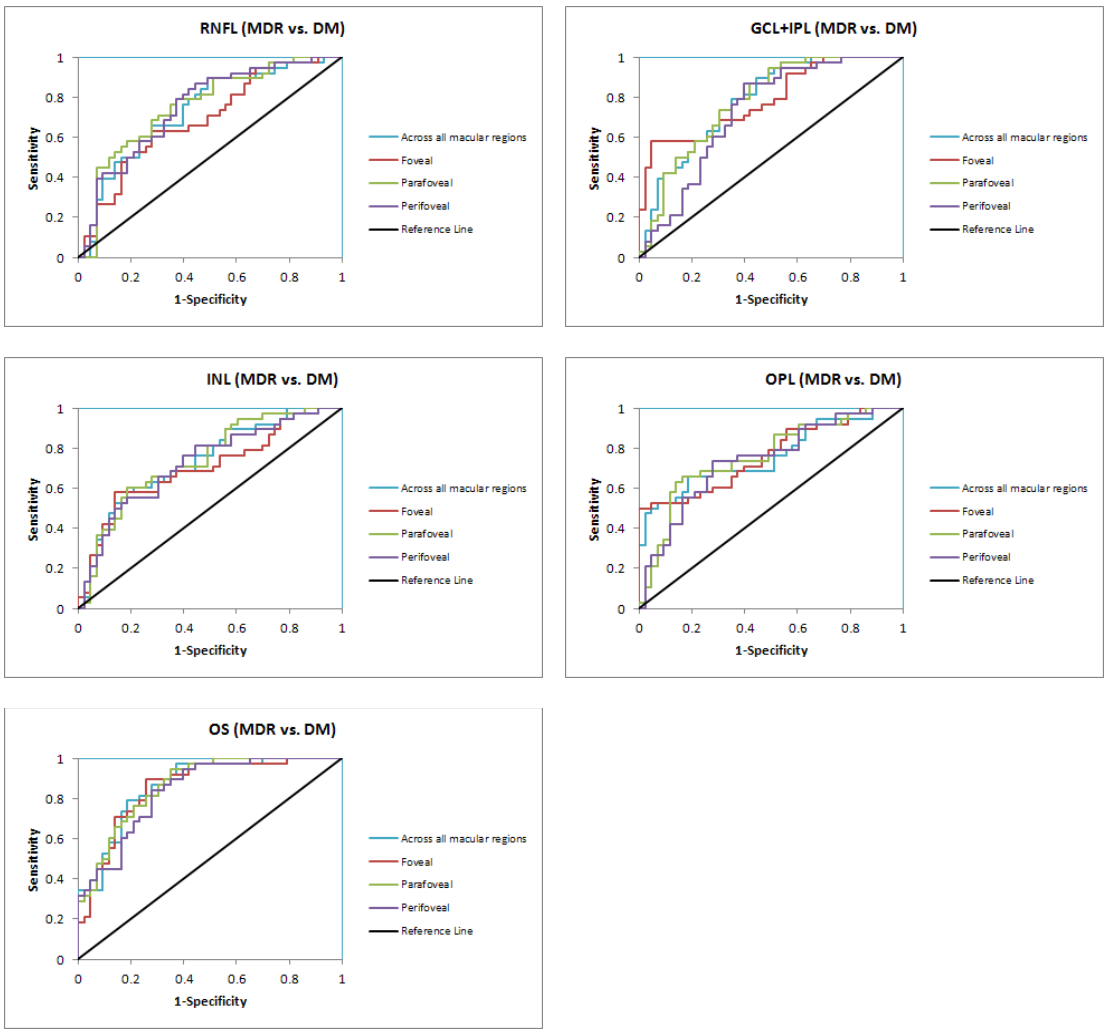

Figure 5.14 Receiver operating characteristic (ROC) curves for the detection of early DR using total reflectance measurements of the RNFL, GCL+IPL, INL, OPL and OS as predictor variables when comparing MDR with DM eyes.

5.3.3 ROC ANALYSIS FOR LAYER INDEX MEASUREMENTS

ROC analyses with corresponding sensitivity and specificity tests were only performed for intraretinal layers that demonstrated statistically significant layer index differences per macular region when comparing MDR eyes with healthy and DM eyes. These layers were the RNFL, GCL+IPL, INL, OPL, ONL+IS and OS. The ROC curves are shown in Figures 5.17 and 5.18. AUROC values are shown in Table 5.16 for each discrimination test. Cutoff values of layer index derived from ROC analyses are shown in Table 5.17 and Table 5.18.

When comparing MDR and healthy eyes, the highest AUROC values were observed in the RNFL, GCL+IPL, INL, OPL, ONL+IS and OS (0.80, 0.85, 0.73, 0.83, 0.71 and 0.81, respectively). The cutoff point for the RNFL was suggested as 11.47 with the sensitivity and specificity at 0.77 and 0.67, respectively. The cutoff point for the GCL+IPL was suggested as 12.20 with the sensitivity and specificity at 0.85 and 0.75, respectively. The cutoff point for the INL was suggested as 3.84 with the sensitivity and specificity at 0.74 and 0.68, respectively. The cutoff point for the OPL was suggested as 5.03 with the sensitivity and specificity at 0.78 and 0.71, respectively. The cutoff point for the ONL+IS was suggested as 6.53 with the sensitivity and specificity at 0.72 and 0.62, respectively. Moreover, the cutoff point for the OS was suggested as 5.55 with the sensitivity and specificity at 0.78 and 0.68, respectively. Additionally, by comparing ROC curves (see Figure 5.17), we found that the most significant layer index changes were obtained for the GCL+IPL, GCL+IPL and RNFL in the foveal, parafoveal and perifoveal macular regions, respectively. In the foveal region, the AUROC for the GCL+IPL was 0.91 with a cutoff point at 6.74. Likewise, the AUROC for the GCL+IPL

(RNFL) in the parafoveal (perifoveal) region was 0.83 (0.79) with a cutoff point at 14.53 (12.88).

The highest AUROC values obtained when comparing MDR and DM eyes were observed in the GCL+IPL, INL, OPL and OS (0.79, 0.75, 0.78 and 0.92, respectively). The cutoff point for the GCL+IPL was suggested as 11.60 with the sensitivity and specificity at 0.71 and 0.61, respectively. The cutoff point for the INL was suggested as 3.79 with the sensitivity and specificity at 0.71 and 0.61, respectively. Furthermore, the cutoff point for the OPL was suggested as 4.93 with the sensitivity and specificity at 0.71 and 0.61, respectively. Moreover, the cutoff point for the OS was suggested as 5.67 with the sensitivity and specificity at 0.90 and 0.80, respectively. Additionally, by comparing ROC curves (see Figure 5.18), we found that the most significant layer index changes were obtained for the OS in the foveal, parafoveal and perifoveal macular region. In the foveal region, the AUROC for the OS was 0.89 with a cutoff point at 5.81. Likewise, the AUROC for the RNFL in the parafoveal (perifoveal) region was 0.91 (0.88) with a cutoff point at 5.69 (5.68).

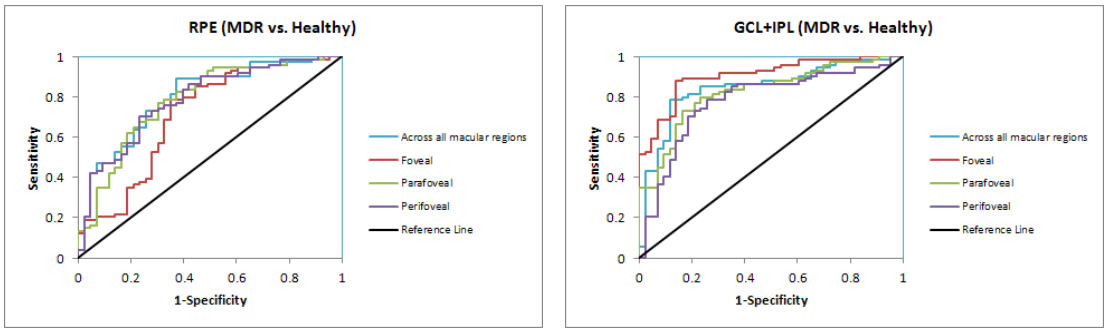

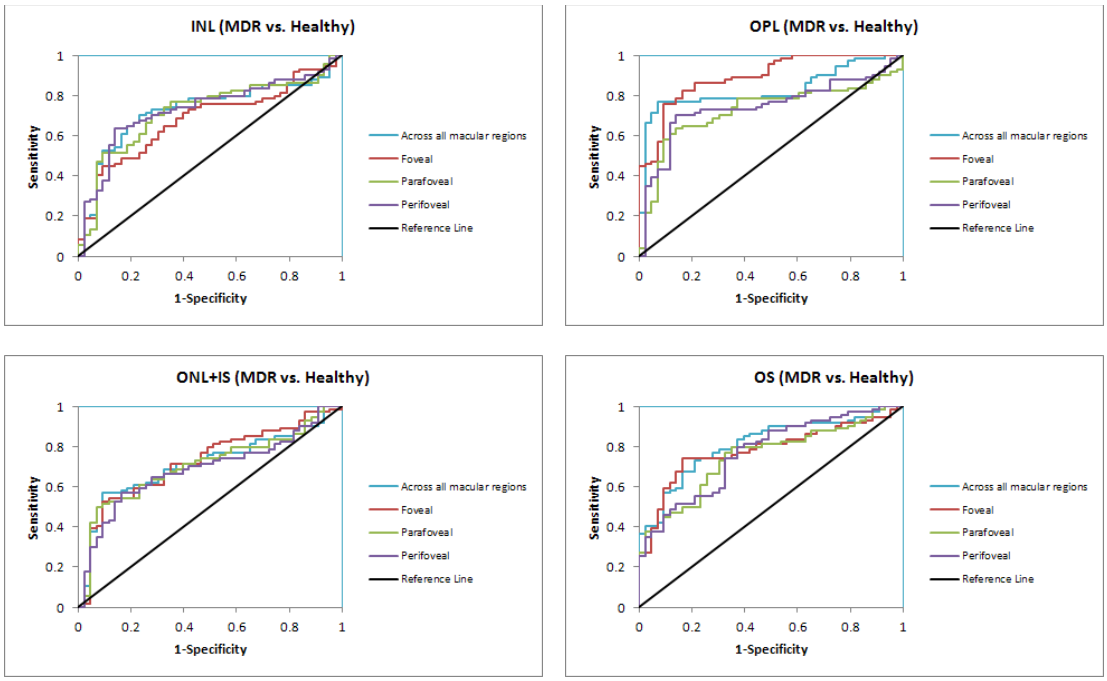

Figure 5.15 Receiver operating characteristic (ROC) curves for the detection of early DR using layer index measurements of the RNFL, GCL+IPL, INL, OPL, ONL+IS and OS as predictor variables when comparing MDR with healthy eyes.

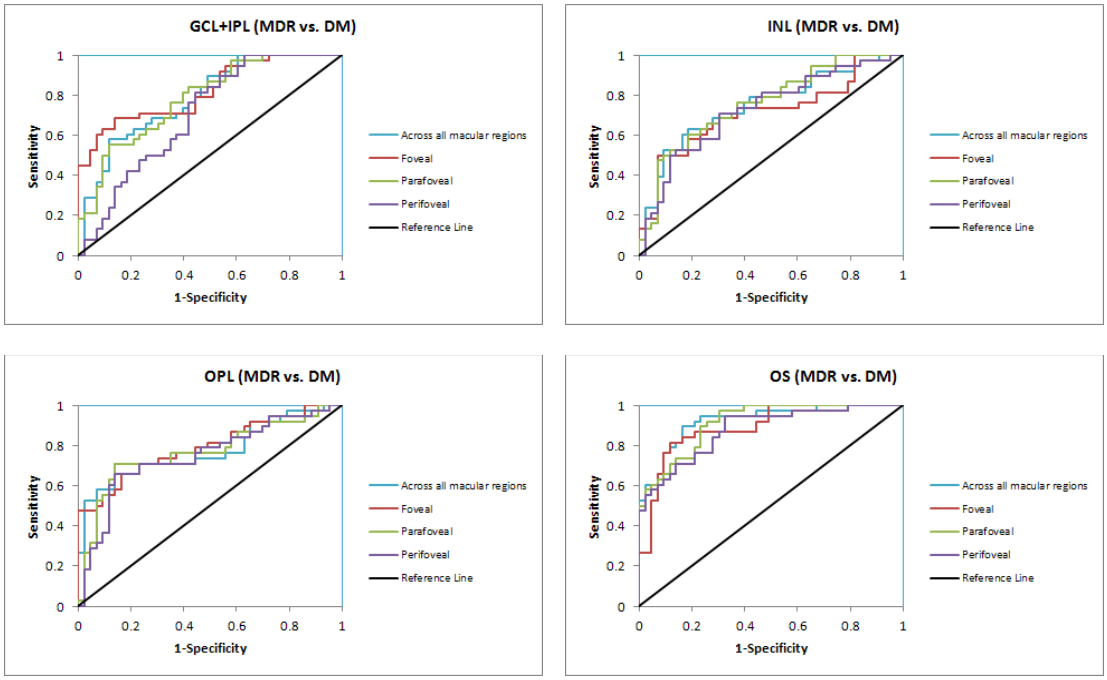

Figure 5.16 Receiver operating characteristic (ROC) curves for the detection of early DR using layer index measurements of the GCL+IPL, INL, OPL and OS as predictor variables when comparing MDR with DM eyes

5.3.4 ROC ANALYSIS FOR SCATTERING COEFFICIENT MEASUREMENTS

5.3.4.1 ROC ANALYSIS FOR SCATTERING COEFFICIENT MEASUREMENTS OBTAINED WITH THE SINGLE-SCATTERING MODEL AND THE NRIR METHOD

The ROC analyses with corresponding sensitivity and specificity tests were only performed for the intraretinal layers that showed statistically significant scattering coefficient differences per macular region when comparing MDR eyes with healthy and DM eyes. These layers were the INL and OPL. The ROC curves are shown in Figures 5.19 and 5.20. AUROC values are presented in Table 5.19 for each discrimination test. Cutoff values of total reflectance derived from the ROC analyses are shown in Table 5.20 and Table 5.21, respectively.

When comparing MDR and healthy eyes, the highest AUROC values were observed in the INL and OPL (0.68 and 0.67, respectively). The cutoff point for the INL was suggested as 2.65 mm^{-1} with the sensitivity and specificity at 0.73 and 0.63, respectively. The cutoff point for the OPL was suggested as 1.93 mm^{-1} with the sensitivity and specificity at 0.77 and 0.67, respectively. Additionally, by comparing ROC curves (see Table 5.19), we found that the most significant scattering coefficients changes were obtained for the INL, OPL and RNFL in the foveal, parafoveal and perifoveal macular regions. In the foveal region, the AUROC for the INL was 0.65 with a cutoff point at 2.22 mm^{-1}. Likewise, the AUROC for the OPL (RNFL) in the parafoveal (perifoveal) region was 0.66 (0.65) with a cutoff point at 1.68 (3.13) mm^{-1}.

The highest AUROC values obtained when comparing MDR and DM eyes were observed in the INL and OPL (0.69 and 0.72, respectively). The cutoff point for the INL was suggested as 2.62 mm^{-1} with the sensitivity and specificity at 0.71 and 0.61, respectively. The cutoff point for the OPL was suggested as 1.92 mm^{-1} with the

sensitivity and specificity at 0.77 and 0.67, respectively. Additionally, by comparing ROC curves (see Table 5.19) we found that the most significant scattering coefficient changes were obtained for the INL, INL and GCL+IPL in the foveal, parafoveal and perifoveal macular regions. In the foveal region, the AUROC for the INL was 0.68 with a cutoff point at 2.24 mm^{-1}. Likewise, the AUROC for the INL (GCL+IPL) in the parafoveal (perifoveal) region was 0.68 (0.66) with a cutoff point at 2.24 (1.90) mm^{-1}.

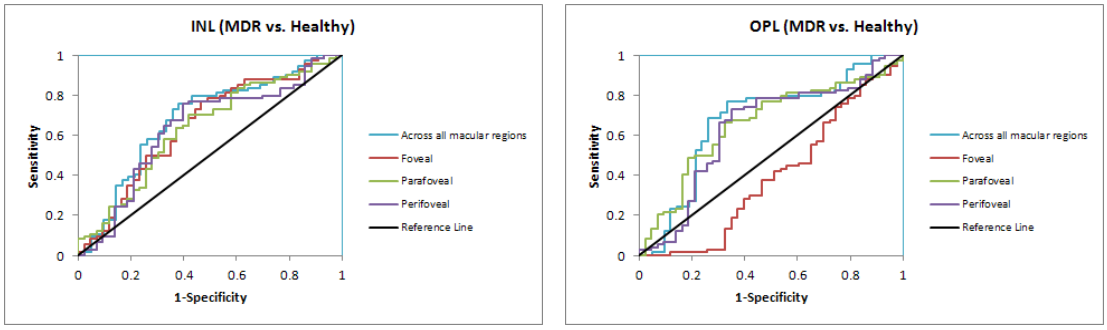

Figure 5.17 Receiver operating characteristic (ROC) curves for the detection of early DR using scattering coefficients of the INL and OPL as predictor variables when comparing MDR with healthy eyes.

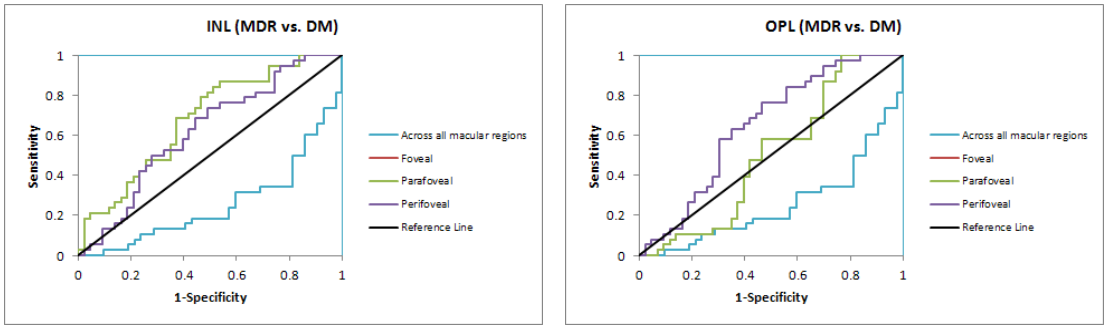

Figure 5.18 Receiver operating characteristic (ROC) curves for the detection of early DR using scattering coefficients of the INL and OPL as predictor variables when comparing MDR with DM eyes.

5.3.4.2 ROC ANALYSIS FOR SCATTERING COEFFICIENT MEASUREMENTS OBTAINED WITH THE SINGLE-SCATTERING MODEL AND THE NRPE METHOD

ROC analyses with corresponding sensitivity and specificity tests were only performed for the intraretinal layers that showed statistically significant scattering coefficient differences per macular region when comparing MDR eyes with healthy and DM eyes. These layers were the INL and OPL. The ROC curves are shown in Figures 5.21 and 5.22. AUROC values are shown in Table 5.22 for each discrimination test. Cutoff values of total reflectance derived from the ROC analyses are presented in Table 5.23 and Table 5.24, respectively.

When comparing MDR eyes and healthy eyes, the highest AUROC values were observed in the INL and OPL (0.65 and 0.65, respectively). The cutoff point for the INL was suggested as 4.02 mm^{-1} with the sensitivity and specificity at 0.68 and 0.58, respectively. The cutoff point for the OPL was suggested as 2.87 mm^{-1} with the sensitivity and specificity at 0.70 and 0.60, respectively. Additionally, by comparing ROC curves (see Table 5.12), we found that the most significant scattering coefficient changes were obtained for the INL, OPL and RNFL in the foveal, parafoveal and perifoveal macular regions. In the foveal region, the AUROC for the INL was 0.63 with a cutoff point at 3.06 mm^{-1}. Likewise, the AUROC for the OPL (RNFL) in the parafoveal (perifoveal) region was 0.63 (0.61) with a cutoff point at 2.37 (4.83) mm^{-1}.

The highest AUROC values obtained when comparing MDR and DM eyes were observed in the INL and OPL (0.66 and 0.71, respectively). The cutoff point for the INL was suggested as 4.04 mm^{-1} with the sensitivity and specificity at 0.70 and 0.60, respectively. The cutoff point for the OPL was suggested as 2.87 mm^{-1} with the sensitivity and specificity at 0.71 and 0.61, respectively. Additionally, by comparing

ROC curves (see Table 5.22), we found that the most significant scattering coefficients changes were obtained for the INL, OPL and OPL in the foveal, parafoveal and perifoveal macular regions. In the foveal region, the AUROC for the INL was 0.70 with a cutoff point at 3.81 mm^{-1}. Likewise, the AUROC for the OPL in the parafoveal (perifoveal) region was 0.68 (0.61) with a cutoff point at 2.39 (2.88) mm^{-1}.

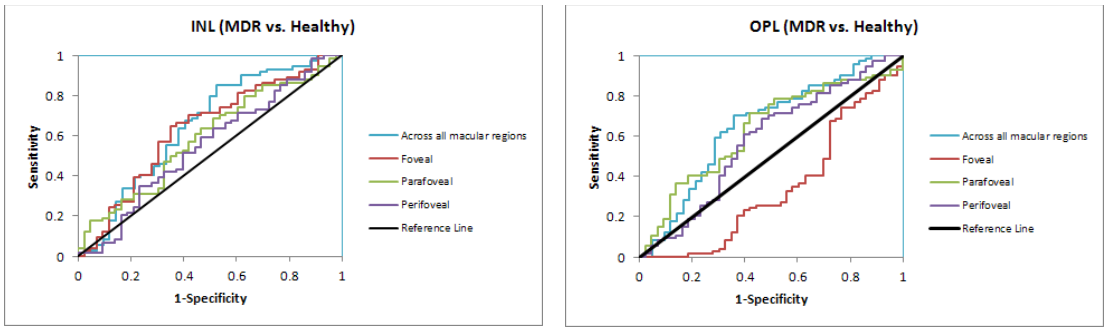

Figure 5.19 Receiver operating characteristic (ROC) curves for the detection of early DR using scattering coefficients of the INL and OPL as predictor variables when comparing MDR with healthy eyes.

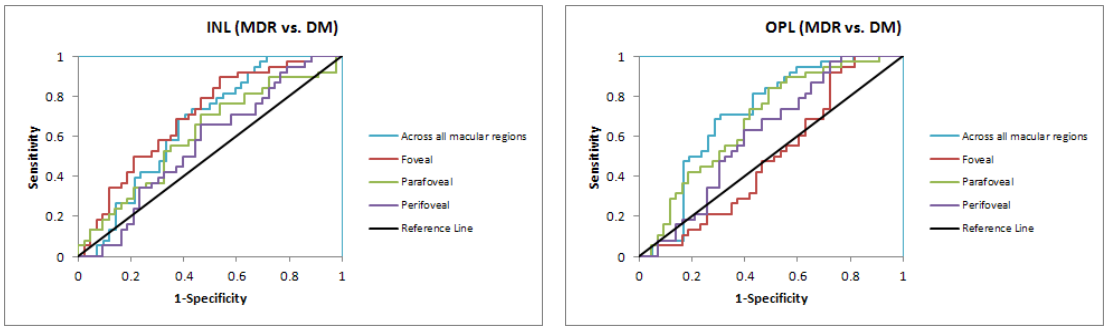

Figure 5.20 Receiver operating characteristic (ROC) curves for the detection of early DR using scattering coefficients of the INL and OPL as predictor variables when comparing MDR with DM eyes.

5.3.4.3 ROC ANALYSIS FOR SCATTERING COEFFICIENT MEASUREMENTS OBTAINED WITH THE MULTIPLE-SCATTERING MODEL AND THE NRIR METHOD

ROC analyses with corresponding sensitivity and specificity tests were only performed for the intraretinal layers that showed statistically significant scattering coefficient differences per macular region when comparing MDR eyes with healthy eyes

and DM eyes. These layers were the INL and OPL. The ROC curves are shown in Figures 5.23 and 5.24. AUROC values are presented in Table 5.25 for each discrimination test. Cutoff values of total reflectance derived from ROC analyses are shown in Table 5.26 and Table 5.27, respectively.

When comparing MDR and healthy eyes, the highest AUROC values were observed in the INL and OPL (0.67 and 0.67, respectively). The cutoff point for the INL was suggested as 3.32 mm^{-1} with the sensitivity and specificity at 0.72 and 0.62, respectively. The cutoff point for the OPL was suggested as 3.03 mm^{-1} with the sensitivity and specificity at 0.77 and 0.67, respectively. Furthermore, by comparing ROC curves (see Table 5.25), we found that the most significant scattering coefficient changes were obtained for the INL, OPL and OPL in the foveal, parafoveal and perifoveal macular regions. In the foveal region, the AUROC for the INL was 0.63 with a cutoff point at 2.77 mm^{-1}. Likewise, the AUROC for the OPL (OPL) in the parafoveal (perifoveal) region was 0.66 (0.64) with a cutoff point at 2.74 (3.00) mm^{-1}.

The highest AUROC values obtained when comparing MDR and DM eyes were observed in the INL and OPL (0.69 and 0.71, respectively). The cutoff point for the INL was suggested as 3.21 mm^{-1} with the sensitivity and specificity at 0.70 and 0.60, respectively. The cutoff point for the OPL was suggested as 3.04 mm^{-1} with the sensitivity and specificity at 0.77 and 0.67, respectively. Additionally, by comparing ROC curves (see Table 5.25), we found that the most significant scattering coefficients' changes were obtained for the RNFL, OPL and OPL in the foveal, parafoveal and perifoveal macular region. In the foveal region, the AUROC for the RNFL was 0.70 with

a cutoff point at 4.16 mm^{-1}. Likewise, the AUROC for the OPL (OPL) in the parafoveal (perifoveal) region was 0.69 (0.67) with a cutoff point at 2.74 (2.97) mm^{-1}.

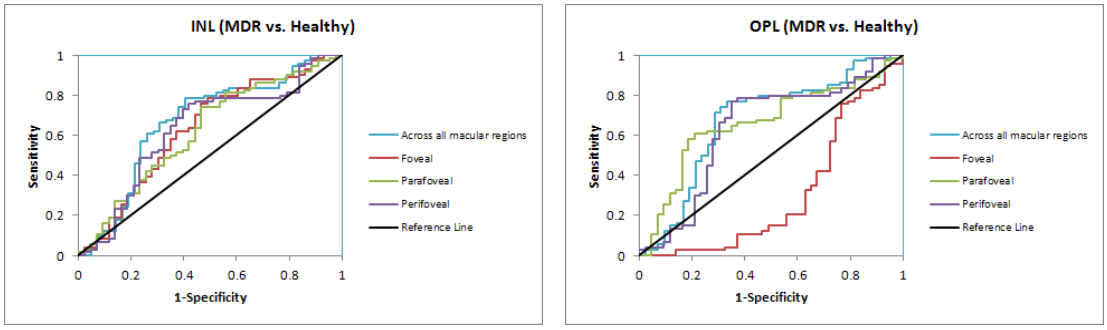

Figure 5.21 Receiver operating characteristic (ROC) curves for the detection of early DR using scattering coefficients of the INL and OPL as predictor variables when comparing MDR with healthy eyes.

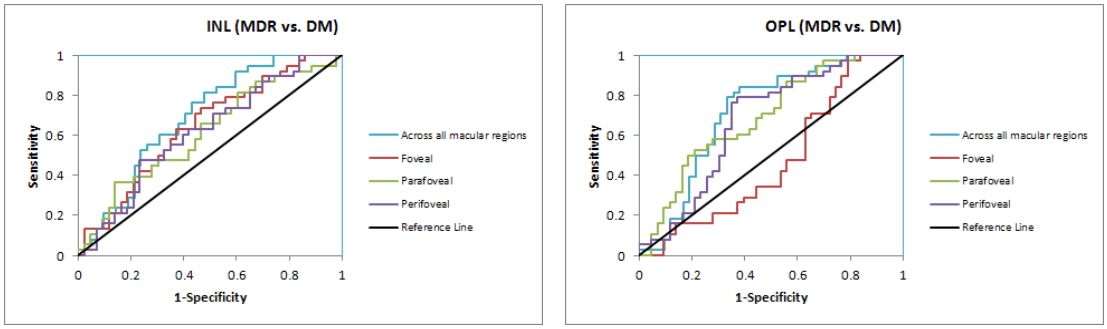

Figure 5.22 Receiver operating characteristic (ROC) curves for the detection of early DR using scattering coefficients of the INL and OPL as predictor variables when comparing MDR with DM eyes.

5.3.4.4 ROC ANALYSIS FOR SCATTERING COEFFICIENT MEASUREMENTS OBTAINED WITH THE MULTIPLE-SCATTERING MODEL AND THE NRPE METHOD

ROC analyses with corresponding sensitivity and specificity tests were only performed for the intraretinal layers that showed statistically significant scattering coefficient differences per macular region when comparing MDR eyes with healthy and DM eyes. These layers were the INL and OPL. The ROC curves are presented in Figures 5.25 and 5.26. AUROC values are shown in Table 5.28 for each discrimination test.

Cutoff values of total reflectance derived from the ROC analyses are shown in Table 5.29 and Table 5.30, respectively.

When comparing MDR eyes and healthy eyes, the highest AUROC values were observed in the INL and OPL (0.64 and 0.65, respectively). The cutoff point for the INL was suggested as 4.61 mm^{-1} with the sensitivity and specificity at 0.70 and 0.60, respectively. The cutoff point for the OPL was suggested as 4.14 mm^{-1} with the sensitivity and specificity at 0.70 and 0.60, respectively. Additionally, by comparing ROC curves (see Table 5.28), we found that the most significant scattering coefficient changes were obtained for the INL, OPL and OPL in the foveal, parafoveal and perifoveal macular regions. In the foveal region, the AUROC for the INL was 0.61 with a cutoff point at 3.58 mm^{-1}. Likewise, the AUROC for the OPL (OPL) in the parafoveal (perifoveal) region was 0.63 (0.58) with a cutoff point at 3.56 (4.17) mm^{-1}.

The highest AUROC values obtained when comparing MDR and DM eyes were observed in the GCL+IPL and OPL (0.67 and 0.71, respectively). The cutoff point for the GCL+IPL was suggested as 2.85 mm^{-1} with the sensitivity and specificity at 0.68 and 0.58, respectively. The cutoff point for the OPL was suggested as 4.26 mm^{-1} with the sensitivity and specificity at 0.74 and 0.64, respectively. In addition, by comparing ROC curves (see Table 5.28), we found that the most significant scattering coefficient (single-scattering model, NRPE) changes were obtained for the RNFL, OPL and OPL in the foveal, parafoveal and perifoveal macular regions. In the foveal region, the AUROC for the RNFL was 0.69 with a cutoff point at 5.84 mm^{-1}. Likewise, the AUROC for the OPL in the parafoveal (perifoveal) region was 0.70 (0.64) with a cutoff point at 3.64 (4.19) mm^{-1}.

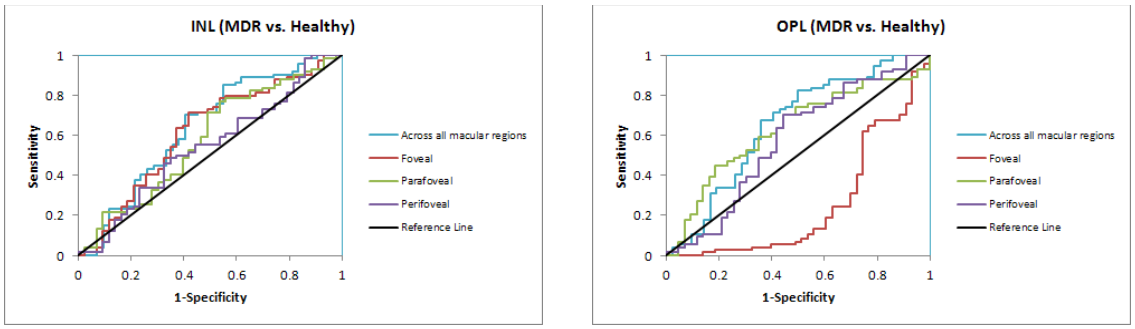

Figure 5.23 Receiver operating characteristic (ROC) curves for the detection of early DR using scattering coefficients (multiple, NRPE) of the INL and OPL as predictor variables when comparing MDR with healthy eyes.

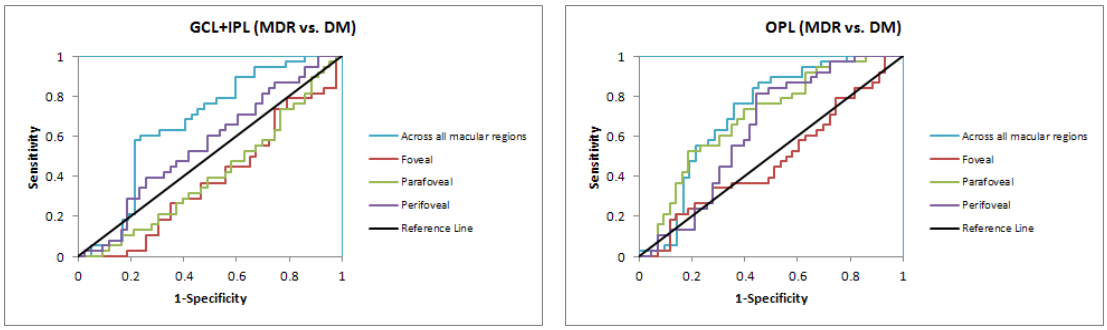

Figure 5.24 Receiver operating characteristic (ROC) curves for the detection of early DR using scattering coefficients (multiple, NRPE) of the GCL+IPL and OPL as predictor variables when comparing MDR with DM eyes.

5.4 SUMMARY

In this chapter, optical parameters, such as mean reflectance, total reflectance, layer index and scattering coefficients, were evaluated as biomarkers of early retinopathy in the diabetic macula. Although OCT is typically used to measure retinal thickness, we have demonstrated that measurements of optical properties may provide additional information relevant to characterizing abnormalities at the early stage of retinopathy in diabetic subjects. Therefore, changes in optical descriptors may provide further knowledge regarding cellular layers and early damage in diabetic ocular disease.

Our findings indicate that significant decreases of total reflectance using both normalization methods (i.e., NRIR and NRPE) were observed for all layers in the MDR eyes compared with controls and DM eyes. Particularly, total reflectance significantly decreased for GCL+IPL (8%), OPL (14%) and OS (7%) in MDR eyes compared with healthy eyes. The layer index values decreased for all layers in MDR eyes compared with healthy and DM eyes. Moreover, scattering coefficients increased for all the layers (except the INL) in MDR eyes compared with healthy eyes. When comparing MDR and DM eyes, scattering coefficients increased for all layers (except in the RNFL, INL and OPL). Moreover, the scattering coefficient value (13.03 mm^{-1}) calculated from the RNFL to ONL+IS was comparable to the results of our previous work based on *in vitro* measurements (12.00 mm^{-1}) from bovine retina using a single backscattering model.[70] Despite the scattering model and normalization method used, the scattering coefficient parameter was not as good a predictor of early retinopathy development compared with the other optical parameters. This particular finding may be associated with the fact that in many OCT systems, the optimal system design for rapid image acquisition is not optimal for measuring optical properties (the design works better at higher numerical aperture values). Moreover, the multiple-scattering model is limited in its ability to handle multiple scattering effects. These limitations might have also affected the accuracy of our experimental results using phantom data (see chapter 3, section 3.6.3).

Furthermore, the ROC curve was estimated for all diagnostic optical parameters using features measured locally for each intraretinal layer. Specifically, the ROC analysis showed that several optical parameters were superior to the standard thickness measurements used in commercial OCT devices. The highest AUROC values estimated

for the total reflectance were observed for the GCL+IPL complex, OPL and OS when comparing MDR eyes with healthy eyes and DM eyes. The highest values estimated for the layer index were observed for the RNFL, OPL and OS when comparing MDR eyes with healthy eyes and DM eyes. Total reflectance and layer index also showed maximum discrimination values for all layers except RPE and INL (only for the layer index parameter).

In general, total reflectance and layer index showed better discriminating power for retinal abnormalities localized to the inner retina (mostly in the GCL+IPL complex) when comparing MDR and healthy eyes. Nearly equivalent diagnostic power was obtained for the layer index and total reflectance for retinal abnormalities localized in the OPL and OS when comparing MDR eyes and healthy eyes. In addition, when comparing MDR with DM eyes, total reflectance showed a better discriminating power for retinal abnormalities localized to the GCL+IPL complex. Nearly equivalent diagnostic power was also obtained for the layer index and total reflectance for retinal abnormalities localized to the OPL and OS when comparing MDR with DM eyes. Moreover, for the diagnosis of MDR eyes versus healthy and DM eyes, no advantage was found for reflectivity measurements and tissue optical-derived measures, such as scattering coefficients obtained with single and multiple backscattering approaches.

Our results suggest that the total reflectance and layer index displayed the most powerful diagnostic utility for detecting early changes in the diabetic retina. Our results also show that looking for abnormalities in the GCL+IPL complex in the OPL and OS could lead to earlier DR detection. In particular, the decreasing trend observed for total reflectance of the RNFL and GCL+IPL complex in MDR eyes could be associated with

pathological metabolic changes in the retina, which might reflect neurodegenerative changes in the diabetic retina. These findings have possible implications for the early detection of macular damage in diabetes. Because the macular region is rich in retinal ganglion cells, it could be suggested that diabetic damage to this central region might occur early in the disease process. In fact, animal models of DR show significant loss of macular ganglion cells.[93-98] Interestingly, our results show for the first time that the total reflectance of the OPL in MDR eyes was significantly reduced compared with similar measures in healthy eyes. In addition, scattering coefficients increased in MDR eyes (except the INL) compared with healthy eyes, which might be due to macular diabetic damage leading to reduced transparence and increased disorganization in these layers. This result is supported by previous results from *in vitro and in vivo* experiments, in which apoptosis was induced in animal models of diabetic eyes.[96] Accordingly, our results suggest that an early indication of neurodegenerative development could be detected by investigating the changes in optical properties and thickness of the OPL. Conversely, the highest AUROC values were obtained for the total reflectance and layer index of the OS when comparing MDR with DM eyes. This particular result suggests that diabetes also inflicts additional damage to the outer photoreceptor segment, which could be an early indication of visual function degeneration. Therefore, this finding could be used as an additional indicator for early detection of diabetic retinal damage and/or disease progression.

In this study, the AUROC results show a similar trend for total reflectance using both normalization methods. This comparable trend might rule out a dependence on the sensitivity to the direction of the light beam incidence. In fact, taking into account that

the RPE layer apparently behaves like a diffuse reflector, which is an assumption that could be valid when the RPE is more or less flat, this layer could be fairly insensitive to the direction of the light beam incidence. Accordingly, our results appear to be unaffected by the directionality of the light beam in the OCT system.

In summary, we have developed a novel methodology that combines structural measures with optical-based diagnostic parameters. The optical parameters were able to discriminate diabetic eyes with early retinopathy from healthy and diabetic eyes (with no retinopathy) with higher sensitivity and specificity compared with the standard thickness parameters. Altogether, these results may have potential applications in therapeutic interventions aimed towards preventing early diabetic retinopathy in diabetic subjects. Given the results of our study, we conclude that obtaining layer index and total reflectance values for the RNFL, GCL+IPL complex, OPL and OS may provide beneficial information for diagnosing early diabetic retinopathy in DM subjects. In our population (or a similar population), a GCL+IPL (OPL, OS) total reflectance of $\leq$ 80.57 dB (72.97 dB, 74.22 dB, respectively) and RNFL (OPL, OS) layer index of $\leq$ 11.47 (5.03, 5.55, respectively) were used successfully to select diabetic patients who might benefit from intervention trials to prevent the onset of early diabetic retinopathy. In conclusion, our results show that optical parameters extracted from OCT images have the potential to differentiate diabetic eyes with early retinopathy from healthy and diabetic eyes without retinopathy.

Table 5.1 Distribution statistics of the mean reflectance (dB) by study groups

Mean Reflectance (dB)	Healthy	DM	MDR
Across All Macular Regions			
RNFL	54.38 ± 1.54	53.46 ± 1.28 ‡	52.19 ± 1.53 ‡
GCL+IPL	50.43 ± 2.13	49.66 ± 1.78 ‡	48.06 ± 1.93 ‡
INL	47.06 ± 2.60	46.44 ± 2.10 ‡	44.71 ± 2.31 ‡
OPL	48.89 ± 2.40	48.39 ± 1.85 ‡	46.53 ± 2.07 ‡
ONL+IS	44.50 ± 2.61	43.70 ± 1.97 ‡	41.96 ± 2.56 ‡
OS	56.57 ± 1.37	55.68 ± 1.54	55.19 ± 1.63 ‡
RPE	58.53 ± 1.08	57.85 ± 0.99 †	57.30 ± 1.06 ‡
Foveal Region			
RNFL	52.09 ± 1.81	51.67 ± 1.69 ‡	50.06 ± 1.80 ‡
GCL+IPL	49.92 ± 2.25	49.23 ± 2.08 ‡	47.44 ± 2.26 ‡
INL	47.26 ± 2.72	46.81 ± 2.20 ‡	44.98 ± 2.59 ‡
OPL	48.94 ± 2.43	48.84 ± 1.85 ‡	46.85 ± 2.26 ‡
ONL+IS	44.69 ± 2.73	44.04 ± 2.12 ‡	42.22 ± 2.76 ‡
OS	56.47 ± 1.47	55.56 ± 1.67	55.06 ± 1.91 ‡
RPE	59.09 ± 1.15	58.32 ± 1.11	57.91 ± 1.19 ‡
Parafoveal Region			
RNFL	53.82 ± 1.69	53.12 ± 1.43 ‡	51.62 ± 1.70 ‡
GCL+IPL	50.27 ± 2.19	49.62 ± 1.77 ‡	48.14 ± 1.93 ‡
INL	46.94 ± 2.69	46.38 ± 2.17 ‡	44.63 ± 2.28 ‡
OPL	49.34 ± 2.42	48.90 ± 1.89 ‡	47.08 ± 1.97 ‡
ONL+IS	44.93 ± 2.68	44.11 ± 1.96 ‡	42.42 ± 2.48 ‡
OS	57.20 ± 1.43	56.32 ± 1.65	55.84 ± 1.71 ‡
RPE	58.68 ± 1.12	57.98 ± 1.06 †	57.51 ± 1.11 ‡
Perifoveal Region			
RNFL	54.82 ± 1.53	53.90 ± 1.20 ‡	52.59 ± 1.57 ‡
GCL+IPL	50.63 ± 2.15	49.85 ± 1.70 ‡	48.31 ± 2.02 ‡
INL	47.01 ± 2.60	46.28 ± 2.13 ‡	44.61 ± 2.44 ‡
OPL	48.64 ± 2.50	47.91 ± 1.91 ‡	46.08 ± 2.28 ‡
ONL+IS	44.37 ± 2.66	43.49 ± 1.97 ‡	41.71 ± 2.71 ‡
OS	56.69 ± 1.40	55.83 ± 1.49	55.29 ± 1.62 ‡
RPE	58.09 ± 1.12	57.47 ± 0.97 †	56.79 ± 1.10 ‡

† $0.001<p<0.05$ and ‡ $p<0.001$ (ANOVA followed by Newman-Keuls post hoc analysis) between MDR and healthy eyes (see MDR column) and between MDR and DM eyes (see DM column).

Table 5.2 Distribution statistics of the total reflectance (dB) by study groups

Total Reflectance (dB)	Healthy	DM	MDR
Across All Macular Regions			
RNFL	81.41 ± 1.77	80.32 ± 1.41 ‡	79.08 ± 1.67 ‡
GCL+IPL	82.49 ± 2.23	81.42 ± 1.76 ‡	79.36 ± 2.14 ‡
INL	72.41 ± 2.59	71.96 ± 2.14 ‡	70.01 ± 2.26 ‡
OPL	75.70 ± 2.57	74.93 ± 2.68 ‡	72.21 ± 2.01 ‡
ONL+IS	77.34 ± 2.77	76.41 ± 2.26 †	74.97 ± 2.50 ‡
OS	75.44 ± 1.49	75.38 ± 1.18 ‡	73.21 ± 1.44 ‡
RPE	75.70 ± 1.05	75.66 ± 0.99 ‡	74.54 ± 0.95 ‡
Foveal Region			
RNFL	77.15 ± 1.87	76.32 ± 1.84 ‡	75.00 ± 2.00 ‡
GCL+IPL	83.46 ± 2.31	82.20 ± 2.39 ‡	79.44 ± 2.27 ‡
INL	72.81 ± 2.69	72.63 ± 2.41 ‡	70.70 ± 2.31 ‡
OPL	78.94 ± 2.72	77.77 ± 3.80 ‡	74.00 ± 2.48 ‡
ONL+IS	78.63 ± 2.86	77.76 ± 2.45 †	76.19 ± 2.76 ‡
OS	76.11 ± 1.65	75.93 ± 1.17 ‡	73.90 ± 1.48 ‡
RPE	76.33 ± 0.98	76.26 ± 0.99 ‡	75.34 ± 0.97 ‡
Parafoveal Region			
RNFL	79.70 ± 1.80	79.01 ± 1.45 ‡	77.45 ± 1.82 ‡
GCL+IPL	83.96 ± 2.25	83.12 ± 1.73 ‡	80.98 ± 2.20 ‡
INL	73.31 ± 2.64	72.93 ± 2.11 ‡	70.88 ± 2.30 ‡
OPL	75.24 ± 2.56	75.01 ± 2.06 ‡	72.94 ± 2.03 ‡
ONL+IS	77.61 ± 2.81	76.57 ± 2.25 †	75.28 ± 2.43 ‡
OS	75.40 ± 1.64	75.62 ± 1.28 ‡	73.10 ± 1.75 ‡
RPE	75.11 ± 1.10	75.37 ± 1.09 ‡	74.25 ± 1.08 ‡
Perifoveal Region			
RNFL	82.37 ± 1.84	81.36 ± 1.38 ‡	79.94 ± 1.77 ‡
GCL+IPL	81.46 ± 2.31	80.29 ± 1.71 ‡	78.61 ± 2.32 ‡
INL	71.88 ± 2.61	71.24 ± 2.18 ‡	69.35 ± 2.45 ‡
OPL	73.21 ± 2.60	72.57 ± 2.04 ‡	70.61 ± 2.32 ‡
ONL+IS	76.12 ± 2.80	75.11 ± 2.23 †	73.76 ± 2.65 ‡
OS	74.85 ± 1.59	74.91 ± 1.34 ‡	72.55 ± 1.66 ‡
RPE	75.14 ± 1.21	75.01 ± 1.22 ‡	73.79 ± 1.23 ‡

† $0.001<p<0.05$ and ‡ $p<0.001$ (ANOVA followed by Newman-Keuls post hoc analysis) between MDR and healthy eyes (see MDR column) and between MDR and DM eyes (see DM column).

Table 5.3 Distribution statistics of the layer index (a.u.) by study groups

Layer Index	Healthy	DM	MDR
Across All Macular Regions			
RNFL	12.38 ± 1.36	11.59 ± 1.19 †	10.81 ± 1.38 ‡
GCL+IPL	13.81 ± 2.10	12.98 ± 1.79 ‡	10.96 ± 1.87 ‡
INL	4.36 ± 0.84	4.40 ± 0.78 ‡	3.74 ± 0.69 ‡
OPL	6.28 ± 1.25	6.20 ± 1.48 ‡	4.75 ± 0.74 ‡
ONL+IS	7.59 ± 1.58	7.22 ± 1.22 †	6.52 ± 1.48 †
OS	6.09 ± 0.77	6.42 ± 0.61 ‡	5.32 ± 0.49 ‡
RPE	6.26 ± 0.52	6.61 ± 0.53 ‡	6.19 ± 0.43
Foveal Region			
RNFL	7.27 ± 0.93	7.03 ± 1.07 †	6.43 ± 1.13 ‡
GCL+IPL	14.93 ± 2.50	13.98 ± 2.93 ‡	10.66 ± 2.01 ‡
INL	4.42 ± 0.95	4.64 ± 1.02 ‡	3.87 ± 0.71 †
OPL	8.95 ± 2.04	8.72 ± 3.15 ‡	5.71 ± 1.40 ‡
ONL+IS	8.55 ± 1.85	8.23 ± 1.48 †	7.28 ± 1.94 †
OS	6.37 ± 0.99	6.62 ± 0.68 ‡	5.51 ± 0.60 ‡
RPE	6.48 ± 0.63	6.85 ± 0.60 †	6.48 ± 0.52
Parafoveal Region			
RNFL	9.84 ± 1.05	9.62 ± 1.00 ‡	8.57 ± 1.23 ‡
GCL+IPL	16.11 ± 2.53	15.55 ± 2.12 ‡	12.97 ± 2.33 ‡
INL	4.75 ± 0.96	4.82 ± 0.87 ‡	4.04 ± 0.75 ‡
OPL	5.96 ± 1.26	6.15 ± 1.25 ‡	5.11 ± 0.86 ‡
ONL+IS	7.75 ± 1.62	7.27 ± 1.19 †	6.66 ± 1.32 ‡
OS	6.02 ± 1.00	6.52 ± 0.74 ‡	5.18 ± 0.71 ‡
RPE	5.79 ± 0.64	6.32 ± 0.69 †	5.91 ± 0.68
Perifoveal Region			
RNFL	14.02 ± 1.69	13.27 ± 1.39 ‡	12.16 ± 1.68 ‡
GCL+IPL	12.56 ± 1.96	11.66 ± 1.61 †	10.46 ± 2.01 ‡
INL	4.19 ± 0.80	4.15 ± 0.72 ‡	3.59 ± 0.74 ‡
OPL	4.87 ± 0.94	4.79 ± 0.79 ‡	4.11 ± 0.74 ‡
ONL+IS	6.79 ± 1.42	6.41 ± 1.12	5.92 ± 1.36 †
OS	5.88 ± 0.75	6.28 ± 0.71 ‡	5.16 ± 0.61 ‡
RPE	6.07 ± 0.55	6.34 ± 0.64 †	5.94 ± 0.54

† $0.001<p<0.05$ and ‡ $p<0.001$ (ANOVA followed by Newman-Keuls post hoc analysis) between MDR and healthy eyes (see MDR column) and between MDR and DM eyes (see DM column).

Table 5.4 Distribution statistics of scattering coefficients (mm^{-1}) (NRIR) by using the single-scattering model

Scattering Coefficients (NRIR)	Healthy	DM	MDR
Across All Macular Regions			
RNFL	3.56 ± 0.50	3.53 ± 0.45	3.38 ± 0.80
GCL+IPL	1.70 ± 0.19	1.77 ± 0.23 †	1.64 ± 0.35
INL	2.90 ± 0.46	2.90 ± 0.41 †	2.57 ± 0.57 †
OPL	2.07 ± 0.40	2.12 ± 0.31 ‡	1.83 ± 0.48 †
ONL+IS	2.80 ± 0.40	2.67 ± 0.52	2.79 ± 0.51
OS	8.90 ± 1.56	8.62 ± 1.43 ‡	11.03 ± 2.68 ‡
RPE	10.12 ± 1.36	10.08 ± 1.45 ‡	11.39 ± 1.39 ‡
Foveal Region			
RNFL	4.15 ± 1.14	4.54 ± 0.88	4.30 ± 1.84
GCL+IPL	1.36 ± 0.26	1.33 ± 0.24 †	1.49 ± 0.38 ‡
INL	2.38 ± 0.35	2.44 ± 0.36 †	2.18 ± 0.42 †
OPL	1.54 ± 0.26	1.67 ± 0.21	1.68 ± 0.38 †
ONL+IS	1.96 ± 0.35	1.82 ± 0.41	1.98 ± 0.56
OS	11.15 ± 2.89	9.59 ± 1.94 ‡	13.23 ± 2.7 †
RPE	9.64 ± 1.22	9.72 ± 1.28 ‡	10.86 ± 1.75 ‡
Parafoveal Region			
RNFL	3.45 ± 0.49	3.51 ± 0.47	3.43 ± 0.62
GCL+IPL	1.06 ± 0.10	1.08 ± 0.13 †	1.14 ± 0.24 †
INL	2.17 ± 0.30	2.16 ± 0.33 †	2.03 ± 0.30
OPL	1.79 ± 0.30	1.79 ± 0.23 †	1.64 ± 0.28 †
ONL+IS	2.46 ± 0.42	2.34 ± 0.50	2.55 ± 0.49
OS	10.79 ± 2.62	8.97 ± 1.56 ‡	12.95 ± 3.17 ‡
RPE	9.97 ± 1.14	10.1 ± 1.42 ‡	11.38 ± 1.35 ‡
Perifoveal Region			
RNFL	3.31 ± 0.33	3.19 ± 0.32	3.09 ± 0.52 †
GCL+IPL	1.93 ± 0.15	2.00± 0.22 †	1.90 ± 0.27
INL	2.82 ± 0.39	2.79 ± 0.34 †	2.63 ± 0.47 †
OPL	2.02 ± 0.36	2.05 ± 0.31 †	1.86 ± 0.42 †
ONL+IS	2.74 ± 0.37	2.67 ± 0.47	2.77 ± 0.42
OS	9.00 ± 1.47	8.46 ± 1.31 ‡	10.87 ± 2.52 ‡
RPE	9.97 ± 1.23	10.03 ± 1.34 ‡	11.21 ± 1.31 ‡

† $0.001<p<0.05$ and ‡ $p<0.001$ (ANOVA followed by Newman-Keuls post hoc analysis) between MDR and healthy eyes (see MDR column) and between MDR and DM eyes (see DM column).

Table 5.5 Distribution statistics of scattering coefficients (mm^{-1}) (NRPE) by using the single-scattering model

Scattering Coefficients (NRPE)	Healthy	DM	MDR
Across All Macular Regions			
RNFL	5.29 ± 0.55	5.23 ± 0.52	5.22 ± 1.06
GCL+IPL	2.56 ± 0.21	2.68 ± 0.30	2.58 ± 0.45
INL	4.29 ± 0.51	4.30 ± 0.44 †	4.00 ± 0.66 †
OPL	3.02 ± 0.46	3.11 ± 0.35 ‡	2.78 ± 0.59 †
ONL+IS	4.16 ± 0.67	3.97 ± 0.84 †	4.32 ± 0.77
OS	13.07 ± 2.42	12.72 ± 2.55 ‡	16.86 ± 3.23 ‡
RPE	14.68 ± 2.02	14.73 ± 2.45 ‡	17.33 ± 2.31 ‡
Foveal Region			
RNFL	5.68 ± 1.48	6.29 ± 1.15	6.15 ± 2.61
GCL+IPL	1.83 ± 0.31	1.81 ± 0.29 †	2.05 ± 0.49 ‡
INL	3.21 ± 0.43	3.34 ± 0.43 †	3.03 ± 0.61
OPL	2.05 ± 0.30	2.28 ± 0.28	2.32 ± 0.56 ‡
ONL+IS	2.61 ± 0.47	2.46 ± 0.52 †	2.70 ± 0.70
OS	14.50 ± 3.70	12.74 ± 2.40 ‡	17.80 ± 3.20 ‡
RPE	12.63 ± 1.69	12.96 ± 1.88 ‡	14.69 ± 2.88 ‡
Parafoveal Region			
RNFL	4.86 ± 0.60	4.97 ± 0.62	4.97 ± 0.85
GCL+IPL	1.49 ± 0.14	1.54 ± 0.17 †	1.66 ± 0.31 ‡
INL	3.06 ± 0.37	3.07 ± 0.39	2.93 ± 0.34
OPL	2.50 ± 0.37	2.53 ± 0.26 †	2.35 ± 0.34 †
ONL+IS	3.45 ± 0.63	3.31 ± 0.72 †	3.67 ± 0.67
OS	14.77 ± 3.57	12.44 ± 2.04 ‡	18.19 ± 4.07 ‡
RPE	13.75 ± 1.70	14.03 ± 2.09 ‡	16.09 ± 2.11 ‡
Perifoveal Region			
RNFL	4.90 ± 0.37	4.76 ± 0.39	4.80 ± 0.71
GCL+IPL	2.92 ± 0.26	3.04 ± 0.32	2.99 ± 0.39
INL	4.22 ± 0.47	4.21 ± 0.37	4.13 ± 0.59
OPL	2.98 ± 0.44	3.04 ± 0.36	2.86 ± 0.57
ONL+IS	4.08 ± 0.64	4.00 ± 0.79	4.29 ± 0.65
OS	13.22 ± 2.26	12.53 ± 2.07 ‡	16.70 ± 3.32 ‡
RPE	14.52 ± 1.79	14.76 ± 2.17 ‡	17.11 ± 2.09 ‡

† $0.001<p<0.05$ and ‡ $p<0.001$ (ANOVA followed by Newman-Keuls post hoc analysis) between MDR and healthy eyes (see MDR column) and between MDR and DM eyes (see DM column).

Table 5.6 Distribution statistics of scattering coefficients (mm^{-1}) (NRIR) by using the multiple-scattering model

Scattering Coefficients (NRIR)	Healthy	DM	MDR
Across All Macular Regions			
RNFL	3.81 ± 0.34	3.90 ± 0.38	3.79 ± 0.68
GCL+IPL	1.98 ± 0.23	2.15 ± 0.28 †	1.96 ± 0.41
INL	3.53 ± 0.49	3.58 ± 0.50 †	3.20 ± 0.65 †
OPL	3.19 ± 0.44	3.26 ± 0.35 ‡	2.89 ± 0.55 †
ONL+IS	2.55 ± 0.34	2.37 ± 0.51	2.52 ± 0.53
OS	10.91 ± 1.54	10.69 ± 1.31 ‡	12.82 ± 2.53 ‡
RPE	12.32 ± 1.38	12.31 ± 1.45 ‡	13.62 ± 1.37 ‡
Foveal Region			
RNFL	4.09 ± 1.16	4.80 ± 0.84	4.34 ± 1.66
GCL+IPL	1.49 ± 0.17	1.60 ± 0.21 †	1.73 ± 0.31 ‡
INL	2.93 ± 0.40	3.00 ± 0.43 †	2.73 ± 0.51 †
OPL	2.29 ± 0.25	2.51 ± 0.28	2.53 ± 0.42 ‡
ONL+IS	1.75 ± 0.24	1.59 ± 0.30	1.75 ± 0.53
OS	14.13 ± 2.66	12.59 ± 1.94 ‡	15.60 ± 2.64 †
RPE	11.76 ± 1.20	11.9 ± 1.33 ‡	12.98 ± 1.77 ‡
Parafoveal Region			
RNFL	3.65 ± 0.38	3.73 ± 0.37	3.69 ± 0.55
GCL+IPL	1.35 ± 0.14	1.39 ± 0.16	1.44 ± 0.27 †
INL	2.63 ± 0.35	2.63 ± 0.39	2.49 ± 0.38
OPL	2.83 ± 0.31	2.85 ± 0.24 †	2.68 ± 0.31 †
ONL+IS	2.15 ± 0.29	2.01 ± 0.46	2.15 ± 0.48
OS	13.14 ± 2.50	11.37 ± 1.59 ‡	14.91 ± 3.06 ‡
RPE	12.07 ± 1.19	12.29 ± 1.43 ‡	13.49 ± 1.38 ‡
Perifoveal Region			
RNFL	3.49 ± 0.23	3.48 ± 0.25	3.47 ± 0.40
GCL+IPL	1.90 ± 0.17	2.05 ± 0.30	1.98 ± 0.39
INL	3.44 ± 0.43	3.45 ± 0.45	3.25 ± 0.55 †
OPL	3.14 ± 0.39	3.17 ± 0.33 †	2.93 ± 0.47 †
ONL+IS	2.49 ± 0.29	2.33 ± 0.51	2.46 ± 0.46
OS	11.01 ± 1.45	10.55 ± 1.23 ‡	12.70 ± 2.37 ‡
RPE	12.18 ± 1.23	12.23 ± 1.31 ‡	13.41 ± 1.28 ‡

† $0.001<p<0.05$ and ‡ $p<0.001$ (ANOVA followed by Newman-Keuls post hoc analysis) between MDR and healthy eyes (see MDR column) and between MDR and DM eyes (see DM column).

Table 5.7 Distribution statistics of scattering coefficients (mm^{-1}) (NRPE) by using the multiple-scattering model

Scattering Coefficients (NRPE)	Healthy	DM	MDR
Across All Macular Regions			
RNFL	5.46 ± 0.44	5.58 ± 0.53	5.62 ± 0.93
GCL+IPL	2.71 ± 0.23	2.97 ± 0.34 †	2.80 ± 0.53
INL	4.90 ± 0.54	5.00 ± 0.58 †	4.62 ± 0.75 †
OPL	4.33 ± 0.44	4.44 ± 0.37 ‡	4.05 ± 0.61 †
ONL+IS	3.45 ± 0.43	3.23 ± 0.80 †	3.53 ± 0.63
OS	15.14 ± 2.36	14.88 ± 2.40 ‡	18.63 ± 3.04 ‡
RPE	16.85 ± 2.06	16.93 ± 2.42 ‡	19.51 ± 2.28 ‡
Foveal Region			
RNFL	5.49 ± 1.56	6.54 ± 1.16	6.07 ± 2.40
GCL+IPL	1.87 ± 0.20	2.04 ± 0.26 ‡	2.23 ± 0.41 ‡
INL	3.74 ± 0.48	3.88 ± 0.51 †	3.57 ± 0.68
OPL	2.88 ± 0.28	3.22 ± 0.40	3.28 ± 0.60 ‡
ONL+IS	2.20 ± 0.28	2.04 ± 0.37 †	2.26 ± 0.65
OS	17.82 ± 3.41	16.10 ± 2.43 ‡	20.38 ± 3.11 ‡
RPE	14.74 ± 1.69	15.13 ± 1.93 ‡	16.77 ± 2.86 ‡
Parafoveal Region			
RNFL	5.00 ± 0.53	5.14 ± 0.56	5.18 ± 0.78
GCL+IPL	1.75 ± 0.16	1.82 ± 0.19 †	1.93 ± 0.34 ‡
INL	3.45 ± 0.42	3.49 ± 0.46	3.33 ± 0.45
OPL	3.69 ± 0.35	3.75 ± 0.24 †	3.57 ± 0.35
ONL+IS	2.80 ± 0.38	2.64 ± 0.61	2.87 ± 0.62
OS	17.30 ± 3.40	15.03 ± 2.05 ‡	20.23 ± 3.95 ‡
RPE	15.82 ± 1.74	16.20 ± 2.09 ‡	18.16 ± 2.13 ‡
Perifoveal Region			
RNFL	4.97 ± 0.35	4.98 ± 0.37 †	5.15 ± 0.55
GCL+IPL	2.62 ± 0.21	2.86 ± 0.37	2.85 ± 0.53 †
INL	4.82 ± 0.53	4.87 ± 0.52	4.74 ± 0.68
OPL	4.28 ± 0.43	4.36 ± 0.35	4.14 ± 0.58
ONL+IS	3.38 ± 0.38	3.20 ± 0.79	3.46 ± 0.58
OS	15.29 ± 2.20	14.73 ± 1.96 ‡	18.53 ± 3.16 ‡
RPE	16.72 ± 1.79	16.92 ± 2.12 ‡	19.26 ± 2.05 ‡

† $0.001<p<0.05$ and ‡ $p<0.001$ (ANOVA followed by Newman-Keuls post hoc analysis) between MDR and healthy eyes (see MDR column) and between MDR and DM eyes (see DM column).

Table 5.8 Statistically significant differences of optical parameters between MDR and healthy eyes

MDR vs. Healthy	Mean Reflectance	Total Reflectance	Layer Index	Scattering (Single, NRIR)	Scattering (Single, NRPE)	Scattering (Multiple, NRIR)	Scattering (Multiple, NRPE)
Across All Macular Regions							
RNFL	x	x					
GCL+IPL	x	x	x				
INL	x	x	x				
OPL	x	x	x	x	x	x	x
ONL+IS	x						
OS		x	x	x	x	x	x
RPE		x	x	x	x	x	x
Foveal Region							
RNFL	x	x					
GCL+IPL	x	x	x				x
INL	x	x	x				
OPL	x	x	x				
ONL+IS	x						
OS		x	x	x	x	x	x
RPE		x		x	x	x	x
Parafoveal Region							
RNFL	x	x	x				
GCL+IPL	x	x	x				
INL	x	x	x				
OPL	x	x	x				
ONL+IS	x						
OS		x	x	x	x	x	x
RPE		x		x	x	x	x
Perifoveal Region							
RNFL	x	x	x				
GCL+IPL	x	x					
INL	x	x	x				
OPL	x	x	x				
ONL+IS	x						
OS		x	x	x	x	x	x
RPE		x		x	x	x	x

"X" denotes the intraretinal layer and regional sector in which the structural feature change showed a statistically significant difference ($p<0.001$) by using ANOVA followed by Newman-Keuls post hoc analysis.

Table 5.9 Statistically significant differences of optical parameters between MDR and DM eyes

MDR vs. DM	Mean Reflectance	Total Reflectance	Layer Index	Scattering (Single, NRIR)	Scattering (Single, NRPE)	Scattering (Multiple, NRIR)	Scattering (Multiple, NRPE)
Across All Macular Regions							
RNFL	x	x	x				
GCL+IPL	x	x	x				
INL	x	x	x				
OPL	x	x	x				
ONL+IS	x	x					
OS	x	x	x	x	x	x	x
RPE	x	x		x	x	x	x
Foveal Region							
RNFL	x	x	x				
GCL+IPL	x	x	x	x	x	x	x
INL	x	x					
OPL	x	x	x		x	x	x
ONL+IS	x	x					
OS	x	x	x		x		x
RPE	x	x		x	x	x	x
Parafoveal Region							
RNFL	x	x	x				
GCL+IPL	x	x	x		x		x
INL	x	x	x				
OPL	x	x	x				
ONL+IS	x	x	x				
OS	x	x	x	x	x	x	x
RPE	x	x		x	x	x	x
Perifoveal Region							
RNFL	x	x	x				
GCL+IPL	x	x	x				
INL	x	x	x				
OPL	x	x	x				
ONL+IS	x	x					
OS	x	x	x	x	x	x	x
RPE	x	x		x	x	x	x

"X" denotes the intraretinal layer and regional sector in which the structural feature change showed a statistically significant difference ($p<0.001$) by using ANOVA followed by Newman-Keuls post hoc analysis.

Table 5.10 AUROC values of mean reflectance measurements by study groups

AUROC	MDR vs. Healthy	MDR vs. DM	DM vs. Healthy
Across All Macular Regions			
RNFL	0.84 **	0.75 *	0.68
GCL+IPL	0.79 *	0.72 *	0.62
INL	0.75 *	0.70 *	0.58
OPL	0.77 *	0.74 *	0.59
ONL+IS	0.75 *	0.72 *	0.61
OS	0.74 *	0.58	0.66
RPE	0.79 *	0.64	0.68
Foveal Region			
RNFL	0.79 *	0.74 *	0.57
GCL+IPL	0.79 *	0.70 *	0.60
INL	0.74 *	0.70 *	0.57
OPL	0.74 *	0.75 *	0.54
ONL+IS	0.75 *	0.72 *	0.59
OS	0.72 *	0.58	0.65
RPE	0.76 *	0.61	0.68
Parafoveal region			
RNFL	0.82 **	0.76 *	0.62
GCL+IPL	0.77 *	0.70 *	0.60
INL	0.75 *	0.69	0.57
OPL	0.76 *	0.74 *	0.58
ONL+IS	0.74 *	0.71 *	0.61
OS	0.74 *	0.58	0.64
RPE	0.76 *	0.62	0.67
Perifoveal Region			
RNFL	0.84 **	0.75 *	0.69
GCL+IPL	0.77 *	0.72 *	0.62
INL	0.75 *	0.70 *	0.59
OPL	0.77 *	0.73 *	0.61
ONL+IS	0.75 *	0.70 *	0.62
OS	0.74 *	0.57	0.66
RPE	0.80 **	0.66	0.68

*0.70≤AUROC<0.80, **0.80≤AUROC

Table 5.11 Cutoff values of the mean reflectance (dB) derived from ROC analyses between MDR and healthy eyes

Intraretinal Layer	AUROC	95% CI		Cutoff Point (dB)	Sensitivity	Specificity
		Lower Bound	Upper Bound			
Across All Macular Regions						
RNFL	0.84 ± 0.04	0.77	0.92	52.91	0.80	0.70
GCL+IPL	0.79 ± 0.04	0.71	0.87	48.55	0.78	0.68
INL	0.75 ± 0.05	0.66	0.84	45.36	0.73	0.63
OPL	0.77 ± 0.04	0.68	0.86	47.03	0.74	0.64
ONL+IS	0.75 ± 0.05	0.66	0.85	42.37	0.77	0.67
OS	0.74 ± 0.05	0.64	0.83	55.59	0.73	0.63
RPE	0.79 ± 0.04	0.70	0.87	57.76	0.77	0.67
Foveal Region						
RNFL	0.79 ± 0.04	0.71	0.87	50.86	0.76	0.66
GCL+IPL	0.79 ± 0.04	0.70	0.87	48.39	0.76	0.66
INL	0.74 ± 0.05	0.65	0.83	45.69	0.75	0.65
OPL	0.74 ± 0.05	0.65	0.84	47.40	0.75	0.65
ONL+IS	0.75 ± 0.05	0.65	0.84	42.79	0.75	0.65
OS	0.72 ± 0.05	0.63	0.82	55.67	0.73	0.63
RPE	0.76 ± 0.05	0.67	0.85	58.32	0.77	0.67
Parafoveal Region						
RNFL	0.82 ± 0.04	0.74	0.90	52.29	0.82	0.72
GCL+IPL	0.77 ± 0.04	0.68	0.86	48.65	0.76	0.66
INL	0.75 ± 0.05	0.66	0.84	45.10	0.75	0.65
OPL	0.76 ± 0.05	0.68	0.85	47.57	0.76	0.66
ONL+IS	0.74 ± 0.05	0.65	0.84	42.68	0.77	0.67
OS	0.74 ± 0.05	0.64	0.83	56.27	0.72	0.62
RPE	0.76 ± 0.05	0.67	0.85	57.80	0.76	0.66
Perifoveal Region						
RNFL	0.84 ± 0.04	0.77	0.91	53.44	0.80	0.70
GCL+IPL	0.77 ± 0.04	0.69	0.86	48.82	0.77	0.67
INL	0.75 ± 0.05	0.66	0.84	45.16	0.73	0.63
OPL	0.77 ± 0.04	0.68	0.85	46.74	0.75	0.65
ONL+IS	0.75 ± 0.05	0.66	0.84	42.44	0.75	0.65
OS	0.74 ± 0.05	0.64	0.83	55.66	0.73	0.63
RPE	0.80 ± 0.04	0.72	0.88	57.37	0.77	0.67

Table 5.12 Cutoff values of the mean reflectance (dB) derived from ROC analyses between MDR and DM eyes

Intraretinal Layer	AUROC	95% CI		Cutoff Point (dB)	Sensitivity	Specificity
		Lower Bound	Upper Bound			
Across All Macular Regions						
RNFL	0.75 ± 0.06	0.64	0.85	52.46	0.75	0.65
GCL+IPL	0.72 ± 0.06	0.61	0.83	48.22	0.71	0.61
INL	0.70 ± 0.06	0.59	0.82	44.93	0.66	0.56
OPL	0.74 ± 0.06	0.63	0.85	46.98	0.71	0.61
ONL+IS	0.72 ± 0.06	0.60	0.83	42.25	0.71	0.61
OS	0.58 ± 0.06	0.46	0.71	55.37	0.59	0.49
RPE	0.64 ± 0.06	0.52	0.77	57.53	0.66	0.56
Foveal Region						
RNFL	0.74 ± 0.06	0.63	0.84	50.47	0.68	0.58
GCL+IPL	0.70 ± 0.06	0.59	0.82	47.65	0.68	0.58
INL	0.70 ± 0.06	0.58	0.81	45.19	0.66	0.56
OPL	0.75 ± 0.06	0.64	0.85	47.32	0.74	0.64
ONL+IS	0.72 ± 0.06	0.60	0.83	42.56	0.74	0.64
OS	0.58 ± 0.06	0.46	0.71	55.22	0.61	0.51
RPE	0.61 ± 0.06	0.48	0.73	57.95	0.68	0.58
Parafoveal Region						
RNFL	0.76 ± 0.05	0.65	0.86	52.08	0.76	0.66
GCL+IPL	0.70 ± 0.06	0.59	0.82	48.23	0.68	0.58
INL	0.69 ± 0.06	0.58	0.81	44.91	0.66	0.56
OPL	0.74 ± 0.06	0.63	0.85	47.41	0.71	0.61
ONL+IS	0.71 ± 0.06	0.59	0.82	42.49	0.74	0.64
OS	0.58 ± 0.06	0.46	0.71	56.02	0.63	0.53
RPE	0.62 ± 0.06	0.50	0.75	57.65	0.66	0.56
Perifoveal Region						
RNFL	0.75 ± 0.06	0.64	0.86	53.05	0.75	0.65
GCL+IPL	0.72 ± 0.06	0.60	0.83	48.67	0.68	0.58
INL	0.70 ± 0.06	0.58	0.81	44.84	0.68	0.58
OPL	0.73 ± 0.06	0.62	0.84	46.66	0.71	0.61
ONL+IS	0.70 ± 0.06	0.59	0.82	42.02	0.71	0.61
OS	0.57 ± 0.06	0.45	0.70	55.44	0.58	0.48
RPE	0.66 ± 0.06	0.54	0.78	57.02	0.64	0.54

Table 5.13 AUROC values of the total reflectance (dB) by study groups

AUROC	MDR vs. Healthy	MDR vs. DM	DM vs. Healthy
Across All Macular Regions			
RNFL	0.83 **	0.73 *	0.68
GCL+IPL	0.84 **	0.78 *	0.67
INL	0.76 *	0.74 *	0.57
OPL	0.84 **	0.76 *	0.58
ONL+IS	0.74 *	0.68	0.61
OS	0.85 **	0.86 **	0.54
RPE	0.80 **	0.80 **	0.52
Foveal Region			
RNFL	0.78 *	0.69	0.62
GCL+IPL	0.89 **	0.79 *	0.65
INL	0.73 *	0.70 *	0.54
OPL	0.90 **	0.77 *	0.58
ONL+IS	0.74 *	0.69	0.60
OS	0.85 **	0.86 **	0.56
RPE	0.76 *	0.75 *	0.52
Parafoveal region			
RNFL	0.81 **	0.76 *	0.61
GCL+IPL	0.82 **	0.78 *	0.63
INL	0.75 *	0.74 *	0.57
OPL	0.76 *	0.76 *	0.56
ONL+IS	0.73 *	0.66	0.62
OS	0.83 **	0.87 **	0.47
RPE	0.71 *	0.77 *	0.43
Perifoveal Region			
RNFL	0.83 **	0.75 *	0.66
GCL+IPL	0.80 **	0.73 *	0.69
INL	0.76 *	0.73 *	0.59
OPL	0.77 *	0.74 *	0.61
ONL+IS	0.72 *	0.65	0.62
OS	0.84 **	0.84 **	0.51
RPE	0.78 *	0.77 *	0.53

*0.70≤AUROC<0.80, **0.80≤AUROC

Table 5.14 Cutoff values of the total reflectance (dB) derived from ROC analyses between MDR and healthy eyes

Intraretinal Layer	AUROC	95% CI		Cutoff Point (dB)	Sensitivity	Specificity
		Lower Bound	Upper Bound			
Across All Macular Regions						
RNFL	0.83 ± 0.04	0.75	0.91	79.89	0.80	0.70
GCL+IPL	0.84 ± 0.04	0.77	0.91	80.57	0.82	0.72
INL	0.76 ± 0.05	0.67	0.85	70.47	0.74	0.64
OPL	0.84 ± 0.04	0.77	0.91	72.97	0.81	0.71
ONL+IS	0.74 ± 0.05	0.65	0.83	75.33	0.73	0.63
OS	0.85 ± 0.04	0.78	0.92	74.22	0.80	0.70
RPE	0.80 ± 0.04	0.72	0.87	75.06	0.73	0.63
Foveal Region						
RNFL	0.78 ± 0.04	0.70	0.87	75.84	0.77	0.67
GCL+IPL	0.89 ± 0.03	0.83	0.95	81.34	0.85	0.75
INL	0.73 ± 0.05	0.64	0.82	71.22	0.73	0.63
OPL	0.90 ± 0.03	0.85	0.95	75.56	0.84	0.74
ONL+IS	0.74 ± 0.05	0.65	0.84	76.76	0.73	0.63
OS	0.85 ± 0.04	0.77	0.92	74.69	0.84	0.74
RPE	0.76 ± 0.05	0.67	0.85	75.68	0.72	0.62
Parafoveal Region						
RNFL	0.81 ± 0.04	0.73	0.89	78.22	0.81	0.71
GCL+IPL	0.82 ± 0.04	0.75	0.90	82.28	0.80	0.70
INL	0.75 ± 0.05	0.67	0.84	71.60	0.75	0.65
OPL	0.76 ± 0.05	0.67	0.85	73.46	0.76	0.66
ONL+IS	0.73 ± 0.05	0.64	0.82	75.88	0.73	0.63
OS	0.83 ± 0.04	0.75	0.90	74.31	0.80	0.70
RPE	0.71 ± 0.05	0.62	0.81	74.61	0.71	0.61
Perifoveal Region						
RNFL	0.83 ± 0.04	0.76	0.91	10.33	0.36	0.26
GCL+IPL	0.80 ± 0.04	0.72	0.89	79.85	0.81	0.71
INL	0.76 ± 0.05	0.67	0.85	69.88	0.75	0.65
OPL	0.77 ± 0.04	0.69	0.86	71.21	0.74	0.64
ONL+IS	0.72 ± 0.05	0.63	0.82	74.17	0.72	0.62
OS	0.84 ± 0.04	0.77	0.91	73.56	0.78	0.68
RPE	0.78 ± 0.04	0.70	0.86	74.49	0.73	0.63

Table 5.15 Cutoff values of the total reflectance (dB) derived from ROC analyses between MDR and DM eyes

Intraretinal Layer	AUROC	95% CI		Cutoff Point (dB)	Sensitivity	Specificity
		Lower Bound	Upper Bound			
Across All Macular Regions						
RNFL	0.73 ± 0.06	0.62	0.84	79.41	0.71	0.61
GCL+IPL	0.78 ± 0.05	0.68	0.88	79.91	0.75	0.65
INL	0.74 ± 0.06	0.63	0.84	70.38	0.68	0.58
OPL	0.76 ± 0.05	0.66	0.87	72.73	0.68	0.58
ONL+IS	0.68 ± 0.06	0.56	0.80	75.19	0.68	0.58
OS	0.86 ± 0.04	0.79	0.94	74.29	0.82	0.72
RPE	0.80 ± 0.05	0.70	0.89	74.97	0.71	0.61
Foveal Region						
RNFL	0.69 ± 0.06	0.58	0.81	75.30	0.66	0.56
GCL+IPL	0.79 ± 0.05	0.69	0.89	80.12	0.71	0.61
INL	0.70 ± 0.06	0.59	0.82	71.13	0.68	0.58
OPL	0.77 ± 0.05	0.66	0.87	74.89	0.71	0.61
ONL+IS	0.69 ± 0.06	0.57	0.80	76.62	0.66	0.56
OS	0.86 ± 0.04	0.78	0.94	74.83	0.84	0.74
RPE	0.75 ± 0.06	0.64	0.86	75.70	0.74	0.64
Parafoveal Region						
RNFL	0.76 ± 0.06	0.65	0.86	78.11	0.75	0.65
GCL+IPL	0.78 ± 0.05	0.68	0.88	81.63	0.75	0.65
INL	0.74 ± 0.06	0.63	0.85	71.31	0.71	0.61
OPL	0.76 ± 0.05	0.65	0.86	73.32	0.74	0.64
ONL+IS	0.66 ± 0.06	0.54	0.78	75.27	0.66	0.56
OS	0.87 ± 0.04	0.79	0.94	74.40	0.82	0.72
RPE	0.77 ± 0.05	0.67	0.88	74.71	0.74	0.64
Perifoveal Region						
RNFL	0.75 ± 0.05	0.64	0.86	80.43	0.73	0.63
GCL+IPL	0.73 ± 0.06	0.62	0.84	79.09	0.75	0.65
INL	0.73 ± 0.06	0.62	0.84	69.75	0.71	0.61
OPL	0.74 ± 0.06	0.63	0.85	71.22	0.74	0.64
ONL+IS	0.65 ± 0.06	0.54	0.77	73.79	0.66	0.56
OS	0.84 ± 0.04	0.76	0.93	73.83	0.82	0.72
RPE	0.77 ± 0.05	0.67	0.87	74.48	0.74	0.64

Table 5.16 AUROC values of the layer index (a.u.) by study groups

AUROC	MDR vs. Healthy	MDR vs. DM	DM vs. Healthy
Across All Macular Regions			
RNFL	0.80 **	0.69	0.66
GCL+IPL	0.85 **	0.79 *	0.63
INL	0.73 *	0.75 *	0.50
OPL	0.83 **	0.78 *	0.52
ONL+IS	0.71 *	0.68	0.57
OS	0.81 **	0.92 **	0.36
RPE	0.54	0.75 *	0.32
Foveal Region			
RNFL	0.71 *	0.65	0.56
GCL+IPL	0.91 **	0.82 **	0.59
INL	0.68	0.71 *	0.46
OPL	0.89 **	0.79 *	0.54
ONL+IS	0.72 *	0.71 *	0.55
OS	0.78 *	0.89 **	0.42
RPE	0.48	0.70 *	0.34
Parafoveal region			
RNFL	0.79 *	0.75 *	0.55
GCL+IPL	0.83 **	0.78 *	0.58
INL	0.72 *	0.76 *	0.50
OPL	0.73 *	0.77 *	0.47
ONL+IS	0.71 *	0.65	0.59
OS	0.75 *	0.91 **	0.33
RPE	0.44	0.68	0.27
Perifoveal Region			
RNFL	0.79 *	0.71 *	0.62
GCL+IPL	0.78 *	0.70 *	0.66
INL	0.73 *	0.73 *	0.52
OPL	0.75 *	0.75 *	0.54
ONL+IS	0.69	0.64	0.58
OS	0.77 *	0.88 **	0.34
RPE	0.57	0.68	0.38

*0.70≤AUROC<0.80, **0.80≤AUROC

Table 5.17 Cutoff values of the layer index (a.u.) derived from ROC analyses between MDR and healthy eyes

Intraretinal Layer	AUROC	95% CI		Cutoff Point (a.u.)	Sensitivity	Specificity
		Lower Bound	Upper Bound			
Across All Macular Regions						
RNFL	0.80 ± 0.04	0.71	0.88	11.47	0.77	0.67
GCL+IPL	0.85 ± 0.04	0.77	0.92	12.20	0.85	0.75
INL	0.73 ± 0.05	0.63	0.82	3.84	0.74	0.64
OPL	0.83 ± 0.04	0.75	0.91	5.03	0.78	0.68
ONL+IS	0.71 ± 0.05	0.62	0.81	6.53	0.72	0.62
OS	0.81 ± 0.04	0.74	0.89	5.55	0.78	0.68
RPE	0.54 ± 0.05	0.44	0.65	6.10	0.57	0.47
Foveal Region						
RNFL	0.71 ± 0.05	0.61	0.82	6.74	0.75	0.65
GCL+IPL	0.91 ± 0.03	0.85	0.96	12.31	0.89	0.79
INL	0.68 ± 0.05	0.58	0.78	3.91	0.71	0.61
OPL	0.89 ± 0.03	0.83	0.95	6.26	0.87	0.77
ONL+IS	0.72 ± 0.05	0.63	0.82	7.36	0.72	0.62
OS	0.78 ± 0.04	0.70	0.87	5.75	0.75	0.65
RPE	0.48 ± 0.05	0.38	0.59	6.36	0.49	0.39
Parafoveal Region						
RNFL	0.79 ± 0.05	0.70	0.87	9.14	0.77	0.67
GCL+IPL	0.83 ± 0.04	0.75	0.90	14.53	0.81	0.71
INL	0.72 ± 0.05	0.63	0.82	4.21	0.75	0.65
OPL	0.73 ± 0.05	0.63	0.82	5.34	0.74	0.64
ONL+IS	0.71 ± 0.05	0.61	0.80	6.72	0.71	0.61
OS	0.75 ± 0.05	0.66	0.84	5.36	0.77	0.67
RPE	0.44 ± 0.06	0.34	0.55	5.81	0.51	0.41
Perifoveal Region						
RNFL	0.79 ± 0.04	0.70	0.87	12.88	0.76	0.66
GCL+IPL	0.78 ± 0.05	0.69	0.87	11.14	0.78	0.68
INL	0.73 ± 0.05	0.64	0.82	3.70	0.73	0.63
OPL	0.75 ± 0.05	0.65	0.84	4.36	0.73	0.63
ONL+IS	0.69 ± 0.05	0.59	0.78	6.15	0.69	0.59
OS	0.77 ± 0.04	0.68	0.85	5.39	0.74	0.64
RPE	0.57 ± 0.06	0.46	0.67	5.86	0.61	0.51

Table 5.18 Cutoff values of the layer index (a.u.) derived from ROC analyses between MDR and DM eyes

Intraretinal Layer	AUROC	95% CI		Cutoff Point (a.u.)	Sensitivity	Specificity
		Lower Bound	Upper Bound			
Across All Macular Regions						
RNFL	0.69 ± 0.06	0.57	0.80	11.08	0.73	0.63
GCL+IPL	0.79 ± 0.05	0.69	0.88	11.60	0.71	0.61
INL	0.75 ± 0.06	0.64	0.86	3.79	0.71	0.61
OPL	0.78 ± 0.05	0.67	0.89	4.93	0.71	0.61
ONL+IS	0.68 ± 0.06	0.56	0.80	6.45	0.68	0.58
OS	0.92 ± 0.03	0.87	0.98	5.67	0.90	0.80
RPE	0.75 ± 0.06	0.64	0.86	6.33	0.77	0.67
Foveal Region						
RNFL	0.65 ± 0.06	0.53	0.77	6.47	0.68	0.58
GCL+IPL	0.82 ± 0.05	0.73	0.91	11.59	0.71	0.61
INL	0.71 ± 0.06	0.60	0.83	4.00	0.73	0.63
OPL	0.79 ± 0.05	0.70	0.89	5.92	0.74	0.64
ONL+IS	0.71 ± 0.06	0.59	0.83	7.21	0.66	0.56
OS	0.89 ± 0.04	0.82	0.96	5.81	0.87	0.77
RPE	0.70 ± 0.06	0.59	0.82	6.63	0.73	0.63
Parafoveal Region						
RNFL	0.75 ± 0.06	0.64	0.86	9.09	0.76	0.66
GCL+IPL	0.78 ± 0.05	0.69	0.88	13.99	0.75	0.65
INL	0.76 ± 0.05	0.66	0.86	4.14	0.73	0.63
OPL	0.77 ± 0.06	0.66	0.88	5.40	0.75	0.65
ONL+IS	0.65 ± 0.06	0.53	0.78	6.68	0.68	0.58
OS	0.91 ± 0.03	0.86	0.97	5.69	0.87	0.77
RPE	0.68 ± 0.06	0.57	0.80	6.08	0.68	0.58
Perifoveal Region						
RNFL	0.71 ± 0.06	0.60	0.83	12.75	0.73	0.63
GCL+IPL	0.70 ± 0.06	0.59	0.82	10.54	0.68	0.58
INL	0.73 ± 0.06	0.62	0.84	3.63	0.73	0.63
OPL	0.75 ± 0.06	0.64	0.86	4.33	0.71	0.61
ONL+IS	0.64 ± 0.06	0.52	0.76	5.82	0.61	0.51
OS	0.88 ± 0.04	0.81	0.95	5.68	0.82	0.72
RPE	0.68 ± 0.06	0.56	0.80	5.93	0.68	0.58

Table 5.19 AUROC values of scattering coefficients (mm^{-1}) (calculated by using the single-scattering model with the normalization method NRIR) by study groups

AUROC	MDR vs. Healthy	MDR vs. DM	DM vs. Healthy
Across All Macular Regions			
RNFL	0.60	0.58	0.53
GCL+IPL	0.60	0.64	0.43
INL	0.68	0.69	0.52
OPL	0.67	0.72 *	0.49
ONL+IS	0.47	0.42	0.58
OS	0.24	0.19	0.55
RPE	0.26	0.26	0.51
Foveal Region			
RNFL	0.53	0.64	0.36
GCL+IPL	0.42	0.38	0.56
INL	0.65	0.68	0.47
OPL	0.39	0.50	0.38
ONL+IS	0.53	0.42	0.62
OS	0.31	0.14	0.68
RPE	0.28	0.30	0.49
Parafoveal region			
RNFL	0.53	0.64	0.46
GCL+IPL	0.41	0.38	0.46
INL	0.64	0.68	0.53
OPL	0.66	0.50	0.52
ONL+IS	0.43	0.42	0.57
OS	0.31	0.14	0.73 *
RPE	0.20	0.30	0.50
Perifoveal Region			
RNFL	0.65	0.58	0.61
GCL+IPL	0.59	0.66	0.39
INL	0.64	0.62	0.53
OPL	0.64	0.65	0.51
ONL+IS	0.45	0.41	0.56
OS	0.24	0.17	0.62
RPE	0.25	0.28	0.48

*0.70≤AUROC<0.80, **0.80≤AUROC

Table 5.20 Cutoff values of scattering coefficients (mm^{-1}) (calculated by using the single-scattering model with the normalization method NRIR) derived from ROC analyses between MDR and healthy eyes

Intraretinal Layer	AUROC	95% CI		Cutoff Point (mm^{-1})	Sensitivity	Specificity
		Lower Bound	Upper Bound			
Across All Macular Regions						
RNFL	0.60 ± 0.06	0.49	0.72	3.46	0.65	0.55
GCL+IPL	0.60 ± 0.06	0.48	0.72	1.66	0.66	0.56
INL	0.68 ± 0.05	0.57	0.79	2.65	0.73	0.63
OPL	0.67 ± 0.06	0.56	0.78	1.93	0.77	0.67
ONL+IS	0.47 ± 0.06	0.35	0.59	2.76	0.54	0.44
OS	0.24 ± 0.04	0.15	0.33	9.36	0.41	0.31
RPE	0.26 ± 0.05	0.17	0.35	10.60	0.41	0.31
Foveal Region						
RNFL	0.53 ± 0.06	0.42	0.65	3.74	0.57	0.47
GCL+IPL	0.42 ± 0.06	0.31	0.53	1.36	0.52	0.42
INL	0.65 ± 0.05	0.54	0.76	2.22	0.68	0.58
OPL	0.39 ± 0.06	0.28	0.51	1.59	0.46	0.36
ONL+IS	0.53 ± 0.06	0.41	0.64	1.84	0.59	0.49
OS	0.31 ± 0.05	0.21	0.40	11.56	0.41	0.31
RPE	0.28 ± 0.05	0.18	0.37	9.70	0.43	0.33
Parafoveal Region						
RNFL	0.53 ± 0.06	0.41	0.64	3.38	0.59	0.49
GCL+IPL	0.41 ± 0.06	0.30	0.53	1.07	0.52	0.42
INL	0.64 ± 0.05	0.53	0.74	2.08	0.68	0.58
OPL	0.66 ± 0.05	0.56	0.76	1.68	0.68	0.58
ONL+IS	0.43 ± 0.06	0.32	0.54	2.49	0.49	0.39
OS	0.31 ± 0.05	0.22	0.41	11.05	0.41	0.31
RPE	0.20 ± 0.04	0.12	0.29	10.30	0.33	0.23
Perifoveal Region						
RNFL	0.65 ± 0.06	0.54	0.76	3.13	0.66	0.56
GCL+IPL	0.59 ± 0.06	0.48	0.71	1.88	0.64	0.54
INL	0.64 ± 0.06	0.53	0.75	2.70	0.71	0.61
OPL	0.64 ± 0.06	0.52	0.75	1.92	0.73	0.63
ONL+IS	0.45 ± 0.06	0.34	0.56	2.77	0.51	0.41
OS	0.24 ± 0.04	0.15	0.32	9.42	0.38	0.28
RPE	0.25 ± 0.05	0.16	0.33	10.33	0.36	0.26

Table 5.21 Cutoff values of scattering coefficients (mm^{-1}) (calculated by using the single-scattering model with the normalization method NRIR) derived from ROC analyses between MDR and DM eyes

Intraretinal Layer	AUROC	95% CI		Cutoff Point (mm^{-1})	Sensitivity	Specificity
		Lower Bound	Upper Bound			
Across All Macular Regions						
RNFL	0.58 ± 0.07	0.46	0.71	3.35	0.61	0.51
GCL+IPL	0.64 ± 0.06	0.52	0.76	1.67	0.68	0.58
INL	0.69 ± 0.06	0.57	0.80	2.62	0.71	0.61
OPL	0.72 ± 0.06	0.60	0.83	1.92	0.77	0.67
ONL+IS	0.42 ± 0.07	0.29	0.55	2.64	0.48	0.38
OS	0.19 ± 0.05	0.10	0.29	9.10	0.34	0.24
RPE	0.26 ± 0.06	0.15	0.36	10.45	0.34	0.24
Foveal Region						
RNFL	0.64 ± 0.06	0.52	0.77	4.13	0.71	0.61
GCL+IPL	0.38 ± 0.06	0.25	0.50	1.33	0.50	0.40
INL	0.68 ± 0.06	0.56	0.80	2.24	0.68	0.58
OPL	0.50 ± 0.07	0.37	0.63	1.61	0.58	0.48
ONL+IS	0.42 ± 0.06	0.29	0.54	1.78	0.50	0.40
OS	0.14 ± 0.04	0.06	0.22	10.68	0.32	0.22
RPE	0.30 ± 0.06	0.18	0.41	9.63	0.40	0.30
Parafoveal Region						
RNFL	0.64 ± 0.06	0.52	0.77	4.13	0.71	0.61
GCL+IPL	0.38 ± 0.06	0.25	0.50	1.33	0.50	0.40
INL	0.68 ± 0.06	0.56	0.80	2.24	0.68	0.58
OPL	0.50 ± 0.07	0.37	0.63	1.61	0.58	0.48
ONL+IS	0.42 ± 0.06	0.29	0.54	1.78	0.50	0.40
OS	0.14 ± 0.04	0.06	0.22	10.68	0.32	0.22
RPE	0.30 ± 0.06	0.18	0.41	9.63	0.40	0.30
Perifoveal Region						
RNFL	0.58 ± 0.06	0.46	0.71	3.07	0.61	0.51
GCL+IPL	0.66 ± 0.06	0.54	0.78	1.90	0.68	0.58
INL	0.62 ± 0.06	0.50	0.74	2.58	0.66	0.56
OPL	0.65 ± 0.06	0.53	0.77	1.89	0.68	0.58
ONL+IS	0.41 ± 0.06	0.28	0.54	2.65	0.43	0.33
OS	0.17 ± 0.05	0.08	0.26	8.99	0.36	0.26
RPE	0.28 ± 0.06	0.17	0.39	10.44	0.42	0.32

Table 5.22 AUROC values of scattering coefficients (mm^{-1}) (calculated by using the single-scattering model with the normalization method NRPE) by study groups

AUROC	MDR vs. Healthy	MDR vs. DM	DM vs. Healthy
Across All Macular Regions			
RNFL	0.59	0.56	0.55
GCL+IPL	0.54	0.61	0.37
INL	0.65	0.66	0.50
OPL	0.65	0.71 *	0.44
ONL+IS	0.41	0.35	0.60
OS	0.17	0.14	0.56
RPE	0.19	0.22	0.50
Foveal Region			
RNFL	0.49	0.63	0.33
GCL+IPL	0.39	0.36	0.53
INL	0.63	0.70 *	0.42
OPL	0.34	0.50	0.31
ONL+IS	0.48	0.40	0.58
OS	0.25	0.11	0.65
RPE	0.27	0.31	0.47
Parafoveal region			
RNFL	0.48	0.52	0.44
GCL+IPL	0.31	0.40	0.43
INL	0.59	0.61	0.49
OPL	0.63	0.68	0.48
ONL+IS	0.37	0.34	0.55
OS	0.27	0.07	0.71 *
RPE	0.19	0.25	0.48
Perifoveal Region			
RNFL	0.61	0.52	0.61
GCL+IPL	0.47	0.58	0.37
INL	0.55	0.56	0.50
OPL	0.58	0.61	0.47
ONL+IS	0.39	0.36	0.55
OS	0.18	0.12	0.60
RPE	0.17	0.21	0.48

*0.70≤AUROC<0.80, **0.80≤AUROC

Table 5.23 Cutoff values of scattering coefficients (mm^{-1}) (calculated by using the single-scattering model with the normalization method NRPE) derived from ROC analyses between MDR and healthy eyes

Intraretinal Layer	AUROC	95% CI		Cutoff Point (mm^{-1})	Sensitivity	Specificity
		Lower Bound	Upper Bound			
Across All Macular Regions						
RNFL	0.59 ± 0.06	0.48	0.71	5.15	0.65	0.55
GCL+IPL	0.54 ± 0.06	0.42	0.66	2.47	0.62	0.52
INL	0.65 ± 0.06	0.54	0.76	4.02	0.68	0.58
OPL	0.65 ± 0.06	0.54	0.76	2.87	0.70	0.60
ONL+IS	0.41 ± 0.06	0.30	0.52	4.14	0.46	0.36
OS	0.17 ± 0.04	0.10	0.24	14.09	0.34	0.24
RPE	0.19 ± 0.04	0.11	0.27	15.44	0.30	0.20
Foveal Region						
RNFL	0.49 ± 0.06	0.38	0.61	5.17	0.52	0.42
GCL+IPL	0.39 ± 0.06	0.28	0.50	1.84	0.50	0.40
INL	0.63 ± 0.06	0.53	0.74	3.06	0.68	0.58
OPL	0.34 ± 0.06	0.23	0.45	2.13	0.41	0.31
ONL+IS	0.48 ± 0.06	0.37	0.60	2.48	0.57	0.47
OS	0.25 ± 0.05	0.16	0.34	15.77	0.35	0.25
RPE	0.27 ± 0.05	0.17	0.36	12.84	0.38	0.28
Parafoveal Region						
RNFL	0.48 ± 0.06	0.36	0.59	4.76	0.57	0.47
GCL+IPL	0.31 ± 0.05	0.21	0.41	1.51	0.41	0.31
INL	0.59 ± 0.05	0.48	0.70	2.90	0.64	0.54
OPL	0.63 ± 0.05	0.53	0.74	2.37	0.68	0.58
ONL+IS	0.37 ± 0.05	0.26	0.47	3.50	0.45	0.35
OS	0.27 ± 0.05	0.18	0.36	15.44	0.41	0.31
RPE	0.19 ± 0.04	0.11	0.27	14.25	0.30	0.20
Perifoveal Region						
RNFL	0.61 ± 0.06	0.49	0.72	4.83	0.66	0.56
GCL+IPL	0.47 ± 0.06	0.36	0.58	2.88	0.54	0.44
INL	0.55 ± 0.06	0.44	0.66	4.06	0.60	0.50
OPL	0.58 ± 0.06	0.47	0.69	2.88	0.64	0.54
ONL+IS	0.39 ± 0.05	0.28	0.49	4.17	0.45	0.35
OS	0.18 ± 0.04	0.10	0.25	14.13	0.36	0.26
RPE	0.17 ± 0.04	0.10	0.25	15.43	0.29	0.19

Table 5.24 Cutoff values of scattering coefficients (mm^{-1}) (calculated by using the single-scattering model with the normalization method NRPE) derived from ROC analyses between MDR and DM eyes

Intraretinal Layer	AUROC	95% CI		Cutoff Point (mm^{-1})	Sensitivity	Specificity
		Lower Bound	Upper Bound			
Across All Macular Regions						
RNFL	0.56 ± 0.07	0.43	0.68	5.03	0.58	0.48
GCL+IPL	0.61 ± 0.06	0.49	0.74	2.54	0.66	0.56
INL	0.66 ± 0.06	0.54	0.78	4.04	0.70	0.60
OPL	0.71 ± 0.06	0.60	0.83	2.87	0.71	0.61
ONL+IS	0.35 ± 0.06	0.22	0.47	4.03	0.41	0.31
OS	0.14 ± 0.04	0.06	0.22	13.70	0.29	0.19
RPE	0.22 ± 0.05	0.12	0.33	15.67	0.39	0.29
Foveal Region						
RNFL	0.63 ± 0.06	0.51	0.76	5.69	0.68	0.58
GCL+IPL	0.36 ± 0.06	0.24	0.48	1.84	0.47	0.37
INL	0.70 ± 0.06	0.59	0.81	3.09	0.68	0.58
OPL	0.50 ± 0.07	0.37	0.63	2.21	0.54	0.44
ONL+IS	0.40 ± 0.06	0.28	0.52	2.43	0.53	0.43
OS	0.11 ± 0.04	0.04	0.18	14.55	0.26	0.16
RPE	0.31 ± 0.06	0.19	0.43	12.97	0.40	0.30
Parafoveal Region						
RNFL	0.52 ± 0.07	0.39	0.64	4.90	0.61	0.51
GCL+IPL	0.40 ± 0.06	0.28	0.53	1.54	0.52	0.42
INL	0.61 ± 0.06	0.49	0.73	2.94	0.66	0.56
OPL	0.68 ± 0.06	0.57	0.80	2.39	0.68	0.58
ONL+IS	0.34 ± 0.06	0.22	0.46	3.44	0.40	0.30
OS	0.07 ± 0.03	0.02	0.13	13.97	0.19	0.09
RPE	0.25 ± 0.05	0.14	0.35	14.71	0.37	0.27
Perifoveal Region						
RNFL	0.52 ± 0.07	0.40	0.65	4.63	0.57	0.47
GCL+IPL	0.58 ± 0.06	0.46	0.71	2.92	0.66	0.56
INL	0.56 ± 0.06	0.44	0.69	4.11	0.64	0.54
OPL	0.61 ± 0.06	0.49	0.74	2.88	0.64	0.54
ONL+IS	0.36 ± 0.06	0.23	0.48	4.13	0.42	0.32
OS	0.12 ± 0.04	0.05	0.19	13.59	0.29	0.19
RPE	0.21 ± 0.05	0.11	0.32	15.54	0.34	0.24

Table 5.25 AUROC values of scattering coefficients (mm^{-1}) (calculated by using the multiple-scattering model with the normalization method NRIR) by study groups

AUROC	MDR vs. Healthy	MDR vs. DM	DM vs. Healthy
Across All Macular Regions			
RNFL	0.55	0.59	0.45
GCL+IPL	0.56	0.68	0.33
INL	0.67	0.69	0.50
OPL	0.67	0.71 *	0.48
ONL+IS	0.53	0.39	0.67
OS	0.26	0.21	0.54
RPE	0.26	0.25	0.51
Foveal Region			
RNFL	0.49	0.70	0.26
GCL+IPL	0.26	0.39	0.34
INL	0.63	0.64	0.48
OPL	0.31	0.47	0.29
ONL+IS	0.55	0.42	0.71 *
OS	0.36	0.19	0.69
RPE	0.29	0.31	0.49
Parafoveal region			
RNFL	0.48	0.54	0.43
GCL+IPL	0.42	0.47	0.45
INL	0.62	0.61	0.51
OPL	0.66	0.69	0.50
ONL+IS	0.51	0.37	0.68
OS	0.35	0.13	0.74 *
RPE	0.22	0.27	0.48
Perifoveal Region			
RNFL	0.55	0.53	0.53
GCL+IPL	0.50	0.61	0.35
INL	0.63	0.62	0.51
OPL	0.64	0.67	0.51
ONL+IS	0.55	0.38	0.69
OS	0.25	0.18	0.60
RPE	0.25	0.26	0.49

*0.70≤AUROC<0.8, **0.80≤AUROC

Table 5.26 Cutoff values of scattering coefficients (mm^{-1}) (calculated by using the multiple-scattering model with the normalization method NRIR) derived from ROC analyses between MDR and healthy eyes

Intraretinal Layer	AUROC	95% CI		Cutoff Point (mm^{-1})	Sensitivity	Specificity
		Lower Bound	Upper Bound			
Across All Macular Regions						
RNFL	0.55 ± 0.06	0.43	0.67	3.76	0.61	0.51
GCL+IPL	0.56 ± 0.06	0.44	0.68	1.90	0.62	0.52
INL	0.67 ± 0.06	0.56	0.78	3.32	0.72	0.62
OPL	0.67 ± 0.06	0.57	0.78	3.03	0.77	0.67
ONL+IS	0.53 ± 0.06	0.41	0.65	2.45	0.60	0.50
OS	0.26 ± 0.05	0.17	0.35	11.25	0.42	0.32
RPE	0.26 ± 0.05	0.16	0.35	12.83	0.41	0.31
Foveal Region						
RNFL	0.49 ± 0.06	0.37	0.60	3.63	0.57	0.47
GCL+IPL	0.26 ± 0.05	0.16	0.36	1.52	0.40	0.30
INL	0.63 ± 0.06	0.52	0.74	2.77	0.66	0.56
OPL	0.31 ± 0.06	0.20	0.42	2.34	0.42	0.32
ONL+IS	0.55 ± 0.06	0.42	0.67	1.70	0.59	0.49
OS	0.36 ± 0.05	0.25	0.46	14.44	0.43	0.33
RPE	0.29 ± 0.05	0.19	0.38	11.84	0.43	0.33
Parafoveal Region						
RNFL	0.48 ± 0.06	0.36	0.60	3.57	0.57	0.47
GCL+IPL	0.42 ± 0.06	0.30	0.54	1.33	0.52	0.42
INL	0.62 ± 0.06	0.51	0.73	2.52	0.64	0.54
OPL	0.66 ± 0.05	0.56	0.77	2.74	0.66	0.56
ONL+IS	0.51 ± 0.06	0.39	0.63	2.09	0.54	0.44
OS	0.35 ± 0.05	0.24	0.45	13.06	0.50	0.40
RPE	0.22 ± 0.04	0.13	0.31	12.32	0.38	0.28
Perifoveal Region						
RNFL	0.55 ± 0.06	0.43	0.66	3.45	0.58	0.48
GCL+IPL	0.50 ± 0.06	0.38	0.61	1.89	0.54	0.44
INL	0.63 ± 0.06	0.52	0.74	3.27	0.71	0.61
OPL	0.64 ± 0.06	0.53	0.75	3.00	0.75	0.65
ONL+IS	0.55 ± 0.06	0.43	0.66	2.39	0.62	0.52
OS	0.25 ± 0.05	0.17	0.34	11.41	0.39	0.29
RPE	0.25 ± 0.05	0.16	0.34	12.60	0.38	0.28

Table 5.27 Cutoff values of scattering coefficients (mm^{-1}) (calculated by using the multiple-scattering model with the normalization method NRIR) derived from ROC analyses between MDR and DM eyes

Intraretinal Layer	AUROC	95% CI		Cutoff Point (mm^{-1})	Sensitivity	Specificity
		Lower Bound	Upper Bound			
Across All Macular Regions						
RNFL	0.59 ± 0.06	0.47	0.72	3.75	0.60	0.50
GCL+IPL	0.68 ± 0.06	0.56	0.80	1.98	0.70	0.60
INL	0.69 ± 0.06	0.58	0.81	3.21	0.70	0.60
OPL	0.71 ± 0.06	0.60	0.83	3.04	0.77	0.67
ONL+IS	0.39 ± 0.06	0.27	0.52	2.33	0.46	0.36
OS	0.21 ± 0.05	0.11	0.30	11.08	0.36	0.26
RPE	0.25 ± 0.06	0.14	0.36	12.60	0.34	0.24
Foveal Region						
RNFL	0.70 ± 0.06	0.57	0.82	4.16	0.73	0.63
GCL+IPL	0.39 ± 0.06	0.26	0.51	1.58	0.47	0.37
INL	0.64 ± 0.06	0.52	0.76	2.80	0.66	0.56
OPL	0.47 ± 0.07	0.34	0.60	2.47	0.47	0.37
ONL+IS	0.42 ± 0.07	0.29	0.55	1.55	0.47	0.37
OS	0.19 ± 0.05	0.10	0.28	13.22	0.34	0.24
RPE	0.31 ± 0.06	0.19	0.42	11.74	0.42	0.32
Parafoveal Region						
RNFL	0.54 ± 0.07	0.42	0.67	3.59	0.59	0.49
GCL+IPL	0.47 ± 0.07	0.34	0.59	1.34	0.52	0.42
INL	0.61 ± 0.06	0.49	0.74	2.50	0.64	0.54
OPL	0.69 ± 0.06	0.58	0.81	2.74	0.66	0.56
ONL+IS	0.37 ± 0.06	0.25	0.49	1.95	0.45	0.35
OS	0.13 ± 0.04	0.06	0.21	12.40	0.26	0.16
RPE	0.27 ± 0.06	0.16	0.38	12.42	0.40	0.30
Perifoveal Region						
RNFL	0.53 ± 0.06	0.40	0.66	3.43	0.54	0.44
GCL+IPL	0.61 ± 0.06	0.49	0.74	1.92	0.63	0.53
INL	0.62 ± 0.06	0.49	0.74	3.18	0.63	0.53
OPL	0.67 ± 0.06	0.55	0.79	2.97	0.75	0.65
ONL+IS	0.38 ± 0.06	0.25	0.50	2.22	0.40	0.30
OS	0.18 ± 0.05	0.09	0.27	11.02	0.37	0.27
RPE	0.26 ± 0.06	0.15	0.37	12.60	0.38	0.28

Table 5.28 AUROC values of scattering coefficients (mm^{-1}) (calculated by using the multiple-scattering model with the normalization method NRPE) by study groups

AUROC	MDR vs. Healthy	MDR vs. DM	DM vs. Healthy
Across All Macular Regions			
RNFL	0.50	0.55	0.45
GCL+IPL	0.48	0.67	0.25
INL	0.64	0.66	0.46
OPL	0.65	0.71 *	0.42
ONL+IS	0.46	0.31	0.70 *
OS	0.17	0.14	0.56
RPE	0.19	0.21	0.50
Foveal Region			
RNFL	0.45	0.69	0.24
GCL+IPL	0.21	0.38	0.30
INL	0.61	0.66	0.44
OPL	0.25	0.48	0.26
ONL+IS	0.52	0.41	0.70
OS	0.29	0.15	0.67
RPE	0.27	0.32	0.46
Parafoveal region			
RNFL	0.44	0.51	0.42
GCL+IPL	0.33	0.41	0.41
INL	0.58	0.61	0.47
OPL	0.63	0.70	0.46
ONL+IS	0.47	0.35	0.68
OS	0.30	0.09	0.73
RPE	0.19	0.26	0.47
Perifoveal Region			
RNFL	0.44	0.43	0.50
GCL+IPL	0.36	0.56	0.29
INL	0.54	0.57	0.46
OPL	0.58	0.64	0.45
ONL+IS	0.46	0.31	0.69
OS	0.19	0.13	0.59
RPE	0.17	0.21	0.48

*0.70≤AUROC<0.80, **0.80≤AUROC

Table 5.29 Cutoff values of scattering coefficients (mm^{-1}) (calculated by using the multiple-scattering model with the normalization method NRPE) derived from ROC analyses between MDR and healthy eyes

Intraretinal Layer	AUROC	95% CI		Cutoff Point	Sensitivity	Specificity
		Lower Bound	Upper Bound			
Across All Macular Regions						
RNFL	0.50 ± 0.06	0.39	0.62	5.37	0.58	0.48
GCL+IPL	0.48 ± 0.06	0.36	0.60	2.65	0.55	0.45
INL	0.64 ± 0.06	0.53	0.75	4.61	0.70	0.60
OPL	0.65 ± 0.06	0.54	0.76	4.14	0.70	0.60
ONL+IS	0.46 ± 0.06	0.35	0.58	3.39	0.54	0.44
OS	0.17 ± 0.04	0.10	0.25	16.08	0.34	0.24
RPE	0.19 ± 0.04	0.11	0.27	17.45	0.34	0.24
Foveal Region						
RNFL	0.45 ± 0.06	0.34	0.56	4.91	0.57	0.47
GCL+IPL	0.21 ± 0.04	0.12	0.29	1.95	0.36	0.26
INL	0.61 ± 0.06	0.51	0.72	3.58	0.68	0.58
OPL	0.25 ± 0.05	0.15	0.36	2.95	0.38	0.28
ONL+IS	0.52 ± 0.06	0.39	0.64	2.16	0.59	0.49
OS	0.29 ± 0.05	0.20	0.39	18.54	0.45	0.35
RPE	0.27 ± 0.05	0.18	0.37	14.90	0.37	0.27
Parafoveal Region						
RNFL	0.44 ± 0.06	0.33	0.56	4.92	0.57	0.47
GCL+IPL	0.33 ± 0.05	0.23	0.43	1.77	0.45	0.35
INL	0.58 ± 0.06	0.47	0.69	3.34	0.61	0.51
OPL	0.63 ± 0.05	0.53	0.73	3.56	0.66	0.56
ONL+IS	0.47 ± 0.06	0.35	0.59	2.72	0.52	0.42
OS	0.30 ± 0.05	0.20	0.39	17.72	0.42	0.32
RPE	0.19 ± 0.04	0.12	0.27	16.34	0.31	0.21
Perifoveal Region						
RNFL	0.44 ± 0.06	0.33	0.55	4.98	0.50	0.40
GCL+IPL	0.36 ± 0.06	0.25	0.47	2.64	0.45	0.35
INL	0.54 ± 0.06	0.43	0.65	4.69	0.57	0.47
OPL	0.58 ± 0.06	0.46	0.69	4.17	0.66	0.56
ONL+IS	0.46 ± 0.06	0.35	0.57	3.30	0.52	0.42
OS	0.19 ± 0.04	0.11	0.26	16.11	0.34	0.24
RPE	0.17 ± 0.04	0.10	0.25	17.59	0.31	0.21

Table 5.30 Cutoff values of scattering coefficients (mm^{-1}) (calculated by using the multiple-scattering model with the normalization method NRPE) derived from ROC analyses between MDR and DM eyes

Intraretinal Layer	AUROC	95% CI		Cutoff Point	Sensitivity	Specificity
		Lower Bound	Upper Bound			
Across All Macular Regions						
RNFL	0.55 ± 0.07	0.42	0.67	5.37	0.58	0.48
GCL+IPL	0.67 ± 0.06	0.55	0.79	2.85	0.68	0.58
INL	0.66 ± 0.06	0.54	0.78	4.67	0.70	0.60
OPL	0.71 ± 0.06	0.60	0.83	4.23	0.74	0.64
ONL+IS	0.31 ± 0.06	0.19	0.43	3.24	0.40	0.30
OS	0.14 ± 0.04	0.06	0.22	15.72	0.29	0.19
RPE	0.21 ± 0.05	0.11	0.31	17.62	0.36	0.26
Foveal Region						
RNFL	0.69 ± 0.06	0.57	0.81	5.84	0.71	0.61
GCL+IPL	0.38 ± 0.06	0.26	0.50	2.05	0.45	0.35
INL	0.66 ± 0.06	0.54	0.78	3.58	0.68	0.58
OPL	0.48 ± 0.07	0.36	0.61	3.16	0.52	0.42
ONL+IS	0.41 ± 0.07	0.28	0.54	2.01	0.47	0.37
OS	0.15 ± 0.04	0.07	0.23	17.44	0.29	0.19
RPE	0.32 ± 0.06	0.20	0.43	15.13	0.40	0.30
Parafoveal Region						
RNFL	0.51 ± 0.07	0.38	0.64	4.94	0.59	0.49
GCL+IPL	0.41 ± 0.06	0.28	0.53	1.79	0.47	0.37
INL	0.61 ± 0.06	0.48	0.73	3.35	0.63	0.53
OPL	0.70 ± 0.06	0.58	0.81	3.64	0.71	0.61
ONL+IS	0.35 ± 0.06	0.23	0.47	2.56	0.42	0.32
OS	0.09 ± 0.03	0.03	0.15	16.23	0.24	0.14
RPE	0.26 ± 0.06	0.15	0.36	16.75	0.37	0.27
Perifoveal Region						
RNFL	0.43 ± 0.06	0.30	0.55	4.98	0.50	0.40
GCL+IPL	0.56 ± 0.06	0.43	0.68	2.74	0.61	0.51
INL	0.57 ± 0.06	0.45	0.70	4.73	0.59	0.49
OPL	0.64 ± 0.06	0.51	0.76	4.19	0.66	0.56
ONL+IS	0.31 ± 0.06	0.19	0.43	3.18	0.40	0.30
OS	0.13 ± 0.04	0.05	0.20	15.70	0.29	0.19
RPE	0.21 ± 0.05	0.11	0.31	17.60	0.32	0.22

CHAPTER 6. AUTOMATED CLASSIFIERS FOR EARLY DETECTION AND DIAGNOSIS OF RETINOPATHY IN DIABETIC EYES

6.1 OVERVIEW

Interest in neural networks has exploded over the last few years and this research is being successfully applied across an extraordinary range of problem domains in areas as diverse as finance, medicine, engineering, geology and physics. Neural networks are traditionally used to refer to networks of biological neurons that are connected or functionally related in the nervous system.[101] However, the modern usage of the term often refers to artificial neural networks (ANNs). The basic architecture of ANNs consists of three layers: an input layer, a hidden layer and an output layer (see Figure 6.1).

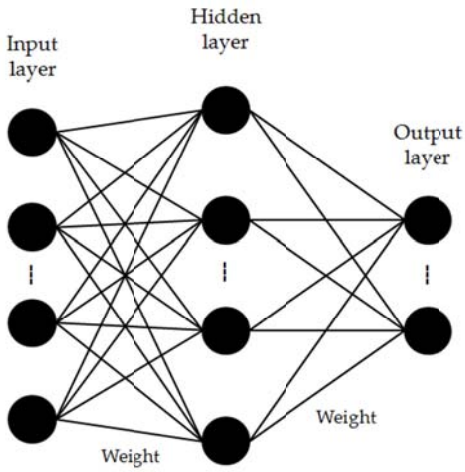

Figure 6.1 A basic artificial neural network architecture

Each neuron in the input layer receives the input signal from outside of the system and then distributes the input signal into the hidden layer via the interconnections that link the neurons. The signal is transformed by all active neurons in the hidden layer and is subsequently exported to the output layer. The function of an ANN is determined

largely by its interconnections and the manner in which the various neurons in the hidden layer process the input signal.

Commonly, an ANN is trained by the use of a program that compares the output and target until the ANN's output matches the target. Based on Kolmogorov's theorem, an ANN with appropriate nonlinear hidden neurons can output the value that matches the target.[102] Typically, many such input/target pairs are needed to train an ANN. By adjusting the values of the connections between neurons and applying the appropriate nonlinear model in the hidden layer, a trained ANN can perform like a black box, requiring no knowledge of the internal workings to perform. Independent of the complexity of the transfer characteristic, a trained ANN implements a particular function between the two categories of signals. Therefore, a trained ANN could be used as a function or predictor to output the target feature of interest by importing the corresponding input feature.

Owing to the well-known capabilities of self-learning and self-adjustment demonstrated in the training and testing procedures, ANNs have been widely used in both modern industries and scientific research to perform diverse and sophisticated tasks, such as data processing, pattern recognition, system controls and medical diagnosis.[103-107]

6.1.1 ARTIFICIAL NEURAL NETWORKS IN MEDICAL DIAGNOSIS

In the field of medical diagnosis, ANNs are recognized as a useful computer-assisted technique. After training with the input and the target features, ANNs can map the relationship between them and perform as black box systems. The same input features used to train ANNs output exactly the same target features used for training. Furthermore, an appropriate ANN can perform a certain function not only for the two features used in training but also for the features extracted from the same type of study subject.

Consequently, well-trained ANNs can not only validate the known input and target features, but they can also predict the target features of interest from the questionable study subjects with corresponding input features. Therefore, ANNs have been widely applied in different areas of medical diagnosis, including cardiology, oncology, radiology and ophthalmology.[108-111]

Because of the prediction capability of ANNs, they can be used to diagnose diseased subjects in clinical practice. This tool is very useful in situations for which the relevant features are not immediately observable in patients. It is therefore effective to train ANNs with both potentially easily obtained features and less obvious features as the input and target signals, respectively, both of which were extracted for training from the same types of diseased subjects in the existing database. Afterward, the target features of interest in the questionable subjects could be predicted with the trained ANNs with the corresponding input features.

Moreover, ANNs have been acknowledged as effective screening tools in clinical practice. ANNs can be treated as an application owing to further development in the prediction capabilities. The basic idea is to compare the measured target features with the predicted target features using a trained ANN that was specifically designed for a particular type of patient group. The results from comparisons using one criterion could determine whether the questionable subjects have a disease or not. With multiple criteria, ANNs could classify the questionable subjects according to differences in disease type or disease stage. In general, criteria are defined as statistically determined values or ranges that represent typical disease characteristics.

The prediction and classification performed by ANNs could save doctors and patients time by determining the diagnosis of the questionable subjects in advance of treatments. The use of ANNs could improve overall positive predictive performance and reduce diagnostic time and medical costs.

6.1.2 ARTIFICIAL NEURAL NETWORKS IN RETINAL DIAGNOSIS

In ophthalmology, the detection of functional vision abnormalities plays a fundamental role in the diagnosis of eye diseases. Such a task depends not only on the use of a variety of precise optical instruments but also on technicians who are well trained in accurate operative techniques. The use of multiple instruments and technicians could decrease measurement precision, whereas the implementation of ANNs could improve it, in addition to reducing waiting times and medical costs.

For example, the visual field is the spatial array of visual sensations available to observation. In the clinic, it is used to detect vision loss or reduced sensitivity. Traditionally, the visual field is mapped and quantified with perimetry, which determines light sensitivity by assessing a subject's ability to detect the presence of test targets on a defined background. The accuracy of the visual field depends heavily on the manner in which the patient responds to the test. Visual function is mainly related to retinal structure changes, which are measured with imaging techniques such as funduscopy, scanning laser polarimetry (SLP) and optical coherence tomography.

Currently, most ANN mapping of eye structure and function involves training with measurements of retinal structure and visual function. For example, Zhu et al. developed an ANN using Bayesian radial basis function (BRBF, see section 1.3) to map the structure-function relationship between the retinal nerve fiber layer and visual function in glaucoma. The results demonstrated that ANNs using BRBF can effectively

improve the agreement between predicted visual function and measured visual function compared with results obtained using linear regression (2.9 ± 2.7 dB vs. 4.9 ± 4.0 dB).[112] Furthermore, Zhu et al. quantitatively evaluated the discordance between the visual function predicted by a trained ANN and the measured visual function in glaucoma. Specifically, 39% of the predicted visual function showed significant discordance with the measured visual function.[113]

Aside from the prediction of visual function, these ANNs have also been used to classify eye diseases, such as diabetic retinopathy. Moreover, the input feature is no longer restricted to the thickness of the retinal nerve fiber layer; it can be expanded to different types of features such as the diameter of blood vessels, the radius of the corneal surface curvature and the cross-sectional area of blood vessels. Yun et al. classified the different stages of diabetic retinopathy (i.e., moderate, severe and proliferative DR) and differentiated them from the healthy retina using a three-layer backpropagation (BPA) ANN. In their method, the perimeter and area of the veins, hemorrhages and microaneurysms were extracted from retinal fundus images and used as input to the classifier. The ANN was trained with 74 subjects (20 healthy, 27 moderate, 13 severe and 27 proliferative) and was tested with 37 subjects (9 healthy, 11 moderate, 5 severe and 12 proliferative). Their system achieved a sensitivity of 90% and a specificity of 100% for the 37 test subjects.[114]

Sinthanayothin et al. proposed an automated screening system to detect blood vessels in fundus images with a three-layer ANN that has 6 input neurons, 20 hidden neurons and 2 output neurons. They achieved a sensitivity of 80.21% and a specificity of

70.66% for 484 healthy retina images and 283 diabetic retinopathy images, of which 5/6 were used for training and 1/6 were used for testing.[115]

Garden et al. developed an ANN to differentiate diabetic retinopathy patients from healthy subjects by extracting the blood vessels, exudates and hemorrhages from images captured by a fundus camera. They achieved a sensitivity of 88.4% and a specificity of 83.5% for the detection of diabetic retinopathy when 147 diabetic and 32 healthy images were used to train the backpropagation and 200 diabetic and 101 healthy images were used for testing.[116]

Most current research has used blood vessels and related features extracted from fundus images to train different types of ANNs to identify diseased eyes.[18-20] To the best of our knowledge, only a few studies have used the thickness measurement extracted from OCT images to train ANNs. For example, the retinal nerve fiber layer thickness was extracted from OCT images to train ANNs to predict visual function in glaucoma.[117]

As demonstrated in Chapters 4 and 5, the structural and optical features of various intraretinal layers can be used as discriminators to differentiate diabetic eyes with and without retinopathy from healthy eyes. Therefore, it is necessary to evaluate the capability of structural and optical features to train ANNs and classify healthy eyes and diabetic eyes with and without retinopathy.

6.2 BAYESIAN RADIAL BASIS FUNCTION NETWORK

6.2.1 RADIAL BASIS FUNCTION

Among the various types of ANNs, a radial basis function (RBF) network is a popular classification tool by which the radial basis functions perform the activation functions of the network. Radial basis function networks are widely used to build up function approximations and have been used in time series prediction and control of

nonlinear systems. In general, a radial basis function network can be represented by the output $\varphi: R^n \rightarrow R$ (from the hidden layer to the output layer):

$$\varphi(x) = \sum_{i=1}^{N} w_i \rho\left(\left|\left|x - c_i\right|\right|\right) \tag{6.1}$$

where N is the number of neurons in the hidden layer, ρ is the radial basis function, c_i is the center vector for the neuron i and w_i is the weight of the output neuron. Additionally, $\|x - c_i\|$ represents the distance from the center of the neuron i. In the basic form, all inputs are connected to each hidden neuron.

The unique characteristic of the radial basis function network is the process performed by radial basis functions in the hidden layer. In radial basis function networks, radial basis functions act as activation functions. The most commonly used radial basis function is a Gaussian function that can be expressed by:

$$\rho(\|x - c_i\|) = \exp(-\beta \|x - c_i\|^2) \tag{6.2}$$

Figure 6.2 illustrates a Gaussian basis function with $c_i = 0$ and $\beta = 2$.

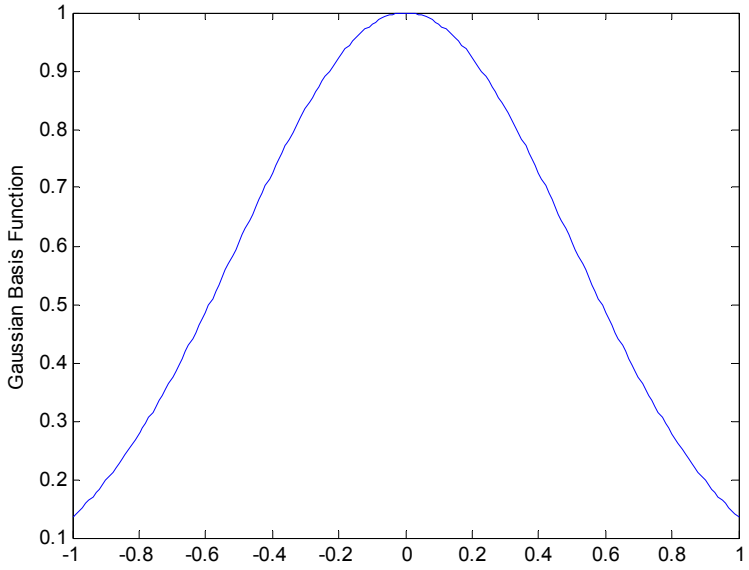

Figure 6.2 A Gaussian bell-shaped curve with $\boldsymbol{c_i = 0}$ and $\boldsymbol{\beta = 2}$

As evident in Figure 6.2 and Equation (6.1), a Gaussian basis function has the following properties:

$$\lim_{\|x\|\to c_i} \rho(\|x - c_i\|) = 1 \tag{6.3}$$

$$\lim_{\|x\|\to \infty} \rho(\|x - c_i\|) = 0 \tag{6.4}$$

With reference to the properties described in equations 6.3 and 6.4, a Gaussian basis function means that a radial basis function network with enough hidden neurons can approximate any continuous function with arbitrary precision. Moreover, in radial basis function networks, the changes of one neuron in the network have only a small effect on input values that are far from the center of that neuron. Therefore, radial basis function networks are valuable for the prediction of a specific target feature.

6.2.2 PREDICTION USING A RADIAL BASIS FUNCTION NETWORK

Generally speaking, a radial basis function network acts as a black box that links the input x and output y. Consequently, the function G is usually used to describe the relationship between the input and output:

$$y = G(x) \tag{6.5}$$

A radial basis function network can predict not only the target feature, but it can also predict the target feature change Δy that may be caused by the input feature change Δx. The relationship between the target feature change Δy and the input feature change Δx can be derived as:

$$\Delta y = G(x + \Delta x) - G(x) \tag{6.6}$$

By assuming the input feature change Δx tends to be 0, equation (6.6) can be rewritten as:

$$\lim_{\Delta x\to 0} \frac{\Delta y}{\Delta x} = \lim_{\Delta x\to 0} \frac{G(x + \Delta x) - G(x)}{\Delta x} = \frac{\partial G}{\partial x} \tag{6.7}$$

where $\partial G/\partial x$ is the deviation of G at x.

Equation (6.7) clearly denotes that the target feature change is related to the function gradient in x. This property is more valuable for classifying eyes into different disease stages. Specifically, eyes at different disease stages might only show a minor structural change such that the interested functional change of the retinal tissue would not be easy to discriminate; whereas, with ANNs, the relevant functional change of the retinal tissue could be determined and then used for classification of the diseased retina.

6.2.3 BAYESIAN RADIAL BASIS FUNCTION NETWORK

Generally, a radial basis function network can be expressed as:[112]

$$y_d^n = w_d^n \phi(x^n) + \varepsilon_d \tag{6.8}$$

where y_d^n is the dth element in the measurement of the nth subject, x^n is the input feature vector, w_d is a weight vector, ε_d is an additive zero-mean Gaussian noise $N(0, \delta_d^2)$ with variance δ_d^2 and the radial basis function vector $\phi(x^n)$ is defined to be M+1 dimensional for M bases: $\phi(x^n) = (1,\ \phi_1(x^n),\ \phi_2(x^n), \ldots, \phi_M(x^n))^T$, where each element is a radial basis function.

Conventionally, the weight w_d^n in radial basis function networks is determined by minimizing the error at the output, which is computed with a linear pseudoinverse solution. Bayesian methodology is used for the weight matrix W to improve the precision:[112]

$$w_d \sim N(0, \Psi) \tag{6.9}$$

where Ψ is a diagonal matrix whose elements are α_1^{-1}, α_2^{-1},..., α_M^{-1} on diagonal and 0 otherwise. Each α_M^{-1} represents the average variance in the weights for the mth basis.

According to Bayesian methodology, prior distributions of hyper-parameters are defined over α_m and $\beta_d = \delta_d^{-2}$ as: [112]

$$p(\alpha) = \prod_{m} \gamma(\alpha_m | a, b) \tag{6.10}$$

$$p(\beta) = \prod_{m} \gamma(\beta_d | c, d) \tag{6.11}$$

where α and β are vectors of α_m and β_d, respectively. $\gamma(\alpha_m|a,b)$ is a Gamma distribution with parameters a and b. Further information about the Bayesian approach can be found in Bernardo et al. [118]

6.2.4 ASSUMPTION OF GAUSSIAN DISTRIBUTION

Assuming that V denotes the measured values of the output parameters extracted from the unknown subjects and that V_P denotes the predicted values of the output parameters using the Bayesian radial basis function network, a simple way to evaluate the predicted values is to calculate the relative error E_P between the predicted and measured values.

$$E_P = (V_P - V)/V \tag{6.12}$$

The distribution of the relative errors E_P is assumed to be the Gaussian function,

$$f(x) = \frac{1}{\sqrt{2\pi\sigma^2}} e^{-\frac{(x-\mu)^2}{2\sigma^2}} \tag{6.13}$$

where μ is the average value of E_P; σ is the deviation of E_P. Then, a proper positive parameter c_p is used to define the range $[\mu - c_p\sigma, \mu + c_p\sigma]$. By integrating the Gaussian function within this range, the Gaussian error function can be calculated as:

$$\begin{aligned} S(c_p) = \int_{\mu - c_p\sigma}^{\mu + c_p\sigma} f(x)dx &= \int_{\mu - c_p\sigma}^{\mu + c_p\sigma} \frac{1}{\sqrt{2\pi\sigma^2}} e^{-\frac{(x-\mu)^2}{2\sigma^2}} dx \\ &= erf(c_p/\sqrt{2}) \end{aligned} \tag{6.14}$$

The value of the Gaussian error function $S(c_p)$ reflects the possibility ratio of the set of relative errors E_P in the range $[\mu - c_p\sigma, \mu + c_p\sigma]$. A series of typical values of

$[c_p, S(c_p)]$ is listed in Table 6.1. In this project, the parameter c_p was initialized as 1.65, which yielded 90% accuracy for the classification.

Once the parameter c_p is obtained from the training set used for training the Bayesian radial basis function network, the discrimination task can be performed on all subjects by comparing the measured values and the predicted values using the Bayesian radial basis function network.

Table 6.1 Typical values of c_p and Gaussian error function

c_p	$S(c_p)$
1.28	80%
1.44	85%
1.65	90%
1.96	95%
2.58	99%

6.3 DIFFERENTIATION OF MDR EYES FROM HEALTHY EYES AND/OR DM EYES

In this section, we present the classification task results obtained when attempting to differentiate MDR eyes from healthy eyes and DM eyes. Specifically, structural and optical parameters of intraretinal layers were chosen as the input and output features for the Bayesian radial basis function networks that would discriminate among MDR eyes; healthy eyes; and DM eyes. As indicated in chapters 4 and 5, thickness measurement (TH), fractal dimension (FD) and total reflectance (TR) can show better discrimination power than other parameters among MDR eyes; healthy eyes; and DM eyes. Therefore, these three parameters were used as the input and output values required in the training task of Bayesian radial basis function networks. Then, trained Bayesian radial basis function networks were used to classify the mixed test subjects (excluding the training subjects).

6.3.1 DIFFERENTIATION OF MDR EYES FROM HEALTHY EYES

To explore the probabilistic relationships between the diabetic retinal disease and target features (i.e., symptoms), we first performed the training task using a sample of the data and different pairs of input and output target features. Then, classification tasks were performed to obtain the optimum distribution over the set of allowed models. Additionally, different sizes of the training set were explored and the corresponding results were compared.

6.3.1.1 EXPLORING THE PROBABILISTIC RELATIONSHIPS BETWEEN THE DIABETIC RETINAL DISEASE AND TARGET FEATURES

A total of 20 healthy eyes were randomly selected from the healthy group (out of 74 healthy eyes) to train the Bayesian radial basis function network. Different pairs of input and target features extracted from all intraretinal layers were used to train the Bayesian radial basis function network and to classify a total of 43 MDR eyes using the remaining 54 healthy eyes (not used in training) from the healthy group.

Results for true positive (TP), false negative (FN), true negative (TN), false positive (FP), positive predictive value (PPV), sensitivity and specificity were calculated to evaluate the classifications and are shown in Tables 6.2 and 6.3. As shown, high sensitivity and specificity ($\geq$0.80) values were obtained.

Table 6.2 shows the sensitivity, specificity, predictive values and positive predictive values obtained when training the Bayesian radial basis function network using the thickness and fractal dimension as the input and target features, respectively. Our results indicated that the true positive (TP) test for the healthy eyes was in the 48- 51 range. Particularly, TP achieved high values (49, 50 and 51, respectively) in the GCL+IPL, OS and RPE. The true negative (TN) test was in the 9-36 range and high TN

values (35 and 36, respectively) were achieved in the GCL+IPL and OPL. Moreover, high values for sensitivity, specificity and accuracy (≥0.80) were only obtained in the GCL+IPL and OPL.

Table 6.2 Sensitivity, specificity, predictive values (TP, FN, TN, FP) and positive predictive values (PPV) obtained when training the Bayesian radial basis function network using the thickness (TH) and fractal dimension (FD) as the input and target features, respectively.

TH vs. FD	RNFL (eye/scans)	GCL+IPL (eye/scans)	INL (eye/scans)	OPL (eye/scans)	ONL+IS (eye/scans)	OS (eye/scans)	RPE (eye/scans)
TP	48/288	49/294	48/288	48/288	48/288	50/300	51/306
FN	6/36	5/30	6/36	6/36	6/36	4/24	3/18
TN	10/60	35/210	23/138	36/216	10/60	9/54	11/66
FP	33/198	8/48	20/120	7/42	33/198	34/204	32/192
PPV	0.59	0.86 *	0.71	0.87 *	0.59	0.60	0.61
Sensitivity	0.89	0.91*	0.89	0.89*	0.89	0.93	0.94
Specificity	0.23	0.81*	0.53	0.84*	0.23	0.21	0.26

* denotes the intraretinal layer for which the sensitivity, specificity and PPV are greater than 80%

Table 6.3 shows the sensitivity, specificity, accuracy, predictive values and positive predictive values obtained when training the Bayesian radial basis function network using the total reflectance and fractal dimension as the input and target features, respectively. Our results indicated that the true positive (TP) and true negative (TN) tests for the healthy eyes were in the 48- 51 and 8- 34 ranges, respectively. Specifically, high TN values (35 and 37, respectively) were achieved in the GCL+IPL and OPL. Moreover, high values for sensitivity, specificity and accuracy (≥0.80) were only obtained in the GCL+IPL and OPL.

Table 6.3 Sensitivity, specificity, predictive values (TP, FN, TN, FP) and positive predictive values (PPV) obtained when training the Bayesian radial basis function network using the total reflectance (TR) and fractal dimension (FD) as the input and target features, respectively

TR vs. FD	RNFL (eye/scans)	GCL+IPL (eye/scans)	INL (eye/scans)	OPL (eye/scans)	ONL+IS (eye/scans)	OS (eye/scans)	RPE (eye/scans)
TP	48/288	49/294	48/288	48/288	48/288	50/300	51/306
FN	6/36	5/30	6/36	6/36	6/36	4/24	3/18
TN	10/60	35/210	23/138	37/222	9/54	9/54	11/66
FP	33/198	8/48	20/120	6/36	34/204	34/204	32/192
PPV	0.59	0.86	0.71	0.89	0.59	0.60	0.61
Sensitivity	0.89	0.91*	0.89	0.89*	0.89	0.93	0.94
Specificity	0.23	0.81*	0.53	0.86*	0.21	0.21	0.26

* denotes the intraretinal layer for which the sensitivity, specificity and PPV are greater than 80%

6.3.1.2 MODEL TESTING BY EXPLORING DIFFERENT SIZES OF THE TRAINING SET

In the previous subsection, structural and optical parameters of 20 healthy eyes were randomly selected to train the Bayesian radial basis function network for differentiating MDR eyes from healthy eyes. The results demonstrated that the GCL+IPL and OPL parameters could be predicted and used to discriminate the MDR eyes from healthy eyes by using either the TH/FD or TR/FD pairs as the input/target features of the Bayesian radial basis function networks.

In this test, different sizes of the training set (20, 30 and 40 healthy eyes) were chosen to train the Bayesian radial basis function network and corresponding results were compared. Tables 6.4 and 6.5 show results obtained from three classification tests for the 43 MDR eyes and the remaining healthy eyes (54, 44 and 34, respectively). Our results demonstrated that the FN value (5) in the GCL+IPL complex was stable despite the amount of healthy eyes used in the training task, whereas the values of FN in the OPL were slightly reduced from 6 to 5 with the increased number of healthy eyes used to train the ANN. Additionally, the TN (35) value in the GCL+IPL complex was stable. Our

results showed relatively high positive predicted values, as well as high sensitivity and specificity (>0.80) in both the GCL+IPL complex and OPL. Our results showed that positive predicted values had a slight decreasing trend for both the GCL+IPL complex and OPL when the number of healthy subjects increased from 20 to 40 in the training task, which was due to a decrease in test subjects (healthy eyes).

Table 6.4 Results of sensitivity, specificity, accuracy, predictive values and positive predictive values obtained for the GCL+IPL complex and OPL when training the Bayesian radial basis function network with 20, 30 and 40 healthy eyes with the thickness (TH) and fractal dimension (FD) as the input and target features, respectively.

Number for training	20 healthy eyes		30 healthy eyes		40 healthy eyes	
TH vs. FD	GCL+IPL (eye/scans)	OPL (eye/scans)	GCL+IPL (eye/scans)	OPL (eye/scans)	GCL+IPL (eye/scans)	OPL (eye/scans)
TP	49/294	48/288	39/234	39/234	29/174	29/174
FN	5/30	6/36	5/30	5/30	5/30	5/30
TN	35/210	36/216	35/210	36/216	35/210	36/216
FP	8/48	7/42	8/48	7/42	8/48	7/42
PPV	0.86	0.87	0.83	0.85	0.78	0.81
Sensitivity	0.91	0.89	0.89	0.89	0.85	0.85
Specificity	0.81	0.84	0.81	0.84	0.81	0.84

Table 6.5 Results of sensitivity, specificity, accuracy, predictive values and positive predictive values obtained for the GCL+IPL complex and OPL when training the Bayesian radial basis function network with 20, 30 and 40 healthy eyes with the total reflectance (TR) and fractal dimension (FD) as the input and target features, respectively.

Number for training	20 healthy eyes		30 healthy eyes		40 healthy eyes	
TR vs. FD	GCL+IPL (eye/scans)	OPL (eye/scans)	GCL+IPL (eye/scans)	OPL (eye/scans)	GCL+IPL (eye/scans)	OPL (eye/scans)
TP	49/294	48/288	39/234	39/234	29/174	29/174
FN	5/30	6/36	5/30	5/30	5/30	5/30
TN	35/210	37/222	35/210	36/216	35/210	37/222
FP	8/48	6/36	8/48	7/42	8/48	6/36
PPV	0.86	0.89	0.83	0.85	0.78	0.83
Sensitivity	0.91	0.89	0.89	0.89	0.85	0.85
Specificity	0.81	0.86	0.81	0.84	0.81	0.86

6.3.2 DIFFERENTIATION OF MDR EYES FROM DIABETIC EYES WITHOUT MDR

As in the previous section, 20 MDR eyes/scans were randomly selected from the total 43 MDR eyes to train the Bayesian radial basis function network with the TH/FD and TR/FD as the input and target features, respectively. Then, the trained Bayesian radial basis function network was used to classify the remaining 23 MDR eyes and 38 DM eyes.

Table 6.6 shows the results obtained when training Bayesian radial basis function networks with the thickness measurement and fractal dimension as the input and target features, respectively. Our results indicated the true positive (TP) test was in the 4-20 range (out of 23 test MDR eyes) for the MDR eyes. Specifically, high TP values were found for the RNFL, GCL+IPL, OS and RPE. The true negative (TN) test for the MDR eyes is in the 9-36 range and high TN values were achieved in the RNFL, INL, OS and RPE. Additionally, the sensitivity, specificity and positive predicted values (PPV) were greater or close to 0.80 in the RNFL, OS and RPE.

Table 6.6 Sensitivity, specificity, predictive values (TP, FN, TN, FP) and positive predictive values (PPV) obtained when training the Bayesian radial basis function network using the thickness (TH) and fractal dimension (FD) as the input and target features, respectively

TH vs. FD	RNFL (eye/scans)	GCL+IPL. (eye/scans)	INL (eye/scans)	OPL (eye/scans)	ONL+IS (eye/scans)	OS (eye/scans)	RPE (eye/scans)
TP	18/108	18/108	15/90	4/24	10/60	18/108	20/120
FN	5/30	5/30	8/48	19/114	13/78	5/30	3/18
TN	30/180	26/156	32/192	28/168	26/162	31/186	33/198
FP	8/48	12/72	6/36	10/60	12/72	7/42	5/30
PPV	0.69	0.60	0.71	0.29	0.45	0.72	0.80*
Sensitivity	0.78	0.78	0.65	0.17	0.43	0.78	0.87*
Specificity	0.79	0.68	0.84	0.74	0.68	0.82	0.87*

* denotes the intraretinal layer for which the sensitivity, specificity and PPV are greater than 80%

6.4 SUMMARY

In this study, the number of TP (of healthy testing eyes) and TN (of MDR testing eyes) confirmed the assumptions that the distribution of error is a Gaussian function and that approximately 90% of the predicted target features would be within the range. Moreover, the stable trend or slight decrease of the FN values (of healthy testing eyes) validates the reliability of the methodology. The high sensitivity and specificity values obtained when using structural and optical parameters of the GCL+IPL complex and OPL suggest that the Bayesian radial basis function network can be used to discriminate MDR eyes from healthy eyes with the selected input and target features extracted from OCT images. In particular, the fractal dimension, which represents the roughness of intraretinal layer structure, could certainly be used to differentiate MDR from healthy eyes. Our results suggest that the GCL+IPL complex and OPL are more susceptible to early damage in MDR eyes. The results also confirmed our previous finding that the thickness and total reflectance of the OPL were significantly different in MDR eyes compared to the corresponding measurements in healthy eyes. The low RNFL specificity value indicated that RNFL parameters were not good input/output targets for use in ANNs to differentiate MDR eyes from healthy eyes. However, our previous results (see Table 4.6) showed that the RNFL fractal dimension in MDR eyes was significantly different from that of healthy eyes. This particular result could be due to the minor changes in the thickness measurement observed for the RNFL (compared with the statistically significant changes observed for the OPL and GCL+IPL) between the healthy eyes and diabetic eyes.

As already established, a Bayesian radial basis function network can accommodate uncertainty in the dimension of the model by adjusting the sizes to the complexity of the data. A distribution is defined over the space of all RBF models of a given basis function and posterior densities are computed using reversible jump Markov chain Monte Carlo samplers. This process alleviates the need to select the architecture during the modeling process. Therefore, in this study, the TN, TP and the positive predicted values remained stable despite the different sizes of training sets (see Tables 6.4 and 6.5). However, training the Bayesian radial basis function network may require more test subjects, which would improve the precision of the differentiation between healthy eyes and DM eyes with and without retinopathy.

In summary, we have employed Bayesian ANNs with four pairs of input and target features to discriminate among MDR eyes; healthy eyes; and DM eyes. The input features used were the intraretinal layer thickness measurement and total reflectance extracted from OCT images. The fractal dimension of the GCL+IPL complex and OPL predicted by the Bayesian radial basis function network effectively discriminated MDR eyes from healthy eyes. Moreover, the thickness and fractal dimension parameters of the RNFL and OS could show discriminating power between MDR eyes and DM eyes.

CHAPTER 7. POTENTIAL CLINICAL APPLICATIONS TO NEURODEGENERATIVE DISEASES

7.1 OVERVIEW

As summarized in chapters 4 and 5, specific structural and optical parameters extracted from OCT images can be used to differentiate diabetic eyes with mild retinopathy from healthy eyes. Specifically, changes in tissue optical properties, thickness and texture descriptors may provide further information regarding cellular layers and early damage in diabetic ocular disease. As demonstrated by studies in animal models, our results support the view of neurodegeneration in the early stages of diabetes-related retinopathy, which seems to mainly involve the ganglion cells and cells of the inner plexiform layers. Therefore, we used the same methodology to explore abnormalities in the retinal tissue of patients with multiple sclerosis (MS), which is also a neurodegenerative disease. Specifically, we aimed to determine the capability of each parameter to discriminate MS eyes from healthy eyes by using the same approach employed to obtain the data on diabetics' eyes.

7.1.1 MULTIPLE SCLEROSIS STUDY

Multiple sclerosis (MS) is an inflammatory disease in which the fatty myelin sheaths around the axons of the brain and spinal cord are damaged.[119] The disease is characterized by demyelination, which leads to axonal dysfunction and neuronal loss. A serious consequence of MS is the diminished ability of nerve cells in the brain and spinal cord to communicate with each other effectively because the axons can no longer effectively conduct signals. Though the symptoms of MS are understood, its cause remains unknown. Thus, early detection of this insidious disease is very important.

As already established, the retinal nerve fiber layer (RNFL) contains the axons of the retinal ganglion cells, which reach the myelin sheath only after leaving the eye through the lamina cribrosa. Therefore, the damage to axons in MS could affect the structural and optical properties of the retinal tissue. Recently, thinning has been observed in the GCL+IPL complex due to the neural loss.[120, 121]

This chapter investigates the changes in structural morphology and optical properties of the intraretinal layers in MS patients with or without optic neuritis (ON). In this study, 14 MS ON- eyes, 13 MS ON+ eyes and 74 healthy eyes were used. OCT examination was performed on each eye using a Stratus OCT device. First, the speckle noise of each raw OCT image exported from the OCT device was removed using a nonlinear complex diffusion filter. Second, the boundaries of intraretinal layers were segmented. Eyes of the MS patients were divided into 2 groups for statistical analysis. The MS ON^+ group contained 13 eyes with a history of ON for least 6 months prior to enrollment. The 14 eyes in the MS ON^- group had no history of ON. The patients underwent a comprehensive neurological examination within one week of the ophthalmic examination. To assess physical disability, an Expanded Disability Status Scale (EDSS) score was determined for each patient. As in the DR study, the comparisons between the study groups were performed using an ANOVA followed by Newman-Keuls post hoc analysis and ROC analysis.

7.2 QUANTITATIVE MEASUREMENTS OF THE STRUCTURAL MORPHOLOGY

7.2.1 THICKNESS MEASUREMENTS

The mean thickness per intraretinal layer was calculated by averaging the local thickness across all macular regions for MS ON^-, MS ON^+ and healthy eyes. The

thickness per macular region per intraretinal layer was also measured, except in the foveola. The thickness measurements are given in Table 7.1. The values are expressed in the form of the mean ± SD (SD: standard deviation).

Thickness measurement changes between MS ON^-, MS ON^+ and healthy eyes were analyzed using an ANOVA followed by Newman-Keuls post-hoc analysis. Significant differences between the study groups are also reported in Table 7.1.

7.2.1.1 INTRARETINAL LAYER THICKNESS CHANGES PER EYE

The mean thickness per intraretinal layer for all study groups is given in Table 7.1. The data clearly demonstrate that in MS ON^-, MS ON^+ and healthy eyes, the highest and lowest intraretinal layer thickness was achieved for the ONL+IS and RPE, respectively. Specifically, the thickness showed a statistically significant decrease (11%) for the GCL+IPL and a non-significant tendency towards thinning for the RNFL and OPL when comparing MS ON^- with healthy eyes.

Moreover, when comparing MS ON^+ with MS ON^- eyes, the thickness of the RNFL and GCL+IPL showed a statistically significant decrease (9% and 16%, respectively). In addition, the thickness showed a non-significant tendency towards thickening for the INL, ONL+IS and OS and a non-significant tendency towards thinning for the OPL and RPE.

7.2.1.2 INTRARETINAL LAYER THICKNESS CHANGES IN THE FOVEAL REGION

The foveal thickness in MS ON^- compared with healthy eyes showed a statistically significant decrease (9%) for the GCL+IPL. However, the foveal thickness showed a tendency towards thickening for the INL, OPL, OS and RPE and a non-significant tendency towards thinning for the RNFL and ONL+IS.

Moreover, when comparing MS ON$^+$ with MS ON$^-$ eyes, the foveal thickness of the GCL+IPL showed a statistically significant decrease (12%). In addition, the foveal thickness showed a non-significant tendency towards thickening for the ONL+IS and OS and a non-significant tendency towards thinning for the RNFL, INL, OPL and RPE.

7.2.1.3 INTRARETINAL LAYER THICKNESS CHANGES IN THE PARAFOVEAL REGION

The parafoveal thickness of MS ON$^-$ compared with that of healthy eyes showed a statistically significant decrease (12%) for the GCL+IPL. However, the parafoveal thickness showed a non-significant tendency towards thickening for the INL, OPL, OS and RPE as well as a non-significant tendency towards thinning for the RNFL and ONL+IS.

Moreover, when comparing MS ON$^+$ with MS ON$^-$ eyes, the parafoveal thickness of the RNFL and GCL+IPL showed a statistically significant decrease (11% and 17%, respectively). In addition, the parafoveal thickness showed a non-significant tendency towards thickening for the INL, OPL, ONL+IS and OS as well as a non-significant tendency towards thinning for the RPE.

7.2.1.4 INTRARETINAL LAYER THICKNESS CHANGES IN THE PERIFOVEAL REGION

The perifoveal thickness in MS ON$^-$ eyes compared with healthy eyes showed a statistically significant decrease (11%) for the GCL+IPL. However, the perifoveal thickness showed a non-significant tendency towards thickening for the INL, ONL+IS, OS and RPE and a non-significant tendency towards thinning for the RNFL and OPL.

Moreover, when comparing MS ON+ with MS ON- eyes, the perifoveal thickness of the RNFL and GCL+IPL showed a statistically significant decrease (11% and 17%, respectively). In addition, the perifoveal thickness showed a non-significant tendency

towards thickening for the INL, ONL+IS, OS and RPE and a non-significant tendency towards thinning for the OPL.

7.2.2 CONTRAST MEASUREMENTS

The contrast measurement for each intraretinal layer was calculated across all macular regions for the MS ON$^-$, MS ON$^+$ and healthy eyes. The contrast measurement per macular region per intraretinal layer was also measured except in the foveola. The contrast measurements are given in Table 7.2. The values are expressed in the form of the mean ± SD (SD: standard deviation).

The contrast measurement changes between the MS ON$^-$, MS ON$^+$ and healthy eyes were analyzed using an ANOVA followed by Newman-Keuls post-hoc analysis. Significant differences between the study groups are also reported in Table 7.2.

7.2.2.1 INTRARETINAL LAYER CONTRAST MEASUREMENT CHANGES PER EYE

The contrast measurements per intraretinal layer for all study groups are given in Table 7.2. The findings clearly demonstrate that in MS ON$^-$, MS ON$^+$ and healthy eyes, the highest and lowest intraretinal layer contrast measurement was achieved for the ONL+IS and RPE, respectively. Despite contrast measurement differences between the study groups, the contrast measurement distribution per intraretinal layer followed the same trend in all groups. Therefore, contrast measurement changes might provide information relevant to the differentiation between MS ON$^-$, MS ON$^+$ and healthy eyes.

When comparing MS ON$^-$ with healthy eyes, the contrast measurement showed no statistical significance for all intraretinal layers. However, the contrast measurement per intraretinal layer showed a non-significant increasing trend for the RNFL, GCL+IPL, INL, OPL and ONL+IS as well as a non-significant decreasing trend for the OS and RPE.

When comparing MS ON^+ with MS ON^- eyes, the contrast measurement of the RNFL and GCL+IPL showed a statistically significant decrease (10% and 7%, respectively). Additionally, the contrast measurement per intraretinal layer showed a non-significant increasing trend for all other intraretinal layers.

7.2.2.2 INTRARETINAL LAYER CONTRAST MEASUREMENT CHANGES IN THE FOVEAL REGION

The foveal contrast measurement in MS ON^- eyes compared with healthy eyes showed no statistical significance for all intraretinal layers. However, the foveal contrast measurement showed a non-significant increasing trend for the RNFL, GCL+IPL, INL, OPL, ONL+IS and RPE and a non-significant decreasing trend for the OS.

When comparing MS ON^+ with MS ON^- eyes, the foveal contrast measurement also showed no statistical significance for all intraretinal layers. In addition, the foveal contrast measurement showed a non-significant increasing trend for the RNFL, GCL+IPL, INL, OPL and ONL+IS as well as a non-significant decreasing trend for the OS and RPE.

7.2.2.3 INTRARETINAL LAYER CONTRAST MEASUREMENT CHANGES IN THE PARAFOVEAL REGION

The parafoveal contrast measurement in MS ON^- compared with healthy eyes showed a statistically significant increase (10%) for the GCL+IPL. However, the parafoveal contrast measurement showed a non-significant increasing trend for the RNFL, ONL+IS, OS and RPE and a non-significant decreasing trend for the INL and OPL.

When comparing MS ON^+ with MS ON^- eyes, the parafoveal contrast measurement showed a statistically significant increase (14%) for the GCL+IPL. Furthermore, the parafoveal contrast measurement showed a non-significant increasing trend for the RNFL and RPE as well as a non-significant decreasing trend for the INL, OPL, ONL+IS and OS.

7.2.2.4 INTRARETINAL LAYER CONTRAST MEASUREMENT CHANGES IN THE PERIFOVEAL REGION

The perifoveal contrast measurement in MS ON^- eyes compared with healthy eyes showed no statistical significance for all intraretinal layers. However, the perifoveal contrast measurement showed a non-significant increasing trend for the RNFL, GCL+IPL, ONL+IS, OS and RPE and a non-significant decreasing trend for the INL.

When comparing MS ON^+ with MS ON^- eyes, the perifoveal contrast measurement of the RNFL and GCL+IPL showed a statistically significant increase (15% and 18%, respectively). Moreover, the perifoveal contrast measurement showed a non-significant increasing trend for the INL, OPL and OS and a non-significant decreasing trend for the RPE.

7.2.3 FRACTAL DIMENSION MEASUREMENTS

The fractal dimension measurement per intraretinal layer was calculated across all macular regions for MS ON^-, MS ON^+ and healthy eyes. The fractal dimension measurement per macular region per intraretinal layer was also measured, except in the foveola. The contrast measurements are given in Table 7.2. The values are expressed in the form of the mean ± SD (SD: standard deviation).

Changes in the fractal dimension measurements between MS ON^-, MS ON^+ and healthy eyes were analyzed using an ANOVA followed by Newman-Keuls post-hoc analysis. Significant differences between the study groups are also reported in Table 7.3.

7.2.3.1 INTRARETINAL LAYER FRACTAL DIMENSION MEASUREMENT CHANGES PER EYE

The fractal dimension measurement per intraretinal layer for all study groups are given in Table 7.3. The findings clearly demonstrate that in MS ON^-, MS ON^+ and healthy eyes, the highest and lowest intraretinal layer fractal dimension measurement was

achieved for the ONL+IS (except for the RNFL in MS ON$^+$ eyes) and OPL, respectively. When comparing MS ON$^-$ eyes with healthy eyes, the fractal dimension measurement showed no statistical significance for all intraretinal layers. However, the fractal dimension measurement per intraretinal layer showed a non-significant increasing trend for the RNFL and ONL+IS.

When comparing MS ON$^+$ with MS ON- eyes, the fractal dimension measurement per intraretinal layer showed a statistically significant increase (3%) for the RNFL. In addition, the fractal dimension measurement per intraretinal layer showed a non-significant decreasing trend for the GCL+IPL and ONL+IS.

7.2.3.2 INTRARETINAL LAYER FRACTAL DIMENSION MEASUREMENT CHANGES IN THE FOVEAL REGION

The foveal fractal dimension measurements in MS ON$^-$ eyes compared with healthy eyes showed no statistical significance for all intraretinal layers. However, the foveal fractal dimension measurement showed a non-significant increasing trend for the RNFL and ONL+IS and a non-significant decreasing trend for the GCL+IPL and OPL.

When comparing MS ON$^+$ with MS ON$^-$ eyes, the foveal fractal dimension measurement also showed no statistical significance for all intraretinal layers. Moreover, the foveal fractal dimension measurement showed a non-significant increasing trend for the RNFL, INL and OPL as well as a non-significant decreasing trend for the GCL+IPL, ONL+IS and OS.

7.2.3.3 INTRARETINAL LAYER FRACTAL DIMENSION MEASUREMENT CHANGES IN THE PARAFOVEAL REGION

The parafoveal fractal dimension measurement in MS ON- eyes compared with healthy eyes showed no statistically significant differences for all intraretinal layers. However, the parafoveal fractal dimension measurement showed a non-significant

increasing trend for the RNFL and a non-significant decreasing trend for the GCL+IPL and OS.

When comparing MS ON^+ with MS ON^- eyes, the parafoveal fractal dimension measurement also showed a statistically significant increase (5%) for the RNFL. In addition, the parafoveal fractal dimension measurement showed a non-significant decreasing trend for the GCL+IPL and ONL+IS.

7.2.3.4 INTRARETINAL LAYER FRACTAL DIMENSION MEASUREMENT CHANGES IN THE PERIFOVEAL REGION

The perifoveal fractal dimension measurement in MS ON^- eyes compared with healthy eyes showed no statistical significance for all intraretinal layers. However, the foveal fractal dimension measurement showed a non-significant increasing trend for the OPL and a non-significant decreasing trend for the OS.

When comparing MS ON^+ with MS ON^- eyes, the foveal fractal dimension measurement also showed no statistical significance for all intraretinal layers. Furthermore, the foveal fractal dimension measurement showed a non-significant increasing trend for the RNFL and OS as well as a non-significant decreasing trend for the GCL+IPL, ONL+IS and RPE.

7.3 QUANTITATIVE MEASUREMENTS OF OPTICAL PARAMETERS

7.3.1 MEAN REFLECTANCE MEASUREMENTS

The mean reflectance measurement per intraretinal layer was calculated across all macular regions for MS ON^-, MS ON^+ and healthy eyes. The mean reflectance measurement per macular region per intraretinal layer was also measured, except in the foveola. The mean reflectance measurements are given in Table 7.4. The values are expressed in the form of the mean ± SD (SD: standard deviation).

The mean reflectance measurement changes between MS ON$^-$, MS ON$^+$ and healthy eyes were analyzed using an ANOVA followed by Newman-Keuls post-hoc analysis. Significant differences between the study groups are also reported in Table 7.4.

7.3.1.1 INTRARETINAL LAYER MEAN REFLECTANCE MEASUREMENT CHANGES PER EYE

The mean reflectance measurements per intraretinal layer for all study groups are given in Table 7.3. The data clearly demonstrate that in MS ON$^-$, MS ON$^+$ and healthy eyes, the highest and lowest intraretinal layer mean reflectance measurement was achieved for the ONL+IS and OPL, respectively. When comparing MS ON$^-$ eyes with healthy eyes, the mean reflectance measurement showed no statistical significance for all intraretinal layers. However, the mean reflectance measurement per intraretinal layer showed a non-significant decreasing trend for all intraretinal layers.

When comparing MS ON$^+$ with MS ON$^-$ eyes, the mean reflectance measurement per intraretinal layer showed no statistical significance for all intraretinal layers. In addition, the mean reflectance measurement per intraretinal layer showed a non-significant decreasing trend for the RNFL and a non-significant increasing trend for all other intraretinal layers.

7.3.1.2 INTRARETINAL LAYER MEAN REFLECTANCE MEASUREMENT CHANGES IN THE FOVEAL REGION

The foveal mean reflectance measurement in MS ON$^-$ eyes compared with healthy eyes showed no statistical significance for all intraretinal layers. However, the foveal mean reflectance measurement showed a non-significant decreasing trend for all intraretinal layers.

When comparing MS ON$^+$ with MS ON$^-$ eyes, the foveal mean reflectance measurement also showed no statistical significance for all intraretinal layers. Moreover,

the foveal mean reflectance measurement showed a non-significant increasing trend for all intraretinal layers.

7.3.1.3 INTRARETINAL LAYER MEAN REFLECTANCE MEASUREMENT CHANGES IN THE PARAFOVEAL REGION

The parafoveal mean reflectance measurement in MS ON^- eyes compared with healthy eyes showed no statistical significance for all intraretinal layers. However, the parafoveal mean reflectance measurement showed a non-significant decreasing trend for all intraretinal layers.

When comparing MS ON^+ with MS ON^- eyes, the parafoveal mean reflectance measurement also showed no statistical significance for all intraretinal layers. In addition, the parafoveal mean reflectance measurement showed a non-significant decreasing trend for the RNFL and a non-significant increasing trend for all other intraretinal layers.

7.3.1.4 INTRARETINAL LAYER MEAN REFLECTANCE MEASUREMENT CHANGES IN THE PERIFOVEAL REGION

The perifoveal mean reflectance measurement in MS ON^- eyes compared with healthy eyes showed no statistical significance for all intraretinal layers. However, the perifoveal mean reflectance measurement showed a non-significant decreasing trend for all intraretinal layers.

When comparing MS ON^+ with MS ON^- eyes, the perifoveal mean reflectance measurement also showed no statistical significance for all intraretinal layers. In addition, the perifoveal mean reflectance measurement showed a non-significant decreasing trend for the RNFL and a non-significant increasing trend for all other intraretinal layers.

7.3.2 TOTAL REFLECTANCE MEASUREMENTS

The total reflectance measurement per intraretinal layer was calculated across all macular regions for MS ON^-, MS ON^+ and healthy eyes. The total reflectance

measurement per macular region per intraretinal layer was also measured, except in the foveola. The total reflectance measurements are given in Table 7.5. The values are expressed in the form of the mean ± SD (SD: standard deviation).

The total reflectance measurement changes between MS ON$^-$, MS ON$^+$ and healthy eyes were analyzed using an ANOVA followed by Newman-Keuls post-hoc analysis. Significant differences between study groups are also reported in Table 7.5.

7.3.2.1 INTRARETINAL LAYER TOTAL REFLECTANCE MEASUREMENT CHANGES PER EYE

The total reflectance measurements per intraretinal layer for all study groups are given in Table 7.5. The findings clearly demonstrate that in MS ON$^-$, MS ON$^+$ and healthy eyes, the highest and lowest total reflectance measurement of the intraretinal layers was achieved for the GCL+IPL and INL, respectively. When comparing MS ON$^-$ with healthy eyes, the total reflectance measurement showed no statistical significance for all intraretinal layers. However, the total reflectance measurement per intraretinal layer showed a non-significant decreasing trend for all intraretinal layers.

Moreover, when comparing MS ON$^+$ with MS ON$^-$ eyes, the total reflectance measurement per intraretinal layer showed no statistical significance for all intraretinal layers. In addition, the total reflectance measurement per intraretinal layer showed a non-significant decreasing trend for the RNFL and GCL+IPL as well as a non-significant increasing trend for all other intraretinal layers.

7.3.2.2 INTRARETINAL LAYER TOTAL REFLECTANCE MEASUREMENT CHANGES IN THE FOVEAL REGION

The foveal total reflectance measurement in MS ON$^-$ eyes compared with healthy eyes showed no statistical significance for all intraretinal layers. However, the foveal

total reflectance measurement showed a non-significant decreasing trend for all intraretinal layers.

When comparing MS ON^+ with MS ON^- eyes, the foveal total reflectance measurement also showed no statistical significance for all intraretinal layers. In addition, the foveal total reflectance measurement showed a non-significant decreasing trend for the RNFL and GCL+IPL and a non-significant increasing trend for all other intraretinal layers.

7.3.2.3 INTRARETINAL LAYER TOTAL REFLECTANCE MEASUREMENT CHANGES IN THE PARAFOVEAL REGION

The parafoveal total reflectance measurement in MS ON^- eyes compared with healthy eyes showed no statistical significance for all intraretinal layers. However, the parafoveal total reflectance measurement showed a non-significant decreasing trend for all intraretinal layers.

When comparing MS ON^+ with MS ON^- eyes, the parafoveal total reflectance measurement also showed no statistical significance for all intraretinal layers. In addition, the parafoveal total reflectance measurement showed a non-significant decreasing trend for the RNFL and GCL+IPL and a non-significant increasing trend for all other intraretinal layers.

7.3.2.4 INTRARETINAL LAYER TOTAL REFLECTANCE MEASUREMENT CHANGES IN THE PERIFOVEAL REGION

The perifoveal total reflectance measurement in MS ON^- eyes compared with healthy eyes showed no statistical significance for all intraretinal layers. However, the perifoveal total reflectance measurement showed a non-significant decreasing trend for all intraretinal layers.

When comparing MS ON$^+$ with MS ON$^-$ eyes, the perifoveal total reflectance measurement also showed no statistical significance for all intraretinal layers. In addition, the perifoveal total reflectance measurement showed a non-significant decreasing trend for the RNFL and GCL+IPL and a non-significant increasing trend for all other intraretinal layers.

7.3.3 LAYER INDEX MEASUREMENTS

The layer index measurement per intraretinal layer was calculated across all macular regions for MS ON$^-$, MS ON$^+$ and healthy eyes. The layer index measurement per macular region per intraretinal layer was also measured, except in the foveola. The layer index measurements are given in Table 7.6. The values are expressed in the form of the mean ± SD (SD: standard deviation).

The layer index measurement changes between MS ON$^-$, MS ON$^+$ and healthy eyes were analyzed using an ANOVA followed by Newman-Keuls post-hoc analysis. Significant differences between study groups are also reported in Table 7.6.

7.3.3.1 INTRARETINAL LAYER INDEX MEASUREMENT CHANGES PER EYE

The layer index measurement per intraretinal layer for all study groups are given in Table 7.6. The data clearly demonstrate that in MS ON$^-$, MS ON$^+$ and healthy eyes, the highest and lowest layer index measurement of the intraretinal layers was achieved for the GCL+IPL and INL, respectively. Despite layer index measurement differences between the study groups, the layer index measurement distribution per intraretinal layer followed the same trend in all groups. Therefore, layer index measurement changes might provide relevant information to differentiate MS ON$^-$ and MS ON$^+$ eyes from healthy eyes.

When comparing MS ON$^-$ with healthy eyes, the layer index measurement showed a statistically significant decrease (13%) for the RNFL. However, the layer index measurement per intraretinal layer showed a non-significant increasing trend for the RPE and a non-significant decreasing trend for the GCL+IPL, INL, OPL, ONL+IS and OS.

When comparing MS ON$^+$ with MS ON$^-$ eyes, the layer index measurement per intraretinal layer showed a statistically significant decrease (14%) for the RNFL. In addition, the layer index measurement per intraretinal layer showed a non-significant increasing trend for the INL, OPL, ONL+IS and OS as well as a non-significant decreasing trend for the GCL+IPL.

7.3.3.2 INTRARETINAL LAYER INDEX MEASUREMENT CHANGES IN THE FOVEAL REGION

The foveal layer index measurement in MS ON$^-$ eyes compared with healthy eyes showed no statistical significance for all intraretinal layers. However, the foveal layer index measurement showed a non-significant decreasing trend for the RNFL, GCL+IPL, INL, OPL and ONL+IS and a non-significant increasing trend for the OS and RPE.

When comparing MS ON$^+$ with MS ON$^-$ eyes, the foveal layer index measurement also showed no statistical significance for all intraretinal layers. In addition, the foveal layer index measurement showed a non-significant decreasing trend for the RNFL, GCL+IPL and RPE as well as a non-significant increasing trend for all other intraretinal layers.

7.3.3.3 INTRARETINAL LAYER INDEX MEASUREMENT CHANGES IN THE PARAFOVEAL REGION

The parafoveal layer index measurement in MS ON$^-$ eyes compared with healthy eyes showed no statistical significance for all intraretinal layers. However, the parafoveal layer index measurement showed a non-significant decreasing trend for the RNFL,

GCL+IPL, INL, OPL and ONL+IS as well as a non-significant increasing trend for the OS and RPE.

When comparing MS ON^+ with MS ON^- eyes, the parafoveal layer index measurement also showed no statistical significance for all intraretinal layers. In addition, the parafoveal layer index measurement showed a non-significant decreasing trend for the RNFL, GCL+IPL and RPE as well as a non-significant increasing trend for all other intraretinal layers.

7.3.3.4 INTRARETINAL LAYER INDEX MEASUREMENT CHANGES IN THE PERIFOVEAL REGION

The parafoveal layer index measurement in MS ON^- eyes compared with healthy eyes showed a statistically significant decrease (14%) for the RNFL. However, the parafoveal layer index measurement showed a non-significant decreasing trend for the GCL+IPL, INL, OPL, ONL+IS and OS as well as a non-significant increasing trend for the RPE.

When comparing MS ON^+ with MS ON^- eyes, the parafoveal layer index measurement also showed a statistically significant decrease (16%) for the RNFL. Furthermore, the parafoveal layer index measurement showed a decreasing trend for the GCL+IPL and a non-significant increasing trend for the INL, OPL, ONL+IS, OS and RPE.

7.3.4 SCATTERING COEFFICIENT MEASUREMENTS

The scattering coefficient measurement per intraretinal layer was calculated across all macular regions for MS ON^-, MS ON^+ and healthy eyes. The layer index measurement per macular region per intraretinal layer was also measured, except in the foveola. Two normalization methods were used in the calculations for both the single-

and multiple-scattering models: 1. Reflectivity normalized to the maximum value within the whole retina (NRIR) and 2. Reflectivity normalized with respect to the RPE reflectance (NRPE). The scattering coefficient measurements are given in Tables 7.7-7.10. The values are expressed in the form of the mean ± SD (SD: standard deviation).

The scattering coefficient measurement changes between MS ON^-, MS ON^+ and healthy eyes were analyzed using an ANOVA followed by Newman-Keuls post-hoc analysis. Significant differences between study groups are also reported in Tables 7.7-7.10.

7.3.4.1 SCATTERING COEFFICIENTS CALCULATED USING THE SINGLE-SCATTERING MODEL AND THE NRIR METHOD

Table 7.7 shows significant differences between study groups.

7.3.4.1.1 INTRARETINAL LAYER SCATTERING COEFFICIENT CHANGES PER EYE

The scattering coefficient per intraretinal layer in MS ON^- eyes compared with healthy eyes showed a statistically significant increase (11%) for the RPE. However, the scattering coefficient per intraretinal layer showed a non-significant decreasing trend for the INL, OPL and ONL+IS and a non-significant increasing trend for the RNFL, GCL+IPL and OS.

When comparing MS ON^+ with MS ON^- eyes, the scattering coefficient per intraretinal layer showed a statistically significant increase (21%) for the RNFL. In addition, the scattering coefficient per intraretinal layer showed a non-significant increasing trend for the RNFL, GCL+IPL, INL, OPL, ONL+IS and OS and a non-significant decreasing trend for the RPE.

7.3.4.1.2 INTRARETINAL LAYER SCATTERING COEFFICIENT CHANGES IN THE FOVEAL REGION

The foveal scattering coefficient in MS ON$^-$ eyes compared with healthy eyes showed no statistical significance for all intraretinal layers. However, the foveal scattering coefficient showed an increasing trend for the RNFL, GCL+IPL and RPE as well as a non-significant decreasing trend for all other intraretinal layers.

When comparing MS ON$^+$ with MS ON- eyes, the foveal scattering coefficient showed a statistically significant increase (45%) for the RNFL. In addition, the scattering coefficient showed a non-significant increasing trend for the GCL+IPL, INL and OPL as well as a non-significant decreasing trend for the ONL+IS, OS and RPE.

7.3.4.1.3 INTRARETINAL LAYER SCATTERING COEFFICIENT CHANGES IN THE PARAFOVEAL REGION

The parafoveal scattering coefficient in MS ON$^-$ eyes compared with healthy eyes showed a statistically significant increase (15%) for the RPE. However, the parafoveal scattering coefficient showed a non-significant increasing trend for the RNFL and GCL+IPL and a non-significant decreasing trend for the INL, OPL, ONL+IS and OS.

When comparing MS ON$^+$ with MS ON$^-$ eyes, the parafoveal scattering coefficient of the RNFL and GCL+IPL showed a statistically significant increase (35% and 25%, respectively). In addition, the parafoveal scattering coefficient showed a non-significant increasing trend for the INL and OPL and a non-significant decreasing trend for the ONL+IS, OS and RPE.

7.3.4.1.4 INTRARETINAL LAYER SCATTERING COEFFICIENT CHANGES IN THE PERIFOVEAL REGION

The perifoveal scattering coefficient in MS ON$^-$ eyes compared with healthy eyes showed a statistically significant increase (17%) for the RPE. However, the perifoveal

scattering coefficient showed a non-significant increasing trend for the RNFL, GCL+IPL and OS and a non-significant decreasing trend for the INL, OPL and ONL+IS.

When comparing MS ON^+ with MS ON^- eyes, the perifoveal scattering coefficient showed a statistically significant increase (22%) for the RNFL. Moreover, the perifoveal scattering coefficient showed a non-significant increasing trend for the GCL+IPL, INL and ONL+IS and a non-significant decreasing trend for the OPL, OS and RPE.

7.3.4.2 SCATTERING COEFFICIENTS CALCULATED USING THE SINGLE-SCATTERING MODEL AND THE NRPE METHOD

Table 7.8 shows the significant differences between the study groups.

7.3.4.2.1 INTRARETINAL LAYER SCATTERING COEFFICIENT CHANGES PER EYE

The scattering coefficient per intraretinal layer in MS ON^- eyes compared with healthy eyes showed no statistical significance for all intraretinal layers. However, the scattering coefficient per intraretinal layer showed a non-significant increasing trend for the RNFL, GCL+IPL, OS and RPE and a non-significant decreasing trend for all other intraretinal layers.

When comparing MS ON^+ with MS ON^- eyes, the scattering coefficient per intraretinal layer of the RNFL and GCL+IPL showed a statistically significant increase (18% and 13%, respectively). In addition, the scattering coefficient per intraretinal layer showed a non-significant increasing trend for the INL and a non-significant decreasing trend for the OPL, ONL+IS, OS and RPE.

7.3.4.2.2 INTRARETINAL LAYER SCATTERING COEFFICIENT CHANGES IN THE FOVEAL REGION

The foveal scattering coefficient in MS ON^- eyes compared with healthy eyes showed no statistical significance for all intraretinal layers. However, the foveal scattering coefficient showed an increasing trend for the RNFL, GCL+IPL and RPE and a non-significant decreasing trend for all other intraretinal layers.

When comparing MS ON^+ with MS ON^- eyes, the foveal scattering coefficient showed a statistically significant increase (41%) for the RNFL. In addition, the scattering coefficient showed a non-significant increasing trend for the GCL+IPL, INL and OPL and a non-significant decreasing trend for the ONL+IS, OS and RPE.

7.3.4.2.3 INTRARETINAL LAYER SCATTERING COEFFICIENT CHANGES IN THE PARAFOVEAL REGION

The parafoveal scattering coefficient in MS ON^- eyes compared with healthy eyes showed a statistically significant increase (15%) for the GCL+IPL. However, the parafoveal scattering coefficient showed a non-significant increasing trend for the RNFL and RPE as well as a non-significant decreasing trend for the INL, OPL, ONL+IS and OS.

When comparing MS ON^+ with MS ON^- eyes, the parafoveal scattering coefficient of the RNFL and GCL+IPL showed a statistically significant increase (32% and 21%, respectively). Furthermore, the parafoveal scattering coefficient showed a non-significant decreasing trend for all other intraretinal layers.

7.3.4.2.4 INTRARETINAL LAYER SCATTERING COEFFICIENTCHANGES IN THE PERIFOVEAL REGION

The perifoveal scattering coefficient in MS ON^- eyes compared with healthy eyes showed a statistically significant increase (15%) for the RPE. However, the perifoveal

scattering coefficient showed a non-significant increasing trend for the RNFL, GCL+IPL and OS and a non-significant decreasing trend for the INL, OPL and ONL+IS.

When comparing MS ON^+ with MS ON^- eyes, the perifoveal scattering coefficient showed a statistically significant increase (21%) for the RNFL. In addition, the perifoveal scattering coefficient showed a non-significant increasing trend for the GCL+IPL, INL, OPL and ONL+IS as well as a non-significant decreasing trend for the OS and RPE.

7.3.4.3 SCATTERING COEFFICIENTS CALCULATED USING THE MULTIPLE-SCATTERING MODEL AND THE NRIR METHOD

Table 7.9 shows the significant differences between the study groups.

7.3.4.3.1 INTRARETINAL LAYER SCATTERING COEFFICIENT CHANGES PER EYE

The scattering coefficient per intraretinal layer in MS ON^- eyes compared with healthy eyes showed no statistical significance for all intraretinal layers. However, the scattering coefficient per intraretinal layer showed a non-significant decreasing trend for the RNFL, INL, OPL and ONL+IS as well as a non-significant increasing trend for all other intraretinal layers.

When comparing MS ON^+ with MS ON^- eyes, the scattering coefficient per intraretinal layer showed a statistically significant increase (17%) for the GCL+IPL. In addition, the scattering coefficient per intraretinal layer showed a non-significant increasing trend for the RNFL, INL and ONL+IS and a non-significant decreasing trend for the OPL, OS and RPE.

7.3.4.3.2 INTRARETINAL LAYER SCATTERING COEFFICIENT CHANGES IN THE FOVEAL REGION

The foveal scattering coefficient in MS ON^- eyes compared with healthy eyes showed no statistical significance for all intraretinal layers. However, the foveal

scattering coefficient showed an increasing trend for the GCL+IPL and RPE and a non-significant decreasing trend for all other intraretinal layers.

When comparing MS ON^+ with MS ON^- eyes, the foveal scattering coefficient showed no statistical significance for all intraretinal layers. In addition, the scattering coefficient showed a non-significant increasing trend for the RNFL, GCL+IPL, INL, OPL and ONL+IS and a non-significant decreasing trend for the OS.

7.3.4.3.3 INTRARETINAL LAYER SCATTERING COEFFICIENT CHANGES IN THE PARAFOVEAL REGION

The parafoveal scattering coefficient in MS ON^- eyes compared with healthy eyes showed a statistically significant increase (13%) for the RPE. However, the parafoveal scattering coefficient showed a non-significant increasing trend for the GCL+IPL and a non-significant decreasing trend for the RNFL, INL, OPL, ONL+IS and OS.

When comparing MS ON^+ with MS ON^- eyes, the parafoveal scattering coefficient of the RNFL and GCL+IPL showed a statistically significant increase (31% and 19%, respectively). Furthermore, the parafoveal scattering coefficient showed a non-significant decreasing trend for the INL, OS and RPE and a non-significant increasing trend for the OPL and ONL+IS.

7.3.4.3.4 INTRARETINAL LAYER SCATTERING COEFFICIENTCHANGES IN THE PERIFOVEAL REGION

The perifoveal scattering coefficient in MS ON^- eyes compared with healthy eyes showed a statistically significant increase (13%) for the RPE. However, the perifoveal scattering coefficient showed a non-significant increasing trend for the RNFL, GCL+IPL, INL and OS as well as a non-significant decreasing trend for the OPL and ONL+IS.

When comparing MS ON^+ with MS ON^- eyes, the perifoveal scattering coefficient of the RNFL, GCL+IPL and INL showed a statistically significant increase (17%, 19% and 3%, respectively). In addition, the perifoveal scattering coefficient showed a non-significant increasing trend for the ONL+IS and a non-significant decreasing trend for the OPL, OS and RPE.

7.3.4.4 SCATTERING COEFFICIENTS CALCULATED USING THE MULTIPLE-SCATTERING MODEL AND THE NRPE METHOD

Table 7.10 shows the significant differences between the study groups.

7.3.4.4.1 INTRARETINAL LAYER SCATTERING COEFFICIENT CHANGES PER EYE

The scattering coefficient per intraretinal layer in MS ON^- eyes compared with healthy eyes showed no statistical significance for all intraretinal layers. However, the scattering coefficient per intraretinal layer showed a non-significant decreasing trend for the RNFL, INL, OPL and ONL+IS as well as a non-significant increasing trend for all other intraretinal layers.

When comparing MS ON^+ with MS ON^- eyes, the scattering coefficient per intraretinal layer showed a statistically significant increase (15%) for the GCL+IPL. In addition, the scattering coefficient per intraretinal layer showed a non-significant increasing trend for the RNFL and INL and a non-significant decreasing trend for the OPL, ONL+IS, OS and RPE.

7.3.4.4.2 INTRARETINAL LAYER SCATTERING COEFFICIENT CHANGES IN THE FOVEAL REGION

The foveal scattering coefficient in MS ON^- eyes compared with healthy eyes showed no statistical significance for all intraretinal layers. However, the foveal

scattering coefficient showed an increasing trend for the GCL+IPL and RPE and a non-significant decreasing trend for all other intraretinal layers.

When comparing MS ON^+ with MS ON^- eyes, the foveal scattering coefficient showed no statistical significance for all intraretinal layers. In addition, the scattering coefficient showed a non-significant increasing trend for the RNFL, GCL+IPL, INL, OPL and ONL+IS and a non-significant decreasing trend for the OS and RPE.

7.3.4.4.3 INTRARETINAL LAYER SCATTERING COEFFICIENT CHANGES IN THE PARAFOVEAL REGION

The parafoveal scattering coefficient in MS ON^- eyes compared with healthy eyes showed no statistical significance for all intraretinal layers. However, the parafoveal scattering coefficient showed a non-significant decreasing trend for the INL, OPL, ONL+IS and OS and a non-significant increasing trend for the GCL+IPL and RPE.

When comparing MS ON^+ with MS ON^- eyes, the parafoveal scattering coefficient of the RNFL and GCL+IPL showed a statistically significant increase (28% and 17%, respectively). In addition, the parafoveal scattering coefficient showed a non-significant decreasing trend for the INL, OPL, OS an RPE and a non-significant increasing trend for the ONL+IS.

7.3.4.4.4 INTRARETINAL LAYER SCATTERING COEFFICIENT CHANGES IN THE PERIFOVEAL REGION

The perifoveal scattering coefficient in MS ON^- eyes compared with healthy eyes showed a statistically significant increase (13%) for the RPE. However, the perifoveal scattering coefficient showed a non-significant increasing trend for the RNFL, GCL+IPL and OS and a non-significant decreasing trend for the INL, OPL and ONL+IS.

When comparing MS ON^+ with MS ON^- eyes, the perifoveal scattering coefficient of the RNFL and GCL+IPL showed a statistically significant increase (17% and 21%,

respectively). Furthermore, the perifoveal scattering coefficient showed a non-significant increasing trend for the INL, OPL and ONL+IS and a non-significant decreasing trend for the OS and RPE.

7.4 RECEIVER OPERATING CHARACTERISTIC (ROC) ANALYSIS

As discussed in the previous section, structural and optical characteristics were extracted from the OCT images and their changes were investigated for each intraretinal layer. Statistically significant changes in these parameters per macular region were found in several particular intraretinal layers and were therefore used as indicators to discriminate MS ON^- and MS ON^+ eyes from healthy eyes. However, the discriminating power of these structural and optical parameters per macular region needs to be determined. Accordingly, a receiver operating characteristic (ROC) analysis was utilized to determine the discriminating power of the structural and optical parameters per macular region. The area under the ROC (AUROC) curve was calculated.

7.4.1 ROC ANALYSIS FOR STRUCTURAL PARAMETERS

7.4.1.1 ROC ANALYSIS FOR THICKNESS MEASUREMENTS

The ROC analyses with corresponding sensitivity and specificity tests were only performed for the intraretinal layers that showed statistically significant thickness differences per macular region when comparing MS ON^- and MS ON^+ eyes with healthy eyes. These layers were the RNFL and GCL+IPL. The AUROC values are shown in Table 7.11 for each discrimination test. Cutoff values of the thickness measurements derived from ROC analyses are shown in Table 7.12 and Table 7.13, respectively.

When comparing MS ON^- with healthy eyes, the highest AUROC values were observed in the RNFL and GCL+IPL (0.82 and 0.90, respectively). The cutoff point for

the RNFL was suggested as 40.53 µm with the sensitivity and specificity at 0.79 and 0.69, respectively. The cutoff point for the GCL+IPL was suggested as 73.07 μm with the sensitivity and specificity at 0.88 and 0.78, respectively. Additionally, by comparing AUROC values (see Table 7.11), we found that the most significant thickness changes were obtained for the GCL+IPL in all macular regions. In the foveal region, the AUROC for the GCL+IPL was 0.85 with a cutoff point at 53.35 μm. In the parafoveal region, the AUROC for the GCL+IPL was 0.90 with a cutoff point at 88.84 μm. In the perifoveal region, the AUROC for the GCL+IPL was 0.85 with a cutoff point at 62.51 μm.

The highest AUROC values obtained when comparing MS ON^- with MS ON^+ eyes were also observed in the RNFL and GCL+IPL (0.84 and 0.89, respectively). The cutoff point for the RNFL was suggested as 38.32 μm with the sensitivity and specificity at 0.72 and 0.62, respectively. The cutoff point for the GCL+IPL was suggested as 65.21 μm with the sensitivity and specificity at 0.87 and 0.77, respectively. Additionally, by comparing AUROC values (see Table 7.11), we found that the most significant thickness changes were obtained for the GCL+IPL in the foveal and parafoveal macular region and for the RNFL in the perifoveal macular region. In the foveal region, the AUROC for the GCL+IPL was 0.82 with a cutoff point at 46.82 μm. In the parafoveal region, the AUROC for the GCL+IPL was 0.88 with a cutoff point at 76.14 μm. Lastly, in the perifoveal region, the AUROC for the RNFL was 0.86 with a cutoff point at 56.82 μm.

7.4.1.2 ROC ANALYSIS FOR CONTRAST MEASUREMENTS

The ROC analyses with corresponding sensitivity and specificity tests were only performed for the intraretinal layers that showed statistically significant thickness

differences per macular region when comparing MS ON$^-$ and MS ON$^+$ eyes with healthy eyes.

The ROC analyses with corresponding sensitivity and specificity tests were performed for the intraretinal layers to determine the discriminating power for contrast measurement changes when comparing MS ON$^-$ and MS ON$^+$ eyes with healthy eyes. The AUROC values are shown in Table 7.14 for each discrimination test. Cutoff values of the thickness measurements derived from ROC analyses are shown in Table 7.15 and Table 7.16, respectively.

When comparing MS ON$^-$ with healthy eyes, the highest AUROC values were observed in the OS (0.68). The cutoff point for the OS was suggested as 3397.46 (a.u.) with the sensitivity and specificity at 0.70 and 0.60, respectively. Additionally, by comparing AUROC values (see Table 7.14), we found that the most significant contrast changes were obtained for the OS, INL and INL in the foveal, parafoveal and perifoveal regions, respectively. In the foveal region, the AUROC for the OS was 0.65 with a cutoff point at 3977.65 (a.u.). In the parafoveal region, the AUROC for the GCL+IPL was 0.70 with a cutoff point at 3891.22 (a.u.). Finally, in the perifoveal region, the AUROC for the GCL+IPL was 0.58 with a cutoff point at 3461.83 (a.u.).

When comparing MS ON$^+$ with MS ON$^-$ eyes, the AUROC values obtained for all intraretinal layers were less than 0.50 (see Table 7.14), which indicated no discriminating power.

7.4.1.3 ROC ANALYSIS FOR FRACTAL DIMENSION MEASUREMENTS

The ROC analyses with corresponding sensitivity and specificity tests were only performed for the intraretinal layers that showed statistically significant fractal dimension differences per macular region when comparing MS ON$^+$ and MS ON$^-$ eyes with healthy

eyes. These layers were the RNFL and GCL+IPL. The AUROC values are shown in Table 7.17 for each discrimination test. Cutoff values of the fractal dimension measurements derived from ROC analyses are shown in Table 7.18 and Table 7.19, respectively.

When comparing MS ON^- with healthy eyes, the highest AUROC values were observed in the OPL (0.75). The cutoff point for the OPL was suggested as 1.51 with the sensitivity and specificity at 0.74 and 0.64, respectively. We found that the most significant fractal dimension changes were obtained for the GCL+IPL, OPL and OPL in the foveal, parafoveal and perifoveal macular region, respectively. In the foveal region, the AUROC for the GCL+IPL was 0.68 with a cutoff point at 1.89. In the parafoveal region, the AUROC for the OPL was 0.71 with a cutoff point at 1.51. Lastly, in the perifoveal region, the AUROC for the OPL was 0.75 with a cutoff point at 1.52.

The highest AUROC values obtained when comparing MS ON^- with MS ON^+ eyes were observed in the GCL+IPL (0.73). The cutoff point for the GCL+IPL was suggested as 1.67 with the sensitivity and specificity at 0.71 and 0.61, respectively. Additionally, by comparing AUROC values (see Table 7.17), we found that the most significant thickness changes were obtained for the GCL+IPL for all macular regions. In the foveal region, the AUROC for the GCL+IPL was 0.75 with a cutoff point at 1.89. In the parafoveal region, the AUROC for the GCL+IPL was 0.69 with a cutoff point at 1.54. Finally, in the perifoveal region, the AUROC for the RNFL was 0.67 with a cutoff point at 1.59.

7.4.2 ROC ANALYSIS FOR OPTICAL PARAMETERS

7.4.2.1 ROC ANALYSIS FOR MEAN REFLECTANCE MEASUREMENTS

The ROC analyses with corresponding sensitivity and specificity tests were only performed for the intraretinal layers that showed statistically significant mean reflectance differences per macular region when comparing MS ON^- and MS ON^+ eyes with healthy eyes. These layers were the RNFL and OS. The AUROC values are shown in Table 7.20 for each discrimination test. Cutoff values of the mean reflectance measurements derived from the ROC analyses are shown in Table 7.21 and Table 7.22, respectively.

When comparing MS ON^- with healthy eyes, the highest AUROC values were observed in the RNFL and OS (0.72 and 0.70, respectively). The cutoff point for the RNFL was suggested as 53.57 dB with the sensitivity and specificity at 0.70 and 0.60, respectively. The cutoff point for the OS was suggested as 55.95 dB with the sensitivity and specificity at 0.66 and 0.56, respectively. Additionally, by comparing AUROC values (see Table 7.20), we found that the most significant mean reflectance changes were obtained for the OS, ONL+IS (OS) and RNFL in the foveal, parafoveal and perifoveal macular regions, respectively. In the foveal region, the AUROC for the OS was 0.68 with a cutoff point at 55.89 dB. In the parafoveal region, the AUROC for the ONL+IS (OS) was 0.68 (0.68) with a cutoff point at 43.44 dB (56.64 dB). Additionally, in the perifoveal region, the AUROC for the RNFL was 0.73 with a cutoff point at 53.82 dB.

When comparing MS ON^+ with MS ON^- eyes, the AUROC values obtained for all intraretinal layers and all macular regions were low, which indicated no discriminating power.

7.4.2.2 ROC ANALYSIS FOR TOTAL REFLECTANCE MEASUREMENTS

The ROC analyses with corresponding sensitivity and specificity tests were only performed for the intraretinal layers that showed statistically significant total reflectance differences per macular region when comparing MS ON^+ and MS ON^- eyes with healthy eyes. These layers were the RNFL and OS. The AUROC values are shown in Table 7.23 for each discrimination test. Cutoff values of the total reflectance measurements derived from the ROC analyses are shown in Table 7.24 and Table 7.25, respectively.

When comparing MS ON^- with healthy eyes, the highest AUROC values were observed in the RNFL and GCL+IPL (0.84 and 0.79, respectively). The cutoff point for the RNFL was suggested as 80.15 dB with the sensitivity and specificity at 0.74 and 0.64, respectively. The cutoff point for the GCL+IPL was suggested as 80.89 dB with the sensitivity and specificity at 0.80 and 0.70, respectively. Additionally, by comparing AUROC values (see Table 7.23), we found that the most significant total reflectance changes were obtained for the GCL+IPL, GCL+IPL and RNFL in the foveal, parafoveal and perifoveal macular region, respectively. In the foveal region, the AUROC for the GCL+IPL was 0.71 with a cutoff point at 82.38 dB. In the parafoveal region, the AUROC for the GCL+IPL was 0.81 with a cutoff point at 82.72 dB. Finally, in the perifoveal region, the AUROC for the RNFL was 0.85 with a cutoff point at 81.25 dB.

The highest AUROC values obtained when comparing MS ON^+ with MS ON^- eyes were also observed in the RNFL (0.68). The cutoff point for the RNFL was suggested as 79.05 dB with the sensitivity and specificity at 0.64 and 0.54, respectively. Additionally, by comparing AUROC values (see Table 7.23), we found that the most significant thickness changes were obtained for the RNFL in the perifoveal macular

region. In the perifoveal region, the AUROC for the RNFL was 0.74 with a cutoff point at 79.75 dB.

7.4.2.3 ROC ANALYSIS FOR LAYER INDEX MEASUREMENTS

The ROC analyses with corresponding sensitivity and specificity tests were only performed for the intraretinal layers that showed statistically significant layer index differences per macular region when comparing MS ON^- and MS ON^+ eyes with healthy eyes. These layers were the RNFL and GCL+IPL. The AUROC values are shown in Table 7.26 for each discrimination test. Cutoff values of the layer index measurements derived from the ROC analyses are shown in Table 7.27 and Table 7.28, respectively.

When comparing MS ON^- with healthy eyes, the highest AUROC values were observed in the RNFL and GCL+IPL (0.78 and 0.77, respectively). The cutoff point for the RNFL was suggested as 11.39 with the sensitivity and specificity at 0.81 and 0.71, respectively. The cutoff point for the GCL+IPL was suggested as 12.34 with the sensitivity and specificity at 0.81 and 0.71, respectively. Additionally, by comparing AUROC values (see Table 7.26), we found that the most significant layer index changes were obtained for the GCL+IPL, GCL+IPL and RNFL in the foveal, parafoveal and perifoveal macular region, respectively. In the foveal region, the AUROC for the GCL+IPL was 0.71 with a cutoff point at 13.51. In the parafoveal region, the AUROC for the GCL+IPL was 0.75 with a cutoff point at 14.72. Lastly, in the perifoveal region, the AUROC for the RNFL was 0.81 with a cutoff point at 12.50.

The highest AUROC values obtained when comparing MS ON^- with MS ON^+ eyes were also observed in the RNFL and GCL+IPL (0.81 and 0.75, respectively). The cutoff point for the RNFL was suggested as 10.07 with the sensitivity and specificity at 0.79 and 0.69, respectively. The cutoff point for the GCL+IPL was suggested as 11.23

with the sensitivity and specificity at 0.72 and 0.62, respectively. Additionally, by comparing AUROC values (see Table 7.26), we found that the most significant thickness changes were obtained for the RNFL and GCL+IPL in the parafoveal and perifoveal macular region. In the parafoveal region, the AUROC for the RNFL (GCL+IPL) was 0.75 (0.76) with a cutoff point at 8.33 (12.79). In the perifoveal region, the AUROC for the RNFL (GCL+IPL) was 0.86 (0.73) with a cutoff point at 11.16 (9.83).

7.4.2.4 ROC ANALYSIS FOR SCATTERING COEFFICIENT MEASUREMENTS

7.4.2.4.1 ROC ANALYSIS FOR SCATTERING COEFFICIENTS OBTAINED WITH THE SINGLE-SCATTERING MODEL AND THE NRIR METHOD

The ROC analyses with corresponding sensitivity and specificity tests were only performed for the intraretinal layers that showed statistically significant scattering coefficient differences per macular region when comparing MS ON^- and MS ON^+ eyes with healthy eyes. These layers were the RNFL and GCL+IPL. The AUROC values are shown in Table 7.29 for each discrimination test. Cutoff values of the layer index measurements derived from the ROC analyses are shown in Table 7.30 and Table 7.31, respectively.

When comparing MS ON^- with healthy eyes, the highest AUROC values were observed in the INL and OPL (0.61 and 0.61, respectively). The cutoff point for the INL was suggested as 2.75 mm^{-1} with the sensitivity and specificity at 0.67 and 0.57, respectively. The cutoff point for the GCL+IPL was suggested as 1.98 mm^{-1} with the sensitivity and specificity at 0.70 and 0.60, respectively. Additionally, by comparing AUROC values (see Table 7.29), we found that the most significant scattering coefficient changes were obtained for the ONL+IS for all macular regions. In the foveal region, the

AUROC for the ONL+IS was 0.67 with a cutoff point at 1.79 mm^{-1}. Additionally, in the parafoveal region, the AUROC for the ONL+IS was 0.68 with a cutoff point at 2.22 mm^{-1}. In the perifoveal region, the AUROC for the ONL+IS was 0.64 with a cutoff point at 2.63 mm^{-1}.

The highest AUROC values obtained when comparing MS ON^- with MS ON^+ eyes were also observed in the RPE. The cutoff point for the RPE was suggested as 11.16 mm^{-1} with the sensitivity and specificity at 0.64 and 0.54, respectively. Additionally, by comparing AUROC values (see Table 7.29), we found that the most significant thickness changes were obtained for the OS, OS and RPE in the foveal, parafoveal and perifoveal macular region, respectively. In the foveal region, the AUROC for the OS was 0.68 with a cutoff point at 9.55 mm^{-1}. In the parafoveal region, the AUROC for the OS was 0.65 with a cutoff point at 9.50 mm^{-1}. In the perifoveal region, the AUROC for the RPE was 0.63 with a cutoff point at 11.49 mm^{-1}.

7.4.2.4.2 ROC ANALYSIS FOR SCATTERING COEFFICIENTS OBTAINED WITH THE SINGLE-SCATTERING MODEL AND THE NRPE METHOD

The ROC analyses with corresponding sensitivity and specificity tests were only performed for the intraretinal layers that showed statistically significant scattering coefficient differences per macular region when comparing MS ON^- and MS ON^+ eyes with healthy eyes. These layers were the RNFL and GCL+IPL. The AUROC values are shown in Table 7.32 for each discrimination test. Cutoff values of the scattering coefficient measurements derived from ROC analyses are shown in Table 7.33 and Table 7.34, respectively.

When comparing MS ON$^-$ with healthy eyes, the highest AUROC value was observed in the OPL (0.60). The cutoff point for the OPL was suggested as 2.94 mm^{-1} with the sensitivity and specificity at 0.66 and 0.56, respectively. Additionally, by comparing AUROC values (see Table 7.32), we found that the most significant scattering coefficient changes were obtained for the ONL+IS for all macular regions. In the foveal region, the AUROC for the ONL+IS was 0.68 with a cutoff point at 2.36 mm^{-1}. In the parafoveal region, the AUROC for the ONL+IS was 0.67 with a cutoff point at 3.09 mm^{-1}. Lastly, in the perifoveal region, the AUROC for the ONL+IS was 0.62 with a cutoff point at 3.79 mm^{-1}.

The highest AUROC value obtained when comparing MS ON$^-$ with MS ON$^+$ eyes was observed in the RPE (0.64). The cutoff point for the RPE was suggested as 15.73 mm^{-1} with the sensitivity and specificity at 0.57 and 0.47, respectively. Additionally, by comparing AUROC values (see Table 7.32), we found that the most significant scattering coefficient changes were obtained for the OS, OS and RPE in the foveal, parafoveal and perifoveal macular regions, respectively. In the foveal region, the AUROC for the OS was 0.70 with a cutoff point at 12.85 mm^{-1}. In the parafoveal region, the AUROC for the OS was 0.67 with a cutoff point at 12.41 mm^{-1}. Additionally, in the perifoveal region, the AUROC for the RPE was 0.64 with a cutoff point at 16.10 mm^{-1}.

7.4.2.4.3 ROC ANALYSIS FOR SCATTERING COEFFICIENTS OBTAINED WITH THE MULTIPLE-SCATTERING MODEL AND THE NRIR METHOD

The ROC analyses with corresponding sensitivity and specificity tests were only performed for the intraretinal layers that showed statistically significant scattering coefficient differences per macular region when comparing MS ON$^-$ and MS ON$^+$ eyes

with healthy eyes. These layers were the INL and OPL. The AUROC values are shown in Table 7.35 for each discrimination test. Cutoff values of the scattering coefficient measurements derived from ROC analyses are shown in Table 7.36 and Table 7.37, respectively.

When comparing MS ON^- with healthy eyes, the highest AUROC value was observed in the INL and ONL+IS (0.63 and 0.68, respectively). The cutoff point for the INL was suggested as 3.36 mm^{-1} with the sensitivity and specificity at 0.67 and 0.57, respectively. The cutoff point for the ONL+IS was suggested as 2.38 mm^{-1} with the sensitivity and specificity at 0.62 and 0.52, respectively. Additionally, by comparing AUROC values (see Table 7.35), we found that the most significant scattering coefficient changes were obtained for the ONL+IS for all macular regions. In the foveal region, the AUROC for the ONL+IS was 0.73 with a cutoff point at 1.63 mm^{-1}. In the parafoveal region, the AUROC for the ONL+IS was 0.71 with a cutoff point at 1.98 mm^{-1}. In the perifoveal region, the AUROC for the ONL+IS was 0.75 with a cutoff point at 3.10 mm^{-1}.

The highest AUROC value obtained when comparing MS ON^+ with MS ON^- eyes was observed in the RPE (0.58). The cutoff point for the RPE was suggested as 13.34 mm^{-1} with the sensitivity and specificity at 0.64 and 0.54, respectively. Additionally, by comparing AUROC values (see Table 7.35), we found that the most significant scattering coefficient changes were obtained for the OS, OS and RPE in the foveal, parafoveal and perifoveal macular region, respectively. In the foveal region, the AUROC for the OS was 0.62 with a cutoff point at 12.44 mm^{-1}. In the parafoveal region, the AUROC for the OS was 0.65 with a cutoff point at 11.84 mm^{-1}. Lastly, in the perifoveal region, the AUROC for the RPE was 0.63 with a cutoff point at 13.64 mm^{-1}.

7.4.2.4.4 ROC ANALYSIS FOR SCATTERING COEFFICIENTS OBTAINED WITH THE MULTIPLE-SCATTERING MODEL AND THE NRPE METHOD

The ROC analyses with corresponding sensitivity and specificity tests were only performed for the intraretinal layers that showed statistically significant scattering coefficient differences per macular region when comparing MS ON^- and MS ON^+ eyes with healthy eyes. These layers were the INL and OPL. The AUROC values are shown in Table 7.38 for each discrimination test. Cutoff values of the scattering coefficient measurements derived from ROC analyses are shown in Table 7.39 and Table 7.40, respectively.

When comparing MS ON^- with healthy eyes, the highest AUROC value was observed in the INL and ONL+IS (0.62 and 0.69, respectively). The cutoff point for the INL was suggested as 4.69 mm^{-1} with the sensitivity and specificity at 0.61 and 0.51, respectively. The cutoff point for the ONL+IS was suggested as 3.26 mm^{-1} with the sensitivity and specificity at 0.67 and 0.57, respectively. Additionally, by comparing AUROC values (see Table 7.38), we found that the most significant scattering coefficient changes were obtained for the ONL+IS for all macular regions. In the foveal region, the AUROC for the ONL+IS was 0.74 with a cutoff point at 2.02 mm^{-1}. In the parafoveal region, the AUROC for the ONL+IS was 0.74 with a cutoff point at 2.56 mm^{-1}. Lastly, in the perifoveal region, the AUROC for the ONL+IS was 0.77 with a cutoff point at 3.09 mm^{-1}.

The highest AUROC value obtained when comparing MS ON^- with MS ON^+ eyes was observed in the RPE (0.62). The cutoff point for the RPE was suggested as 17.91 mm^{-1} with the sensitivity and specificity at 0.56 and 0.46, respectively. Additionally, by

comparing AUROC values (see Table 7.40), we found that the most significant scattering coefficient changes were obtained for the OS, OS and RPE in the foveal, parafoveal and perifoveal macular regions, respectively. In the foveal region, the AUROC for the OS was 0.63 with a cutoff point at 16.10 mm^{-1}. In the parafoveal region, the AUROC for the OS was 0.68 with a cutoff point at 14.94 mm^{-1}. Additionally, in the perifoveal region, the AUROC for the RPE was 0.65 with a cutoff point at 18.26 mm^{-1}.

7.5 SUMMARY

In this chapter, we evaluated the optical and structural parameters from macular OCT images in patients with MS to determine which parameter could best discriminate MS eyes from healthy eyes.

Our findings indicate that the thickness of the GCL+IPL complex showed a significant decrease (11%) in MS ON^- eyes compared with healthy eyes. The thickness showed a tendency towards thickening for all other intraretinal layers (except in the OPL). The thickness in other layers (except in the ONL+IS and RPE) showed a tendency towards thickening without reaching significance compared with healthy eyes. The thickness of the OPL and OS showed a significant decrease (9% and 16%, respectively) in MS ON^+ eyes compared with MS ON^- eyes. Moreover, the fractal dimension increased for the RNFL and ONL+IS in MS ON^+ eyes compared with healthy eyes. When comparing MS ON^+ with MS ON- eyes, the fractal dimension showed a statistically significant increase (3%) for the RNFL.

Multiple sclerosis is a neurodegenerative disease characterized by both demyelination and axonal degeneration.[119] Objective markers are necessary for MS patients' diagnoses and follow-ups, and markers could also help to determine the effect of

therapy. Our results demonstrate the superiority of the GCL+IPL thickness as a good discriminator between healthy eyes and eyes affected by MS. Specifically, we found that the thickness of the macular ganglion cell complex had the highest sensitivity and specificity, outperforming the RNFL thickness data provided by the analysis software of the commercially available Stratus OCT device. Our study also suggests that optic neuritis is followed by a targeted loss of ganglion cells in the macula, which can be objectively assessed by OCT image processing.

Several studies have reported atrophy of the RNFL around the optic nerve in patients with MS with and even without a history of optic neuritis.[122-126] Our findings confirmed that the mean overall RNFL thickness in the eyes of MS patients with and without a history of ON is smaller than in healthy eyes. More than a reduction in the RNFL, our results showed a statistically significant decrease (11%) for the GCL+IPL. This finding agrees with previous OCT studies, which confirmed that the fibers of the papillomacular bundle are most susceptible to damage in the ON.[125, 127] One important aspect of this finding is that the evaluation of the mean thickness values may provide a way to discriminate between the RNFL atrophy caused by glaucomatous damage and neurodegenerative disorders.[128]

The RNFL atrophy observed in eyes previously unaffected with ON might have been the result of the occurrence of subclinical axonal degeneration.[119] As a result of axonal degeneration, the RNFL decreases and the number of retinal ganglion cells diminishes, which manifests in macular thinning. Burkholder et al. showed that ON-affected eyes had significantly decreased macular volume and thickness compared with healthy eyes.[129] To the best of our knowledge, no direct measurement of macular

structures has yet been performed in order to determine which retinal layers are affected in MS patients. Histopathological studies have qualitatively revealed atrophy of the inner retina in the eyes of MS patients but not in the outer nuclear layer.[130, 131] However, no quantitative measurements were performed because of technical difficulties, e.g., partial post-mortem detachment of the retina in many of the eyes.

Our results showed that the atrophy of the RNFL and GCL+IPL was present in the macula of patients with MS even in eyes previously unaffected with ON. Furthermore, we demonstrated that the outer layers of the retina were not involved in this process. The value most capable of determining the presence of axonal loss appeared to be the thickness of the GCL+IPL complex with a cutoff value of 73.07 μm and the highest sensitivity and specificity.

Neurodegeneration in MS patients can be quantitatively assessed using MRI or OCT. Measurements of brain atrophy, brain parenchymal fraction and also the thickness of RNFL show correlation with clinical disability (usually assessed with the EDSS and multiple sclerosis functional composite (MSFC)), which is considered to be the consequence of axonal damage.[132-134] Previous studies have also shown that thinning of the RNFL correlates with the MRI-based measurements of axonal loss.[133, 135, 136, 124] Our study shows the superiority of the GCL+IPL thickness as a good discriminator between healthy eyes and eyes with MS. Therefore, macular GCL segmentation may be able to provide a comparably good parameter to MRI-based measurements for the description of neurodegenerative changes in MS. Although GCL+IPL thickness may provide a sensitive tool for the assessment of axonal degeneration, care should be taken when interpreting its

value for numerous other neurodegenerative disorders, such as glaucoma, Alzheimer's disease or Parkinson's disease, which may also lead to ganglion cell death. [137-139]

Our results imply that MS mainly affects the ganglion cells. Furthermore, changes can occur in eyes without a previous history of ON, which may reflect axonal degeneration due to the MS disease process. This finding could facilitate cost-effective follow-up strategies for patients with neurodegeneration due to MS. With OCT image segmentation, we also demonstrated in vivo that neurodegeneration affected the ganglion cells and not the outer retina, whereas episodes of ON resulted in further pronounced loss of retinal ganglion cells.[140]

Table 7.1 Distribution statistics of thickness measurements (µm) of intraretinal layers by study groups

Thickness (µm)	Healthy	MS ON-	MS ON+
Across All Macular Regions			
RNFL	42.02 ± 2.11	39.70 ± 1.57 †	36.22 ± 3.30 ‡
GCL+IPL	78.30 ± 4.09	70.03 ± 4.86 ‡	58.95 ± 7.77 ‡
INL	35.02 ± 1.60	35.78 ± 1.67	36.16 ± 1.82
OPL	41.30 ± 2.49	41.16 ± 2.70	40.58 ± 2.77
ONL+IS	86.41 ± 5.21	86.61 ± 5.83	87.39 ± 5.60
OS	16.27 ± 3.06	17.70 ± 2.31	18.29 ± 3.13
RPE	12.71 ± 1.32	13.04 ± 1.13	12.91 ± 1.24
Foveal Region			
RNFL	8.85 ± 2.37	8.22 ± 2.83	6.05 ± 2.99 †
GCL+IPL	55.80 ± 3.87	50.65 ± 3.64 ‡	44.44 ± 5.34 ‡
INL	20.93 ± 1.82	21.59 ± 1.75	21.47 ± 2.29
OPL	61.24 ± 6.83	59.67 ± 7.13	57.51 ± 6.85
ONL+IS	99.26 ± 6.79	100.34 ± 6.91	101.4 ± 6.83
OS	18.05 ± 4.03	19.85 ± 3.24	20.86 ± 3.86
RPE	12.84 ± 1.72	13.35 ± 1.80	13.21 ± 1.58
Parafoveal Region			
RNFL	33.72 ± 1.85	31.68 ± 1.85 †	28.05 ± 4.60 ‡
GCL+IPL	94.71 ± 5.73	83.37 ± 6.93 ‡	69.44 ± 9.28 ‡
INL	39.60 ± 2.17	41.07 ± 2.35 †	41.62 ± 2.50
OPL	37.17 ± 2.68	37.32 ± 2.40	38.04 ± 2.38
ONL+IS	84.89 ± 6.11	84.75 ± 7.00	85.57 ± 6.43
OS	14.80 ± 3.58	16.48 ± 2.99	17.57 ± 4.04
RPE	11.57 ± 1.59	12.13 ± 1.80	11.66 ± 1.87
Perifoveal Region			
RNFL	41.87 ± 2.94	38.68 ± 2.15 †	34.50 ± 4.09 ‡
GCL+IPL	67.36 ± 4.52	60.34 ± 5.30 ‡	50.04 ± 7.57 ‡
INL	33.00 ± 1.67	33.33 ± 1.67	33.56 ± 1.75
OPL	31.54 ± 1.38	32.05 ± 1.31	31.82 ± 1.31
ONL+IS	75.27 ± 4.84	74.96 ± 5.53	75.87 ± 5.58
OS	14.59 ± 2.81	15.72 ± 2.11	15.93 ± 3.00
RPE	12.54 ± 1.39	12.66 ± 1.21	12.69 ± 1.15

† $0.001<p<0.05$ and ‡ $p<0.001$ (ANOVA followed by Newman-Keuls post hoc analysis) between MS ON- and healthy eyes (see MS ON- column) and between MS ON- and MS ON+ eyes (see MS ON+ column).

Table 7.2 Distribution statistics of the contrast (a.u.) of intraretinal layers by study groups

Contrast (a.u.)	Healthy	MS ON-	MS ON+
Across All Macular Regions			
RNFL	1516.30 ± 117.28	1637.67 ± 88.92 †	1799.47 ± 96.51 ‡
GCL+IPL	1457.80 ± 83.51	1525.78 ± 65.28 †	1635.36 ± 112.27 ‡
INL	1404.58 ± 129.70	1446.90 ± 195.39	1594.87 ± 211.54 †
OPL	1333.37 ± 88.44	1342.07 ± 134.14	1443.21 ± 141.43 †
ONL+IS	874.95 ± 105.71	883.14 ± 68.69	882.12 ± 36.40
OS	3613.71 ± 405.61	3376.80 ± 281.57	3402.84 ± 278.84
RPE	5014.53 ± 420.37	4941.36 ± 352.04	4958.04 ± 409.38
Foveal Region			
RNFL	2088.32 ± 333.82	2186.56 ± 578.05	2407.19 ± 298.73
GCL+IPL	2362.71 ± 134.64	2441.86 ± 144.29	2662.07 ± 169.55 ‡
INL	2077.17 ± 337.04	2362.66 ± 399.90 †	2505.89 ± 372.83
OPL	2099.11 ± 221.11	2234.24 ± 282.90	2283.58 ± 242.21
ONL+IS	995.01 ± 168.37	1003.85 ± 120.31	966.00 ± 80.04
OS	4116.37 ± 556.12	3779.14 ± 519.07	3882.56 ± 506.53
RPE	7308.22 ± 655.20	7382.35 ± 719.48	7800.33 ± 530.23
Parafoveal Region			
RNFL	5128.67 ± 1305.11	5299.89 ± 1330.35	5631.39 ± 1111.49
GCL+IPL	1863.24 ± 116.70	2058.49 ± 133.05 ‡	2340.50 ± 202.36 ‡
INL	3983.85 ± 240.79	3828.07 ± 234.99 †	3732.34 ± 213.72
OPL	4272.54 ± 241.98	4120.81 ± 255.48	4076.91 ± 252.54
ONL+IS	1122.66 ± 120.42	1190.80 ± 181.04	1147.78 ± 134.27
OS	3214.98 ± 1485.33	3187.52 ± 1051.02	3165.02 ± 1368.64
RPE	7803.44 ± 1093.91	8003.71 ± 1176.83	8392.73 ± 1051.05
Perifoveal Region			
RNFL	2260.49 ± 176.31	2423.13 ± 194.98 †	2795.20 ± 360.48 ‡
GCL+IPL	1879.89 ± 120.80	1997.80 ± 164.95 †	2352.11 ± 242.51 ‡
INL	3546.13 ± 210.98	3487.03 ± 272.95	3554.55 ± 276.19
OPL	4036.11 ± 233.66	4034.55 ± 219.45	4090.54 ± 260.08
ONL+IS	1291.61 ± 117.39	1341.60 ± 193.57	1322.04 ± 139.86
OS	3986.67 ± 1088.46	4086.73 ± 1106.22	4293.40 ± 868.09
RPE	7292.01 ± 789.99	7729.87 ± 951.42	7495.44 ± 727.40

† $0.001<p<0.05$ and ‡ $p<0.001$ (ANOVA followed by Newman-Keuls post hoc analysis) between MS ON- and healthy eyes (see MS ON- column) and between MS ON- and MS ON+ eyes (see MS ON+ column).

Table 7.3 Distribution statistics of the fractal dimension (a.u.) of intraretinal layers by study groups

Fractal Dimension	Healthy	MS ON-	MS ON+
Across All Macular Regions			
RNFL	1.74 ± 0.04	1.75 ± 0.04	1.80 ± 0.07 ‡
GCL+IPL	1.68 ± 0.01	1.68 ± 0.01 †	1.67 ± 0.01 †
INL	1.78 ± 0.01	1.78 ± 0.01	1.78 ± 0.01
OPL	1.51 ± 0.01	1.51 ± 0.01 †	1.51 ± 0.01
ONL+IS	1.78 ± 0.03	1.79 ± 0.04	1.78 ± 0.03
OS	1.70 ± 0.02	1.70 ± 0.01	1.70 ± 0.01
RPE	1.68 ± 0.01	1.68 ± 0.01	1.68 ± 0.01
Foveal Region			
RNFL	2.22 ± 0.07	2.24 ± 0.08	2.30 ± 0.09 †
GCL+IPL	1.90 ± 0.01	1.89 ± 0.01	1.88 ± 0.01 †
INL	2.02 ± 0.02	2.02 ± 0.01	2.03 ± 0.03
OPL	1.49 ± 0.01	1.48 ± 0.01	1.49 ± 0.01
ONL+IS	1.76 ± 0.03	1.77 ± 0.04	1.75 ± 0.03
OS	1.71 ± 0.02	1.71 ± 0.01	1.70 ± 0.02
RPE	1.67 ± 0.01	1.67 ± 0.01	1.67 ± 0.01
Parafoveal Region			
RNFL	1.53 ± 0.05	1.55 ± 0.06	1.63 ± 0.12 ‡
GCL+IPL	1.56 ± 0.01	1.55 ± 0.01	1.54 ± 0.01 †
INL	1.67 ± 0.01	1.67 ± 0.01	1.67 ± 0.01
OPL	1.51 ± 0.01	1.51 ± 0.01	1.51 ± 0.01
ONL+IS	1.79 ± 0.03	1.79 ± 0.04	1.78 ± 0.03
OS	1.70 ± 0.02	1.69 ± 0.02	1.69 ± 0.02
RPE	1.69 ± 0.02	1.69 ± 0.02	1.69 ± 0.02
Perifoveal Region			
RNFL	1.52 ± 0.04	1.52 ± 0.03	1.55 ± 0.05 †
GCL+IPL	1.60 ± 0.01	1.60 ± 0.01	1.59 ± 0.01 †
INL	1.68 ± 0.01	1.68 ± 0.01	1.68 ± 0.01
OPL	1.52 ± 0.01	1.52 ± 0.01 †	1.52 ± 0.01
ONL+IS	1.79 ± 0.03	1.81 ± 0.03	1.80 ± 0.03
OS	1.70 ± 0.02	1.69 ± 0.01	1.70 ± 0.01
RPE	1.69 ± 0.01	1.69 ± 0.02	1.68 ± 0.02

† $0.001<p<0.05$ and ‡ $p<0.001$ (ANOVA followed by Newman-Keuls post hoc analysis) between MS ON- and healthy eyes (see MS ON- column) and between MS ON- and MS ON+ eyes (see MS ON+ column).

Table 7.4 Distribution statistics of the mean reflectance (dB) of intraretinal layers by study groups

Mean Reflectance (dB)	Healthy	MS ON-	MS ON+
Across All Macular Regions			
RNFL	54.38 ± 1.54	53.28 ± 1.27 †	52.99 ± 1.14
GCL+IPL	50.43 ± 2.13	49.60 ± 1.57	50.35 ± 1.35
INL	47.06 ± 2.60	45.95 ± 1.83	46.57 ± 1.72
OPL	48.89 ± 2.40	47.93 ± 1.63	48.44 ± 1.45
ONL+IS	44.50 ± 2.61	42.91 ± 2.03	43.64 ± 1.93
OS	56.57 ± 1.37	55.44 ± 1.50 †	55.78 ± 1.21
RPE	58.53 ± 1.08	57.95 ± 0.77	58.27 ± 0.68
Foveal Region			
RNFL	52.09 ± 1.81	51.36 ± 1.76	51.72 ± 1.04
GCL+IPL	49.92 ± 2.25	49.28 ± 1.72	50.42 ± 1.36
INL	47.26 ± 2.72	46.36 ± 1.98	47.09 ± 1.57
OPL	48.94 ± 2.43	48.17 ± 1.71	48.76 ± 1.20
ONL+IS	44.69 ± 2.73	43.17 ± 2.32	44.07 ± 1.87
OS	56.47 ± 1.47	55.36 ± 1.77	55.78 ± 1.23
RPE	59.09 ± 1.15	58.49 ± 0.91	58.77 ± 0.68
Parafoveal Region			
RNFL	53.82 ± 1.69	52.91 ± 1.55	52.66 ± 1.13
GCL+IPL	50.27 ± 2.19	49.60 ± 1.68	50.56 ± 1.37
INL	46.94 ± 2.69	45.89 ± 1.91	46.70 ± 1.70
OPL	49.34 ± 2.42	48.55 ± 1.60	49.17 ± 1.44
ONL+IS	44.93 ± 2.68	43.39 ± 2.04	44.23 ± 1.94
OS	57.20 ± 1.43	56.09 ± 1.69	56.44 ± 1.30
RPE	58.68 ± 1.12	58.04 ± 0.81	58.43 ± 0.72
Perifoveal Region			
RNFL	54.82 ± 1.53	53.62 ± 1.19 †	53.18 ± 1.18
GCL+IPL	50.63 ± 2.15	49.68 ± 1.59	50.24 ± 1.38
INL	47.01 ± 2.60	45.81 ± 1.87	46.33 ± 1.82
OPL	48.64 ± 2.50	47.48 ± 1.81	47.94 ± 1.66
ONL+IS	44.37 ± 2.66	42.69 ± 2.06	43.27 ± 2.03
OS	56.69 ± 1.40	55.56 ± 1.40 †	55.82 ± 1.25
RPE	58.09 ± 1.12	57.52 ± 0.76	57.84 ± 0.74

† $0.001<p<0.05$ and ‡ $p<0.001$ (ANOVA followed by Newman-Keuls post hoc analysis) between MS ON- and healthy eyes (see MS ON- column) and between MS ON- and MS ON+ eyes (see MS ON+ column).

Table 7.5 Distribution statistics of the total reflectance (dB) of intraretinal layers by study groups

Total Reflectance (dB)	Healthy	MS ON-	MS ON+
Across All Macular Regions			
RNFL	81.41 ± 1.77	79.76 ± 1.20 †	78.67 ± 1.57 †
GCL+IPL	82.49 ± 2.23	80.74 ± 1.42 †	80.01 ± 1.39
INL	72.41 ± 2.59	71.51 ± 1.93	72.20 ± 1.84
OPL	75.70 ± 2.57	74.76 ± 1.50	75.14 ± 1.51
ONL+IS	77.34 ± 2.77	75.80 ± 2.12	76.62 ± 1.56
OS	75.44 ± 1.49	74.96 ± 1.09	75.58 ± 1.24
RPE	75.70 ± 1.05	75.34 ± 0.99	75.60 ± 1.04
Foveal Region			
RNFL	77.15 ± 1.87	76.29 ± 1.94	75.92 ± 1.86
GCL+IPL	83.46 ± 2.31	81.98 ± 1.69 †	81.94 ± 1.34
INL	72.81 ± 2.69	72.19 ± 1.99	73.04 ± 1.72
OPL	78.94 ± 2.72	77.94 ± 1.57	78.25 ± 1.55
ONL+IS	78.63 ± 2.86	77.21 ± 2.37	78.18 ± 1.52
OS	76.11 ± 1.65	75.79 ± 1.12	76.60 ± 1.30
RPE	76.33 ± 0.98	76.03 ± 0.95	76.28 ± 0.99
Parafoveal Region			
RNFL	79.70 ± 1.80	78.44 ± 1.51 †	77.60 ± 1.45
GCL+IPL	83.96 ± 2.25	82.18 ± 1.48 †	81.56 ± 1.30
INL	73.31 ± 2.64	72.55 ± 2.06	73.48 ± 1.89
OPL	75.24 ± 2.56	74.51 ± 1.68	75.20 ± 1.61
ONL+IS	77.61 ± 2.81	76.07 ± 2.14	76.97 ± 1.55
OS	75.40 ± 1.64	75.12 ± 1.39	75.94 ± 1.45
RPE	75.11 ± 1.10	74.84 ± 1.38	74.95 ± 1.41
Perifoveal Region			
RNFL	82.37 ± 1.84	80.52 ± 1.10 †	79.15 ± 1.67 †
GCL+IPL	81.46 ± 2.31	79.57 ± 1.64 †	78.49 ± 1.61
INL	71.88 ± 2.61	70.78 ± 2.00	71.33 ± 1.94
OPL	73.21 ± 2.60	72.19 ± 1.92	72.57 ± 1.74
ONL+IS	76.12 ± 2.80	74.42 ± 2.17	75.09 ± 1.73
OS	74.85 ± 1.59	74.32 ± 1.14	74.64 ± 1.38
RPE	75.14 ± 1.21	74.69 ± 1.13	75.02 ± 1.15

† $0.001<p<0.05$ and ‡ $p<0.001$ (ANOVA followed by Newman-Keuls post hoc analysis) between MS ON- and healthy eyes (see MS ON- column) and between MS ON- and MS ON+ eyes (see MS ON+ column).

Table 7.6 Distribution statistics of the layer index (a.u.) of intraretinal layers by study groups

Layer Index	Healthy	MS ON-	MS ON+
Across All Macular Regions			
RNFL	12.38 ± 1.36	10.83 ± 0.80 ‡	9.34 ± 1.39 ‡
GCL+IPL	13.81 ± 2.10	11.83 ± 1.12 †	10.65 ± 1.18
INL	4.36 ± 0.84	4.13 ± 0.67	4.36 ± 0.74
OPL	6.28 ± 1.25	5.88 ± 0.78	5.98 ± 0.87
ONL+IS	7.59 ± 1.58	6.64 ± 1.14	7.07 ± 0.91
OS	6.09 ± 0.77	6.06 ± 0.47	6.34 ± 0.77
RPE	6.26 ± 0.52	6.34 ± 0.50	6.34 ± 0.56
Foveal Region			
RNFL	7.27 ± 0.93	6.95 ± 1.07	6.59 ± 1.19
GCL+IPL	14.93 ± 2.50	13.21 ± 1.81 †	12.76 ± 1.45
INL	4.42 ± 0.95	4.31 ± 0.79	4.62 ± 0.82
OPL	8.95 ± 2.04	8.26 ± 1.18	8.30 ± 1.38
ONL+IS	8.55 ± 1.85	7.57 ± 1.43	8.16 ± 1.08
OS	6.37 ± 0.99	6.39 ± 0.64	6.86 ± 0.99
RPE	6.48 ± 0.63	6.60 ± 0.73	6.56 ± 0.64
Parafoveal Region			
RNFL	9.84 ± 1.05	8.95 ± 0.82 †	7.95 ± 1.10 †
GCL+IPL	16.11 ± 2.53	13.72 ± 1.30 †	12.43 ± 1.21
INL	4.75 ± 0.96	4.58 ± 0.83	4.95 ± 0.92
OPL	5.96 ± 1.26	5.74 ± 1.00	6.02 ± 0.95
ONL+IS	7.75 ± 1.62	6.78 ± 1.17	7.28 ± 0.91
OS	6.02 ± 1.00	6.10 ± 0.75	6.54 ± 1.02
RPE	5.79 ± 0.64	5.94 ± 0.81	5.83 ± 0.84
Perifoveal Region			
RNFL	14.02 ± 1.69	12.00 ± 0.88 ‡	10.04 ± 1.66 ‡
GCL+IPL	12.56 ± 1.96	10.66 ± 1.28 †	9.25 ± 1.33 †
INL	4.19 ± 0.80	3.90 ± 0.64	4.05 ± 0.68
OPL	4.87 ± 0.94	4.57 ± 0.75	4.64 ± 0.71
ONL+IS	6.79 ± 1.42	5.89 ± 1.05	6.18 ± 0.87
OS	5.88 ± 0.75	5.84 ± 0.46	5.93 ± 0.77
RPE	6.07 ± 0.55	6.10 ± 0.53	6.17 ± 0.56

† $0.001<p<0.05$ and ‡ $p<0.001$ (ANOVA followed by Newman-Keuls post hoc analysis) between MS ON- and healthy eyes (see MS ON- column) and between MS ON- and MS ON+ eyes (see MS ON+ column).

Table 7.7 Distribution statistics of scattering coefficients (mm^{-1}) calculated by using the single-scattering model with the normalization method NRIR by study groups

Scattering Coefficients (Single, NRIR)	Healthy	MS ON-	MS ON+
Across All Macular Regions			
RNFL	3.56 ± 0.50	3.60 ± 0.58	4.36 ± 1.02 ‡
GCL+IPL	1.70 ± 0.19	1.75 ± 0.16	2.03 ± 0.28 †
INL	2.90 ± 0.46	2.78 ± 0.31	2.90 ± 0.30
OPL	2.07 ± 0.40	2.01 ± 0.31	2.02 ± 0.37
ONL+IS	2.80 ± 0.40	2.69 ± 0.46	2.72 ± 0.52
OS	8.90 ± 1.56	9.19 ± 1.60	9.25 ± 1.99
RPE	10.12 ± 1.36	11.27 ± 1.15 ‡	10.88 ± 1.27
Foveal Region			
RNFL	4.15 ± 1.14	4.21 ± 1.65	6.11 ± 3.30 ‡
GCL+IPL	1.36 ± 0.26	1.51 ± 0.36	1.77 ± 0.27 †
INL	2.38 ± 0.35	2.32 ± 0.30	2.37 ± 0.27
OPL	1.54 ± 0.26	1.52 ± 0.27	1.59 ± 0.22
ONL+IS	1.96 ± 0.35	1.71 ± 0.39 †	1.63 ± 0.46
OS	11.15 ± 2.89	11.08 ± 2.32	9.90 ± 2.81
RPE	9.64 ± 1.22	10.67 ± 1.26 †	10.59 ± 0.91
Parafoveal Region			
RNFL	3.45 ± 0.49	3.73 ± 0.57	5.04 ± 1.55 ‡
GCL+IPL	1.06 ± 0.10	1.21 ± 0.15 †	1.50 ± 0.28 ‡
INL	2.17 ± 0.30	2.13 ± 0.21	2.14 ± 0.20
OPL	1.79 ± 0.30	1.78 ± 0.24	1.80 ± 0.23
ONL+IS	2.46 ± 0.42	2.17 ± 0.54	2.15 ± 0.69
OS	10.79 ± 2.62	10.54 ± 1.95	9.33 ± 2.18
RPE	9.97 ± 1.14	11.47 ± 1.50 ‡	11.35 ± 1.12
Perifoveal Region			
RNFL	3.31 ± 0.33	3.42 ± 0.47	4.16 ± 1.03 ‡
GCL+IPL	1.93 ± 0.15	2.00 ± 0.16	2.16 ± 0.21 †
INL	2.82 ± 0.39	2.79 ± 0.29	2.87 ± 0.29
OPL	2.02 ± 0.36	1.98 ± 0.24	1.97 ± 0.31
ONL+IS	2.74 ± 0.37	2.54 ± 0.41	2.59 ± 0.51
OS	9.00 ± 1.47	9.39 ± 1.48	9.09 ± 1.53
RPE	9.97 ± 1.23	11.64 ± 1.46 ‡	11.16 ± 1.25

† $0.001<p<0.05$ and ‡ $p<0.001$ (ANOVA followed by Newman-Keuls post hoc analysis) between MS ON- and healthy eyes (see MS ON- column) and between MS ON- and MS ON+ eyes (see MS ON+ column).

Table 7.8 Distribution statistics of scattering coefficients (mm^{-1}) calculated by using the single-scattering model with the normalization method NRPE by study groups

Scattering Coefficients (Single, NRPE)	Healthy	MS ON-	MS ON+
Across All Macular Regions			
RNFL	5.29 ± 0.55	5.37 ± 0.60	6.32 ± 1.21 ‡
GCL+IPL	2.56 ± 0.21	2.64 ± 0.20	2.97 ± 0.29 ‡
INL	4.29 ± 0.51	4.13 ± 0.32	4.24 ± 0.36
OPL	3.02 ± 0.46	2.95 ± 0.28	2.91 ± 0.40
ONL+IS	4.16 ± 0.67	4.02 ± 0.79	3.97 ± 0.83
OS	13.07 ± 2.42	13.49 ± 2.20	13.32 ± 2.78
RPE	14.68 ± 2.02	16.3 ± 1.50 †	15.46 ± 1.61
Foveal Region			
RNFL	5.68 ± 1.48	5.82 ± 2.28	8.21 ± 4.18 ‡
GCL+IPL	1.83 ± 0.31	2.03 ± 0.44	2.35 ± 0.31 †
INL	3.21 ± 0.43	3.12 ± 0.36	3.16 ± 0.33
OPL	2.05 ± 0.30	2.02 ± 0.30	2.10 ± 0.26
ONL+IS	2.61 ± 0.47	2.27 ± 0.50 †	2.14 ± 0.59
OS	14.50 ± 3.70	14.41 ± 2.66	12.80 ± 3.49
RPE	12.63 ± 1.69	13.92 ± 1.73 †	13.57 ± 1.09
Parafoveal Region			
RNFL	4.86 ± 0.60	5.24 ± 0.63	6.90 ± 1.90 ‡
GCL+IPL	1.49 ± 0.14	1.71 ± 0.17 ‡	2.07 ± 0.33 ‡
INL	3.06 ± 0.37	2.99 ± 0.25	2.97 ± 0.27
OPL	2.50 ± 0.37	2.49 ± 0.23	2.47 ± 0.24
ONL+IS	3.45 ± 0.63	3.05 ± 0.83	2.97 ± 1.00
OS	14.77 ± 3.57	14.54 ± 2.78	12.67 ± 3.03
RPE	13.75 ± 1.70	15.73 ± 2.04 †	15.24 ± 1.53
Perifoveal Region			
RNFL	4.90 ± 0.37	5.02 ± 0.46	6.06 ± 1.28 ‡
GCL+IPL	2.92 ± 0.26	2.98 ± 0.20	3.23 ± 0.35 †
INL	4.22 ± 0.47	4.14 ± 0.30	4.28 ± 0.39
OPL	2.98 ± 0.44	2.90 ± 0.21	2.97 ± 0.64
ONL+IS	4.08 ± 0.64	3.77 ± 0.70	3.85 ± 0.87
OS	13.22 ± 2.26	13.68 ± 1.94	13.32 ± 1.79
RPE	14.52 ± 1.79	16.77 ± 1.84 ‡	15.96 ± 1.59

† $0.001<p<0.05$ and ‡ $p<0.001$ (ANOVA followed by Newman-Keuls post hoc analysis) between MS ON- and healthy eyes (see MS ON- column) and between MS ON- and MS ON+ eyes (see MS ON+ column).

Table 7.9 Distribution statistics of scattering coefficients (mm^{-1}) calculated by using the multiple-scattering model with the normalization method NRIR by study groups

Scattering Coefficients (Multiple, NRIR)	Healthy	MS ON-	MS ON+
Across All Macular Regions			
RNFL	3.81 ± 0.34	3.75 ± 0.43	4.27 ± 0.99 †
GCL+IPL	1.98 ± 0.23	2.09 ± 0.18	2.45 ± 0.33 ‡
INL	3.53 ± 0.49	3.36 ± 0.33	3.50 ± 0.35
OPL	3.19 ± 0.44	3.13 ± 0.32	3.12 ± 0.40
ONL+IS	2.55 ± 0.34	2.33 ± 0.26	2.36 ± 0.38
OS	10.91 ± 1.54	11.22 ± 1.52	11.18 ± 1.95
RPE	12.32 ± 1.38	13.43 ± 1.09 †	13.06 ± 1.25
Foveal Region			
RNFL	4.09 ± 1.16	3.76 ± 1.43	5.65 ± 3.40 †
GCL+IPL	1.49 ± 0.17	1.58 ± 0.21	1.79 ± 0.29 †
INL	2.93 ± 0.40	2.81 ± 0.31	2.86 ± 0.29
OPL	2.29 ± 0.25	2.27 ± 0.26	2.34 ± 0.21
ONL+IS	1.75 ± 0.24	1.53 ± 0.27 †	1.58 ± 0.35
OS	14.13 ± 2.66	13.93 ± 2.32	13.00 ± 2.48
RPE	11.76 ± 1.20	12.80 ± 1.25 †	12.80 ± 0.95
Parafoveal Region			
RNFL	3.65 ± 0.38	3.64 ± 0.35	4.76 ± 1.48 ‡
GCL+IPL	1.35 ± 0.14	1.48 ± 0.21 †	1.76 ± 0.26 ‡
INL	2.63 ± 0.35	2.56 ± 0.23	2.54 ± 0.25
OPL	2.83 ± 0.31	2.80 ± 0.27	2.81 ± 0.23
ONL+IS	2.15 ± 0.29	1.89 ± 0.31	1.93 ± 0.48
OS	13.14 ± 2.5	12.82 ± 1.97	11.68 ± 1.99
RPE	12.07 ± 1.19	13.65 ± 1.55 ‡	13.48 ± 1.04
Perifoveal Region			
RNFL	3.49 ± 0.23	3.55 ± 0.33	4.14 ± 1.02 ‡
GCL+IPL	1.90 ± 0.17	2.07 ± 0.22 †	2.47 ± 0.35 ‡
INL	3.44 ± 0.43	3.36 ± 0.32 †	3.47 ± 0.36 ‡
OPL	3.14 ± 0.39	3.09 ± 0.25	3.06 ± 0.30
ONL+IS	2.49 ± 0.29	2.22 ± 0.25 †	2.27 ± 0.41
OS	11.01 ± 1.45	11.38 ± 1.43	11.04 ± 1.48
RPE	12.18 ± 1.23	13.81 ± 1.39 ‡	13.31 ± 1.26

† $0.001<p<0.05$ and ‡ $p<0.001$ (ANOVA followed by Newman-Keuls post hoc analysis) between MS ON- and healthy eyes (see MS ON- column) and between MS ON- and MS ON+ eyes (see MS ON+ column).

Table 7.10 Distribution statistics of scattering coefficients (mm^{-1}) calculated by using the multiple-scattering model with the normalization method NRPE by study groups

Scattering Coefficients (Multiple, NRPE)	Healthy	MS ON-	MS ON+
Across All Macular Regions			
RNFL	5.46 ± 0.44	5.39 ± 0.50	6.02 ± 1.23 †
GCL+IPL	2.71 ± 0.23	2.88 ± 0.16 †	3.32 ± 0.35 ‡
INL	4.90 ± 0.54	4.68 ± 0.37	4.81 ± 0.44
OPL	4.33 ± 0.44	4.27 ± 0.27	4.19 ± 0.40
ONL+IS	3.45 ± 0.43	3.18 ± 0.36	3.17 ± 0.53
OS	15.14 ± 2.36	15.61 ± 2.13	15.30 ± 2.72
RPE	16.85 ± 2.06	18.41 ± 1.42 †	17.60 ± 1.52
Foveal Region			
RNFL	5.49 ± 1.56	5.06 ± 2.02	7.45 ± 4.33 †
GCL+IPL	1.87 ± 0.20	1.99 ± 0.26	2.24 ± 0.34 †
INL	3.74 ± 0.48	3.58 ± 0.38	3.61 ± 0.33
OPL	2.88 ± 0.28	2.85 ± 0.28	2.92 ± 0.25
ONL+IS	2.20 ± 0.28	1.93 ± 0.30 †	1.97 ± 0.41
OS	17.82 ± 3.41	17.58 ± 2.79	16.26 ± 3.12
RPE	14.74 ± 1.69	16.01 ± 1.67 †	15.76 ± 1.11
Parafoveal Region			
RNFL	5.00 ± 0.53	5.00 ± 0.50	6.38 ± 1.85 ‡
GCL+IPL	1.75 ± 0.16	1.93 ± 0.23 †	2.26 ± 0.30 ‡
INL	3.45 ± 0.42	3.35 ± 0.27	3.28 ± 0.31
OPL	3.69 ± 0.35	3.66 ± 0.26	3.61 ± 0.21
ONL+IS	2.80 ± 0.38	2.48 ± 0.40	2.49 ± 0.60
OS	17.30 ± 3.40	16.96 ± 2.83	15.18 ± 2.77
RPE	15.82 ± 1.74	17.89 ± 2.06 †	17.31 ± 1.40
Perifoveal Region			
RNFL	4.97 ± 0.35	5.00 ± 0.31	5.87 ± 1.33 ‡
GCL+IPL	2.62 ± 0.21	2.84 ± 0.25 †	3.43 ± 0.47 ‡
INL	4.82 ± 0.53	4.67 ± 0.35	4.89 ± 0.58
OPL	4.28 ± 0.43	4.19 ± 0.19	4.24 ± 0.65
ONL+IS	3.38 ± 0.38	3.02 ± 0.33 †	3.13 ± 0.66
OS	15.29 ± 2.20	15.73 ± 1.88	15.32 ± 1.77
RPE	16.72 ± 1.79	18.89 ± 1.74 ‡	18.06 ± 1.58

† $0.001<p<0.05$ and ‡ $p<0.001$ (ANOVA followed by Newman-Keuls post hoc analysis) between MS ON- and healthy eyes (see MS ON- column) and between MS ON- and MS ON+ eyes (see MS ON+ column).

Table 7.11 AUROC values of thickness measurements (µm) by study groups

AUROC	MS ON- vs. Healthy	MS ON+ vs. MS ON-
Across All Macular Regions		
RNFL	0.82 **	0.84 **
GCL+IPL	0.90 **	0.89 **
INL	0.39	0.46
OPL	0.53	0.61
ONL+IS	0.48	0.49
OS	0.32	0.40
RPE	0.41	0.53
Foveal Region		
RNFL	0.57	0.70 *
GCL+IPL	0.85 **	0.82 **
INL	0.41	0.52
OPL	0.58	0.61
ONL+IS	0.47	0.46
OS	0.35	0.39
RPE	0.42	0.53
Parafoveal region		
RNFL	0.77 *	0.80 **
GCL+IPL	0.90 **	0.88 **
INL	0.31	0.42
OPL	0.47	0.43
ONL+IS	0.49	0.50
OS	0.34	0.39
RPE	0.39	0.55
Perifoveal Region		
RNFL	0.81 **	0.86 **
GCL+IPL	0.85 **	0.85 **
INL	0.46	0.48
OPL	0.38	0.53
ONL+IS	0.50	0.45
OS	0.34	0.46
RPE	0.47	0.47

*0.70≤AUROC<0.80, **0.80≤AUROC

Table 7.12 Cutoff values of the thickness measurement (μm) derived from ROC analyses between MS ON- and healthy eyes

Intraretinal Layer	AUROC	95% CI		Cutoff Point (μm)	Sensitivity	Specificity
		Lower Bound	Upper Bound			
Across All Macular Regions						
RNFL	0.82 ± 0.06	0.71	0.93	40.53	0.78	0.68
GCL+IPL	0.90 ± 0.05	0.79	1.00	73.07	0.88	0.78
INL	0.39 ± 0.08	0.24	0.55	34.94	0.53	0.43
OPL	0.53 ± 0.08	0.37	0.69	40.72	0.60	0.50
ONL+IS	0.48 ± 0.09	0.31	0.66	85.54	0.57	0.47
OS	0.32 ± 0.07	0.18	0.46	16.16	0.46	0.36
RPE	0.41 ± 0.08	0.26	0.57	12.82	0.46	0.36
Foveal Region						
RNFL	0.57 ± 0.08	0.40	0.73	8.21	0.57	0.47
GCL+IPL	0.85 ± 0.05	0.75	0.95	53.35	0.77	0.67
INL	0.41 ± 0.08	0.25	0.58	21.24	0.53	0.43
OPL	0.58 ± 0.08	0.43	0.73	60.16	0.60	0.50
ONL+IS	0.47 ± 0.09	0.30	0.64	99.75	0.53	0.43
OS	0.35 ± 0.07	0.20	0.49	18.31	0.46	0.36
RPE	0.42 ± 0.09	0.25	0.58	12.50	0.51	0.41
Parafoveal Region						
RNFL	0.77 ± 0.06	0.65	0.89	32.99	0.67	0.57
GCL+IPL	0.90 ± 0.05	0.81	1.00	88.84	0.89	0.79
INL	0.31 ± 0.08	0.15	0.47	40.06	0.41	0.31
OPL	0.47 ± 0.08	0.32	0.63	36.59	0.53	0.43
ONL+IS	0.49 ± 0.09	0.31	0.67	84.02	0.58	0.48
OS	0.34 ± 0.07	0.19	0.48	14.40	0.47	0.37
RPE	0.39 ± 0.09	0.22	0.56	11.77	0.50	0.40
Perifoveal Region						
RNFL	0.81 ± 0.06	0.70	0.92	39.52	0.80	0.70
GCL+IPL	0.85 ± 0.07	0.72	0.98	62.51	0.84	0.74
INL	0.46 ± 0.08	0.31	0.62	32.89	0.47	0.37
OPL	0.38 ± 0.07	0.23	0.52	31.47	0.46	0.36
ONL+IS	0.50 ± 0.09	0.32	0.68	74.70	0.53	0.43
OS	0.34 ± 0.07	0.20	0.47	14.66	0.42	0.32
RPE	0.47 ± 0.08	0.31	0.62	12.40	0.53	0.43

Table 7.13 Cutoff values of the thickness measurement (μm) derived from ROC analyses between MS ON+ and MS ON- eyes

Intraretinal Layer	AUROC	95% CI		Cutoff Point (μm)	Sensitivity	Specificity
		Lower Bound	Upper Bound			
Across All Macular Regions						
RNFL	0.84 ± 0.08	0.68	0.99	38.32	0.72	0.62
GCL+IPL	0.89 ± 0.06	0.76	1.01	65.22	0.87	0.77
INL	0.46 ± 0.12	0.23	0.69	35.21	0.56	0.46
OPL	0.61 ± 0.11	0.39	0.83	40.07	0.71	0.61
ONL+IS	0.49 ± 0.12	0.26	0.72	85.80	0.50	0.40
OS	0.40 ± 0.12	0.17	0.63	18.21	0.41	0.31
RPE	0.53 ± 0.12	0.30	0.75	12.98	0.57	0.47
Foveal Region						
RNFL	0.70 ± 0.10	0.50	0.91	6.99	0.72	0.62
GCL+IPL	0.82 ± 0.09	0.65	0.99	46.82	0.79	0.69
INL	0.52 ± 0.12	0.29	0.75	21.36	0.56	0.46
OPL	0.61 ± 0.11	0.39	0.83	57.21	0.71	0.61
ONL+IS	0.46 ± 0.11	0.24	0.69	99.73	0.56	0.46
OS	0.39 ± 0.11	0.16	0.61	20.73	0.41	0.31
RPE	0.53 ± 0.12	0.30	0.76	13.28	0.50	0.40
Parafoveal Region						
RNFL	0.80 ± 0.09	0.63	0.97	30.34	0.79	0.69
GCL+IPL	0.88 ± 0.07	0.75	1.01	76.14	0.79	0.69
INL	0.42 ± 0.11	0.20	0.65	40.99	0.50	0.40
OPL	0.43 ± 0.11	0.21	0.66	36.74	0.49	0.39
ONL+IS	0.50 ± 0.11	0.28	0.72	84.04	0.56	0.46
OS	0.39 ± 0.12	0.15	0.62	17.29	0.41	0.31
RPE	0.55 ± 0.11	0.33	0.77	12.06	0.50	0.40
Perifoveal Region						
RNFL	0.86 ± 0.07	0.72	1.00	36.46	0.72	0.62
GCL+IPL	0.85 ± 0.08	0.70	1.00	56.82	0.79	0.69
INL	0.48 ± 0.12	0.25	0.71	32.96	0.57	0.47
OPL	0.53 ± 0.12	0.30	0.75	31.66	0.56	0.46
ONL+IS	0.45 ± 0.11	0.23	0.67	75.14	0.50	0.40
OS	0.46 ± 0.12	0.23	0.69	15.57	0.56	0.46
RPE	0.47 ± 0.12	0.24	0.70	12.52	0.50	0.40

Table 7.14 AUROC values of the contrast (a.u.) by study groups

AUROC	MS ON- vs. Healthy	MS ON+ vs. MS ON-
Across All Macular Regions		
RNFL	0.21	0.10
GCL+IPL	0.25	0.22
INL	0.48	0.26
OPL	0.52	0.29
ONL+IS	0.45	0.44
OS	0.68	0.46
RPE	0.56	0.47
Foveal Region		
RNFL	0.49	0.23
GCL+IPL	0.32	0.15
INL	0.29	0.39
OPL	0.35	0.44
ONL+IS	0.45	0.59
OS	0.65	0.50
RPE	0.47	0.32
Parafoveal region		
RNFL	0.47	0.40
GCL+IPL	0.12	0.13
INL	0.70	0.63
OPL	0.66	0.56
ONL+IS	0.42	0.55
OS	0.51	0.50
RPE	0.41	0.40
Perifoveal Region		
RNFL	0.25	0.14
GCL+IPL	0.24	0.10
INL	0.58	0.43
OPL	0.49	0.46
ONL+IS	0.42	0.46
OS	0.46	0.50
RPE	0.37	0.55

*0.70≤AUROC<0.80, **0.80≤AUROC

Table 7.15 Cutoff values of the contrast (a.u.) derived from ROC analyses between MS ON+ and healthy eyes

Intraretinal Layer	AUROC	95% CI		Cutoff Point	Sensitivity	Specificity
		Lower Bound	Upper Bound			
Across All Macular Regions						
RNFL	0.21 ± 0.06	0.09	0.33	1575.85	0.35	0.25
GCL+IPL	0.25 ± 0.07	0.12	0.38	1486.45	0.39	0.29
INL	0.48 ± 0.09	0.30	0.66	1371.86	0.60	0.50
OPL	0.52 ± 0.09	0.33	0.70	1316.39	0.55	0.45
ONL+IS	0.45 ± 0.09	0.28	0.62	855.20	0.53	0.43
OS	0.68 ± 0.07	0.54	0.82	3397.46	0.70	0.60
RPE	0.56 ± 0.08	0.40	0.71	4910.18	0.60	0.50
Foveal Region						
RNFL	0.49 ± 0.08	0.33	0.65	2015.68	0.53	0.43
GCL+IPL	0.32 ± 0.08	0.16	0.49	2403.86	0.42	0.32
INL	0.29 ± 0.08	0.14	0.45	2101.30	0.37	0.27
OPL	0.35 ± 0.09	0.18	0.52	2098.00	0.39	0.29
ONL+IS	0.45 ± 0.10	0.26	0.64	962.72	0.53	0.43
OS	0.65 ± 0.07	0.51	0.80	3977.65	0.61	0.51
RPE	0.47 ± 0.09	0.30	0.64	7313.48	0.49	0.39
Parafoveal Region						
RNFL	0.47 ± 0.09	0.29	0.64	4801.52	0.50	0.40
GCL+IPL	0.12 ± 0.05	0.03	0.22	1924.27	0.24	0.14
INL	0.70 ± 0.08	0.55	0.85	3891.22	0.69	0.59
OPL	0.66 ± 0.08	0.51	0.82	4152.04	0.65	0.55
ONL+IS	0.42 ± 0.10	0.23	0.60	1098.32	0.47	0.37
OS	0.51 ± 0.07	0.37	0.65	3161.95	0.53	0.43
RPE	0.41 ± 0.08	0.25	0.57	8103.62	0.46	0.36
Perifoveal Region						
RNFL	0.25 ± 0.08	0.09	0.40	2289.46	0.38	0.28
GCL+IPL	0.24 ± 0.08	0.09	0.39	1917.35	0.32	0.22
INL	0.58 ± 0.09	0.40	0.77	3461.83	0.61	0.51
OPL	0.49 ± 0.09	0.32	0.65	3990.89	0.53	0.43
ONL+IS	0.42 ± 0.09	0.25	0.59	1272.28	0.47	0.37
OS	0.46 ± 0.08	0.30	0.63	4138.14	0.50	0.40
RPE	0.37 ± 0.09	0.19	0.54	7366.59	0.85	0.46

Table 7.16 Cutoff values of the contrast (a.u.) derived from ROC analyses between MS ON+ and MS ON- eyes

Intraretinal Layer	AUROC	95% CI		Cutoff Point	Sensitivity	Specificity
		Lower Bound	Upper Bound			
Across All Macular Regions						
RNFL	0.10 ± 0.06	-0.03	0.23	1697.76	0.21	0.11
GCL+IPL	0.22 ± 0.09	0.04	0.40	1553.90	0.36	0.26
INL	0.26 ± 0.10	0.07	0.45	1440.51	0.41	0.31
OPL	0.29 ± 0.10	0.09	0.49	1356.04	0.36	0.26
ONL+IS	0.44 ± 0.12	0.21	0.67	864.04	0.41	0.31
OS	0.46 ± 0.12	0.24	0.69	3341.82	0.49	0.39
RPE	0.47 ± 0.12	0.25	0.70	4941.70	0.50	0.40
Foveal Region						
RNFL	0.23 ± 0.09	0.04	0.41	2145.89	0.36	0.26
GCL+IPL	0.15 ± 0.08	0.00	0.29	2519.03	0.29	0.19
INL	0.39 ± 0.11	0.17	0.61	2409.36	0.50	0.40
OPL	0.44 ± 0.11	0.22	0.66	2219.98	0.56	0.46
ONL+IS	0.59 ± 0.11	0.37	0.81	950.12	0.64	0.54
OS	0.50 ± 0.12	0.27	0.72	3713.14	0.57	0.47
RPE	0.32 ± 0.11	0.12	0.53	7579.20	0.49	0.39
Parafoveal Region						
RNFL	0.40 ± 0.11	0.18	0.61	5242.04	0.49	0.39
GCL+IPL	0.13 ± 0.07	-0.01	0.26	2146.21	0.33	0.23
INL	0.63 ± 0.11	0.41	0.84	3785.80	0.64	0.54
OPL	0.56 ± 0.11	0.33	0.78	4075.88	0.56	0.46
ONL+IS	0.55 ± 0.11	0.33	0.77	1097.91	0.64	0.54
OS	0.50 ± 0.12	0.27	0.73	3403.19	0.50	0.40
RPE	0.40 ± 0.11	0.18	0.62	8296.33	0.56	0.46
Perifoveal Region						
RNFL	0.14 ± 0.07	-0.01	0.28	2552.27	0.25	0.15
GCL+IPL	0.10 ± 0.06	-0.02	0.22	2076.70	0.25	0.15
INL	0.43 ± 0.11	0.21	0.65	3421.51	0.56	0.46
OPL	0.46 ± 0.12	0.24	0.69	4083.63	0.56	0.46
ONL+IS	0.46 ± 0.12	0.24	0.69	1282.71	0.43	0.33
OS	0.50 ± 0.12	0.28	0.73	4154.32	0.57	0.47
RPE	0.55 ± 0.12	0.32	0.78	7513.11	0.50	0.40

Table 7.17 AUROC values of the fractal dimension (a.u.) by study groups

AUROC	MS ON- vs. Healthy	MS ON+ vs. MS ON-
Across All Macular Regions		
RNFL	0.44	0.24
GCL+IPL	0.70	0.73 *
INL	0.35	0.44
OPL	0.75 *	0.50
ONL+IS	0.42	0.58
OS	0.52	0.56
RPE	0.53	0.55
Foveal Region		
RNFL	0.44	0.30
GCL+IPL	0.68	0.75 *
INL	0.42	0.40
OPL	0.66	0.45
ONL+IS	0.45	0.65
OS	0.55	0.63
RPE	0.52	0.48
Parafoveal region		
RNFL	0.47	0.26
GCL+IPL	0.61	0.69
INL	0.48	0.56
OPL	0.71 *	0.51
ONL+IS	0.43	0.57
OS	0.55	0.60
RPE	0.59	0.49
Perifoveal Region		
RNFL	0.59	0.42
GCL+IPL	0.67	0.67
INL	0.32	0.61
OPL	0.75 *	0.58
ONL+IS	0.37	0.53
OS	0.50	0.45
RPE	0.53	0.58

*0.70≤AUROC<0.80, **0.80≤AUROC

Table 7.18 Cutoff values of the fractal dimension (a.u.) derived from ROC analyses between MS ON+ and healthy eyes

Intraretinal Layer	AUROC	95% CI		Cutoff Point	Sensitivity	Specificity
		Lower Bound	Upper Bound			
Across All Macular Regions						
RNFL	0.44 ± 0.09	0.26	0.62	1.74	0.53	0.43
GCL+IPL	0.70 ± 0.08	0.54	0.85	1.68	0.74	0.64
INL	0.35 ± 0.07	0.22	0.48	1.78	0.45	0.35
OPL	0.75 ± 0.07	0.62	0.88	1.51	0.74	0.64
ONL+IS	0.42 ± 0.09	0.24	0.60	1.78	0.46	0.36
OS	0.52 ± 0.08	0.37	0.68	1.70	0.53	0.43
RPE	0.53 ± 0.09	0.35	0.70	1.68	0.60	0.50
Foveal Region						
RNFL	0.44 ± 0.09	0.27	0.60	2.22	0.53	0.43
GCL+IPL	0.68 ± 0.07	0.54	0.81	1.89	0.64	0.54
INL	0.42 ± 0.08	0.27	0.57	2.02	0.46	0.36
OPL	0.66 ± 0.08	0.50	0.82	1.48	0.67	0.57
ONL+IS	0.45 ± 0.09	0.27	0.63	1.76	0.53	0.43
OS	0.55 ± 0.07	0.41	0.69	1.71	0.53	0.43
RPE	0.52 ± 0.10	0.34	0.71	1.67	0.53	0.43
Parafoveal Region						
RNFL	0.47 ± 0.10	0.28	0.66	1.53	0.60	0.50
GCL+IPL	0.61 ± 0.09	0.44	0.79	1.55	0.60	0.50
INL	0.48 ± 0.08	0.31	0.64	1.67	0.53	0.43
OPL	0.71 ± 0.07	0.57	0.85	1.51	0.67	0.57
ONL+IS	0.43 ± 0.10	0.24	0.62	1.78	0.46	0.36
OS	0.55 ± 0.08	0.38	0.71	1.70	0.53	0.43
RPE	0.59 ± 0.10	0.40	0.79	1.68	0.66	0.56
Perifoveal Region						
RNFL	0.59 ± 0.07	0.45	0.72	1.53	0.60	0.50
GCL+IPL	0.67 ± 0.08	0.51	0.82	1.60	0.67	0.57
INL	0.32 ± 0.07	0.18	0.47	1.68	0.39	0.29
OPL	0.75 ± 0.06	0.64	0.85	1.52	0.72	0.62
ONL+IS	0.37 ± 0.09	0.20	0.53	1.79	0.46	0.36
OS	0.50 ± 0.08	0.34	0.66	1.69	0.54	0.44
RPE	0.53 ± 0.09	0.35	0.70	1.68	0.60	0.50

Table 7.19 Cutoff values of the fractal dimension (a.u.) derived from ROC analyses between MS ON+ and MS ON- eyes

Intraretinal Layer	AUROC	95% CI		Cutoff Point	Sensitivity	Specificity
		Lower Bound	Upper Bound			
Across All Macular Regions						
RNFL	0.24 ± 0.09	0.06	0.42	1.77	0.36	0.26
GCL+IPL	0.73 ± 0.10	0.54	0.93	1.67	0.71	0.61
INL	0.44 ± 0.12	0.21	0.67	1.78	0.50	0.40
OPL	0.50 ± 0.12	0.27	0.73	1.50	0.64	0.54
ONL+IS	0.58 ± 0.11	0.36	0.80	1.78	0.64	0.54
OS	0.56 ± 0.11	0.34	0.78	1.70	0.57	0.47
RPE	0.55 ± 0.11	0.33	0.77	1.68	0.56	0.46
Foveal Region						
RNFL	0.30 ± 0.10	0.10	0.51	2.26	0.41	0.31
GCL+IPL	0.75 ± 0.10	0.55	0.95	1.89	0.79	0.69
INL	0.40 ± 0.12	0.17	0.64	2.02	0.56	0.46
OPL	0.45 ± 0.12	0.22	0.67	1.48	0.50	0.40
ONL+IS	0.65 ± 0.11	0.44	0.87	1.76	0.71	0.61
OS	0.63 ± 0.11	0.41	0.85	1.71	0.64	0.54
RPE	0.48 ± 0.12	0.25	0.71	1.67	0.56	0.46
Parafoveal Region						
RNFL	0.26 ± 0.10	0.08	0.45	1.56	0.41	0.31
GCL+IPL	0.69 ± 0.10	0.48	0.89	1.54	0.64	0.54
INL	0.56 ± 0.12	0.33	0.78	1.67	0.57	0.47
OPL	0.51 ± 0.12	0.28	0.74	1.51	0.43	0.33
ONL+IS	0.57 ± 0.11	0.35	0.79	1.79	0.64	0.54
OS	0.60 ± 0.12	0.38	0.83	1.69	0.64	0.54
RPE	0.49 ± 0.11	0.27	0.71	1.68	0.50	0.40
Perifoveal Region						
RNFL	0.42 ± 0.12	0.19	0.65	1.53	0.57	0.47
GCL+IPL	0.67 ± 0.11	0.46	0.88	1.59	0.56	0.46
INL	0.61 ± 0.11	0.39	0.83	1.68	0.64	0.54
OPL	0.58 ± 0.12	0.35	0.80	1.52	0.64	0.54
ONL+IS	0.53 ± 0.11	0.30	0.75	1.80	0.57	0.47
OS	0.45 ± 0.12	0.22	0.67	1.70	0.49	0.39
RPE	0.58 ± 0.11	0.35	0.80	1.68	0.56	0.46

Table 7.20 AUROC values of the mean reflectance (dB) by study groups

AUROC	MS ON- vs. Healthy	MS ON+ vs. MS ON-
Across All Macular Regions		
RNFL	0.72 *	0.54
GCL+IPL	0.64	0.38
INL	0.65	0.41
OPL	0.65	0.41
ONL+IS	0.69	0.39
OS	0.70 *	0.45
RPE	0.67	0.36
Foveal Region		
RNFL	0.62	0.44
GCL+IPL	0.60	0.32
INL	0.62	0.38
OPL	0.62	0.41
ONL+IS	0.67	0.39
OS	0.68	0.44
RPE	0.66	0.39
Parafoveal region		
RNFL	0.65	0.56
GCL+IPL	0.61	0.36
INL	0.65	0.37
OPL	0.64	0.39
ONL+IS	0.68	0.37
OS	0.68	0.47
RPE	0.68	0.35
Perifoveal Region		
RNFL	0.73 *	0.57
GCL+IPL	0.66	0.39
INL	0.66	0.40
OPL	0.66	0.43
ONL+IS	0.69	0.41
OS	0.70	0.45
RPE	0.67	0.36

*0.70≤AUROC<0.80, **0.80≤AUROC

Table 7.21 Cutoff values of the mean reflectance (dB) derived from ROC analyses between MS ON- and healthy eyes

Intraretinal Layer	AUROC	95% CI		Cutoff Point	Sensitivity	Specificity
		Lower Bound	Upper Bound			
Across All Macular Regions						
RNFL	0.72 ± 0.07	0.59	0.85	53.57	0.70	0.60
GCL+IPL	0.64 ± 0.07	0.51	0.77	49.49	0.69	0.59
INL	0.65 ± 0.07	0.52	0.78	45.86	0.69	0.59
OPL	0.65 ± 0.07	0.52	0.77	47.90	0.70	0.60
ONL+IS	0.69 ± 0.07	0.56	0.82	42.93	0.72	0.62
OS	0.70 ± 0.07	0.56	0.85	55.95	0.66	0.56
RPE	0.67 ± 0.07	0.54	0.80	58.03	0.67	0.57
Foveal Region						
RNFL	0.62 ± 0.08	0.47	0.78	51.67	0.60	0.50
GCL+IPL	0.60 ± 0.07	0.46	0.74	49.37	0.61	0.51
INL	0.62 ± 0.07	0.48	0.76	46.55	0.62	0.52
OPL	0.62 ± 0.07	0.49	0.75	48.19	0.61	0.51
ONL+IS	0.67 ± 0.07	0.54	0.80	43.60	0.64	0.54
OS	0.68 ± 0.08	0.53	0.83	55.89	0.66	0.56
RPE	0.66 ± 0.07	0.52	0.81	58.65	0.60	0.50
Parafoveal Region						
RNFL	0.65 ± 0.08	0.50	0.80	53.24	0.62	0.52
GCL+IPL	0.61 ± 0.07	0.47	0.75	49.46	0.65	0.55
INL	0.65 ± 0.07	0.52	0.78	45.94	0.68	0.58
OPL	0.64 ± 0.07	0.51	0.77	48.39	0.72	0.62
ONL+IS	0.68 ± 0.07	0.55	0.81	43.44	0.72	0.62
OS	0.68 ± 0.08	0.53	0.83	56.64	0.67	0.57
RPE	0.68 ± 0.07	0.55	0.82	58.09	0.67	0.57
Perifoveal Region						
RNFL	0.73 ± 0.07	0.61	0.86	53.82	0.74	0.64
GCL+IPL	0.66 ± 0.07	0.52	0.79	49.76	0.69	0.59
INL	0.66 ± 0.07	0.53	0.79	46.13	0.68	0.58
OPL	0.66 ± 0.07	0.52	0.79	47.28	0.73	0.63
ONL+IS	0.69 ± 0.07	0.56	0.82	42.68	0.74	0.64
OS	0.70 ± 0.07	0.56	0.83	55.99	0.65	0.55
RPE	0.67 ± 0.07	0.54	0.80	57.68	0.70	0.60

Table 7.22 Cutoff values of the mean reflectance (dB) derived from ROC analyses between MS ON+ and MS ON- eyes

Intraretinal Layer	AUROC	95% CI		Cutoff Point	Sensitivity	Specificity
		Lower Bound	Upper Bound			
Across All Macular Regions						
RNFL	0.54 ± 0.12	0.31	0.76	53.07	0.50	0.40
GCL+IPL	0.38 ± 0.11	0.16	0.59	49.39	0.49	0.39
INL	0.41 ± 0.11	0.19	0.64	45.62	0.49	0.39
OPL	0.41 ± 0.11	0.19	0.63	47.69	0.49	0.39
ONL+IS	0.39 ± 0.11	0.17	0.61	42.78	0.43	0.33
OS	0.45 ± 0.11	0.22	0.67	55.73	0.57	0.47
RPE	0.36 ± 0.11	0.15	0.58	58.04	0.41	0.31
Foveal Region						
RNFL	0.44 ± 0.12	0.21	0.67	51.31	0.57	0.47
GCL+IPL	0.32 ± 0.10	0.12	0.53	49.40	0.49	0.39
INL	0.38 ± 0.11	0.16	0.59	46.43	0.49	0.39
OPL	0.41 ± 0.11	0.19	0.63	48.16	0.50	0.40
ONL+IS	0.39 ± 0.11	0.17	0.60	43.38	0.56	0.46
OS	0.44 ± 0.11	0.22	0.66	55.84	0.49	0.39
RPE	0.39 ± 0.11	0.17	0.61	58.59	0.50	0.40
Parafoveal Region						
RNFL	0.56 ± 0.12	0.32	0.79	52.71	0.50	0.40
GCL+IPL	0.36 ± 0.11	0.15	0.57	49.46	0.49	0.39
INL	0.37 ± 0.11	0.15	0.58	45.74	0.49	0.39
OPL	0.39 ± 0.11	0.17	0.61	48.35	0.41	0.31
ONL+IS	0.37 ± 0.11	0.16	0.59	43.39	0.41	0.31
OS	0.47 ± 0.12	0.25	0.70	56.17	0.56	0.46
RPE	0.35 ± 0.11	0.14	0.56	58.14	0.41	0.31
Perifoveal Region						
RNFL	0.57 ± 0.11	0.34	0.79	53.40	0.56	0.46
GCL+IPL	0.39 ± 0.11	0.17	0.61	49.53	0.50	0.40
INL	0.40 ± 0.11	0.17	0.62	45.36	0.49	0.39
OPL	0.43 ± 0.11	0.20	0.65	47.19	0.43	0.33
ONL+IS	0.41 ± 0.11	0.19	0.64	42.61	0.41	0.31
OS	0.45 ± 0.12	0.23	0.68	55.58	0.57	0.47
RPE	0.36 ± 0.11	0.15	0.58	57.52	0.43	0.33

Table 7.23 AUROC values of the total reflectance (dB) by study groups

AUROC	MS ON- vs. Healthy	MS ON+ vs. MS ON-
Across All Macular Regions		
RNFL	0.84 **	0.68
GCL+IPL	0.79 *	0.59
INL	0.60	0.42
OPL	0.62	0.45
ONL+IS	0.67	0.39
OS	0.50	0.35
RPE	0.45	0.44
Foveal Region		
RNFL	0.61	0.56
GCL+IPL	0.71 *	0.53
INL	0.55	0.36
OPL	0.62	0.47
ONL+IS	0.66	0.40
OS	0.50	0.31
RPE	0.46	0.42
Parafoveal region		
RNFL	0.75 *	0.63
GCL+IPL	0.81 **	0.61
INL	0.58	0.39
OPL	0.57	0.42
ONL+IS	0.68	0.37
OS	0.47	0.33
RPE	0.43	0.48
Perifoveal Region		
RNFL	0.85 **	0.74 *
GCL+IPL	0.79 *	0.63
INL	0.62	0.46
OPL	0.60	0.44
ONL+IS	0.69	0.39
OS	0.50	0.42
RPE	0.48	0.44

*0.70≤AUROC<0.80, **0.80≤AUROC

Table 7.24 Cutoff values of the total reflectance (dB) derived from ROC analyses between MS ON- and healthy eyes

Intraretinal Layer	AUROC	95% CI		Cutoff Point	Sensitivity	Specificity
		Lower Bound	Upper Bound			
Across All Macular Regions						
RNFL	0.78 ± 0.06	0.66	0.89	80.15	0.74	0.64
GCL+IPL	0.77 ± 0.05	0.66	0.88	80.89	0.80	0.70
INL	0.63 ± 0.07	0.49	0.76	71.65	0.67	0.57
OPL	0.67 ± 0.06	0.56	0.78	74.93	0.69	0.59
ONL+IS	0.67 ± 0.07	0.55	0.80	75.98	0.69	0.59
OS	0.64 ± 0.08	0.49	0.79	74.98	0.70	0.60
RPE	0.61 ± 0.08	0.45	0.77	75.36	0.68	0.58
Foveal Region						
RNFL	0.61 ± 0.08	0.45	0.77	76.90	0.53	0.43
GCL+IPL	0.71 ± 0.06	0.59	0.83	82.38	0.66	0.56
INL	0.60 ± 0.07	0.45	0.74	71.75	0.66	0.56
OPL	0.65 ± 0.06	0.54	0.77	78.56	0.60	0.50
ONL+IS	0.65 ± 0.07	0.51	0.79	77.63	0.61	0.51
OS	0.59 ± 0.08	0.44	0.74	75.61	0.67	0.57
RPE	0.62 ± 0.08	0.46	0.78	75.82	0.70	0.60
Parafoveal Region						
RNFL	0.71 ± 0.07	0.57	0.84	78.76	0.67	0.57
GCL+IPL	0.75 ± 0.06	0.64	0.86	82.72	0.70	0.60
INL	0.61 ± 0.07	0.47	0.75	72.40	0.68	0.58
OPL	0.64 ± 0.07	0.50	0.78	74.72	0.68	0.58
ONL+IS	0.67 ± 0.07	0.54	0.80	76.23	0.66	0.56
OS	0.58 ± 0.08	0.42	0.74	75.05	0.60	0.50
RPE	0.57 ± 0.09	0.39	0.74	74.88	0.60	0.50
Perifoveal Region						
RNFL	0.81 ± 0.05	0.71	0.91	81.25	0.74	0.64
GCL+IPL	0.77 ± 0.06	0.66	0.88	80.31	0.74	0.64
INL	0.64 ± 0.07	0.50	0.78	70.65	0.70	0.60
OPL	0.63 ± 0.07	0.49	0.77	71.74	0.73	0.63
ONL+IS	0.68 ± 0.07	0.55	0.81	74.47	0.72	0.62
OS	0.63 ± 0.07	0.48	0.77	74.18	0.70	0.60
RPE	0.62 ± 0.08	0.47	0.77	74.53	0.73	0.63

Table 7.25 Cutoff values of the total reflectance (dB) derived from ROC analyses between MS ON+ and MS ON- eyes

Intraretinal Layer	AUROC	95% CI		Cutoff Point	Sensitivity	Specificity
		Lower Bound	Upper Bound			
Across All Macular Regions						
RNFL	0.68 ± 0.10	0.48	0.89	79.05	0.64	0.54
GCL+IPL	0.59 ± 0.11	0.37	0.81	80.23	0.57	0.47
INL	0.42 ± 0.11	0.20	0.64	71.20	0.43	0.33
OPL	0.45 ± 0.12	0.22	0.67	74.63	0.50	0.40
ONL+IS	0.39 ± 0.11	0.17	0.61	75.81	0.49	0.39
OS	0.35 ± 0.11	0.14	0.56	74.83	0.49	0.39
RPE	0.44 ± 0.11	0.22	0.66	75.18	0.49	0.39
Foveal Region						
RNFL	0.56 ± 0.12	0.33	0.78	76.37	0.64	0.54
GCL+IPL	0.53 ± 0.12	0.30	0.75	82.03	0.57	0.47
INL	0.36 ± 0.11	0.15	0.58	72.04	0.43	0.33
OPL	0.47 ± 0.11	0.25	0.70	77.98	0.56	0.46
ONL+IS	0.40 ± 0.11	0.18	0.62	77.47	0.56	0.46
OS	0.31 ± 0.10	0.10	0.51	75.89	0.43	0.33
RPE	0.42 ± 0.11	0.20	0.64	75.74	0.49	0.39
Parafoveal Region						
RNFL	0.63 ± 0.11	0.42	0.85	77.69	0.64	0.54
GCL+IPL	0.61 ± 0.11	0.39	0.83	81.74	0.57	0.47
INL	0.39 ± 0.11	0.17	0.60	72.17	0.49	0.39
OPL	0.42 ± 0.11	0.20	0.64	74.53	0.56	0.46
ONL+IS	0.37 ± 0.11	0.16	0.59	76.24	0.41	0.31
OS	0.33 ± 0.11	0.12	0.54	75.01	0.49	0.39
RPE	0.48 ± 0.11	0.26	0.70	74.70	0.50	0.40
Perifoveal Region						
RNFL	0.74 ± 0.10	0.56	0.93	79.75	0.72	0.62
GCL+IPL	0.63 ± 0.11	0.41	0.84	78.73	0.64	0.54
INL	0.46 ± 0.12	0.23	0.68	70.30	0.49	0.39
OPL	0.44 ± 0.11	0.22	0.66	71.55	0.49	0.39
ONL+IS	0.39 ± 0.11	0.17	0.61	74.45	0.41	0.31
OS	0.42 ± 0.11	0.20	0.64	74.08	0.49	0.39
RPE	0.44 ± 0.12	0.21	0.67	74.48	0.43	0.33

Table 7.26 AUROC values of the layer index (a.u.) by study groups

AUROC	MS ON- vs. Healthy	MS ON+ vs. MS ON-
Across All Macular Regions		
RNFL	0.78 *	0.81 **
GCL+IPL	0.77 *	0.75 *
INL	0.63	0.43
OPL	0.67	0.48
ONL+IS	0.67	0.39
OS	0.64	0.40
RPE	0.61	0.49
Foveal Region		
RNFL	0.61	0.56
GCL+IPL	0.71 *	0.59
INL	0.60	0.37
OPL	0.65	0.52
ONL+IS	0.65	0.40
OS	0.59	0.32
RPE	0.62	0.52
Parafoveal region		
RNFL	0.71 *	0.75 *
GCL+IPL	0.75 *	0.76 *
INL	0.61	0.41
OPL	0.64	0.46
ONL+IS	0.67	0.37
OS	0.58	0.34
RPE	0.57	0.54
Perifoveal Region		
RNFL	0.81 **	0.86 **
GCL+IPL	0.77 *	0.73 *
INL	0.64	0.45
OPL	0.63	0.49
ONL+IS	0.68	0.41
OS	0.63	0.50
RPE	0.62	0.45

*0.70≤AUROC<0.80, **0.80≤AUROC

Table 7.27 Cutoff values of the layer index (a.u.) derived from ROC analyses between MS ON- and healthy eyes

Intraretinal Layer	AUROC	95% CI		Cutoff Point	Sensitivity	Specificity
		Lower Bound	Upper Bound			
Across All Macular Regions						
RNFL	0.84 ± 0.05	0.75	0.93	11.39	0.81	0.71
GCL+IPL	0.79 ± 0.05	0.69	0.89	12.34	0.81	0.71
INL	0.60 ± 0.08	0.45	0.75	4.13	0.66	0.56
OPL	0.62 ± 0.07	0.49	0.75	6.12	0.60	0.50
ONL+IS	0.67 ± 0.07	0.54	0.80	6.53	0.72	0.62
OS	0.50 ± 0.07	0.36	0.64	5.91	0.58	0.48
RPE	0.45 ± 0.08	0.28	0.61	6.15	0.53	0.43
Foveal Region						
RNFL	0.61 ± 0.09	0.44	0.78	7.03	0.65	0.55
GCL+IPL	0.71 ± 0.06	0.59	0.84	13.51	0.67	0.57
INL	0.55 ± 0.08	0.39	0.70	4.13	0.60	0.50
OPL	0.62 ± 0.07	0.49	0.75	8.23	0.67	0.57
ONL+IS	0.66 ± 0.07	0.52	0.80	7.55	0.67	0.57
OS	0.50 ± 0.07	0.35	0.64	6.30	0.53	0.43
RPE	0.46 ± 0.09	0.27	0.64	6.32	0.53	0.43
Parafoveal Region						
RNFL	0.75 ± 0.06	0.63	0.87	9.22	0.74	0.64
GCL+IPL	0.81 ± 0.05	0.72	0.90	14.72	0.80	0.70
INL	0.58 ± 0.08	0.43	0.73	4.51	0.60	0.50
OPL	0.57 ± 0.08	0.42	0.72	5.74	0.61	0.51
ONL+IS	0.68 ± 0.07	0.55	0.80	6.85	0.68	0.58
OS	0.47 ± 0.08	0.32	0.62	5.77	0.55	0.45
RPE	0.43 ± 0.10	0.24	0.61	5.80	0.53	0.43
Perifoveal Region						
RNFL	0.85 ± 0.05	0.77	0.94	12.50	0.84	0.74
GCL+IPL	0.79 ± 0.05	0.69	0.89	11.68	0.74	0.64
INL	0.62 ± 0.07	0.48	0.76	3.90	0.69	0.59
OPL	0.60 ± 0.08	0.46	0.75	4.65	0.67	0.57
ONL+IS	0.69 ± 0.07	0.56	0.81	6.04	0.70	0.60
OS	0.50 ± 0.07	0.35	0.64	5.72	0.53	0.43
RPE	0.48 ± 0.08	0.32	0.63	5.98	0.53	0.43

Table 7.28 Cutoff values of the layer index (a.u.) derived from ROC analyses between MS ON+ and MS ON- eyes

Intraretinal Layer	AUROC	95% CI		Cutoff Point	Sensitivity	Specificity
		Lower Bound	Upper Bound			
Across All Macular Regions						
RNFL	0.81 ± 0.08	0.64	0.97	10.07	0.79	0.69
GCL+IPL	0.75 ± 0.09	0.56	0.93	11.23	0.72	0.62
INL	0.43 ± 0.11	0.21	0.66	3.96	0.56	0.46
OPL	0.48 ± 0.12	0.25	0.71	5.60	0.57	0.47
ONL+IS	0.39 ± 0.11	0.17	0.61	6.41	0.49	0.39
OS	0.40 ± 0.12	0.17	0.62	5.97	0.49	0.39
RPE	0.49 ± 0.12	0.26	0.71	6.31	0.50	0.40
Foveal Region						
RNFL	0.56 ± 0.11	0.33	0.78	6.90	0.64	0.54
GCL+IPL	0.59 ± 0.11	0.38	0.81	12.92	0.64	0.54
INL	0.37 ± 0.11	0.15	0.58	4.15	0.49	0.39
OPL	0.52 ± 0.12	0.30	0.75	7.93	0.56	0.46
ONL+IS	0.40 ± 0.11	0.18	0.62	7.52	0.49	0.39
OS	0.32 ± 0.11	0.11	0.54	6.57	0.36	0.26
RPE	0.52 ± 0.12	0.29	0.75	6.59	0.50	0.40
Parafoveal Region						
RNFL	0.75 ± 0.09	0.57	0.94	8.33	0.71	0.61
GCL+IPL	0.76 ± 0.10	0.57	0.95	12.79	0.79	0.69
INL	0.41 ± 0.11	0.19	0.63	4.40	0.57	0.47
OPL	0.46 ± 0.11	0.23	0.68	5.58	0.56	0.46
ONL+IS	0.37 ± 0.11	0.15	0.58	6.76	0.49	0.39
OS	0.34 ± 0.11	0.12	0.56	6.16	0.41	0.31
RPE	0.54 ± 0.11	0.32	0.77	5.99	0.50	0.40
Perifoveal Region						
RNFL	0.86 ± 0.08	0.71	1.00	11.16	0.86	0.76
GCL+IPL	0.73 ± 0.10	0.53	0.93	9.83	0.72	0.62
INL	0.45 ± 0.12	0.22	0.67	3.73	0.49	0.39
OPL	0.49 ± 0.11	0.27	0.71	4.37	0.56	0.46
ONL+IS	0.41 ± 0.11	0.19	0.63	5.69	0.49	0.39
OS	0.50 ± 0.12	0.26	0.73	5.70	0.56	0.46
RPE	0.45 ± 0.11	0.23	0.67	6.07	0.56	0.46

Table 7.29 AUROC values of scattering coefficients (mm^{-1}) (calculated by using the single-scattering model with the normalization method NRIR) by study groups

AUROC	MS ON- vs. Healthy	MS ON+ vs. MS ON-
Across All Macular Regions		
RNFL	0.49	0.28
GCL+IPL	0.41	0.21
INL	0.61	0.37
OPL	0.61	0.50
ONL+IS	0.57	0.50
OS	0.46	0.52
RPE	0.24	0.60
Foveal Region		
RNFL	0.56	0.27
GCL+IPL	0.40	0.28
INL	0.57	0.42
OPL	0.52	0.41
ONL+IS	0.67	0.60
OS	0.52	0.68
RPE	0.26	0.47
Parafoveal region		
RNFL	0.35	0.17
GCL+IPL	0.20	0.20
INL	0.55	0.49
OPL	0.56	0.44
ONL+IS	0.68	0.56
OS	0.52	0.65
RPE	0.21	0.52
Perifoveal Region		
RNFL	0.44	0.25
GCL+IPL	0.36	0.28
INL	0.55	0.42
OPL	0.57	0.53
ONL+IS	0.64	0.48
OS	0.42	0.52
RPE	0.19	0.63

*0.70≤AUROC<0.80, **0.80≤AUROC

Table 7.30 Cutoff values of scattering coefficients (mm^{-1}) (calculated by using the single-scattering model with the normalization method NRIR) derived from ROC analyses between MS ON- and healthy eyes

Intraretinal Layer	AUROC	95% CI		Cutoff Point	Sensitivity	Specificity
		Lower Bound	Upper Bound			
Across All Macular Regions						
RNFL	0.49 ± 0.09	0.31	0.68	3.58	0.60	0.50
GCL+IPL	0.41 ± 0.08	0.25	0.58	1.73	0.47	0.37
INL	0.61 ± 0.07	0.47	0.76	2.75	0.67	0.57
OPL	0.61 ± 0.08	0.46	0.76	1.98	0.70	0.60
ONL+IS	0.57 ± 0.09	0.39	0.75	2.68	0.60	0.50
OS	0.46 ± 0.08	0.30	0.61	8.58	0.53	0.43
RPE	0.24 ± 0.07	0.10	0.38	10.78	0.31	0.21
Foveal Region						
RNFL	0.56 ± 0.09	0.38	0.73	3.64	0.62	0.52
GCL+IPL	0.40 ± 0.09	0.23	0.57	1.39	0.47	0.37
INL	0.57 ± 0.09	0.40	0.73	2.25	0.66	0.56
OPL	0.52 ± 0.09	0.35	0.70	1.53	0.55	0.45
ONL+IS	0.67 ± 0.08	0.51	0.84	1.79	0.67	0.57
OS	0.52 ± 0.08	0.37	0.68	10.59	0.60	0.50
RPE	0.26 ± 0.06	0.14	0.38	9.84	0.39	0.29
Parafoveal Region						
RNFL	0.35 ± 0.09	0.18	0.53	3.47	0.46	0.36
GCL+IPL	0.20 ± 0.08	0.04	0.35	1.11	0.31	0.21
INL	0.55 ± 0.08	0.39	0.70	2.10	0.60	0.50
OPL	0.56 ± 0.08	0.41	0.71	1.74	0.60	0.50
ONL+IS	0.68 ± 0.09	0.51	0.85	2.21	0.67	0.57
OS	0.52 ± 0.08	0.36	0.67	10.43	0.53	0.43
RPE	0.21 ± 0.08	0.06	0.37	10.35	0.31	0.21
Perifoveal Region						
RNFL	0.44 ± 0.09	0.26	0.62	3.36	0.46	0.36
GCL+IPL	0.36 ± 0.09	0.18	0.54	1.93	0.46	0.36
INL	0.55 ± 0.08	0.40	0.70	2.81	0.60	0.50
OPL	0.57 ± 0.08	0.42	0.72	1.99	0.65	0.55
ONL+IS	0.64 ± 0.09	0.46	0.82	2.63	0.70	0.60
OS	0.42 ± 0.09	0.26	0.59	8.94	0.46	0.36
RPE	0.19 ± 0.07	0.05	0.34	10.62	0.31	0.21

Table 7.31 Cutoff values of scattering coefficients (mm^{-1}) (calculated by using the single-scattering model with the normalization method NRIR) derived from ROC analyses between MS ON+ and MS ON- eyes

Intraretinal Layer	AUROC	95% CI		Cutoff Point	Sensitivity	Specificity
		Lower Bound	Upper Bound			
Across All Macular Regions						
RNFL	0.28 ± 0.10	0.08	0.47	3.82	0.43	0.33
GCL+IPL	0.21 ± 0.09	0.03	0.40	1.82	0.41	0.31
INL	0.37 ± 0.11	0.16	0.59	2.75	0.41	0.31
OPL	0.50 ± 0.12	0.27	0.73	1.94	0.56	0.46
ONL+IS	0.50 ± 0.12	0.27	0.72	2.58	0.64	0.54
OS	0.52 ± 0.12	0.30	0.75	8.54	0.57	0.47
RPE	0.60 ± 0.11	0.38	0.82	11.16	0.64	0.54
Foveal Region						
RNFL	0.27 ± 0.10	0.08	0.46	3.93	0.41	0.31
GCL+IPL	0.28 ± 0.10	0.08	0.47	1.58	0.43	0.33
INL	0.42 ± 0.12	0.19	0.64	2.25	0.43	0.33
OPL	0.41 ± 0.11	0.18	0.63	1.53	0.56	0.46
ONL+IS	0.60 ± 0.11	0.38	0.82	1.57	0.64	0.54
OS	0.68 ± 0.11	0.46	0.90	9.55	0.64	0.54
RPE	0.47 ± 0.12	0.24	0.70	10.34	0.41	0.31
Parafoveal Region						
RNFL	0.17 ± 0.08	0.02	0.32	3.94	0.41	0.31
GCL+IPL	0.20 ± 0.09	0.02	0.38	1.29	0.33	0.23
INL	0.49 ± 0.11	0.27	0.71	2.10	0.50	0.40
OPL	0.44 ± 0.11	0.22	0.66	1.72	0.50	0.40
ONL+IS	0.56 ± 0.12	0.33	0.79	1.95	0.64	0.54
OS	0.65 ± 0.11	0.44	0.87	9.50	0.71	0.61
RPE	0.52 ± 0.12	0.30	0.75	11.35	0.56	0.46
Perifoveal Region						
RNFL	0.25 ± 0.09	0.06	0.43	3.51	0.33	0.23
GCL+IPL	0.28 ± 0.10	0.08	0.48	2.07	0.49	0.39
INL	0.42 ± 0.11	0.20	0.64	2.81	0.49	0.39
OPL	0.53 ± 0.12	0.30	0.76	1.90	0.64	0.54
ONL+IS	0.48 ± 0.12	0.26	0.71	2.51	0.56	0.46
OS	0.52 ± 0.12	0.30	0.75	9.02	0.56	0.46
RPE	0.63 ± 0.11	0.41	0.84	11.49	0.64	0.54

Table 7.32 AUROC values of scattering coefficients (mm^{-1}) (calculated by using the single-scattering model with the normalization method NRPE) by study groups

AUROC	MS ON- vs. Healthy	MS ON+ vs. MS ON-
Across All Macular Regions		
RNFL	0.46	0.23
GCL+IPL	0.38	0.17
INL	0.59	0.37
OPL	0.60	0.53
ONL+IS	0.55	0.52
OS	0.45	0.54
RPE	0.25	0.64
Foveal Region		
RNFL	0.56	0.25
GCL+IPL	0.38	0.26
INL	0.57	0.43
OPL	0.55	0.44
ONL+IS	0.68	0.63
OS	0.51	0.70 *
RPE	0.27	0.56
Parafoveal region		
RNFL	0.33	0.16
GCL+IPL	0.17	0.17
INL	0.56	0.54
OPL	0.54	0.51
ONL+IS	0.67	0.56
OS	0.51	0.67
RPE	0.23	0.59
Perifoveal Region		
RNFL	0.42	0.13
GCL+IPL	0.41	0.27
INL	0.54	0.39
OPL	0.60	0.56
ONL+IS	0.62	0.49
OS	0.43	0.57
RPE	0.19	0.64

*0.70≤AUROC<0.80, **0.80≤AUROC

Table 7.33 Cutoff values of scattering coefficients (mm^{-1}) (calculated by using the single-scattering model with the normalization method NRPE) derived from ROC analyses between MS ON- and healthy eyes

Intraretinal Layer	AUROC	95% CI		Cutoff Point	Sensitivity	Specificity
		Lower Bound	Upper Bound			
Across All Macular Regions						
RNFL	0.46 ± 0.09	0.28	0.64	5.29	0.54	0.44
GCL+IPL	0.38 ± 0.08	0.22	0.54	2.60	0.42	0.32
INL	0.59 ± 0.07	0.46	0.72	4.16	0.57	0.47
OPL	0.60 ± 0.07	0.46	0.73	2.94	0.66	0.56
ONL+IS	0.55 ± 0.10	0.37	0.74	3.92	0.60	0.50
OS	0.45 ± 0.08	0.29	0.61	12.88	0.51	0.41
RPE	0.25 ± 0.06	0.13	0.36	15.39	0.31	0.21
Foveal Region						
RNFL	0.56 ± 0.09	0.38	0.74	5.01	0.60	0.50
GCL+IPL	0.38 ± 0.09	0.21	0.55	1.86	0.46	0.36
INL	0.57 ± 0.08	0.40	0.73	3.08	0.67	0.57
OPL	0.55 ± 0.09	0.38	0.71	2.05	0.55	0.45
ONL+IS	0.68 ± 0.08	0.52	0.84	2.36	0.67	0.57
OS	0.51 ± 0.08	0.36	0.66	13.61	0.61	0.51
RPE	0.27 ± 0.07	0.14	0.41	12.80	0.39	0.29
Parafoveal Region						
RNFL	0.33 ± 0.09	0.15	0.50	4.87	0.46	0.36
GCL+IPL	0.17 ± 0.07	0.02	0.32	1.56	0.31	0.21
INL	0.56 ± 0.08	0.41	0.71	2.95	0.60	0.50
OPL	0.54 ± 0.07	0.40	0.68	2.42	0.60	0.50
ONL+IS	0.67 ± 0.09	0.50	0.85	3.09	0.64	0.54
OS	0.51 ± 0.08	0.36	0.67	14.25	0.55	0.45
RPE	0.23 ± 0.08	0.08	0.38	14.18	0.31	0.21
Perifoveal Region						
RNFL	0.42 ± 0.09	0.24	0.60	4.92	0.53	0.43
GCL+IPL	0.41 ± 0.08	0.25	0.56	2.91	0.51	0.41
INL	0.54 ± 0.07	0.40	0.68	4.15	0.54	0.44
OPL	0.60 ± 0.07	0.46	0.73	2.86	0.66	0.56
ONL+IS	0.62 ± 0.09	0.45	0.79	3.79	0.67	0.57
OS	0.43 ± 0.08	0.27	0.59	13.00	0.53	0.43
RPE	0.19 ± 0.06	0.07	0.31	15.68	0.24	0.14

Table 7.34 Cutoff values of scattering coefficients (mm^{-1}) (calculated by using the single-scattering model with the normalization method NRPE) derived from ROC analyses between MS ON+ and MS ON- eyes

Intraretinal Layer	AUROC	95% CI		Cutoff Point	Sensitivity	Specificity
		Lower Bound	Upper Bound			
Across All Macular Regions						
RNFL	0.23 ± 0.09	0.05	0.41	5.61	0.36	0.26
GCL+IPL	0.17 ± 0.08	0.01	0.34	2.79	0.33	0.23
INL	0.37 ± 0.11	0.15	0.59	4.20	0.41	0.31
OPL	0.53 ± 0.12	0.30	0.75	2.87	0.57	0.47
ONL+IS	0.52 ± 0.12	0.30	0.75	3.64	0.57	0.47
OS	0.54 ± 0.12	0.31	0.77	12.86	0.64	0.54
RPE	0.64 ± 0.11	0.43	0.85	15.73	0.57	0.47
Foveal Region						
RNFL	0.25 ± 0.09	0.06	0.43	5.25	0.41	0.31
GCL+IPL	0.26 ± 0.10	0.06	0.45	2.13	0.43	0.33
INL	0.43 ± 0.11	0.21	0.65	2.99	0.43	0.33
OPL	0.44 ± 0.11	0.22	0.66	2.04	0.56	0.46
ONL+IS	0.63 ± 0.11	0.41	0.85	2.08	0.64	0.54
OS	0.70 ± 0.11	0.49	0.92	12.85	0.79	0.69
RPE	0.56 ± 0.11	0.33	0.78	13.63	0.57	0.47
Parafoveal Region						
RNFL	0.16 ± 0.08	0.01	0.31	5.62	0.33	0.23
GCL+IPL	0.17 ± 0.08	0.01	0.33	1.80	0.33	0.23
INL	0.54 ± 0.11	0.32	0.77	2.93	0.56	0.46
OPL	0.51 ± 0.12	0.29	0.74	2.41	0.56	0.46
ONL+IS	0.56 ± 0.12	0.33	0.79	2.66	0.71	0.61
OS	0.67 ± 0.11	0.45	0.88	12.41	0.72	0.62
RPE	0.59 ± 0.11	0.36	0.81	15.56	0.57	0.47
Perifoveal Region						
RNFL	0.13 ± 0.07	0.00	0.26	5.24	0.33	0.23
GCL+IPL	0.27 ± 0.10	0.07	0.47	3.05	0.49	0.39
INL	0.39 ± 0.11	0.17	0.61	4.23	0.50	0.40
OPL	0.56 ± 0.12	0.33	0.79	2.81	0.64	0.54
ONL+IS	0.49 ± 0.12	0.26	0.72	3.47	0.57	0.47
OS	0.57 ± 0.11	0.34	0.79	12.97	0.56	0.46
RPE	0.64 ± 0.11	0.43	0.85	16.10	0.64	0.54

Table 7.35 AUROC values of scattering coefficients (mm^{-1}) (calculated by using the multiple-scattering model with the normalization method NRIR) by study groups

AUROC	MS ON- vs. Healthy	MS ON+ vs. MS ON-
Across All Macular Regions		
RNFL	0.55	0.34
GCL+IPL	0.34	0.21
INL	0.63	0.38
OPL	0.61	0.52
ONL+IS	0.68	0.45
OS	0.45	0.53
RPE	0.24	0.58
Foveal Region		
RNFL	0.66	0.30
GCL+IPL	0.38	0.29
INL	0.61	0.46
OPL	0.50	0.47
ONL+IS	0.73 *	0.48
OS	0.53	0.62
RPE	0.26	0.48
Parafoveal region		
RNFL	0.49	0.21
GCL+IPL	0.30	0.21
INL	0.57	0.51
OPL	0.59	0.50
ONL+IS	0.71 *	0.50
OS	0.53	0.65
RPE	0.21	0.58
Perifoveal Region		
RNFL	0.46	0.29
GCL+IPL	0.25	0.19
INL	0.57	0.41
OPL	0.60	0.58
ONL+IS	0.75 *	0.45
OS	0.43	0.56
RPE	0.19	0.63

*0.70≤AUROC<0.80, **0.80≤AUROC

Table 7.36 Cutoff values of scattering coefficients (mm^{-1}) (calculated by using the multiple-scattering model with the normalization method NRIR) derived from ROC analyses between MS ON- and healthy eyes

Intraretinal Layer	AUROC	95% CI		Cutoff Point	Sensitivity	Specificity
		Lower Bound	Upper Bound			
Across All Macular Regions						
RNFL	0.55 ± 0.09	0.37	0.74	3.71	0.66	0.56
GCL+IPL	0.34 ± 0.08	0.19	0.48	2.01	0.46	0.36
INL	0.63 ± 0.07	0.49	0.77	3.36	0.67	0.57
OPL	0.61 ± 0.08	0.46	0.76	3.12	0.68	0.58
ONL+IS	0.68 ± 0.07	0.54	0.82	2.38	0.62	0.52
OS	0.45 ± 0.08	0.29	0.60	10.62	0.53	0.43
RPE	0.24 ± 0.07	0.11	0.38	12.99	0.32	0.22
Foveal Region						
RNFL	0.66 ± 0.09	0.49	0.84	3.37	0.74	0.64
GCL+IPL	0.38 ± 0.09	0.21	0.56	1.51	0.46	0.36
INL	0.61 ± 0.08	0.46	0.76	2.77	0.66	0.56
OPL	0.50 ± 0.09	0.34	0.67	2.29	0.53	0.43
ONL+IS	0.73 ± 0.08	0.57	0.88	1.63	0.69	0.59
OS	0.53 ± 0.08	0.36	0.69	13.80	0.60	0.50
RPE	0.26 ± 0.06	0.13	0.38	12.17	0.31	0.21
Parafoveal Region						
RNFL	0.49 ± 0.09	0.32	0.66	3.57	0.57	0.47
GCL+IPL	0.30 ± 0.09	0.13	0.48	1.35	0.46	0.36
INL	0.57 ± 0.08	0.42	0.72	2.53	0.61	0.51
OPL	0.59 ± 0.07	0.44	0.74	2.82	0.61	0.51
ONL+IS	0.71 ± 0.08	0.55	0.88	1.98	0.64	0.54
OS	0.53 ± 0.08	0.38	0.69	12.44	0.58	0.48
RPE	0.21 ± 0.08	0.06	0.36	12.44	0.31	0.21
Perifoveal Region						
RNFL	0.46 ± 0.09	0.28	0.65	3.51	0.46	0.36
GCL+IPL	0.25 ± 0.08	0.09	0.41	1.95	0.38	0.28
INL	0.57 ± 0.08	0.42	0.72	3.39	0.62	0.52
OPL	0.60 ± 0.08	0.46	0.75	3.10	0.67	0.57
ONL+IS	0.75 ± 0.07	0.62	0.89	2.28	0.80	0.70
OS	0.43 ± 0.08	0.27	0.59	10.96	0.47	0.37
RPE	0.19 ± 0.07	0.05	0.33	12.88	0.28	0.18

Table 7.37 Cutoff values of scattering coefficients (mm^{-1}) (calculated by using the multiple-scattering model with the normalization method NRIR) derived from ROC analyses between MS ON+ and MS ON- eyes

Intraretinal Layer	AUROC	95% CI		Cutoff Point	Sensitivity	Specificity
		Lower Bound	Upper Bound			
Across All Macular Regions						
RNFL	0.34 ± 0.11	0.12	0.55	3.75	0.43	0.33
GCL+IPL	0.21 ± 0.09	0.03	0.39	2.16	0.41	0.31
INL	0.38 ± 0.11	0.16	0.60	3.30	0.43	0.33
OPL	0.52 ± 0.12	0.29	0.74	3.00	0.64	0.54
ONL+IS	0.45 ± 0.12	0.22	0.68	2.30	0.50	0.40
OS	0.53 ± 0.12	0.31	0.76	10.47	0.57	0.47
RPE	0.58 ± 0.11	0.36	0.80	13.34	0.64	0.54
Foveal Region						
RNFL	0.30 ± 0.10	0.10	0.50	3.53	0.36	0.26
GCL+IPL	0.29 ± 0.10	0.09	0.48	1.62	0.41	0.31
INL	0.46 ± 0.12	0.24	0.69	2.74	0.50	0.40
OPL	0.47 ± 0.12	0.25	0.70	2.30	0.56	0.46
ONL+IS	0.48 ± 0.12	0.25	0.72	1.43	0.64	0.54
OS	0.62 ± 0.11	0.40	0.84	12.44	0.64	0.54
RPE	0.48 ± 0.12	0.25	0.70	12.43	0.49	0.39
Parafoveal Region						
RNFL	0.21 ± 0.10	0.03	0.40	3.78	0.33	0.23
GCL+IPL	0.21 ± 0.09	0.04	0.38	1.53	0.43	0.33
INL	0.51 ± 0.12	0.28	0.73	2.53	0.50	0.40
OPL	0.50 ± 0.11	0.27	0.72	2.74	0.56	0.46
ONL+IS	0.50 ± 0.12	0.27	0.73	1.82	0.56	0.46
OS	0.65 ± 0.11	0.44	0.87	11.84	0.71	0.61
RPE	0.58 ± 0.11	0.35	0.80	13.52	0.56	0.46
Perifoveal Region						
RNFL	0.29 ± 0.10	0.09	0.49	3.59	0.49	0.39
GCL+IPL	0.19 ± 0.09	0.02	0.35	2.16	0.36	0.26
INL	0.41 ± 0.11	0.19	0.63	3.36	0.49	0.39
OPL	0.58 ± 0.12	0.35	0.81	2.98	0.71	0.61
ONL+IS	0.45 ± 0.12	0.21	0.68	2.23	0.49	0.39
OS	0.56 ± 0.11	0.34	0.78	11.03	0.56	0.46
RPE	0.63 ± 0.11	0.42	0.85	13.64	0.64	0.54

Table 7.38 AUROC values of scattering coefficients (mm^{-1}) (calculated by using the multiple-scattering model with the normalization method NRPE) by study groups

AUROC	MS ON- vs. Healthy	MS ON+ vs. MS ON-
Across All Macular Regions		
RNFL	0.54	0.34
GCL+IPL	0.26	0.13
INL	0.62	0.38
OPL	0.58	0.60
ONL+IS	0.69	0.54
OS	0.43	0.55
RPE	0.26	0.62
Foveal Region		
RNFL	0.68	0.30
GCL+IPL	0.37	0.29
INL	0.62	0.45
OPL	0.52	0.45
ONL+IS	0.74 *	0.49
OS	0.53	0.63
RPE	0.29	0.54
Parafoveal region		
RNFL	0.50	0.20
GCL+IPL	0.27	0.19
INL	0.58	0.54
OPL	0.56	0.62
ONL+IS	0.74 *	0.55
OS	0.53	0.68
RPE	0.22	0.62
Perifoveal Region		
RNFL	0.47	0.18
GCL+IPL	0.24	0.11
INL	0.58	0.41
OPL	0.60	0.59
ONL+IS	0.77 *	0.50
OS	0.43	0.56
RPE	0.20	0.65

*0.70≤AUROC<0.80, **0.80≤AUROC

Table 7.39 Cutoff values of scattering coefficients (mm^{-1}) (calculated by using the multiple-scattering model with the normalization method NRPE) derived from ROC analyses between MS ON- and healthy eyes

Intraretinal Layer	AUROC	95% CI		Cutoff Point	Sensitivity	Specificity
		Lower Bound	Upper Bound			
Across All Macular Regions						
RNFL	0.54 ± 0.09	0.36	0.71	5.38	0.57	0.47
GCL+IPL	0.26 ± 0.06	0.13	0.38	2.79	0.39	0.29
INL	0.62 ± 0.07	0.49	0.75	4.69	0.61	0.51
OPL	0.58 ± 0.07	0.44	0.71	4.24	0.61	0.51
ONL+IS	0.69 ± 0.08	0.54	0.85	3.26	0.68	0.58
OS	0.43 ± 0.09	0.27	0.60	14.85	0.53	0.43
RPE	0.26 ± 0.06	0.14	0.37	17.55	0.31	0.21
Foveal Region						
RNFL	0.68 ± 0.09	0.50	0.86	4.38	0.74	0.64
GCL+IPL	0.37 ± 0.08	0.21	0.54	1.90	0.46	0.36
INL	0.62 ± 0.08	0.46	0.77	3.59	0.67	0.57
OPL	0.52 ± 0.09	0.36	0.69	2.85	0.60	0.50
ONL+IS	0.74 ± 0.08	0.59	0.90	2.02	0.73	0.63
OS	0.53 ± 0.08	0.37	0.69	17.22	0.60	0.50
RPE	0.29 ± 0.07	0.15	0.43	14.80	0.39	0.29
Parafoveal Region						
RNFL	0.50 ± 0.09	0.33	0.67	4.87	0.62	0.52
GCL+IPL	0.27 ± 0.09	0.10	0.44	1.80	0.34	0.24
INL	0.58 ± 0.08	0.43	0.73	3.33	0.62	0.52
OPL	0.56 ± 0.07	0.41	0.70	3.65	0.60	0.50
ONL+IS	0.74 ± 0.08	0.59	0.89	2.56	0.67	0.57
OS	0.53 ± 0.09	0.37	0.70	16.62	0.60	0.50
RPE	0.22 ± 0.08	0.07	0.38	16.33	0.31	0.21
Perifoveal Region						
RNFL	0.47 ± 0.08	0.32	0.62	4.97	0.51	0.41
GCL+IPL	0.24 ± 0.08	0.10	0.39	2.71	0.31	0.21
INL	0.58 ± 0.07	0.44	0.72	4.70	0.55	0.45
OPL	0.60 ± 0.06	0.48	0.73	4.19	0.65	0.55
ONL+IS	0.77 ± 0.07	0.63	0.92	3.09	0.81	0.71
OS	0.43 ± 0.08	0.27	0.59	15.14	0.50	0.40
RPE	0.20 ± 0.06	0.08	0.32	17.82	0.27	0.17

Table 7.40 Cutoff values of scattering coefficients (mm^{-1}) (calculated by using the multiple-scattering model with the normalization method NRPE) derived from ROC analyses between MS ON+ and MS ON- eyes

Intraretinal Layer	AUROC	95% CI		Cutoff Point	Sensitivity	Specificity
		Lower Bound	Upper Bound			
Across All Macular Regions						
RNFL	0.34 ± 0.11	0.13	0.55	5.40	0.43	0.33
GCL+IPL	0.13 ± 0.08	-0.03	0.28	3.00	0.25	0.15
INL	0.38 ± 0.11	0.16	0.60	4.73	0.41	0.31
OPL	0.60 ± 0.12	0.37	0.83	4.16	0.64	0.54
ONL+IS	0.54 ± 0.12	0.31	0.78	3.06	0.56	0.46
OS	0.55 ± 0.12	0.32	0.78	14.80	0.64	0.54
RPE	0.62 ± 0.11	0.40	0.83	17.91	0.56	0.46
Foveal Region						
RNFL	0.30 ± 0.10	0.10	0.50	4.54	0.36	0.26
GCL+IPL	0.29 ± 0.10	0.09	0.48	2.01	0.41	0.31
INL	0.45 ± 0.11	0.23	0.68	3.54	0.49	0.39
OPL	0.45 ± 0.11	0.22	0.67	2.86	0.50	0.40
ONL+IS	0.49 ± 0.12	0.26	0.72	1.78	0.64	0.54
OS	0.63 ± 0.11	0.41	0.85	16.10	0.72	0.62
RPE	0.54 ± 0.11	0.32	0.77	15.56	0.57	0.47
Parafoveal Region						
RNFL	0.20 ± 0.09	0.03	0.37	5.19	0.33	0.23
GCL+IPL	0.19 ± 0.08	0.03	0.36	1.99	0.33	0.23
INL	0.54 ± 0.11	0.32	0.77	3.27	0.57	0.47
OPL	0.62 ± 0.11	0.39	0.84	3.59	0.71	0.61
ONL+IS	0.55 ± 0.12	0.32	0.78	2.35	0.64	0.54
OS	0.68 ± 0.10	0.48	0.89	14.94	0.64	0.54
RPE	0.62 ± 0.11	0.39	0.84	17.49	0.57	0.47
Perifoveal Region						
RNFL	0.18 ± 0.09	0.01	0.35	5.08	0.29	0.19
GCL+IPL	0.11 ± 0.07	-0.03	0.25	2.95	0.25	0.15
INL	0.41 ± 0.12	0.18	0.63	4.69	0.56	0.46
OPL	0.59 ± 0.12	0.37	0.82	4.11	0.64	0.54
ONL+IS	0.50 ± 0.12	0.27	0.74	2.87	0.57	0.47
OS	0.56 ± 0.11	0.34	0.78	15.16	0.56	0.46
RPE	0.65 ± 0.11	0.45	0.86	18.26	0.64	0.54

CHAPTER 8. CONCLUDING REMARKS

8.1 SIGNIFICANT FINDINGS

This thesis presented several important findings. This section will provide a brief overview of the key results reported in the thesis and will highlight the relevant conclusions. In this study, structural parameters and optical properties per intraretinal layer per macular region of the retinal tissue were extracted from OCT-based images. In addition to the traditional measurement of thickness, structural parameters including fractal dimension, energy, entropy, correlation, contrast and homogeneity were evaluated and used to discriminate DM eyes with and without DR from healthy eyes. Optical properties, such as the mean reflectance, total reflectance, layer index and scattering coefficients, were also calculated and used to detect early retinopathy indicators in the diabetic macula.

Based on the present study, the following conclusions were drawn:

1. OCT is typically employed for the measurement of retinal thickness. However, coherent reflected light carries more information that is characteristic of retinal tissue's reflectance changes. In addition, texture measures may provide additional information with which to characterize abnormalities at the early stage of retinopathy. Therefore, changes in tissue reflectance and texture descriptors may provide further information regarding cellular layers and early damage in diabetic ocular disease. Compared with the standard thickness measurements provided by current commercial OCT devices, the combination of thickness, texture and reflectance measurements were significantly better at discriminating MDR eyes from healthy and DM eyes. Thus, the diagnostic

power was improved by adding diagnostic parameters based on texture descriptors and reflectance change measures of the backscattered signal from layered retinal structures in diabetic eyes.

2. Our quantitative results indicate that the total reflectance, fractal dimension, thickness and layer index displayed the most powerful diagnostic utility for detecting early changes in the diabetic retina. Our results show that screening for abnormalities in the GCL+IPL complex, OPL and OS could detect DR earlier.
3. The results obtained by the custom-built OCTRIMA software were more sensitive than the measurements extracted by most commercially available OCT devices (e.g., cpRNFL, total macular volume), which reveals the potential clinical usefulness of intraretinal structure quantification by OCT image segmentation. Therefore, macular OCT image segmentation, which shows in vivo structural-optical changes in retinal tissue, may yield deeper insights into macular pathology and should therefore play an important future role in the diagnosis and follow-up of eye diseases.
4. Our results also suggest that the RNFL, GCL+IPL complex, OPL and OS are more susceptible to initial damage when comparing MDR with healthy and DM eyes. Particularly, the trend observed for the thickness (thinning) and total reflectance (decreasing) of the RNFL and GCL+IPL complex in MDR eyes might be associated with pathological metabolic changes in the retina, possibly reflecting neurodegenerative changes in the diabetic retina. These findings also have possible implications for the early detection of macular

damage in diabetes. Because the macular region is rich in retinal ganglion cells, diabetic damage to this central region might occur early in the disease process. In fact, animal models of DR show significant loss of macular ganglion cells. [12-16]

5. Interestingly, our results show for the first time that the thickness and total reflectance of the OPL in MDR eyes was significantly reduced compared with similar measures in healthy eyes. In addition, total reflectance decreased in MDR eyes (except the RPE) compared with controls, possibly due to macular diabetic damage leading to reduced transparence and increased disorganization in these layers, which would result in increased backscattering. This result is supported by previous results from in vitro and in vivo experiments inducing apoptosis in animal models of diabetic eyes. [14] In fact, previous studies have shown that not only are retinal pericytes and endothelial cells susceptible to hyperglycemia, but neuroglial elements of the retina are also involved in the retinal damage caused by diabetes. [1, 2] According to Barber and colleagues, apoptotic cells are likely to include ganglion cells and other neurons in the retina, such as cells of the plexiform and nuclear layers. [15] Thus, the possibility that damage to the neuroglial retina causes or contributes to capillary degeneration is consistent with evidence that neuroglial degeneration precedes the degeneration of retinal capillaries in diabetic retinopathy.[15] Accordingly, our results suggest that an early indicator of vascular and neural degeneration development could be detected by investigating the changes in reflectance and thickness changes in these layers.

6. Interestingly, a significant decrease in fractal dimension was only observed for the GCL+IPL complex of MDR eyes compared with controls. This result is in agreement with previous reports showing a significant reduction of the fractal dimension during induced apoptosis throughout early apoptotic phases in breast cancer cells.[17] On the other hand, the highest AUROC values were obtained for the thickness, total reflectance and layer index of the OS when comparing MDR with DM eyes. This particular result might suggest that diabetes also damages the outer photoreceptor segment. This observation could be an early indication of visual function degeneration and could be used to improve early detection of diabetic retinal damage and/or disease progression.
7. In this study, the AUROC results showed a similar trend for total reflectance using NRIR and NRPE normalizations. This comparable trend might rule out the dependence on the sensitivity to the direction of incidence of the light beam. Considering that the RPE layer apparently behaves like a diffuse reflector, which is an assumption that could be valid when the RPE is more or less flat, this layer could be fairly insensitive to the direction of incidence of the light beam. Accordingly, our results appear not to have been affected by the directionality of the light beam in the OCT system.
8. Despite the scattering model and normalization method used, the scattering coefficient parameter was not a good predictor of early retinopathy development. This finding may be associated with the fact that in many OCT systems, the optimal system design for rapid image acquisition is not optimal

for measuring optical properties (which works better at higher numerical aperture values). Moreover, the low penetration depth of the laser source (820 nm) used in the Stratus OCT device limits its ability to handle multiple scattering effects at deeper retinal locations where multiple scattering becomes an important factor. The multiple scattering model is also limited in its ability to handle multiple scattering effects. However, our quantitative results show a statistically significant scattering coefficient increase in the OS and RPE when comparing MDR with healthy eyes when using both the single- and multiple-scattering model. Additionally, scattering coefficients show a statistically significant decrease for the OPL and a statistically significant increase for OS and RPE when comparing MDR with DM eyes when using both the single- and multiple-scattering model. This finding indicates that scattering coefficients provided better discriminating power for outer retinal abnormalities localized in the OS and RPE in MDR eyes compared with healthy and DM eyes. In addition, when comparing MDR with DM eyes, scattering coefficients also show better discriminating power for outer retinal abnormalities localized in the OPL when using both the single- and multiple-scattering model.

9. When the same methodology was applied to MS eyes, our results demonstrated the superiority of the GCL+IPL thickness as a good discriminator between healthy eyes and eyes with MS. Specifically, we found that the thickness of the macular ganglion cell complex had the highest sensitivity and specificity, outperforming the RNFL thickness data provided

by the analysis software of commercially available OCT devices. Our preliminary MS study also shows that optic neuritis is followed by a targeted loss of ganglion cells in the macula, which can also be objectively assessed by macular image processing.

In summary, we have demonstrated the following:

1. The novel diagnostic parameters were able to discriminate diabetic eyes with early retinopathy from healthy and diabetic eyes with higher sensitivity and specificity compared with standard thickness parameters. These results together validate the potential of these parameters for use in therapeutic interventions to prevent early diabetic retinopathy in diabetic subjects. Given the results of our study, we conclude that obtaining fractal dimension, thickness, layer index and total reflectance values for the RNFL, GCL+IPL complex, OPL and OS may be a beneficial method for diagnosing early diabetic retinopathy in DM subjects. In our population (or a similar population), a GCL+IPL (OPL) thickness of ≤ 75.86 (38.12) μm; a GCL+IPL fractal dimension of ≤ 1.66; a GCL+IPL (OPL, OS) total reflectance of ≤ 80.57 dB (72.97 dB, 74.22 dB, respectively) and a RNFL (OPL, OS)'s layer index of ≤ 11.47 (5.03, 5.55, respectively) can be used to select diabetic patients who may benefit from intervention trials to prevent the onset of early diabetic retinopathy. We conclude that our results have shown the potential of this methodology to differentiate diabetic eyes with early retinopathy from healthy and diabetic eyes without retinopathy.

2. Our methodology can yield deeper insights into the macular pathology and should therefore play an important future role in the diagnosis and follow-up of optic nerve-damaging neurological diseases, such as multiple sclerosis, which influences a continuously increasing number of patients worldwide.

8.2 OUTLOOK

The results presented in this thesis are widely applicable to the diagnosis of retinal neurodegeneration in patients with multiple sclerosis or other neurodegenerative diseases, such as Parkinson's and Alzheimer disease. Additionally, the methodology presented in this thesis is relevant to other therapeutic interventions for which it is important to assess the effects that certain drugs have on the local remodeling of retinal tissue.

In addition, structural and optical property changes, as well as functional derangement (e.g., blood flow alterations) in the retina, are observed in diabetic eyes at the early stage. It is well known that the earliest clinical signs of DR are microaneurysms and dot intraretinal hemorrhages resulting from damage to the capillary pericytes and endothelial cells. This capillary damage leads to an increase in retinal vascular permeability, localized loss of capillaries with resulting ischemia and the growth of abnormal retinal blood vessels known as proliferative diabetic retinopathy (PDR) in the final stage of DR. Therefore, in addition to the study of structural and optical property changes in diabetic eyes, functional information regarding the retinal tissue blood vessels could also assist the diagnosis of diabetic eyes with and without retinopathy

It is also important to note that our results indicated that scattering coefficients did not perform as well for the discrimination between diabetic eyes and healthy eyes as did other structural and optical parameters, such as the thickness, fractal dimension, mean

reflectance and total reflectance. This limitation could be due to the complicated interactions between photons and cellular organelles in the retinal tissue as well as the low numerical aperture and depth penetration of the Stratus OCT system. Until now, there has been no scattering model to precisely describe the interaction between photons and cellular organelles. In particular, different assumptions are made to simplify the scattering model. For example, a single scattering event is assumed in the single-scattering model and a multi-angle event is assumed in the multiple-scattering model. Therefore, the scattering coefficients could not be obtained with high accuracy with the single- and multiple-scattering models using a low resolution OCT device and thus could not provide better discriminating power. Further research is needed to develop more precise light scattering models.

Lastly, improved validation of the current methodology demands a larger patient population for analysis. Future studies will benefit from higher resolution imaging. Moreover, the collection of longitudinal data will facilitate the prediction of disease stage and progression. Despite these basic limitations, this thesis demonstrates how to improve the diagnostic power of OCT imaging systems. Our methodology holds considerable promise for retinal diagnosis.

REFERENCE

1. Huang, D., Swanson, E.A., Lin, C.P., et al. 1991. "Optical coherence tomography." *Science*, Vol. 254, No. 5035, pp. 1178-1181.
2. Erbel, R., Roelandt, J.R.T.C., Ge, J., and Gorge, G, eds.1998. *Intravascular Ultrasound*. London: Martin Dunitz.
3. Szabo, T.L. 2004. *Diagnostic Ultrasound Imaging: Inside Out.* Burlington: Academic Press.
4. Brezinski, M.E., Tearney, G.J., Bouma, B.E., et al. 1996. "Optical coherence tomography for optical biopsy: properties and demonstration of vascular pathology." *Circulation*, Vol. 93, No. 6, pp. 1206-1213.
5. Michelson, A.A., and Morley E.W. 1887. "On the relative motion of the earth and the luminiferous aether." *American Journal of Science*, Vol. 34, No. 203, pp. 333-345.
6. Fercher, A.F., Hitzenberger, C.K., Kamp, G., and El-Zaiat, S.Y. 1995. "Measurement of intraocular distances by backscattering spectral interferometry." *Optics Communications*, Vol. 117, No. 1-2, pp. 43-48.
7. Hausler, G., and Lindner, M.W. 1998. "Coherence radar and spectral radar - new tools for dermatological diagnosis." *Journal of Biomedical Optics*, Vol. 3, No. 1, pp. 21-31.
8. Choma, M.A., Sarunic, M.V., Yang, C., and Izatt, J. 2003. "Sensitivity advantage of swept source and Fourier domain optical coherence tomography." *Optics Express*, Vol. 11, No. 18, pp. 2183-2189.
9. de Boer, J.F., Cense, B., Park B.H., et al. 2003. "Improved signal to-noise ratio in spectral-domain compared with time-domain optical coherence tomography." *Optics Letters*, Vol. 28, No. 21, pp. 2067-2069.
10. Leitgeb, R.A., Schmetterer, S.L., Drexler, W., et al. 2003. "Real-time assessment of retinal blood flow with ultrafast acquisition by color Doppler Fourier domain optical coherence tomography." *Optics Express*, Vol. 11, No. 23, pp. 3116-3121.
11. Mitsui, T. 1999. "Dynamic range of optical reflectometry with spectral interferometry." *Japanese Journal of Applied Physics*, Vol. 38, No. 10, pp. 6133-6137.

12. Nassif, N.A. Cense, B., Park, B.H., et al. 2004. "In vivo high-resolution video-rate spectral-domain optical coherence tomography of the human retina and optic nerve." *Optics Express*, Vol. 12, No. 3, pp. 367-376.
13. Puliafito, C.A., et al. 1996. *Optical Coherence Tomography of Ocular Diseases*. 1st ed. Thorofare, NJ: SLACK.
14. Fercher, A.F., Hitzenberger, C.K., Drexler, W., et al. 1993. "In vivo optical coherence tomography." *American Journal of Ophthalmology*, Vol. 116, No. 1, pp. 113-114.
15. Drexler, W., and Fujimoto, J.G. 2008. "State-of-the-art retinal optical coherence tomography." *Progress in Retinal and Eye Research*, Vol. 27, No. 1, pp. 45–88.
16. Bizheva, K., Pflug, R., Hermann, B., et al. 2006. "Optophysiology: depth-resolved probing of retinal physiology with functional ultrahigh-resolution optical coherence tomography." *Proceedings of the National Academy of Sciences of the United States of America*, Vol. 103, No. 13, pp. 5066-5071.
17. Hermann, B., Povazay, B., Unterhuber, A., et al. 2006. "Optophysiology of the human retina with functional ultrahigh resolution optical coherence tomography." *Investigative Ophthalmology and Visual Science*, Vol. 47: E-Abstract 1672.
18. Shaw, J.E., Sicree, R.A., and Zimmet, P.Z. 2010. "Global estimates of the prevalence of diabetes for 2010 and 2030." *Diabetes Research and Clinical Practice*, Vol. 87, No. 1, pp. 4
19. Piao, J., Lee, J.E., Weon, K.Y., et al. 2009. "Development of novel mucoadhesive pellets of metformin hydrochloride." *Archives of Pharmacal Research*, Vol. 32, No. 3, pp. 391-397.
20. Diabetes, heart disease, and stroke, NIH Publication No. 06–5094, 2005.
21. Malone, J.I., Morrison, A.D., Pavan, P.R., et al. 2001. "Prevalence and significance of retinopathy in subjects with type 1 diabetes of less than 5 years' duration screened for the diabetes control and complications trial." *Diabetes Care*, Vol. 24, No. 3, pp. 522-526.
22. Duh, E.J. 2008. *Diabetic Retinopathy*. ed. Totowa, NJ: Humana Press.
23. Schaudig, U.H., Glaefke, C., Scholz, F., et al. 2000. "Optical coherence tomography for retinal thickness measurement in diabetic patients without clinically significant macular edema." *Ophthalmic Surgery and Lasers*, Vol. 31, No. 3, pp. 182–186.

24. Goebel, W., and Kretzchmar-Gross, T. 2002. "Retinal thickness in diabetic retinopathy: a study using optical coherence tomography (OCT)." *Retina*, Vol. 22, No. 6, pp. 759-767.
25. Oshitar, T., Hanawa, T., and Adachi-Usami, E. 2008. "Changes of macular and RNFL thickness measured by Stratus OCT in patients with early stage diabetes." *Eye*, Vol. 23, No. 4, pp. 884-889.
26. Asefzadeh, B., Fisch, B.M., Parenteau C.E., et al., 2008. "Macular thickness and systemic markers for diabetes in individuals with no or mild diabetic retinopathy." *Clinical and Experimental Ophthalmology*, Vol. 36, No. 5, pp. 455-463.
27. Bressler, N.M., Edwards, A.R., Antoszyk, A.N., et al., 2008. "Retinal thickness on Stratus optical coherence tomography in people with diabetes and minimal or no diabetic retinopathy." *American Journal of Ophthalmology*, Vol. 145, No. 5, pp. 894-901.
28. DeBuc, D.C., and Somfai, G.M. 2010. "Early detection of retinal thickness changes in diabetes using optical coherence tomography." *Medical Science Monitor International Medical Journal of Experimental and Clinical Research*, Vol. 16, No. 3, MT15-21.
29. Kernell, A., Dedorsson, I., Johansson, B., et al. 1997. "Prevalence of diabetic retinopathy in children and adolescents with IDDM. A population-based multicentre study." *Diabetologia*. Vol. 40, No. 3, pp. 307-310.
30. Early Treatment Diabetic Retinopathy Study Research Group, 1991. "Early treatment diabetic retinopathy study design and baseline patient characteristics." *Ophthalmology*, Vol. 98, pp. 741–756.
31. Ishikawa, H., Wollstein, G., Aoyama, M., et al. 2004. "Stratus OCT Image Quality Assessment." *Investigative Ophthalmology and Visual Science,* Vol. 45, E-Abstract 3317.
32. Salinas, H.M., Cabrera Fernandez, D. 2007. "Comparison of PDE-based nonlinear diffusion approaches for image enhancement and denoising in optical coherence tomography." *IEEE Transactions on Medical Imaging*, Vol. 26, No. 6, pp. 761-771.

33. Cabrera Fernandez, D., Salinas, H.M., Puliafito, C.A. 2005. “Automated detection of retinal layer structures on optical coherence tomography images.” *Opt Express*, Vol. 13, No. 25, pp. 10200-10216.
34. Shahidi, M., Wang, Z., Zelkha, R. 2005. “Quantitative thickness measurement of retinal layers imaged by optical coherence tomography.” *American Journal of Ophthalmology,* Vol. 139, No. 6, pp. 1056-1061.
35. Ishikawa, H., Wollstein, G., Aoyama, M., et al. 2004. “Stratus OCT Image Quality Assessment.” *Investigative Ophthalmology and Visual Science,* Vol. 45, E-Abstract 3317.
36. Cabrera Fernández, D. 2005. "Delineating fluid-filled region boundaries in optical coherence tomography images of the retina." *IEEE Transaction on Medical Imaging*, Vol. 24, No. 8, pp. 929-945.
37. Koozekanani, D., Boyer, K., Roberts, C. 2001. “Retinal thickness measurements from optical coherence tomography using a Markov boundary model.” *IEEE Transaction on Medical Imaging*, Vol. 20, No. 9, pp. 900–916.
38. Mujat, M., Chan, R.C., Cense, B., et al. 2005. “Retinal nerve fiber layer thickness map determined from optical coherence tomography images.” *Optics Express,* Vo. 13, No. 23, pp. 9480–9491.
39. Szkulmowski, M., Wojtkowski, M., Sikorski, B., et al. 2007. “Analysis of posterior retinal layers in spectral optical coherence tomography images of the normal retina and retinal pathologies.” *Journal of Biomedical Optics,* Vol. 12, No. 4, 041207.
40. Baroni, M., Fortunato, P., and Torre, A. L. 2007. “Towards quantitative analysis of retinal features in optical coherence tomography.” *Med. Engineering and Physics,* Vol. 29, No. 4, pp. 432–441.
41. Gotzinger, E., Pircher, M., Geitzenauer, W., et al. 2008. “Retinal pigment epithelium segmentation by polarization sensitive optical coherence tomography.” *Optics Express,* Vol. 16, No. 21, pp. 16410–16422.
42. Toth, C.A., Farsiu, S., Chiu, S. J., et al. 2008. “Automatic drusen segmentation and characterization in spectral domain optical coherence tomography (SDOCT) images of AMD Eyes.” *Investigative Ophthalmology and Visual Science,* Vol. 49, E-Abstract 5394.

43. Cabrera Fernández, D., Somfai, G.M., Tátrai, E., et al. 2008. "Potentiality of intraretinal layer segmentation to locally detect early retinal changes in patients with diabetes mellitus using Optical Coherence Tomography." *Investigative Ophthalmology and Visual Science,* Vol. 49, E-Abstract 2751.
44. Ahlers, C., Simader, C., Geitzenauer, W., et al. 2008. "Automatic segmentation in three-dimensional analysis of fibrovascular pigment epithelial detachment using high-definition optical coherence tomography." *The British Journal of Ophthalmology,* Vol. 92, No.2, pp. 197-203.
45. Fabritius, T., Makita, S., Miura, M., et al. 2009. "Automated segmentation of the macula by optical coherence tomography." *Optics Express,* Vol. 17, No. 18, pp. 15659-15669.
46. Garvin, M., Abramoff, M., Kardon, R., et al. 2008. "Intraretinal layer segmentation of macular optical coherence tomography images using optimal 3-D graph search." *IEEE Transactions on Medical Imaging,* Vol. 27, No. 10, pp. 1495-1505.
47. Fuller, A.R., Zawadzki, R.J. Choi, S., et al. 2007. "Segmentation of three-dimensional retinal image data." *IEEE Transactions on Visualization and Computer Graphics.* Vol. 13, No. 6, pp. 1719-1726.
48. Joeres, S., Tsong, J.W., Updike, P.G., et al. 2007. "Reproducibility of quantitative optical coherence tomography subanalysis in neovascular age-related macular degeneration." *Investigative Ophthalmology and Visual Science*, Vol. 48, No. 9, pp. 4300-4307.
49. Somfai, G.M., Tátrai, E., Ranganathan, S. et al. 2008. "Age-related changes in macular structure among young and middle-aged healthy subjects assessed by OCT image segmentation.' *Investigative Ophthalmology and Visual Science*, Vol. 49, E-Abstract 3214.
50. Sadda, S.R., Joeres, S., Wu, Z., et al. 2007. "Error correction and quantitative subanalysis of optical coherence tomography data using computer-assisted grading." *Investigative Ophthalmology and Visual Science*, Vol. 48, No. 2, pp. 839-848.
51. Gao, W., Ranganathan, S., Tátrai, E., et al. 2008. "Development of a Graphic User Interface as an additional tool of diagnostic differentiation of retinal tissue using Optical Coherence Tomography." *Investigative Ophthalmology and Visual Science*, Vol. 49, E-Abstract 1891.

52. Cabrera DeBuc, D., Somfai, G.M., Ranganathan, S., et al. 2009. “Reliability and reproducibility of macular segmentation using a custom-built OCT retinal image analysis software.” *Journal of Biomedical Optics,* Vol. 14, No. 6, 064023.
53. Wehbe, H., Ruggeri, M., Jiao, S., et al. 2007. “Automatic retinal blood flow calculation using spectral domain optical coherence tomography.” *Optics Express*, Vol. 15, No. 23, pp. 15193-15206.
54. Ishikawa, H., Stein, D.M., Wollstein, G., et al. 2005. “Macular segmentation with optical coherence tomography.” *Investigative Ophthalmology and Visual Science*, Vol. 46, No. 6, pp. 2012-2017.
55. Vargas, G., Readinger, A., Dozier, S.S., et al., 2007. “Morphological changes in blood vessels produced by hyperosmotic agents and measured by optical coherence tomography." *Photochemistry and Photobiology*. Vol. 77, No. 5, pp. 541-549
56. Schuman, J.S. 2008. “Spectral domain optical coherence tomography for glaucoma.” *Transactions of the American Ophthalmological Society*, Vol. 106, pp. 426-458.
57. Aquino, A. 2010. “Detecting the optical disc boundary in digital fundus images using morphological, edge detection, and feature extraction techniques.” *IEEE Transactions on Medical Imaging*, Vol. 29, No. 11, pp. 1860-1869.
58. Ziou, D., and Tabbone, S. 1998. “Edge detection techniques - an overview.” *International Journal of Pattern Recognition and Image Analysis*, Vol. 8, No. 4, pp. 537-559.
59. Early Treatment Diabetic Retinopathy Study Research Group, 1991. “Early treatment diabetic retinopathy study design and baseline patient characteristics.” *Ophthalmology*, Vol. 98, pp. 741–756.
60. Srinivasan, G.N., and Shobha, G. 2008. “Statistical texture analysis.” *Proceeding of World Academy of Science, Engineering and Technology*, Vol. 36, pp. 1264-1269.
61. Gossage, K.W., Tkaczyk, T.S., Rodriguez, J.J., et al. 2003. “Texture analysis of optical coherence tomography images: feasibility for tissue classification.” *Journal of Biomedical Optics*, Vol. 8, No. 3, pp 550-575.
62. van de Wouwer, G., Scheunders, P., and van Dyck, D., 1999. “Statistical texture characterization from discrete wavelet representations.” *IEEE Transactions on Image Processing*, Vol 8, No. 8, pp. 592-598.

63. Haralick, R.M. 1979. “Statistical and structural approaches to texture." Proceedings of THE IEEE, Vol, 67, No. 5, pp. 786-804
64. Sharma, M., Markou, M. and Singh, S. 2000. “Evaluation of texture methods for image analysis.” *Pattern Recognition Letters*, pp. 117-121.
65. Sarkar, N., and Chaudhuri, B.B. 1992. “An efficient approach to estimate fractal dimension of textural images.” *Pattern Recognition*, Vol. 25, No. 9, pp. 1035-1041.
66. Gneiting, T., and Chalather, M.S. 2004. “Stochastic models that separate fractal dimension and the Hurst effect.” *SIAM Review,* Vol. 46, No. 2, pp. 269–282.
67. Hasegawa, M., Liu, J., Okuda, K., et al. 1996. “Calculation of the fractal dimensions of machined surface profiles.” *Wear*, Vol. 192, No. 1-2, pp. 40-45
68. Huang, Y. 1997. “Optical coherence tomography (OCT) in hereditary retinal degeneration: layer-by-layer analysis in normal and diseased retinas.” Ph.D. dissertation, University of Pennsylvania.
69. Cabrera DeBuc, D., Somfai, G.M., Tatrai, E., et al. 2009. **“**Assessment of Intraretinal Light-Backscatter in Eyes With No or Minimal Diabetic Retinopathy Using Optical Coherence Tomography.” *Investigative Ophthalmology and Visual Science*, Vol. 50, E-Abstract 1107.
70. Hammer, M., Schweitzer, D., Thamm, E., et al. 2000. “Optical properties of ocular fundus tissues determined by optical coherence tomography.” *Optics Communications*, Vol. 186, No. 1-3, pp. 149-153.
71. Stein, D.M., Ishikawa, H., Hariprasad, R., et al. 2006. “A new quality assessment parameter for optical coherence tomography.” *British Journal of Ophthalmology*, Vol. 90, No. 2, pp. 186-190.
72. Wang, J., Thomas, J., Cox, I., et al. 2004. “Noncontact measurements of central corneal epithelial and flap thickness after laser in situ keratomileusis.” *Investigative Ophthalmology and Visual Science,* Vol.45, No. 6, pp. 1812-1816.
73. Wang, J., Simpson, T.L., and Fonn, D. 2004. “Objective measurements of corneal light-backscatter during corneal swelling, by optical coherence tomography.” *Investigative Ophthalmology and Visual Science,* Vol.45, No. 10, pp. 3493-3498.
74. Bohren, C.F., and Huffmann, D.R. 2010. *Absorption and scattering of light by small particles*. New York: Wiley.

75. Stratton, J. A.1941.*Electromagnetic Theory*. New York: McGraw-Hill.
76. Barnett, C.E. 1942. "Some application of wavelength turbidimetry in the infrared." *The Journal of Physical Chemistry*, Vol. 46, No. 1, pp. 69–75.
77. Lenoble. J. ed. 1985. *Radiative Transfer in Scattering and Absorbing Atmospheres: Standard Computational Procedures.* Hampton, VA: A. Deepak Publishing.
78. Wang, L.V., and Jacques, S.L. 2000. "Sources of error in calculation of optical diffuse reflectance from turbid media using diffusion theory." *Computer Methods and Programs Biomedicine*, Vol. 61, No. 3, pp. 163-170.
79. Alerstam, E., Andersson-Engels, S., and Svensson, T. 2008. "White Monte Carlo for time-resolved photon migration." *Journal of Biomedical Optics*, Vol. 13, No. 4, 041304.
80. Tuchin, V.V. 2004. *Coherent-Domain Optical Methods*: *Biomedical Diagnostics, Environment and Material Science.* Boston: Kluwer Academic Publishers, Corp.
81. Faber, D.J., Aalders, M.C.G., Mik, E.G., et al., 2004. "Oxygen saturation denendent absorption and scattering of blood." *Physical Review Letters*, Vol. 93, No. 2, pp. 0281021-0281024.
82. Stamper, D., Weissman, N.J., FACC, et al. 2006. "Plaque characterization with optical coherence tomography." *Journal of the American College of Cardiology*, Vol. 47, No. 8, pp. 69-79.
83. Lee, P., Gao, W., and Zhang, X. 2010. "Performance of single-scattering model versus multiple-scattering model in the determination of optical properties of biological tissue with optical coherence tomography." *Applied Optics*, Vol. 49, No. 18, pp. 3538-3544.
84. Thrane, L., Yura, H.T., and Andersen, P.E., 2000. "Analysis of optical coherence tomography systems based on the extended Huygens-Fresnel principle." *Journal of the Optical Society of America A*, Vol. 17, No. 3, pp. 484-490.
85. Hillion, P., and Quinnez, S. 1983. "Huygens-Fresnel principle in the spinor theory of light." *Journal of Optics*, Vol. 14, No. 3, pp. 143
86. Gerrard, A., and Burch, J. M. 1975. *Introduction to Matrix Methods in Optics.* New York,NY: Wiley.

87. Cabrera Fernandez, D., and Salinas, H.M. 2004. “A tissue phantom for investigation volume quantification on retinal images obtained with the stratus OCT system.” *International Conference of the IEEE Engineering in Medicine and Biology Society*, Vol. 2, pp. 1225-1228.
88. Somfai, G.M., Salinas, H.M., Puliafito, C.A., et al. 2007. "Evaluation of potential image acquisition pitfalls during optical coherence tomography and their influence on retinal image segmentation." *Journal of Biomedical Optics*, Vol. 12, No. 4, 041209.
89. van der Schoot, J., Vermeer, K.A., de Boer, J.F., et al. 2012. “The effect of glaucoma on the optical attenuation coefficient of the retinal nerve fiber layer in spectral domain optical coherence tomography images.” *Investigative Ophthalmology and Visual Science*, Vol. 53, No. 4, pp. 2424-2430.
90. Knighton, R.W., and Huang, X.R. 1999. “Directional and spectral reflectance of the rat retinal nerve fiber layer.” *Investigative Ophthalmology and Visual Science,* Vol. 40, No. 3, pp. 639-647.
91. Snedecor, G.W. 1989. *Statistical methods*. Iowa: Iowa State University Press.
92. Gao, W., Tatrai, E., Olvedy, V., et al. 2011. "Investigation of changes in thickness and reflectivity from layered retinal structures of healthy and diabetic eyes with optical coherence tomography." *Journal of Biomedical Science and Engineering*, Vol. 4, pp. 657-665.
93. Barber, A.J., Lieth, E., Khin, S.A., et al. 1998. “Neural apoptosis in the retina during experimental and human diabetes. Early onset and effect of insulin.” *The Journal of Clinical Investigation*, Vol. 102, No. 4, pp. 783-791.
94. Park, S.H., Park, J.W., Park, S.J., et al. 2003. “Apoptotic death of photoreceptors in the streptozotocin-induced diabetic rat retina”. *Diabetologia*, Vol. 46, No. 9, pp. 1260-1268.
95. Rungger-Brandle, E., Dosso, A.A. and Leuenberger, P.M. 2000. “Glial reactivity, an early feature of diabetic retinopathy.” *Investigative Ophthalmology and Visual Science*, Vol. 41, No. 7, pp. 1971-1980.
96. Zeng, X.X., Ng, Y.K. and Ling, E.A. 2000. “Neuronal and microglial response in the retina of streptozotocin- induced diabetic rats.” *Visual Neuroscience*, Vol. 17, No. 3, pp. 463-471.

97. Barber, A.J., Antonetti, D.A., Kern, T.S., et al. 2005. "The Ins2Akita mouse as a model of early retinal complications in diabetes." *Investigative Ophthalmology and Visual Science*, Vol. 46, No. 6, pp. 2210-2218.

98. Barber, A.J. 2003. "A new view of diabetic retinopathy: A neurodegenerative disease of the eye." *Progress in Neuropsychopharmacology and Biological Psychiatry*, Vol. 27, No. 2, pp. 283-290.

99. Mizutani, M., Gerhardinger, C., and Lorenzi, M. 1998. "Muller cell changes in human diabetic retinopathy." *Diabetes*, Vol. 47, No. 3, pp. 445-449.

100. Zheng, L., Gong, B., Hatala, D.A., et al. 2007. "Retinal ischemia and reperfusion causes capillary degeneration: similarities to diabetes." *Investigative Ophthalmology and Visual Science*, Vol. 48, No. 1, pp 361-367.

101. Hopfield, J.J. 1982. "Neural networks and physical systems with emergent collective computational abilities." *Proceedings of the National Academy of Sciences*, Vol. 79, No. 8, pp. 2551-2558.

102. Kolmogorov, A.N. 1957. "On the representations of continuous functions of many variables by superposition of continuous functions of one variable and addition." *Doklady Akademii Nauk SSSR*, Vol. 114, pp. 953-956.

103. Agatonovic-Kustrin, S., and Beresford, R. 2000. "Basic concepts of artificial neural network (ANN) modeling and its application in pharmaceutical research." *Journal of Pharmaceutical and Biomedical Analysis*, Vol. 22, No. 5, pp. 717-727.

104. Baxt, W.G. 1990. "Use of artificial neural network for data analysis in clinical decision-making: the diagnosis of acute coronary occlusion." *Neural Computation*, Vol. 2, No. 4, pp. 480-489.

105. Miller, W.T., III, Sutton, R.S., and Werbos, P.J. eds. 1995. *Neural Networks for Control*. Cambridge, MA: MIT Press.

106. Bishop, C.M. 1996. *Neural Networks for Pattern Recognition*. New York, NY: Oxford University Press.

107. Ohno-Machado, L. 1996. *Medical Applications of Artificial Neural Networks: Connectionist Models of Survival*. Ph.D. dissertation, Stanford University.

108. Lapuerta, P., L'italien, G.J., Paul, S., et al. 1998. "Neural network assessment of perioperative cardiac risk in vascular surgery patients." *Medical Decision Marking*. Vol. 18, No. 1, pp. 70-75.

109. Douglas, T.H., and Moul, J.W. 1998 "Applications of neural networks in urologic oncology." *Seminars in Urologic Oncology*, Vol. 16, No. 1, pp. 35-39.

110. Ashizawa, K., MacMahon, H., Ishida, T., et al. 1999. "Effect of an artificial neural network on radiologists' performance in the differential diagnosis of interstitial lung disease using chest radiographs." *American Journal of Roentgenology*, Vol. 172, No. 5, pp.1311-1315.

111. Salvi, M., Dazzi, D., Pellistri, I., et al. 2002. "Classification and prediction of the progression of thyroid-associated ophthalmopathy by an artificial neural network." *Ophthalmology*, Vol. 109, No. 9, pp. 1703-1708.

112. Zhu, H., Crabb, D.P., Schlottmann, P.G., et al. 2010. "Predicting visual function from the measurements of retinal nerve fiber layer structure." *Investigative Ophthalmology and Visual Science*, Vol. 51, No. 1, pp. 5657-5666.

113. Zhu, H., Crabb, D.P., Fredette, M.J., et al. 2011. "Quantifying discordance between structure and function measurements in the clinical assessment of glaucoma," *Achieves of Ophthalmology*, Vol. 129, No. 9, pp. 1167-1174.

114. Yun, W.L., Acharya, U.R., Venkatesh, Y.V., et al. 2008. "Identification of different stages of diabetic retinopathy using retinal optical images." *Information Sciences*, Vol. 178, No. 1, pp. 106-121.

115. Sinthanayothin, C., Kongbunkiat, V., Phoojaruenchanachai, S., et al. 2003 "Automated screening system for diabetic retinopathy." *Proceedings of the 3rd International Symposium on Image and Signal processing and Analysis*, Vol. 2, pp. 915-920.

116. Gardner, G.G., Keating, D., Williamson, T.H., et al., 1996. "Automatic detection of diabetic retinopathy using an artificial neural network: a screening tool." *British Journal of Ophthalmology*, Vol. 80, No. 11, pp. 940-944.

117. Bowd, C., Hao, J., Tavares, I.M., et al. 2008. "Bayesian machine learing classifiers for combining structural and functional measurements to classify healthy and glaucomatous eyes," *Investigative Ophthalmology and Visual Science*, Vol 49, No. 3, pp. 945-953.

118. Bernardo, J.M., and Smith, A.F.M. 2000. *Bayesian Theory.* Wiley.

119. Silber, E., and Sharief, M.K. 1999. "Axonal degeneration in the pathogenesis of multiple sclerosis." *Journal of the neurological Sciences,* Vol. 170, No. 1, pp. 11-18.

120. Tegetmeyer, H., and Kühn, E. 2011. "Quantitative Analysis of Changes in Macular Layers Following Optic Neuritis." *Neuro-Ophthalmology*, Vol. 35, No. 3, pp. 101–107.

121. Davies, E.C., Galetta, K.M., Sackel, D.J., et al. 2011. "Retinal ganglion cell layer volumetric assessment by spectral-domain optical coherence tomography in multiple sclerosis: application of a high-precision manual estimation technique." *Journal of Neuro-ophthalmololgy*, Vol. 31, No. 3, pp. 260–264.

122. Bock, M., Brandt, A.U., Dorr, J., et al. 2010. "Patterns of retinal nerve fiber layer loss in multiple sclerosis patients with or without optic neuritis and glaucoma patients." *Clinical Neurology and Neurosurgery,* Vol. 112, No. 8, pp. 647–652.

123. Fjeldstad, C., Bemben, M., and Pardo, G. 2011. "Reduced retinal nerve fiber layer and macular thickness in patients with multiple sclerosis with no history of optic neuritis identified by the use of spectral domain high-definition optical coherence tomography." *Journal of Clinical Neuroscience,* Vol. 18, No. 11, pp. 1469–1472.

124. Parisi, V., Manni, G., Spadaro, M., et al. 1999. "Correlation between morphological and functional retinal impairment in multiple sclerosis patients." *Investigative Ophthalmology and Visual Science,* Vol. 40, No. 11, pp. 2520–2527.

125. Pueyo V, Martin J, Fernandez J, Almarcegui C, Ara J, et al. (2008) Axonal loss in the retinal nerve fiber layer in patients with multiple sclerosis. *Mult Scler* 14: 609-614.

126. Sepulcre, J., Murie-Fernandez, M., Salinas-Alaman, A., et al. 2007. "Diagnostic accuracy of retinal abnormalities in predicting disease activity in MS." *Neurology,* Vol. 68, No. 18, pp. 1488–1494.

127. Klistorner, A., Arvind, H., Nguyen, T., et al. 2009. "Multifocal VEP and OCT in optic neuritis: a topographical study of the structure-function relationship." *Documenta Ophthalmologica,* Vol. 118, No. 2, pp. 129–137.

128. Garas, A., Vargha, P., and Hollo, G. 2011. "Diagnostic accuracy of nerve fibre layer, macular thickness and optic disc measurements made with the RTVue-100 optical coherence tomograph to detect glaucoma." *Eye (Lond),* Vol. 25, No. 1, pp. 57–65.

129. Burkholder, B.M., Osborne, B., Loguidice, M.J., et al. 2009. "Macular volume determined by optical coherence tomography as a measure of neuronal loss in multiple sclerosis." *Achieves of Neurology,* Vol. 66, No. 11, pp. 1366–1372.

130. Green, A.J., McQuaid, S., Hauser, S.L., et al. 2010. "Ocular pathology in multiple sclerosis: retinal atrophy and inflammation irrespective of disease duration." *Brain* Vol. 133, Pt6, No. 1591–1601.

131. Kerrison, J.B., Flynn, T., and Green, W.R. 1994. "Retinal pathologic changes in multiple sclerosis." *Retina,* Vol. 14, No. 5, pp. 445–451.

132. Fisher, J.B., Jacobs, D.A., Markowitz, C.E., et al. 2006. "Relation of visual function to retinal nerve fiber layer thickness in multiple sclerosis." *Ophthalmology*, Vol. 113, No.2, pp. 324-332.

133. Sepulcre, J., Murie-Fernandez, M., Salinas-Alaman, A., et al. 2007. "Diagnostic accuracy of retinal abnormalities in predicting disease activity in MS." *Neurology*, Vol. 68, No. 18, pp. 1488-1494.

134. Rudick, R.A., Lee, J.C., Nakamura, K., et al. 2009. "Gray matter atrophy correlates with MS disability progression measured with MSFC but not EDSS." *Journal of Neurological Sciences,* Vol. 282, No. 1-2, pp. 106-111.

135. Gordon-Lipkin, E., Chodkowski, B., Reich, D.S., et al. 2007. "Retinal nerve fiber layer is associated with brain atrophy in multiple sclerosis." *Neurology,* Vol. 69, No. 16, pp. 1603-1609.

136. Grazioli, E., Zivadinov, R., Weinstock-Guttman, B., et al. 2008. "Retinal nerve fiber layer thickness is associated with brain MRI outcomes in multiple sclerosis." *Journal of Neurological Sciences*, Vol. 268, No. 1-2, pp. 12-17.

137. Altintas, O., Iseri, P., Ozkan, B., et al. 2008. "Correlation between retinal morphological and functional findings and clinical severity in Parkinson's disease." *Documenta Ophthalmologica,* Vol. 116, No. 2, pp. 137-146.

138. Hajee, M.E., March, W.F., Lazzaro, D.R., et al. 2009. "Inner retinal layer thinning in Parkinson disease." *Archives of Ophthalmol*ogy, Vol. 127, No. 12, pp. 737-741.

139. Inzelberg, R., Ramirez, J.A., Nisipeanu, P., et al. 2004. "Retinal nerve fiber layer thinning in Parkinson disease." *Vision Research*. Vol. 44, No. 24, pp. 2793-2797.

140. Tatrai, E., Simo, M., Iljicsov, A., et al. 2012. "In vivo evaluation of retinal neurodegeneration in patients with multiple sclerosis." *PLoS One*, Vol. 7, No. 1, e30922.

141. Stanga, P.E., and Bird, A.C, 2001, "Optical coherence tomography (OCT): principles of operation, technology, indications in vitreoretinal imaging and interpretation of results." *International Ophthalmology*, Vol. 23, No. 4-6, pp. 191-197.

142. Antonetti, D.A., Klein, R., and Gardner, T.W., 2012, "Diabetic retinopathy." The New England Journal of Medicine, Vol. 366, pp. 1227-1239.

143. Lee, K.M., 2008, "Segmentations of the intraretinal surfaces, optic disc and retinal blood vessels in 3D-OCT scans." Ph.D. dissertation, University of Iowa.

144. Lehtikangas, O., Tarvainen, T., and Kim, A.D., 2012, "Modeling boundary measurements of scattered light using the corrected diffusion approximation." *Biomedical Optics Express*, Vol. 3, No. 3, pp.552-571.

145. Van Dijk, H.W., Kok, P.H.B., Garvin, M., et al., 2009, "Selective loss of inner retinal layer thickness in type 1 diabetic patients with minimal diabetic retinopathy." *Investigative Ophthalmology and Visual Science,* Vol. 50, No. 7, pp. 3404–3409.